WA School of Mines: Minerals, Energy and
Chemical Engineering

Synthesis of Novel Boron Containing Catalyts for the Dry Reforming of Methane reaction

MD Shakir
(19604103)

This thesis is presented for the collaborative Degree of Doctor of Philosophy
of
Indian Institute of Technology (Indian School of Mines) Dhanbad
And
Curtin University

March 2023

Form No: PH16

INDIAN INSTITUTE OF TECHNOLOGY (INDIAN SCHOOL OF MINES) DHANBAD

CERTIFICATE FOR FINAL VERSION OF THESIS

(To be submitted after Final Viva-Voce Examination)

This is to certify that the soft copy of thesis entitled "**SYNTHESIS OF NOVEL BORON CONTAINING CATALYST FOR THE DRY REFORMING OF METHANE REACTION**" submitted by Mr MD Shakir for award of Doctor of Philosophy (Ph.D.) Degree in **Department of Chemical Engineering** incorporates all corrections/modifications including those suggested during viva-voce.

Signature of Scholar
Name: MD Shakir
Date: 15/03/2023

Signature of Supervisor
Name: Dr. Siddhartha Sengupta
Associate Professor
Dept. of Chemical Engineering
IIT (ISM), Dhanbad-826004,
Jharkhand, India
Date: 15/03/2023

Signature of Supervisor
Name: Dr. Hari Vuthaluru
Associate Professor
WASM: Mineral, Energy
and Chemical Engineering,
Curtin University, Australia
Date: 15/03/2023

Signature of Supervisor
Dr. Shaomin Liu
Professor
WASM: Mineral, Energy
and Chemical Engineering,
Curtin University, Australia
Date: 15/03/2023

Form No: PH10

INDIAN INSTITUTE OF TECHNOLOGY (INDIAN SCHOOL OF MINES) DHANBAD

COPYRIGHT AND CONSENT FORM

(To be submitted at the time of Thesis Submission)

To ensure uniformity of treatment among all contributors, other forms may not be substituted for this form, nor may any wording of the form be changed. This form is intended for original material submitted to the IIT (ISM), Dhanbad and must accompany any such material in order to be published by the (IIT)ISM. Please read the form carefully and keep a copy for your files. TITLE OF THESIS: SYNTHESIS OF NOVEL BORON CONTANING CATALYST FOR THE DRY REFORMING OF METHANE REACTION

AUTHOR'S NAME & ADDRESS: MD Shakir

Department of Chemical Engineering, Indian Institute of Technology (Indian School of Mines),
Dhanbad 826004, Jharkhand, India.

COPYRIGHT TRANSFER

1. The undersigned hereby assigns to Indian Institute of Technology (Indian School of Mines), Dhanbad all rights under copyright that may exist in and to: (a) the above Work, including any revised or expanded derivative works submitted to the ISM by the undersigned based on the work; and (b) any associated written or multimedia components or other enhancements accompanying the work.

CONSENT AND RELEASE

2. In the event the undersigned makes a presentation based upon the work at a conference hosted or sponsored in whole or in part by the IIT (ISM) Dhanbad, the undersigned, in consideration for his/her participation in the conference, hereby grants the ISM the unlimited, worldwide, irrevocable permission to use, distribute, publish, license, exhibit, record, digitize, broadcast, reproduce and archive; in any format or medium, whether now known or hereafter developed: (a) his/her presentation and comments at the conference; (b) any written materials or multimedia files used in connection with his/her presentation; and (c) any recorded interviews of him/her (collectively, the "Presentation"). The permission granted includes the transcription and reproduction of the Presentation for inclusion in products sold or distributed by IIT(ISM) Dhanbad and live or recorded broadcast of the Presentation during or after the conference.
3. In connection with the permission granted in Section 2, the undersigned hereby grants IIT (ISM) Dhanbad the unlimited, worldwide, irrevocable right to use his/her name, picture, likeness, voice and biographical information as part of the advertisement, distribution and sale of products incorporating the Work or Presentation, and releases IIT (ISM) Dhanbad from any claim based on right of privacy or publicity.
4. The undersigned hereby warrants that the Work and Presentation (collectively, the "Materials") are original and that he/she is the author of the Materials. To the extent the Materials incorporate text passages, figures, data or other material from the works of others, the undersigned has obtained any necessary permissions. Where necessary, the undersigned has obtained all third-party permissions and consents to grant the license above and has provided copies of such permissions and consents to IIT (ISM) Dhanbad.

GENERAL TERMS

- The undersigned represents that he/she has the power and authority to make and execute this assignment.
- The undersigned agrees to indemnify and hold harmless the IIT (ISM) Dhanbad from any damage or expense that may arise in the event of a breach of any of the warranties set forth above.
- In the event the above work is not accepted and published by the IIT (ISM) Dhanbad or is withdrawn by the author(s) before acceptance by the IIT(ISM) Dhanbad, the foregoing copyright transfer shall become null and void and all materials embodying the Work submitted to the IIT(ISM) Dhanbad will be destroyed.
- For jointly authored Works, all joint authors should sign, or one of the authors should sign as authorized agent for the others.

Signature of the Author

Form No: PH11

INDIAN INSTITUTE OF TECHNOLOGY (INDIAN SCHOOL OF MINES), DHANBAD

CERTIFICATE FOR CLASSIFIED DATA

(To be submitted at the time of Thesis Submission)

This is to certify that the thesis entitled “**Synthesis of novel boron containing catalyst for the dry reforming of methane reaction**” being submitted to the Indian Institute of Technology (Indian School of Mines), Dhanbad by **Mr. MD Shakir** for award of Doctor of Philosophy (Ph.D) Degree in **Chemical Engineering** does not contains any classified information. This work is original and yet not been submitted to any institution or university for the award of any degree.

Signature of Supervisor	Signature of Supervisor	Signature of Supervisor
Dr. Siddhartha Sengupta	A/Prof. Hari Vuthaluru	Prof. Shaomin Liu
Assistant Professor	Associate Professor	Professor
Dept. of Chemical Engineering	WASM: Mineral, Energy	WASM: Mineral, Energy
IIT (ISM), Dhanbad-826004,	and Chemical Engineering,	and Chemical Engineering,
Jharkhand, India	Curtin University, Australia	Curtin University, Australia

Signature of Scholar

Form No: PH12

INDIAN INSTITUTE OF TECHNOLOGY (INDIAN SCHOOL OF MINES), DHANBAD

CERTIFICATE REGARDING ENGLISH CHECKING

(To be submitted at the time of Thesis Submission)

This is to certify that the thesis entitled “**Synthesis of novel boron containing catalyst for the dry reforming of methane reaction**” being submitted to the Indian Institute of Technology (Indian School of Mines), Dhanbad by **Mr. MD Shakir**, Admission No **17DR000390**, for the award of Doctor of Philosophy (Ph.D.) Degree has been thoroughly checked for quality of English and logical sequencing of topics.

It is hereby certified that the standard of English is good and that grammar and typos have been thoroughly checked.

It is now worthy for evaluation by the panel of examiners.

Signature of Supervisor
Dr. Siddhartha Sengupta
Assistant Professor
Dept. of Chemical Engineering
IIT (ISM), Dhanbad-826004,
Jharkhand, India

Signature of Supervisor
A/Prof. Hari Vuthaluru
Associate Professor
WASM: Mineral, Energy
and Chemical Engineering,
Curtin University, Australia

Signature of Supervisor
Prof. Shaomin Liu
Professor
WASM: Mineral, Energy
and Chemical Engineering,
Curtin University, Australia

Signature of Scholar

Form No: PH13

INDIAN INSTITUTE OF TECHNOLOGY (INDIAN SCHOOL OF MINES), DHANBAD
DHANBAD, 826004, JHARKHAND, INDIA

CERTIFICATE FROM THE SUPERVISOR(S)

(To be submitted at the time of Thesis Submission)

This is to certify that the thesis entitled “ **Synthesis of novel boron containing catalyst for the dry reforming of methane reaction**”, submitted by **Mr. MD Shakir, Admission No. (17DR000390)**, in fulfilment of the requirements for the award of degree Doctor of Philosophy (Ph.D.), is a bonafide work carried out by her, in the **Department of Chemical Engineering, IIT (ISM), Dhanbad**, and part of research work has been carried out in the **Department of Chemical Engineering (WASM), Curtin University, Australia**, under our joint supervision and guidance. The thesis has fulfilled all the requirements as per the regulations of IIT (ISM) and, in our opinion, has reached the standard needed for submission. The results embodied in this thesis have not been submitted to any other university or institute for the award of any other degree.

Signature of Supervisor
Dr. Siddhartha Sengupta
Assistant Professor
Dept. of Chemical Engineering
IIT (ISM), Dhanbad-826004,
Jharkhand, India

Signature of Supervisor
A/Prof. Hari Vuthaluru
Associate Professor
WASM: Mineral, Energy
and Chemical Engineering,
Curtin University, Australia

Signature of Supervisor
Prof. Shaomin Liu
Professor
WASM: Mineral, Energy
and Chemical Engineering,
Curtin University, Australia

Signature of Scholar

Acknowledgments

I would like to give my heartiest gratitude to key persons such as my supervisors Dr. Siddhartha Sengupta, A/Professor Hari Vuthaluru, and co-supervisor Professor Shaomin Liu, I would also like to express my sincere gratitude to Dr. Apurba Sinhamahapatra, Professor Chun Zhu Li, Professor I.M. Mishra and Professor San ping Jiang. It's been my honor to get an opportunity to work under supervision of them.

I would also like to express my warm sincere thanks to my parents, family members, Jannat Ochira, my friends and all the IIT(ISM) and WASM members: Rashmi Kumari, Manohar Kumar, Priyanshu Pratap Singh, Manoj Kumar Jena, Sweta Singh, Angelina Rossiter, Nathan Tarom, Lana McQueen, Teejay Ahmed Afolobi, Xiao Hua, Jennifer Wang, Veronica Avery, Jiaquan Li, Aaron Dodd and Shiyong Zhao for the friendship and their personal cooperative help during my PhD.

I would also like to gratefully acknowledge for the financial support for this research work from following sources:

- *Curtin University of Technology through the Curtin International Postgraduate Research Scholarship (CIPRS).*
- *The IIT (ISM) Dhanbad scholarship through MHRD, Government of India fellowship for PhD.*
- *DST, India for INSPIRED-FACULTY FELLOWSHIP (Grant No. IFA 17-MS107).*

Specially, I would like to thank my beloved brothers Shams Tabrez and Mohammad Shamshad for their encouragement. They were the one who constantly supported me on my way of achieving my goal.

Dedicated to my loving family

Table of content

List of figures

List of Tables

Synopsis

Worldwide scientists agree that the rate of climate change is faster than ever before, mainly due to non-renewable fuels like coal and oil (called fossil fuels). The greenhouse gas emissions primarily drive climate change which appears to be an urgent issue to avoid anthropogenic climate change in the coming decades. Since carbon dioxide (CO_2) accounts for 80% of the total GHGs followed by methane, the Inter-governmental Panel on Climate Change (IPCC) also emphasized that net-zero GHGs emissions must reach by 2050. In these aspects, the reforming reaction of methane (DRM) appears as one of the most effective way for utilizations of GHGs into a valuable product. The prime goal of methane reforming is to get the desired final product by converting the syngas energy no matter the specific oxidant. Currently, the steam reforming of methane (SRM), DRM and partial oxidation of methane reaction (POM) are the most common reforming processes for the utilization of methane towards valuable fossil fuels. Compared to other reforming processes, DRM reactions have been effectively utilizing CH_4 and CO_2 into the syngas (mixture of CO and H_2). In addition, the DRM produces a lower H_2/CO ratio, which is suitable for further liquid fuel production such as DME. Subsequently, syngas production is a crucial step for producing fossil fuels *via* Fischer–Tropsch synthesis (FTS). Although the DRM appears to be a potential pathway for the utilization of greenhouse gases to the valuable chemicals and liquid fuels: it has issues for the commercialization mainly due to the deactivation of the catalyst. DRM is an endothermic reaction and requires a higher temperature that also favors some side reactions. The major side reactions of DRM reactions are the reverse water-gas shift (RWGS) reaction, the carbon forming reactions: methane decomposition reaction and the Boudouard reaction, also known as disproportion reaction.

The catalyst deactivation due to carbon deposition at high operating temperature is the major drawback of this reaction, which hinders its application. Despite this limitation, the DRM reaction offers more advantages than other reforming processes. Therefore, developing a suitable catalyst that can withstand high operating temperatures without compromising its activity is of great interest and challenge. The noble metals-based catalysts are reported to be highly active and low sensitive, but high cost and limited availability increase interest in transition metal. Among the transition metals, Ni-based catalysts are most preferable and frequently used at an industrial scale. The selection of support and bimetallic catalyst improves the catalyst performance in terms of dispersion, active sites of metals and activity of the catalyst

but not shows any effective impact on deactivation of catalyst especially on graphitic-carbon formation. So far, several studies have been done to supress the C formation to enhance the activity of catalyst. On this regard, the boron (B) modified catalysts shows impressive results. Hence, the prime objective of this this thesis is to develop a suitable method for the synthesis of B-containing catalyst to enhance the performance for DRM and highly resist towards the carbon deposition. The observation of the series of studies are as follows:

1. A series of B-containing B(x)-Ni-based $MgAl_2O_4$ (MA) supported catalysts were synthesized by the $NaBH_4$ reduction method appears as a one-step catalyst preparation method as $NaBH_4$ plays two crucial roles - doping of B and reduction Ni-salt to Ni^0 and Ni-B. The detailed investigations of the catalysts confirmed the presence of metallic Ni and Ni-B species. It is also realized that smaller particle size (~7 nm) for the B-containing catalyst than the non-B Ni/MA (17 nm). It is generally accepted that the smaller Ni size helps enhance catalyst performance and suppress the deactivation of the catalysts for DRM. The B(x)-Ni/MA catalysts tested for the DRM, which further revealed catalyst with 3 wt.% B showed excellent performance among the prepared catalyst with 2.61 times higher $\mathrm{TOF_{CH_4}}$ compared to the non-B catalyst. The decline in conversion was also insignificant, about ~9.7% for the B(3)-Ni/MA catalyst compared to the Ni/MA catalyst (~49%). Moreover, extremely low carbon deposition was observed at the Ni sites due to the B particles that block carbon diffusion into Ni lattice. Interestingly, the Raman analysis disclosed the nature of deposited carbon over the catalyst surface and suggested a graphitic (carbon) free catalyst for the B(3)-Ni/MA catalyst compared to non-B Ni/MA catalyst due to higher values of I_D/I_G value that further verified by the XPS analysis of the spent catalysts. The retainment of B after the DRM was also revealed by XPS analysis of spent catalysts, which means B was successfully seated at the site that possessed difficulty for the resilient carbon to form over the surface. B inclusion into the catalyst matrix leads to enhancements in multiple aspects, including higher reduction, stabilizing the metallic state, activation of the reactants, and lower carbon deposition.

2. Recent studies also suggested the addition of second metal helps to improve the catalysts activities and prevent catalysts from deactivation. The optimized B (wt.%) was used to determine the effect of addition of second metal on B-Ni/MA catalyst. In this order, we have synthesized a series B-containing Ni-Co bimetallic catalysts, which offered a steady

conversion of CH_4 and CO_2 for the DRM with a reasonable H_2:CO ratio. The lattice spacing and the elemental distribution confirmed the presence of alloy Ni-Co and Ni-Co-B. Additionally, Rod-like Ni-Co alloy and Ni-Co-B species on the two-dimensional flakes of MA is observed. Ni-rich B-containing bimetallic [B-(75Ni-25Co)] catalyst exhibits better methane and carbon dioxide conversions compared to other prepared catalysts. The turnover frequency (CH_4) and produced syngas ratio of the B-catalyst are 1.5 and 1.04 times, respectively, higher than the non-B catalyst prepared by the traditional impregnation method with the same Ni:Co ratio. The catalyst [B-(75Ni-25Co)] exhibits higher activity and almost a steady conversion rate, while continuous decrement is observed for the non-B catalyst. Exceptionally low carbon deposition (~3.57 times) was observed for B-(75Ni-25Co)/MA than the non-B catalyst. The density functional theory (DFT) investigation also revealed the adsorption energy (E_{ads}) of carbon at various sites of 75Ni25Co significantly reduces by ~0.5eV in the presence of B, causing hindrance to the formation of carbon over the surface.

3. Above experimental studies revealed that the ~ 2.68 wt.% B-containing B-(75Ni-25Co)/MA catalyst prepared by one-step $NaBH_4$ reduction method was highly active for the DRM reactions. However, it was also observed that the catalysts were not completely reduced after the synthesis by the $NaBH_4$ reduction method. Hence the effect of further H_2-reduction of the B-(75Ni25Co)/MA catalyst is needed to be examined and compared with the as-prepared catalysts. The characterization of both catalysts revealed that further reduction improves metal dispersion and promotes allow Ni-Co type structure. The catalyst activity test was carried out in a fixed bed reactor (FBR) at the temperature of 600^0C and atmospheric pressure. Further reduction of the catalyst showed improvement in the initial conversion (CH_4= 25.45% & CO_2= 38.24%) as well as the ratio of H_2: CO compared to the as-prepared catalyst (CH_4= 22.56% & CO_2= 34.08%). However, the conversion decline was comparatively higher for the H_2-reduced catalyst than the as-prepared catalyst as the CH_4 cracking was higher for further reduced catalyst. The turnover frequency and conversion of reaction were nearly the same for both catalysts at TOS 24h. Most interestingly the reaction result reveals that the further reduction of catalyst improves the performance. However, the carbon deposition was similar for both as-prepared and further reduced catalysts.

4. A kinetic study for the non-B and B-containing bimetallic catalyst 75Ni25Co/MA catalysts

were also performed for the temperature range of 773-973 K. The concentration and rate of reaction was observed increased with temperature. However, the rate of reaction was comparatively higher for the B-containing catalyst compared to the non-B catalyst. Further, the calculated activation energy was almost similar for both B and non-B catalysts suggested. The spent catalysts were characterized by the ICP-OES and elemental analysis. The loss of metal (Ni and Co) was insignificant compared to the non-B catalysts. Interestingly, the retainment of B was observed in spent catalysts at all temperatures. The carbon deposition was extremely low ~5.8 times lesser than the non-B catalysts. In-depth study suggests that the presence of a small amount of B helps a catalyst to achieve good B-metal dispersion and stable metallic species. Finally, the present study provides a new strategy to perform carbon-free DRM with B-containing catalysts for the temperature range of 773-973K without compromising the activity.

From above research studies it appears that the adding B by the one-step $NaBH_4$ catalyst reduction method for the dry reforming of methane reaction. The catalyst preparation method using $NaBH_4$ appears to be the prime source of dispersing B on Ni-based catalyst and a straightforward way for reducing metal salts. The B(x)-Ni/MA catalysts enhanced the conversion of CH_4 and CO_2 and promoted graphitic free dry reforming of methane reaction. The maximum conversion was CH_4: 18.75% and CO_2: 30.61% for 3% B (wt%) containing B(3)-Ni/MA catalyst and the corresponding $TOF_{CH_4}$was 0.31 s^{-1} which is 2.61 times higher compared to non-B catalyst. Interestingly, the deposition of resilient graphitic carbon for the B catalyst was significantly lower (~11 times) than the non-B catalyst. It was found that the presence of B facilitated the formation of Ni-B species along with metallic Ni (reduced by $NaBH_4$), controlled the particle size and stabilized the metallic state, and influenced the Ni-C interaction leading to the advancement in catalytic performance and diminution in deactivation. Further the optimized B% was used to determine the effect of addition of second metal on B(3)-Ni/MA catalysts. In this order, we have developed a B (3 wt%) containing Ni-Co bimetallic catalyst, which offered a steady conversion of CH_4 and CO_2 for the DRM with a reasonable H_2:CO ratio. The lattice spacing and the elemental distribution confirmed the presence of Ni, Co and Ni-Co-B. The maximum TOF_{CH_4} and TOF_{CO_2} were found to be 0.299 and 0.480 s^{-1} respectively, using a catalyst containing 10.89 wt% of Ni, 3.71 wt% of Co, and 2.68 wt% of B to MA[(75Ni25Co-B)/MA] which were 1.50 and 1.17 times higher than the similar non-B (Traditional 75Ni25Co/MA) catalyst. Interestingly, the carbon deposition was found to be extremely low (~5 times lesser than the non-B) and of non-graphitic nature. B also helps in hindering the formation of carbon on the catalyst surface. The amount of deposited carbon was 0.039 g/g_{cat}^{-1} for the developed catalyst, while it was 0.106 g/g_{cat}^{-1} for the catalyst that does not contain B. Besides the importance of B inclusion, the study also realizes that a particular metallic ratio (Ni-Co =3:1) is also crucial for the supported bimetallic catalyst to achieve maximum activity and stability for DRM.

Chapter 1

Introduction and literature review

"The world is reaching the tipping point beyond which climate change may become irreversible. If this happens, we risk denying present and future generations the right to a healthy and sustainable planet – the whole of humanity stands to lose."

-Kofi Annan,

Former Secretary-General of United Nations

1.1 Motivation:

Global warming driven by greenhouse gas (GHG) emissions has been a primary reason for climate change, and it needs to address to avoid anthropogenic effects in the coming decades [1-4]. The temperature rises and increment of greenhouse gases (GHGs) observed alarming the situation as the global temperature increased by ~1.5 to 1.7°C, which is higher than ever [5, 6]. The United Nations framework convention conference (UNFCC) adopted the Paris agreement (December 2015) on climate change and instructed 196 countries to approach reducing GHGs emissions [7, 8]. The current approach is to achieve net-zero GHGs emissions that can upgrade the existing energy management system to emphasize the mitigation and utilization of GHGs. Several countries are making laws and policies, including government-private regulations, to limit GHG emissions through strict rules on zero-emission guidelines and emphasize to the scientists to find out a significant way to utilize the GHGs.

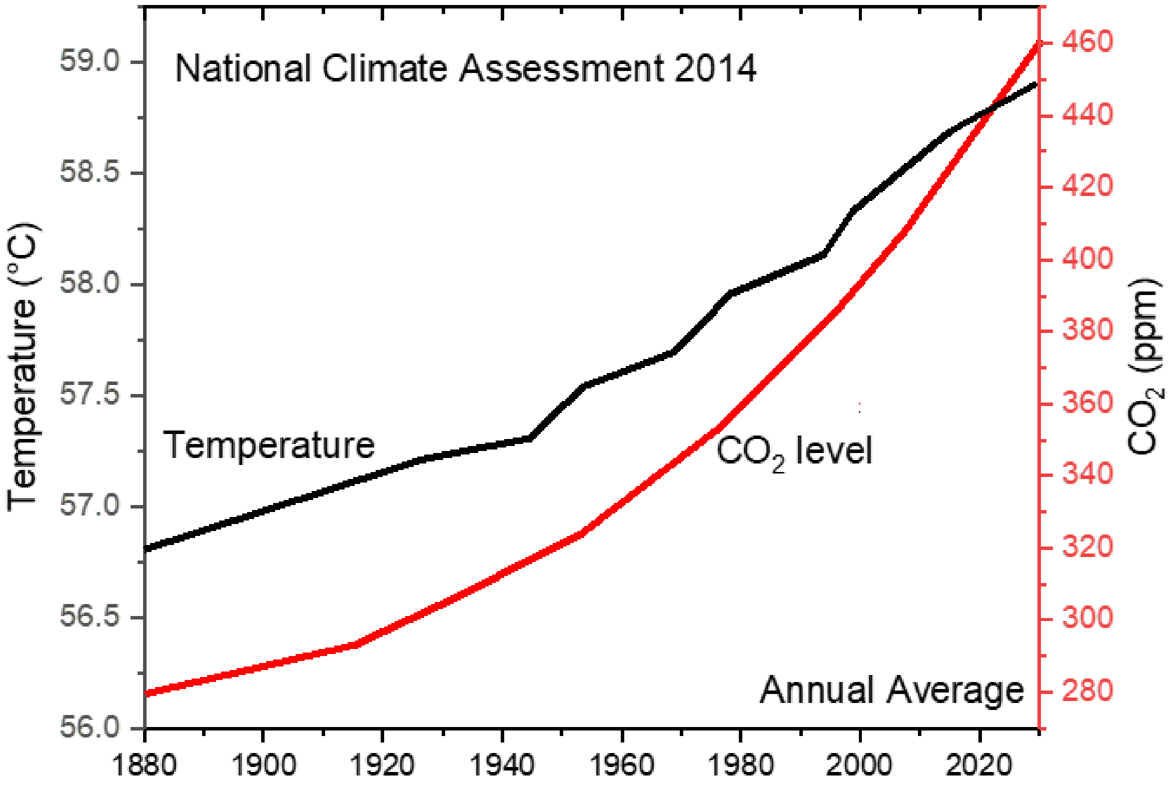

Figure 1.1. Temperature rise and CO_2 emission trend released by UN National Climate Assessment

1.2 Sources of greenhouse gases:

A recent survey by the US Environmental Protection Agency (USEPA) revealed that transportation, power, and industries are the major sectors of GHG emissions (Fig. 1.2) [9]. The burning of fossil fuels (mainly oil and gas) for the existing transportation system is the prime source of GHGs emissions, and concerning to find an alternative solution [10, 11]. Domestic and industrial electricity consumption are the other sources of GHGs emissions; to date, many approaches have been taken to control GHG emissions. Recently, carbon capture and utilization (CCU) techniques have been highly emphasized for the potential solutions to combat GHGs impacts on climate change and ocean acidification [3]. The Intergovernmental Panel on Climate Change (IPCC) also emphasized net-zero GHGs emissions must reach by 2050 and instructed participating countries to prepare and implement policies accordingly [4]. Since carbon dioxide (CO_2) accounts for 82% of the total GHGs, followed by methane (CH_4), showed in Fig. 1.3, the utilization of these two gases is the main challenge for researchers. There are various sources of GHGs emissions that lead to increased overall GHG effects reported in the EPA 2020 studies [9].

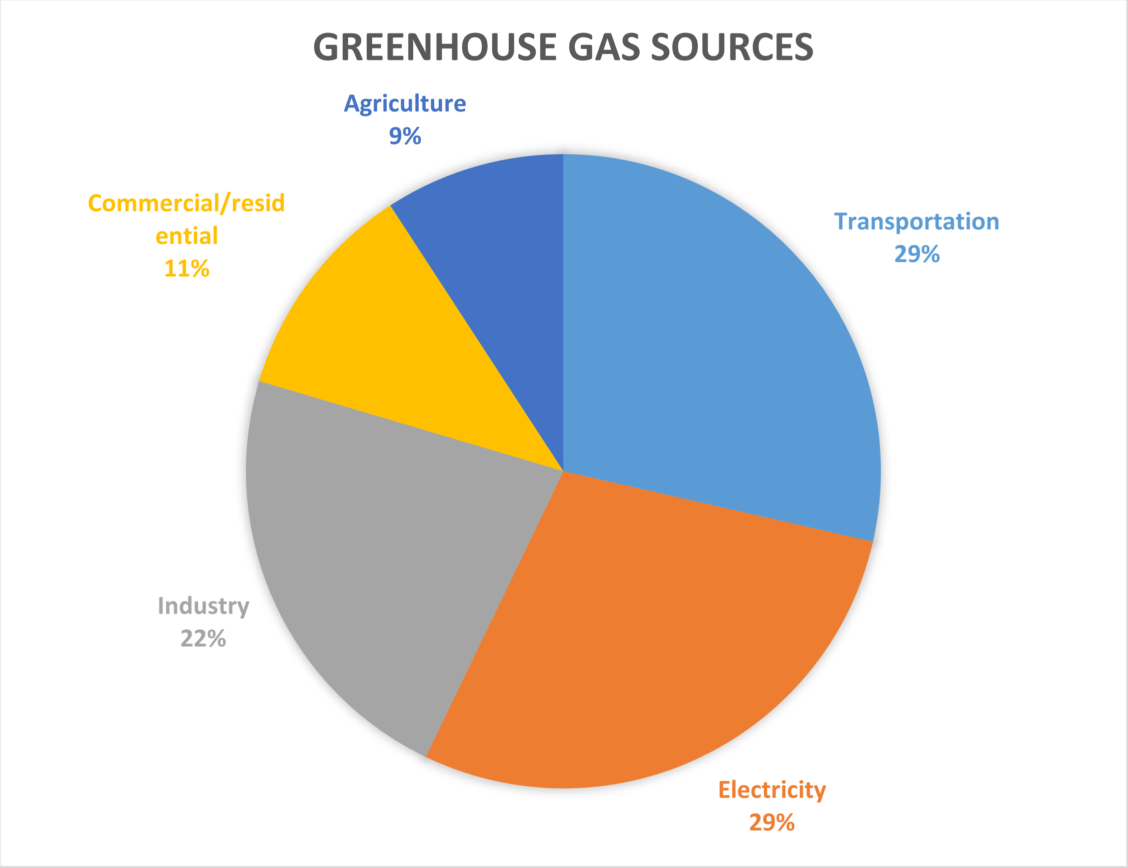

Figure 1.2. Sources of greenhouse gases emission

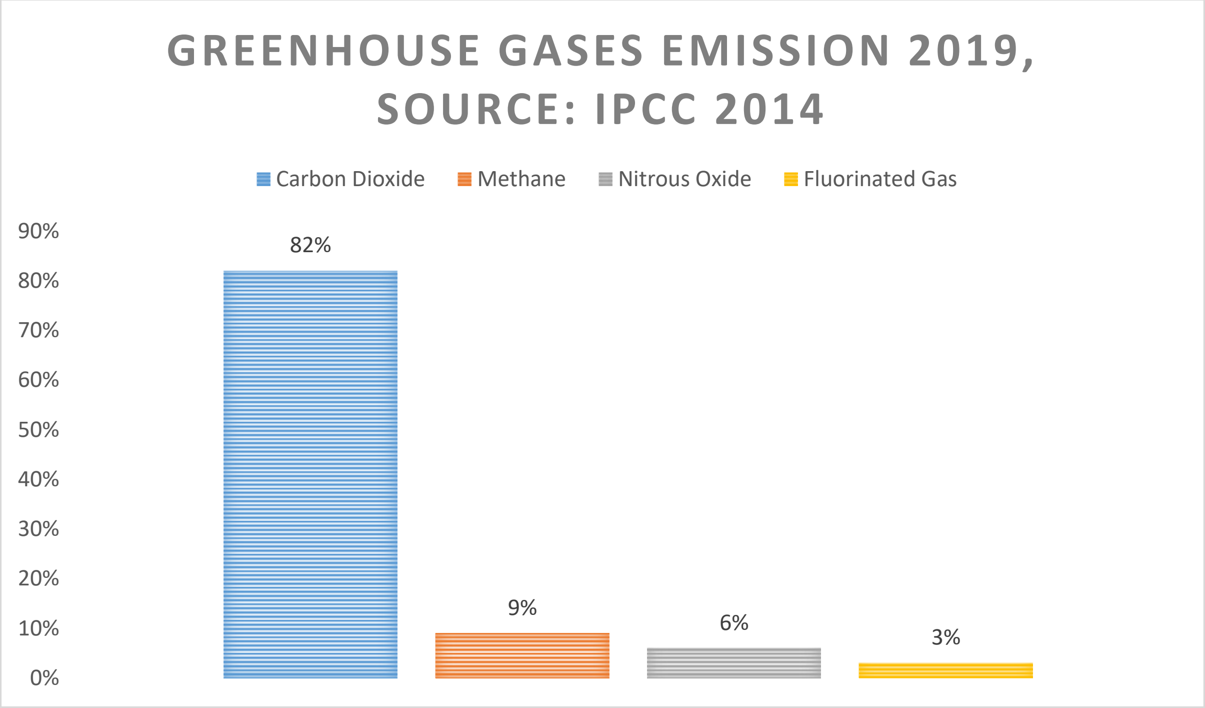

Figure 1.3. Greenhouse gases emission 2019, Source: IPCC 2014

1.2.1 Sources of carbon dioxide:

The rapid growth in the use of fossil fuels (oil, natural gas, and coal) and their burning are the primary source of CO_2 emission, showed in Fig. 1.4. The heavy dependence on petroleum and coals for meeting the current requirement of energy are the prime sources of CO_2 emission [12]. The other sources of CO_2 in the atmosphere are volcanic eruption, plant/animal respiration, soil respiration and decomposition, residential area, transportation, and industrialization are sources of adding CO_2 to the atmosphere. In 2016, 81.60 % of greenhouse gas emissions were reported in the US report, from which the CO2 emissions were 94% [12, 13]. The incineration sources of GHGs of fossil fuels from electricity, transportation, and industrial applications [12, 13]. Presently, several technologies have been commenced to detent CO_2 from combustion flue gases, which is responsible for reducing climate change. These technologies are adsorption, cryogenic distillation, absorption, and membrane separation. For controlling CO_2 emission, the most applied method is to inject and store the CO_2 in a geological formation. However, the major constraint of this method is the limitation of carbon storage for a long time. Chemical feedstock can be an alternative to ensure maximum carbon dioxide utilization.

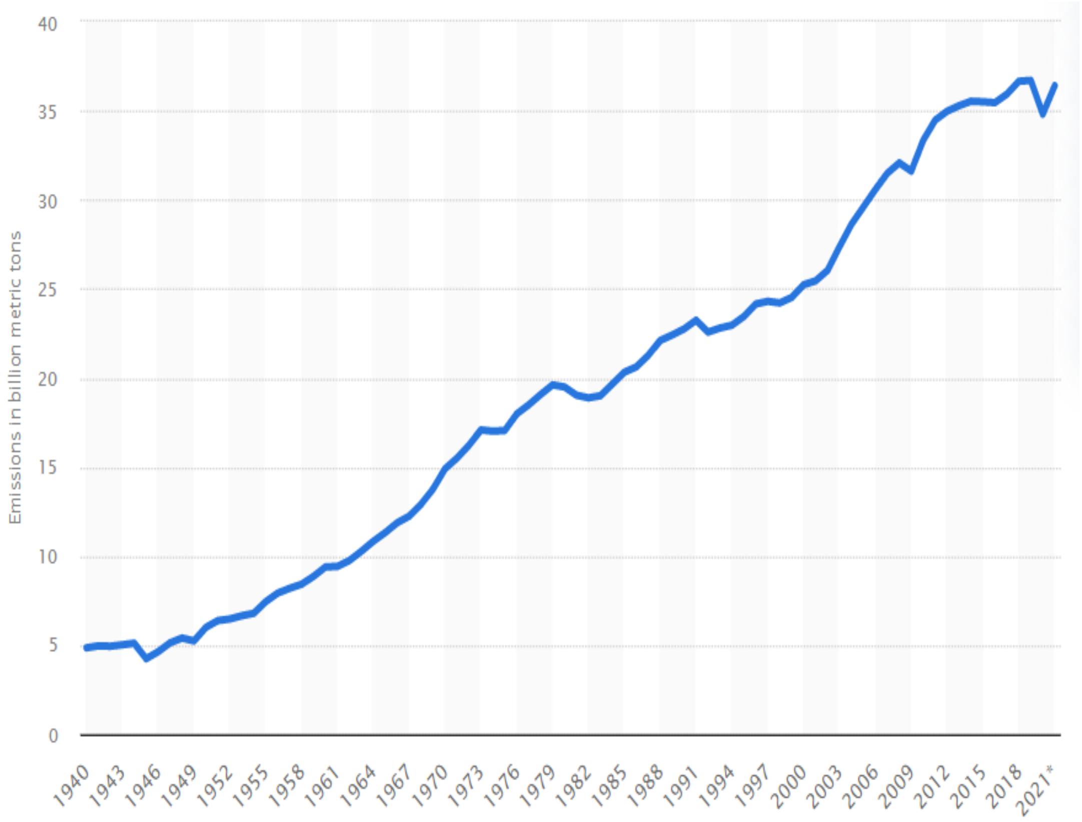

Figure 1.4. Annual global CO_2 emission reported by US council.

1.2.2 Source of methane:

The EPA report stated 11% of GHGs accountable to CH_4. However, the utilization of CH_4 is comparatively more straightforward than CO_2 utilization [14]. The EPA studies mentioned that 50-70% of total CH4 emissions come from human activities that are further classified as agriculture, industries (energy), land use, and household activities. Recently, the United States Center for strategic & international studies (US-CSIS) reported the abundance of CH_4 shown in Fig 1.5. Shale gas (mainly CH_4) is one of the unconventional natural gas recourse since its successful exploration in the US recently showed it to be the largest natural gas source. The sudden increase is shale gas production is mainly due to the projection supply of 40-50% by 2040 to the world market. Ultimately, the utilization of CO_2 and CH_4 becomes crucial to reduce the effects of GHGs.

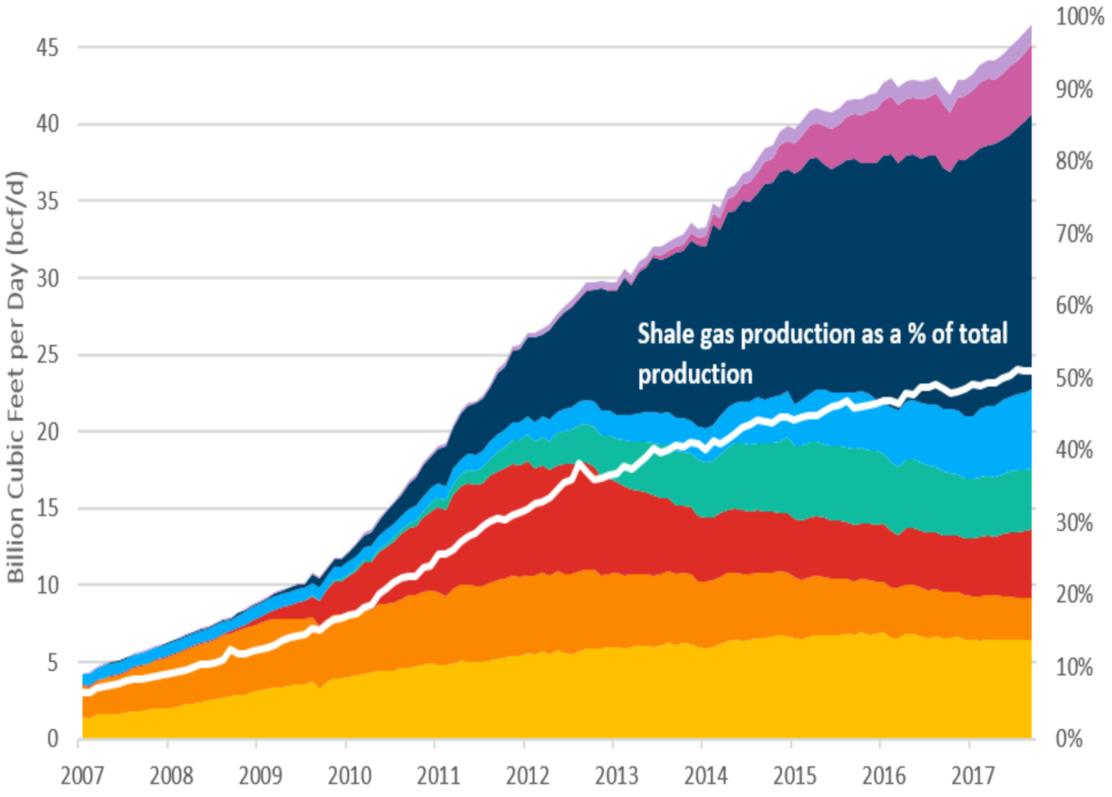

Figure 1.5. Production of global natural gases

1.3 Utilization of greenhouse gases:

There are three possible strategies to reduce CO_2 emissions, such as restricting the amount of CO_2 produced, storage of CO_2, and proper utilization of the emitted CO_2 [5]. Utilization of CO_2 is more promising because storage of captured CO_2 is still complicated. In recent years, the conversion of CO_2 into value-added chemicals has received significant attention as it can deal with several issues, such as the mitigation of CO_2 associated with the global warming problem, producing renewable energy resources, and energy storage issues [4-6]. Many approaches have been made to utilize GHGs by synthesizing fuels, such as gasification of CO_2, reforming reactions, and pyrolysis of CH_4. However, most processes suffer from the low net yield of the desired product and the low conversions of GHGs. The reforming reactions are most effective in utilizing methane; the whole process needs to consider methane to transform it into a valuable product. Fig. 1.6 represents the possible routes for converting methane into desirable products. However, the primary constraint is lowering the yield of the product; it is almost impossible for methane to limit-break the surface C-H bonds because the first bond is stronger than the C-H bond. The reason behind it is the low polarity of bonds. Consequently, every reforming process commercially depends on syngas to get higher-value products. Moreover, methane reactions can occur when it comes close to various oxidants based on fuel reforming while producing syngas. The prime goal of methane reforming is to get the desired final product by converting the syngas energy no matter the specific oxidant. Currently, reforming reactions has been widely used in industries. However, the temperature requirement of this reforming process is 800-900°C, and this reaction process is highly endothermic.

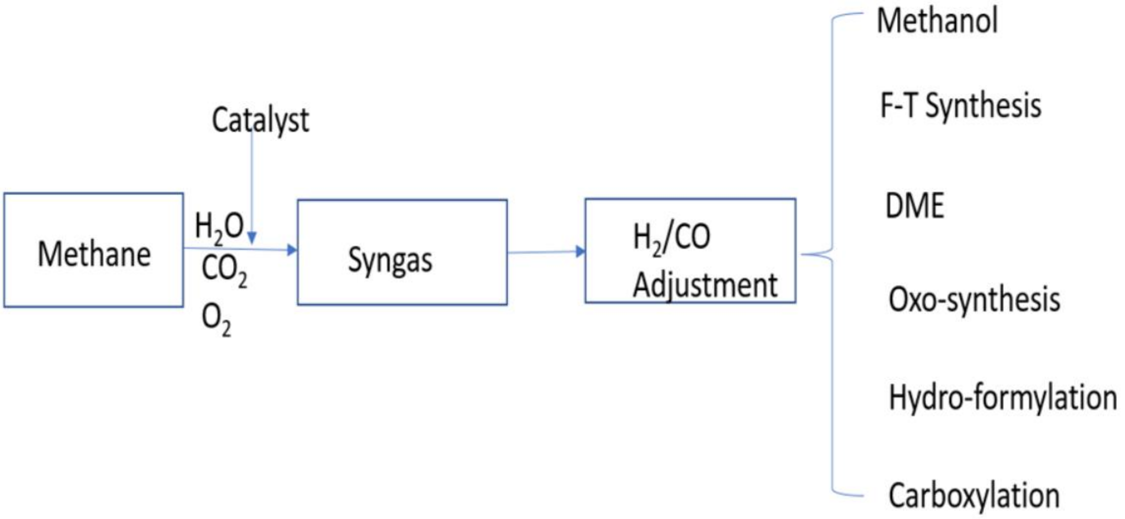

Figure 1.6. Possible routes for the utilization of methane

1.4 Reforming reaction:

The reforming reactions are widely used techniques for the production of hydrogen (H_2) and carbon monoxide (CO), commonly known as syngas [15-18]. The reforming reaction is the most economical, industrially acceptable, and straightforward process to produce syngas from GHGs CO_2 and methane [19-24]. Recently, the production of syngas has become so crucial in the energy sector as it helps chemical industries to synthesize fuel stocks such as methanol (CH_3OH), dimethyl ether (DME), hydroformylation, and promotes Fischer-Tropsch synthesis (FTS) (Fig 1.5) [25-28]. The most common reforming process are steam reforming of methane (SRM), partial oxidation of methane (POM), and dry reforming of methane (DRM).

1.4.1. Steam reforming of methane (SRM):

The SRM is a commercially acceptable and established method for syngas production [29]. It allows the utilization of CH_4 with the steam and is an endothermic reaction (Eq. 1.1) [30-33]. However, this process has some drawbacks as the produced syngas ratio by the SRM is higher (~3), which further needs an additional step to adjust the desired H_2:CO (ratio) ~1. The lower syngas ratio is highly preferable for the Fischer-Tropsch synthesis (FTS) for further production of methanol and other organic compounds such as dimethyl ether (DME). Moreover, the SRM method produces CO_2 through water gas shift reaction along with the H_2 and CO, which is against the zero-emission Paris agreement policy and leads to a significant issue in the petrochemical industry.

$$CH_4 + H_2O \leftrightarrow CO + 3H_2 \qquad \Delta H_{298k} = 206\ (kJ/mol) \qquad (1.1)$$

1.4.2. Partial oxidation of methane (POM):

The POM reaction is also an exothermic process to produce the syngas of ratio ~2 (Eq. 1.2). In the case of POM, the CH_4 reacts with O_2 to form syngas ratios ~2. The main drawback of POM reaction is the unstable nature of reaction formation due to the presence of O_2 and hot spots that make this process difficult to control.

$$CH_4 + 0.5O_2 \leftrightarrow CO + 2H_2 \qquad \Delta H_{298k} = -36\ (kJ/mol) \qquad (1.2)$$

1.4.3. Dry reforming of methane (DRM):

The DRM is an extensively investigated technique to convert the two GHGs into the syngas equation (1.3) [34-37]. Compared to other reforming processes, such as SRM and POM processes, the DRM produces a lower H_2/CO ratio suitable for further liquid fuel production, such as methanol and DME [38-41]. Moreover, the dry reforming process provides the use of biogas containing CH_4 (40–70%) and CO_2 (30-60%), a renewable resource produced by the anaerobic digestion of biomass [39-43]. Subsequently, syngas production is crucial for producing fossil fuels and chemicals *via* Fischer–Tropsch synthesis (FTS).

$$CH_4 + CO_2 \leftrightarrow 2CO + 2H_2 \qquad \Delta H_{298k} = 247\ (kJ/mol) \qquad (1.3)$$

The DRM has the potential to utilize both GHGs (CO_2 and CH_4) and produce valuable syngas with the desired ratio of ~1. However, it has an issue with commercialization mainly due to catalyst deactivation during the reaction. The DRM is endothermic and requires a high temperature that also favors side reactions, such as reverse water-gas shift (RWGS) (Eq. 1.4), the carbon forming reactions: methane decomposition reaction (Eq. 1.5) and the Boudouard reaction, also known as disproportion reaction (Eq. 1.6) [44, 45].

Reverse water-gas shift reactions

$$CO_2 + H_2 \leftrightarrow CO + H_2O \qquad \Delta H^{\circ}_{298} = 41\ (KJ/mol) \qquad (1.4)$$

Methane decomposition reaction

$$CH_4 \leftrightarrow C + 2H_2 \qquad \Delta H^{\circ}_{298} = 74.9\ (KJ/mol) \qquad (1.5)$$

Boudouard reaction

$$2CO \leftrightarrow C + CO_2 \qquad \Delta H^{\circ}_{298} = -172.4\ (KJ/mol) \qquad (1.6)$$

1.5 Applications of DRM:

The DRM appears as a most promising technique for the reduction of GHGs towards the syngas (Fig. 1.7). DRM also provides the use of biogas containing CH_4 (40–70%) and CO_2 (30-60%), a renewable resource produced by anaerobic digestion of biomass. Further, the process facilitates the desirable syngas ratio that is further beneficial for certain downstream processes. The syngas ratio 1 is suitable for FTS for producing valuable feedstocks such as methanol and DME.

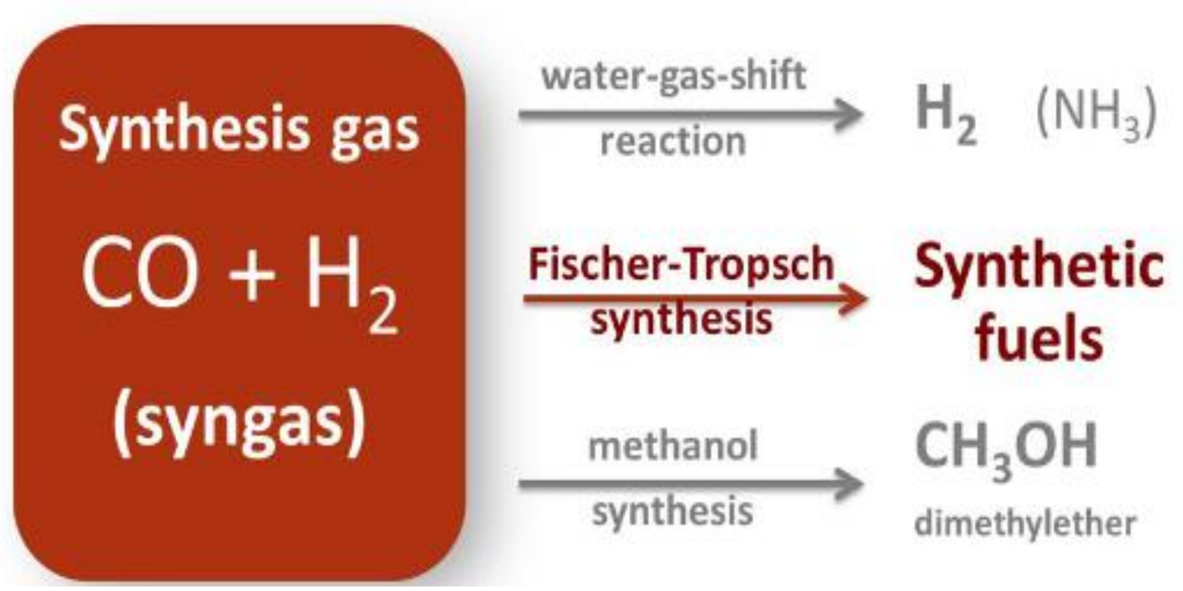

Figure 1.7. Application of DRM and uses of syngas

1.5.1 Fischer-Tropsch synthesis (FTS):

The FTS was developed by two known scientists Franz-Fischer and Hans-Tropsch in 1925. The lower ratio of syngas from the DRM reaction is the main feed for the FTS reaction. The FTS reaction is also called junction reaction as FTS used for further hydrogenation and synthesis of clean fuel such as DME and methanol (Eq. 1.7).

FTS reaction

$$nCO + (2n+1)H_2 \leftrightarrow C_nH_{2n+2} + H_2O \qquad \Delta H^{\circ}_{298} = -172.4\ (KJ/mol) \qquad (1.7)$$

1.5.2 Methanol production:

Methanol is one of the most versatile compounds developed, which can be used as a solvent and industrial feedstock to produce various chemicals (formaldehyde and acetic acid). Moreover, methanol is an efficient alternative fuel as it has lesser NO_x emission than gasoline without producing Sulphur containing compounds [7]. Thus it can be blended with gasoline or completely substituted as a transport fuel. Currently, methanol is produced from syngas on a large scale with several million tons per year capacity [8]. Syngas produced by DRM consists of H_2, CO_2, CO, and CH_4; some inert components are the main feed for methanol production [9–13].

1.5.3 Dimethyl ether (DME):

DME is one of the crucial and industrially accepted products of produced syngas by DRM reaction, as this can be helpful for the further production of lean gases such as dimethyl sulfate and olefins. Comparatively, DME is easier to handle and transport than other non-renewable fossil fuels [46]. As oil and coal resources deplete and the zero GHG emission policy has been implemented, the DME and methanol from syngas are the alternative solutions to meet the energy demand. Like methanol, the DME does not contain hazardous components such as NO_x and SO_x [47]. Hence, it can be summarized that the produced syngas from DRM has multiple applications in terms of clean gases and reduction of GHGs emissions.

1.6 DRM mechanism and carbon formation pathways:

DRM allows both CO2 and CH4 to react to produce syngas at higher temperatures with multiple decomposition and formation reactions. The possible reaction pathways for the DRM reaction based on reported work were observed and represented schematically in Fig 1.7. The CO_2 pathways are related to the deoxidation of the feed and convert it towards the CO and produce H_2 throughout the process. On the other hand, the CH_4 pathways for the DRM reactions are essential as the initial C1 chemistries related to CH_4, the initial C–H bond activation is a rate-limiting step for DRM and this pathway also promotes the Boudouard that further leads to the formation of carbon. As the carbon formation during the DRM deactivates the catalyst, many efforts have been made to overcome this issue to develop a carbon-free catalyst for DRM reaction. This carbon formation during the DRM further leads to the deactivation of the catalysts, which is the most challenging task for researchers.

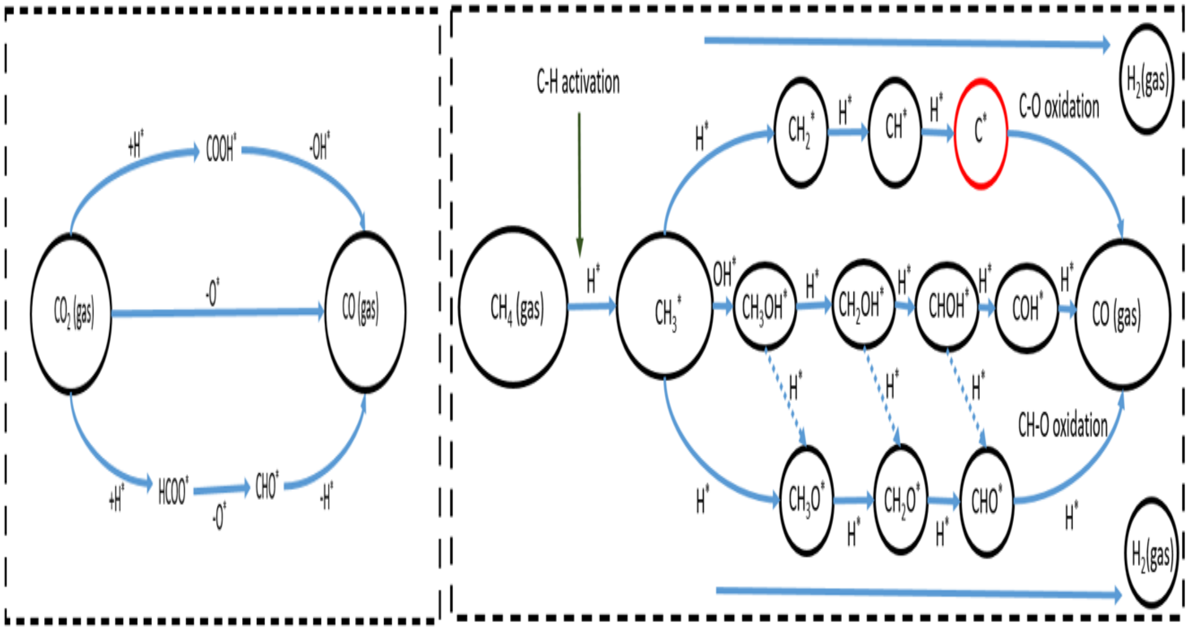

Figure 1.8. Reaction mechanism for DRM reaction (a) pathway of CO_2 conversion towards the CO and H_2 (b) pathway of CH_4 conversion to the CO and H_2 and possible steps of C formation.

1.7 Definition of the problems:

From above, it appears that the DRM reaction is a promising way to utilize GHGs to produce syngas. However, the carbon deposition during the DRM reaction is the prime concern for its industrial implementation. In the last few decades, researchers have made several efforts to overcome catalyst deactivation and suggested designing such catalysts that can be active for a long time for commercial use. In this order, the synthesis of catalysts becomes essential, such as the method of preparation of catalysts, quantitative and qualitative analysis of support and metal used, and selection of additional promotors that can be helpful to prevent catalysts from deactivation. A series of previous studies have suggested that noble metals are highly active and resistant to the deactivation of catalysts for DRM. However, due to limited availability and high cost, most studies suggested using transition metals [33, 43, 48-50]. Among transition metals, Ni-based supported catalysts attracted considerable attention mainly due to their availability, being economical, and high reforming activity [53, 54].

Nonetheless, Ni-based catalysts suffer from deactivation due to the carbon deposition due to the CH_4 decomposition (Fig 1.8) that occurs above ~557°C and Boudouard reaction below ~700°C. Hence, the reaction temperature of 600°C appeared suitable to examine the testing catalyst for DRM. Further, the feed ratio plays a vital role in product selectivity. Recent studies suggested that the feed ratio is a severe condition for the analysis of the catalyst's performance, as a lower reactant ratio (<1) limits the RWGS reaction, and a higher reactant ratio (>1) lowers the H_2 production [116]. Hence, from the above discussion, it appears that a reaction temperature of 600°C and feed ratio is the recommended catalysts evaluation condition.

1.8 Catalysts for DRM:

The DRM reaction appears to be the most suitable method to produce syngas with a ratio of unity, which can be further used to produce the liquid hydrocarbons by the FTS [34, 40]. Besides, the DRM process is an economically and environmentally preferable method compared to other reforming processes as it utilizes two major greenhouse gases, methane (CH_4) and carbon dioxide (CO_2) [21, 25, 28, 55-58]. However, DRM is a highly endothermic reaction cause suffers from various challenges, such as carbon deposition over the catalyst and metal sintering at the high reaction temperature that causes catalyst deactivation [37, 59]. Many approaches have been made to overcome the deactivation of catalysts and design such catalysts that can be highly stable and active during the DRM reactions. On that aspect, a series of recent studies have indicated that noble metals such as Ru, Rh, Pd, and Pt-based catalysts are highly active and resistant to the deactivation of catalysts [60-63]. However, the expensiveness and limited availability of the noble metals the research required with non-noble metals such as transition metals [33, 43, 50]. Among transition metals, Ni-based supported catalysts attracted considerable interest mainly due to their availability, economic, and good reforming activity [51, 52]. Among transition metals, Ni-based supported catalysts attracted considerable attention mainly due to their availability, being economical, and high reforming activity [53, 54].

1.8.1 Nickel-based catalysts:

The Ni-based catalysts are widely used in industries for hydrogenation, methanation, reforming, and hydrocracking processes. A series of previous studies have demonstrated that metal-support interactions can occur in the case of impregnated supported metal catalyst systems [64-66]. Recently, Raupp et al.[67] proposed that supports such as alumina can migrate onto the metal surface and exist there as large crystallites. Yining et al. [68] reported that Ni-based catalysts are highly dispersed on support resulting formation of surface spinel species in octahedral sites. However, larger particle size, low performance, and early deactivation of catalysts were also reported. Hence, the synthesis of Ni-based supported catalysts become essential attributes in terms of activity, stability, and selectivity. There have been some important parameters such as catalyst support, catalyst preparation method, metallic state of the catalyst, and additional promoters that enhance the catalyst performance, so it is crucial to select the catalysts and preparation method for their lifetime use [37, 40]. In order to synthesis suitable catalysts for DRM, a detailed literature survey has been done on the nickel-based catalysts with different types of support in Table. 1.1 focuses on the preparation method, metal loading percent, temperature, and catalyst amount used to measure methane and carbon dioxide activity.

1.8.2 Influence of support:

Supported catalysts constitute an important class of catalytic systems not only because of their direct impact on the chemical industry but also for the variety of reactions they are able to promote. Examples of nickel-based catalysts with different types of supports are listed in Table. 1.1. Among the supported heterogeneous catalysts listed, Al_2O_3-supported nickel catalysts appear to be traditional catalytic support for DRM [18, 37, 41, 43, 69-77]. Hao et al. [70] prepared Ni/Al_2O_3 catalysts by the incipient impregnation (IWI) method and reported the CO_2 and CH_4 conversion was about 63 and 69%, respectively, at 800°C and GHSV of 45000 h^{-1}. However, the poor stability of γ-Al_2O_3 at higher temperatures was reported [37, 69]. The oxide support shows better performance compared to the traditional Al_2O_3 support showed attractive performance for DRM with Ni catalyst [54, 78-80]. Hale et al. [98] showed that a cerium oxide-supported catalyst gave 75 and 79 % conversion of CH_4 and CO_2 at 700°C. Fazal et al. [78] showed low conversion at the same temperature for zirconium oxide-supported catalysts (Table. 1.1). Zhang et al. [22] and Chatla et al. [81] reported Mg-based supported catalysts to have strong metal-support interaction (SMSI) compared to CeO_2, ZrO_2, SiO and TiO_2. Further, the supports with oxygen storage capacity (OSC) have proven significantly enhanced in the reduction of carbon formation, particularly ceria-based (CeO_2 and $Ce_xZr_{(1-X)}O_2$) and magnesium-based oxide-supported catalysts [20, 27, 28, 73, 83]. However, mixed ceria-zirconia oxide showed high conversion at 600° C, indicating mixed oxide-supported catalysts may be used to improve the performance of the catalyst further and prevent early deactivation. Khajenoori et al. [84] performed DRM with MgO-supported Ni-based catalysts and observed that MgO support improves the catalyst activity and improves the overall performance of catalysts compared to traditional support. Researchers also suggested that magnesium aluminate spinel (MA) as a promising support for Ni-based catalysts with good thermal shocking resistance ability and high melting temperature (2135°C) [25, 37]. Recently, Hadian et al. [9] suggested that the MA-supported catalyst shows a low deactivation rate of catalyst as well as a stable conversion of CH_4 & CO_2 at low temperature(550°C) due to its good refractoriness, low acidity, high mechanical strength, and excellent thermal shocking resistance.

Table 1.1. Effect of support on Ni-based catalyst for DRM.

Source	**Metal**	**Support**	**Reaction Condition**		**Conversion (%)**		**Main findings**
			T (℃)	**GHSV (h^{-1})**	**CH_4**	**CO_2**	
Hao et al. [70]	Ni	Al_2O_3	800	45000	63	69	The conversion increases with temperature. However Significant decline in conversion was observed with TOS
Khajenoori et al. [84]	Ni	MgO	700	-	35.5	64	It is clearly observed that MgO support improves the catalyst activity
Jing et al. [85]	Ni	MgO-SiO	700	60000	58	-	The addition of SiO_2 Improves the catalyst performance as well as the deactivation resistance capability
Rouibah et al. [86]	Ni	ZrO_2	700	300000	43.2	50.6	Nickel with zirconium oxide shows lower conversion cerium support; however, the oxygenated support improves the catalyst stability compared to traditional support.

Shin et al. [87]	Ni	ZrO_2-Al_2O_3	700	25000	37.8	50.1	Ni-based zirconia alumina-supported catalyst shows lower conversion compared to solely zirconium-based catalysts.
Wolfbeisser et al. [52]	Ni	CeO_2-ZrO_2	600	60000	52	72	Nickel with cerium-zirconium mixed oxide shows high conversion compared to the CeO_2-supported catalyst
Elsayed at al. [15]	Ni	$Ce_{0.6}Zr_{0.4}O_2$	300	68000	10	10	60% CeO_2 and 40% ZrO_2 appear to be the feasible ratio for Ce, and Zr mixed supported catalyst.
Hadian et al. [17]	Ni	MA	550	300000	22	20	Ni-based MA-supported catalyst shows lower deactivation
Rashmi et al. [37]	Ni	MA	600	300000	14.1	16.8	The performance of MA supported catalyst appears more effective than the Ni/Al_2O_3 catalyst.

1.8.3 Addition of second metal:

Ni-based catalysts also suffer from catalyst deactivation due to carbon deposition [17, 37]. It has always been suggested the addition of the second metal enhances the catalytic activity by lowering the carbon deposition [37, 88-90]. Bimetallic catalysts perform better than monometallic catalysts mainly due to their surface composition, electronic configuration, and interaction support-metal bonding [70-72]. Beneficial effects of the Ni-based bimetallic catalysts with noble metals like Pt, Rh, and Ru were reported [69, 72, 74, 91, 92]. Toey et al. [97] reported that the addition of 1% Pt with the Ni-based catalyst enhances the catalyst activity by 1.66 times that of monometallic catalysts. However, it has also been reported that the addition of noble metals is not effective as it has limited availability and expansiveness. In this regard, the transitional metal is preferable from an economic perspective. Cobalt (Co) has recently attracted much attention among transition metals [37, 93, 94]. It has also been reported Ni-Co bimetallic catalyst shows better metal dispersion and strong metal-support interaction to prevent carbon deposition [37, 39, 95]. Rouibah et al. [86] reported that the Ni-Co bimetallic catalyst shows better conversion compared to the monometallic catalyst in terms of catalyst dispersion and activity for DRM. Hale et al. [98] also reported that the addition of second metal enhances the catalyst performance compared to the monometallic catalysts. Chang et al. [96] prepared Ni-Ca /$CeZrO_2$ catalysts using molten salt and concluded that the addition of a small amount of Ca increases the catalyst performance by a few folds compared to Ni-based catalysts. Recently, Rashmi et al. [37] studied the effect of second metal on this Ni-based catalyst and reported a small amount of Co improves the catalyst performance by 1.8 times compared to the Ni catalyst and decreases the deactivation of the catalyst by 1.05 times (Table. 1.2). The performance of Ni-Co catalyst mainly depends on the metallic ratio of the supported catalysts.

Table 1.2. Effect of bi-metallic catalyst for DRM.

Source	**Metal loading (%)**	**Type of catalyst**	**Preparation method**	**Reaction Condition**		**Conversion (%)**		**Main findings**
				T (℃)	**GHSV (h^{-1})**	**CH_4**	**CO_2**	
Sengupta et al. [41]	15	Ni-Co/Al_2O_3	IWI	600	30000	23	39	The addition of Co on Ni-based Al_2O_3 supported catalyst enhanced the conversion and lowered the deactivation rate of the catalyst compared to monometallic catalyst.
Rouibah et al. [86]	-	Ni-Co/MgO	CP	700		28	42	Ni-Co bimetallic catalyst shows better conversion compared to the monometallic catalyst
Chang et al. [96]	5	Ni-Ca /$CeZrO_2$	Molten salt	700	60000	72	79	The addition of a small amount of Ca increases the catalyst performance by a few folds compared to Ni-based catalysts.
Toey et al. [97]	6	Ni-Pt /Al_2O_3	ALD	600	-	30	-	The addition of (1%) Pt increases the catalyst activity and enhances the catalyst deactivation

								compared to the monometallic Ni/Al_2O_3 catalyst.
Hale et al. [98]	8	Ni-Co/ CeO_2	IWI	700	-	75	79	The bimetallic catalyst enhances the catalyst performance for oxide-supported catalysts compared to traditionally supported catalysts.
Rashmi et al. [37]	15	Ni-Co/ MA	IWI	600	300000	19.65	20.86	The Ni-Co catalyst with 3:1 improves the catalyst performance by 1.8 times compared to the Ni catalysts

IWI = Incipient wetness impregnation
ALD= Atomic layer deposition
CP= Co-precipitation

1.9 Catalyst preparation:

The preparation of catalysts material includes various spectrums of the preparation methods such as impregnation, precipitation, sol-gel, and chemical assist method [2]. The preparation of supported catalysts material includes a broad spectrum of methods, such as impregnation, deposition, ion exchange, and precipitation [101]. Preparation technology is never known for sure as they are being used in industry because of proprietary reasons. Hence, general procedures commonly used will be illustrated. The incipient impregnation method is one most common methods for the preparation of heterogeneous catalysts. The amount of water has been calculated to impregnate the metal-support solution according to the required water for the pores of support and the water already involved in the salt precursor. A well-mixed metal support interaction formed after a complete impregnation in the desired amount of water. However, the big particle size of the catalyst was also reported for the catalyst prepared by the impregnation method. Additionally, the calcination and high-temperature reduction of the catalysts in the H_2 environment are required for the activation of the metal sites. In the context, many approaches have been made to prepare catalysts using different techniques to form an extremely small size and highly metal-dispersed catalyst. Recently one-step studies showed a more impressive and remarkable outcome in catalyst activity and cost by reducing the calcination and reduction steps. The B-based chemical reduction method employs chemical hydrides such as $NaBH_4$, KBH_4, and NH_3BH_3, which is considered a novel approach for the DRM. Recently, Jing et al. [13] proposed that the B-treated Ni catalyst improved the coking resistance capacity mainly due to similar chemisorption of B and carbon on the Ni catalyst. Fouskas et al. [14] suggested that B atoms can effectively block carbon diffusion into nickel lattice, mainly by occupying the subsurface site of the first surface layer. Takanabe et al. [15] reported that the B-based catalyst synthesis process showed a significant increase in the conversion of CH_4 & CO_2 and a very low deactivation rate of the catalyst compared to traditional methods. Among them, $NaBH_4$ is non-toxic, stable, and non-combustible, appeared to be a potential compound for the synthesis of heterogeneous catalysts. This method is simple and often provides better dispersion of the metal on the support and does not generate any waste [16–18].

1.10 Introduction of boron:

Several efforts have addressed the deactivation of Ni-based catalysts because of graphitic carbon formed over the surface during the DRM, which eventually blocks the active sites of the metals [102, 103]. However, the first principal studies suggested that the activity of Ni-based catalysts can be enhanced by the addition of a small amount of boron [103-105]. Xu et al. [102, 104] described that the addition of B on the metal surfaces helps enhance the catalytic activity and promotes low catalyst deactivation during the reaction as B exhibits similar chemisorption over the Ni surface. Aggelos et al. [105] prepared a B-containing (Ni/ γ-Al_2O_3) catalyst using H_3BO_3 by calcination followed by reduction and showed low carbon formation compared to the non-B catalyst.

There have been many efforts made to suppress the deactivation of Ni-based catalysts listed in Table 1.3. The first principle studies using density function theory (DFT) by Jing Xu et al. [106] suggested the promotion of B over the Ni surface can reduce the deactivation rate by six times than the without B catalysts. The reason behind this coking resistance capacity improvement is due to similar chemisorption of B and carbon particles over the Ni surface. Chen et al. [108] performed experimental partial oxidation of methane reaction with B modified Ni-Al_2O_3 catalyst and suggested B reduces the deactivation of the catalyst by 3-fold due to the active site of the Ni. DFT work by kong et al. [110] concluded a similar conclusion as Jing et al. [102] that the Ni surface can reduce the deactivation rate by six times more than the unpromoted Ni. In addition to that, Saeys et al. [106] reported in their first principle study that the B promotion is effective for Ni-based catalysts. An experimental work by Fouskas et al. [103] also reported the significantly smaller size of Ni particle obtained by the addition of B, which further helps to enhance the activity of the catalyst and suppress the carbon deposition. Eva et al. [77] used Co/Al_2O_3 by using H_3BO_3 as the B source to perform propane decomposition reaction and observed the addition of a small amount of catalyst improved the catalyst deactivation rate, which is the most important aspect in order to commercialize the catalyst.

Table 1.3. Effect of B on deactivation of the catalyst

Author	Catalyst	B-Source	Process to used	Remark
Mark et al. [106]	Co-B	-	DFT	B promotion reduced the deactivation rate by six times
Jing et al. [106]	Ni-B	-	DFT	B occupy Ni sub-surface sited to prevent deactivation
Chen et al. [108]	Ni-B/ Al_2O_3	KBH_4	POM	Improved carbon resistance capacity of the catalyst by the addition of B
Jing et al. [105]	Ni-B/ Al_2O_3	H_3BO_3	SRM	B reduced the deactivation of the catalyst
Mark et al. [109]	Co-B/Al_2O_3	H_3BO_3	FTS	B and C display similar binding energy over the Co. Experimentally achieved B reduces deactivation rate by 6-fold compared to without B promotion
Kong et al. [110]	Co-B	DFT	FTS	B promotion reduced the deactivation rate by six times
Fouskas et al. [103]	Ni/Al_2O_3	H_3BO_4	DRM	B reduced the size and deactivation rate
Aly et al. [61]	Pt-B/Al_2O_3	H_3BO_4	DFT and Dehydrogenation of propane	The addition of 3 wt % of B decreases deposited carbon of carbon by 3-fold
Eva et al. [77]	Co/Al_2O_3	H_3BO_4	Propane decomposition	The addition of a small amount of B helps to reduce the deactivation of the catalyst.

DFT = Density function theory
POM = Partial oxidation of methane
FTS = Fischer-Tropsch synthesis

1.11 Research objective:

From the above, it appears that the deactivation of the catalyst is a major issue for the DRM. Although the noble metals-based catalysts reported a highly active and low sensitive but their high cost and have limited-availability increased interest in transition metals. Among the transition metals, Ni-based catalysts are the most preferable and frequently used at an industrial scale. The bimetallic catalyst improves the performance of the catalysts in terms of dispersion, active sites of metals, and activity of the catalysts. Several studies also suggested the formation of graphitic carbon for bimetallic catalysts during DRM, which deactivates the catalysts. In this regard, the B-modified catalysts showed impressive results. Hence, the objectives of this thesis are as follows.

1. Develop suitable Ni-based catalysts which can improve the catalyst performance and the coking resistance capacity.
2. Experimental validation of the first-principles DFT studies suggested that the activity and stability of Ni-based catalysts can be enhanced by the addition of a small amount of boron (B) [106-107].
3. The optimization B amount for the Ni-based catalysts by using $NaBH_4$ as a source of B and monitoring the metal reduction behavior by adding $NaBH_4$ solution.
4. The optimized B amount was further implemented for the bi-metallic catalysts and compared with the monometallic and traditional synthesized catalysts.
5. The effect of further H_2-reduction of optimized catalysts needs to be studied to evaluate the change in structural, compositional, and performance.

1.12 Summary:

From the above extensive literature survey, it appears that the development of Ni catalyst for dry reforming is a crucial step to produce syngas by the utilization of greenhouse gases (CO_2 and CH_4). Support for the DRM catalyst plays and important role in the synthesis of syngas as it directly impacts the dispersion of metal, refractoriness, and the thermal shocking resistance ability, especially for the higher reaction temperature. Many investigators have worked on the Ni-based catalyst and focused on the support and promoters to improve catalyst activity for DRM. The catalyst support constitutes a vital role in enhancing their catalytic performance [37, 40]. Traditionally γ-Al_2O_3 has been used as the support of Ni-based catalyst for DRM reaction; however, the poor stability of γ-Al_2O_3 support at the higher temperature was reported [37, 69]. Researchers found magnesium aluminate spinel (MA) is a promising support for Ni-based catalysts as it showed a good thermal shocking resistance ability and high melting temperature (2135°C). The MA-supported Ni-based catalyst reported a low deactivation rate and a stable conversion of CH_4 & CO_2 due to its good refractoriness, low acidity, high mechanical strength, and excellent thermal shocking resistance [16, 17, 45, 99]. A recent study reported a comparative study of supported traditional (Ni/γ-Al_2O_3) catalysts with Ni/MA for DRM and reported Ni/MA to be more active and stable [37].

The addition of a second metal and modifying the support can help the catalyst improve its performance in terms of metal dispersion, active sites, conversion, and prevention from early deactivation. In this regard, Co appears to be one of the promising second metals for Ni-based catalysts as the suggested noble metals are extensive and limited available. However, the performance of Ni-Co bimetallic catalyst mainly depends on the ratio of the metallic components, which often changes with the catalyst modification, preparation method, treatment procedures, and reaction condition that need to be investigated thoroughly [37, 100]. Unfortunately, the catalyst deactivation due to the deposition of carbonaceous material on the catalyst surface is still the most challenging issue for the DRM as it forms resilient graphitic carbon, which occupies the metal active surface sites. Table. 1.3 suggested B-modified catalysts show impressive results. A series of DFT works reported enhancement of catalyst activity by the addition of a small amount of B over the surfaces of the catalyst. However, experimental validation of B-containing catalysts for reforming reactions is yet to be verified.

Chapter 2

Experimental

2.1 Catalysts preparation:

2.1.1 Support preparation:

Many approaches have been made for the preparation of support magnesium aluminate (MA). Among the existing preparation method, such as co-precipitation, solgel, and high-temperature calcination method, the MA preparation by high-temperature calcination appears to be the easiest and most affordable method suggested in previous studies [33, 37]. Recently, Katheria et al. [33] suggested the preparation of MA by the calcination of MG30, Sasol, Germany) $Mg_{2x}Al_2(OH)_{4X+4}CO_3.nH_2O$ (Aluminum magnesium hydroxy carbonate) MG30 powder at 900˚C for 4h. Kumari et al. [37] also suggested the same method of preparation. Hence, the support MA was prepared by the calcining aluminum magnesium hydroxy carbonate at 900˚C for 4h with a heating rate of 10˚C/min [33, 37, 114].

2.1.2 Catalyst preparation by the traditional method:

The incipient wetness impregnation (IWI) method appears to be traditional catalysts preparation method for the dry reforming of methane (DRM) process. Initially, the required amount of $Ni(NO_3)_2.6H_2O$ (Sigma Aldrich, Australia, purity >99.99%) and $Co(NO_3)_2.6H_2O$ (Sigma Aldrich, Australia, purity >99.99%) was impregnated with pre-synthesized support (Table 2.1). The impregnated paste was dried in an oven, followed by gradual calcination up to 500°C to generate the supported metal oxide species. Before the reaction, this catalyst was reduced at 600°C with 10% H_2 in the reactor itself.

Table 2.1. Amount of metal and support required for the preparation of catalysts.

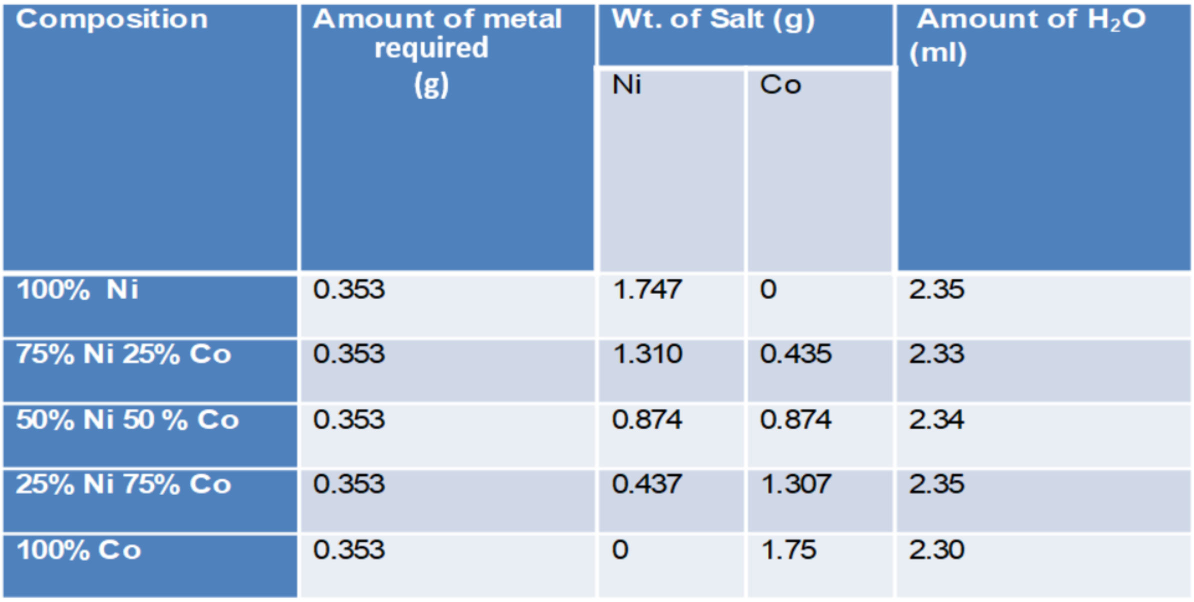

Composition	Amount of metal required (g)	Wt. of Salt (g)		Amount of H_2O (ml)
		Ni	Co	
100% Ni	0.353	1.747	0	2.35
75% Ni 25% Co	0.353	1.310	0.435	2.33
50% Ni 50 % Co	0.353	0.874	0.874	2.34
25% Ni 75% Co	0.353	0.437	1.307	2.35
100% Co	0.353	0	1.75	2.30

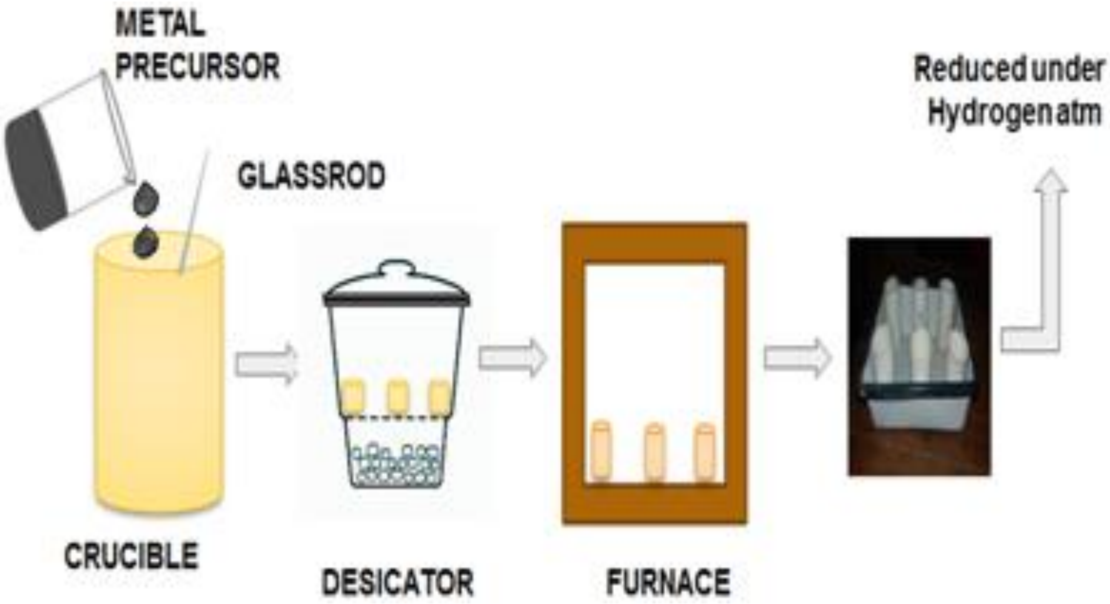

Figure 2.1. Schematic representation of the Ni and/or Co catalysts by the traditional IWI catalysts preparation method.

2.1.3 Catalyst preparation by $NaBH_4$ reduction method:

The B-containing monometallic Ni, Co, and bimetallic Ni-Co over MA-supported catalysts were prepared by the $NaBH_4$ reduction method. $NaBH_4$ is used here with the aim of two reasons; first, for the reduction of metal (MO to M^0) as $NaBH_4$ is a highly reducing agent, and for the doping of B over the catalyst's surfaces. For the preparation of catalysts by $NaBH_4$ reduction method, the calculated amount of support MA was dissolved in the water followed to the addition of metals salt precursor [$Ni(NO_3)_2.6H_2O$ (Sigma Aldrich, Australia, purity >99.99%) and $Co(NO_3)_2.6H_2O$ (Sigma Aldrich, Australia, purity >99.99%)] continues stirring. The color of the metal-support solution changes according to the concentration of $Ni(NO_3)_2.6H_2O$ and/or $Co(NO_3)_2.6H_2O$. The metal-support solution was then put in the ultrasonic bath for 30 min to get a well-mixed solution. Meanwhile, a $NaBH_4$ solution was prepared with the help of 10 mL ethanol and 10 mL deionized water. 0.250 g of $NaBH_4$ was added to the ethanol-water solution, which was immediately transferred to the well-mixed metal-support solution with continuous stirring (300 rpm and 40°C) [113, 114]. A color change of all catalysts was observed, which turned dark black color due to the reduction of metal due to the liberated H_2 from the $NaBH_4$ solution (Fig. 2.2). As a result of this synthesis process, a well-mixed product was formed, which was filtered, and the collected cake was dried in a vacuum oven at 60^o C for 12 h and then used as the catalyst for DRM without any further calcination and H_2-reduction steps.

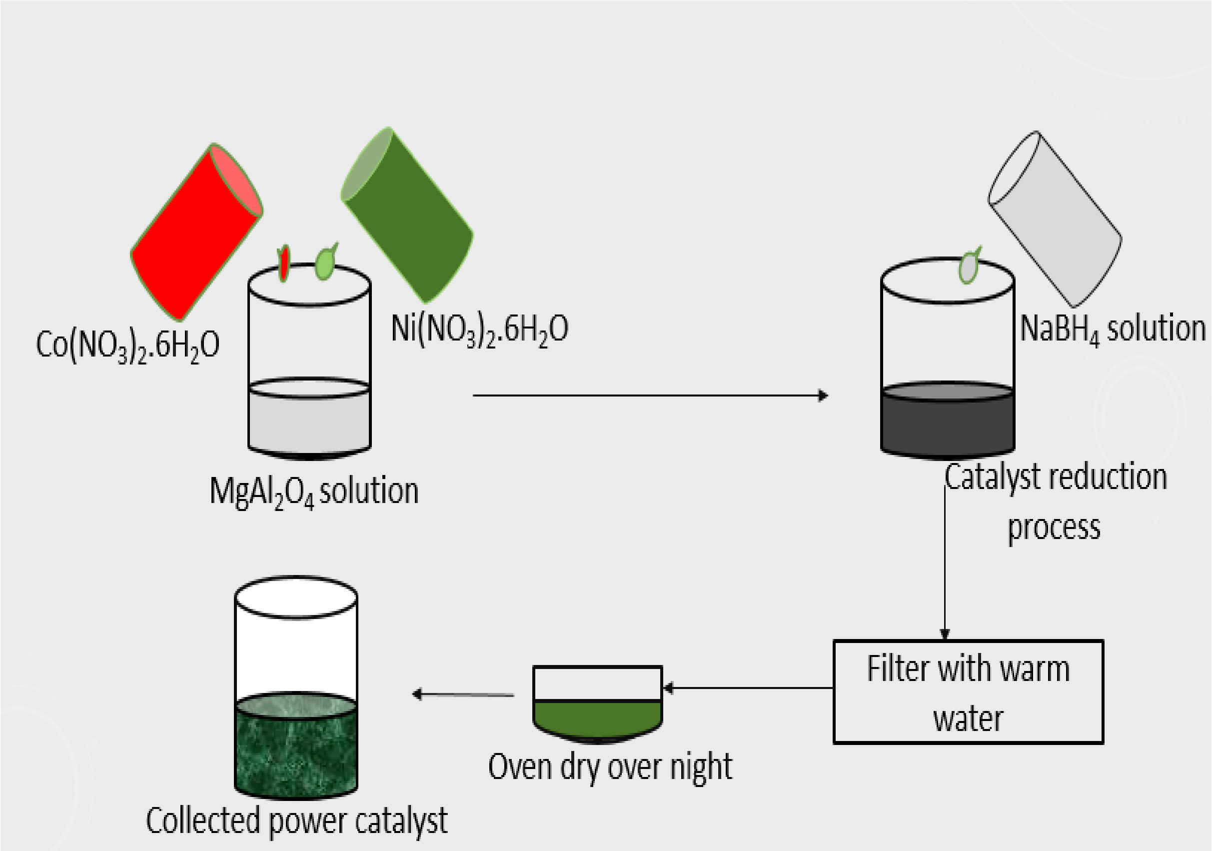

Figure 2.2. Schematic representation of the one-step $NaBH_4$ reduction for (Ni-Co)-B/MA catalysts for the dry reforming reaction.

2.2 Catalyst characterizations:

2.2.1. Inductively coupled plasma-optical emission spectroscopy (ICP-OES) analysis:

The quantitative analysis of the prepared sample can be done by using Thermo-Fischer XR (2013) inductively coupled plasma-optical emission spectroscopy (ICP-OES) analyzer. The principle used by the ICP-OES analyzer suggested the ions can absorb energy by the movement of electrons from the ground to the excited state, then the excited atoms release light at a particular wavelength due to the electron transition to the lower energy level (usually the ground state). Based on the observed calibration curve, the specific concentration of the element can be found. In order to get the accurate concentration of each element, the sample preparation for the ICP-OES analysis is very crucial. The calculated amount of catalysts was digested in the HNO_3 (5%) solution. The 10 mg of the prepared catalyst was dissolved in the HNO_3 solution, and the solution was heated at 60°C with continuous stirring until the solid particle was completely digested in the acid solution.

2.2.2 X-Ray diffraction (XRD) analysis:

The XRD analysis uses for the identification of materials phase based on their diffraction patterns. XRD analysis is a non-destructive analytical method for the analysis of crystalline materials. The Bruker D8A XRD with copper X-ray source and automated sampler were used to analyze the prepared catalysts. A powdered sample of Ni, Co, and Ni-Co-based catalyst was analyzed using a LynxEye position-sensitive detector was used.

2.2.3 H_2 temperature-programmed reduction (H_2-TPR):

A Chembet-3000 equipped with a thermal conductivity detector (TCD) H_2-TPR was used to examine the reduction behavior of prepared catalysts. The reduction of oxide from the present metal oxide (MO) catalysts was monitored in the equipped mass spectrometry acquired in the H_2 environment to reduce MO to M^0. The prepared catalysts initially ramped up the temperature in the N_2 environment till the desired temperature was reached. The H_2-TPR spectra were further acquired to the spectra with the H_2(10%)/N_2 mixture. The TCD showed the hydrogen consumption during the H_2-TPR experiments. The degree of reduction was also calculated from the H_2-consumption profile [37].

2.2.4 H_2 temperature-programmed desorption (H_2-TPD):

the H_2-TPD technique is used to determine the interaction of the catalyst's solid surfaces with the gases. The adsorption and desorption of the carrier gas (He) gives information to calculate the dispersion and active sites of the metal surfaces. Hence, to determine the dispersion and surface-active sites present on the surface of the catalyst, the H_2-TPD experiments were performed, and the profiles were recorded using catalyst characterization equipment BELCAT II (Fig. 2.4). For this, N_2 treated catalyst sample of about 0.035 g was taken and treated with 10% H_2/Ar with 30 ml/ min at 50 °C. The assumption was much such H_2 adsorbed and desorbed were the same [37]. At 50 °C, samples were flushed with N_2 for 30 min; then, the temperature was ramped with N_2 at 10°C/min.

3.2.5 Surface area analysis:

The Brunner-Emmett-Teller (BET) was used to determine the surface area of the catalysts. Micrometric 3-Flex instruments with a separate degassing unit were used to analyze the surface area of the prepared material. The BET analysis gives important information on their physical structure as the area that can be altered during the synthesis of the catalysts. The surface area of the catalysts increases with the pores of the particle. In order to get the surface area, 50 to 100 mg of catalysts were degassed in the degassing unit at 323 K for 12 h. After proper degassing of the catalysts, the catalyst was placed in the Micrometric 3-Flex instrument with the presence of liquid N_2.

2.2.6 X-ray photoelectron spectroscopy (XPS) analysis:

The XPS analysis is used for analyzing the surface chemistry of the catalyst’s material by measuring the elemental composition and electronic state of each atom in the catalysts. Generally, XRD analysis is unable to provide clear information about the elemental composition, especially the presence of lighter elements such as B. The Kratos AXIS ultra DLD XPS (Manufacture: Kratos Analytical, Manchester, UK) is equipped with an Al anode (AlKα = 1486.6 eV) XPS instrument. The spectra were obtained by ray hitting electrons of the catalyst surface, providing kinetic and binding energy of each element along with the photoelectron spectrum. The binding energy was recorded from the range of 0-1200 eV to get all elemental distribution. A separated scan was also recorded for each element of the catalysts, such as Ni, Co, and B.

2.2.7 Morphological analysis of the catalysts:

The transmission electron microscope (TEM) analysis is generally used to define the compositional and crystallographic information of the catalysts. The energetic electron's interactions with the catalyst particles record through the electromagnetic lenses to obtain the images. A high-resolution TEM was used to get the crystal structures and lattice fringes of the metal and support to get more insight information. The FEI Talos FS200X G2 field emission gun (FEG) TEM equipped with highly sensitive Energy-dispersive X-ray spectroscopy (EDS) detectors for elemental analysis was used to analyze the Ni-Co-B based MA-supported catalysts (Fig. 2.5). In addition, a scanning transmission electron microscopy (S-TEM) was also used in this work to obtain the elemental mapping through a high angle annular dark field (HAADF) for each element of the catalysts to confirm their existence. The sample for TEM analysis was prepared by the dilution of solid catalysts in the ethanol solution, followed by the sonicated bath in an ultrasonic bath (UP2200HE 50 kHz, 100 W). Further, a well-mixed liquid solution was placed on the continuous carbon grid to get the TEM images.

2.2.8 Raman analysis:

The Perkin-Elmer Spectrum GX Raman spectrometer was used to investigate the composition of carbonaceous species. The elemental structure of carbonaceous species presents the used catalyst by evaluating the D-band (structural disorder) and G-band (Graphitic carbon). The ratio of Intensity of the D-band and G-band (I_D/I_G) estimated the graphitization of the carbon species present in catalysts. The sample for Raman analysis was prepared by using IR-grade potassium bromide and made mixed powdered in the pellet form to analyze.

2.2.9 Elemental analysis:

The amount of carbon deposited over catalysts after the dry reforming reaction was evaluated by the Perkin-Elmer series II CHNS/O Analyzer 2400 elemental Analyzer. The elemental analyzer is generally used to quantify the amount of carbon, hydrogen, nitrogen, Sulphur, and oxygen contained in the solid sample. However, the spent DRM catalysts possibly had some carbon deposition on the catalyst surface, so the amount of carbon present in the spent catalysts was determined by the CHNS analysis.

2.3 Catalysts evaluation and activity test:

The DRM was carried out in a tubular down flow quartz reactor. The thermodynamic study of DRM and its highly endothermic nature suggested the reaction proceeds above ~ 640 ℃ [37, 115]. Simultaneously, the carbon formation occurs due to CH_4 cracking and CO disproportion reaction in the temperature range of ~557–700°C. Therefore, it is observed that most of the previous studies performed DRM at 600°C [40]. Further, the reactants (CH_4 and CO_2) ratio plays a vital role in product selectivity (H_2:CO). Ayoub et al. [116] suggested that the reactants ratio of unity is a severe condition for the analysis of the catalyst's performance, as a lower reactant ratio (<1) limits the RWGS reaction, and a higher reactant ratio (>1) lowers the H_2 production. The conversions of CH_4 and CO_2, along with the H_2:CO, are the function of the reaction time of DRM. The decline in conversion and syngas selectivity with time on stream (TOS) is one of the most significant issues for DRM due to the deactivation of the catalyst. Therefore, a catalyst with superior activity and resistive to graphitic carbon deposition is highly desirable. GHSV is related to the residence time for the interaction between the catalyst and the feed gases. The GHSV can facilitate the reactant's conversions by providing satisfactory catalyst-reactant interaction. Habibi et al. [117] reported that the conversion of reactants decreases with increasing GHSV. The main reason for the decrement in conversion with increasing GHSV is the decrease in the contact time of the reactants with the catalyst and the decrease in catalyst bed temperature. It is also reported that the higher value of GHSV and small particle size can minimize the amount of internal and external mass-transfer limitations. Hence, from the above discussion, it appears that at a reaction temperature of 600°C, CH_4: CO_2 ~unity and GHSV (~300000 h^{-1}) is the severe condition to examine the prepared catalysts. The Weisz-Prater and Mears' criteria were used with the reaction data to determine the internal and/or external mass transfer effect and observed the negligible impact of internal and external mass transfer effects with adopted reaction condition (Table. D1-D2) [37, 118]. About 0.20 g of the freshly prepared catalyst was loaded in the reactor and heated to 600^0 C in an N_2 (inert) environment. The temperature of the catalyst bed was monitored using a K-type thermocouple (Fig. 2.6). The bed height was uniform for all catalysts, i.e., ~ 0.01m, to prevent the formation of any type of gas channeling. Once the temperature reached 600^0 C and became stable, the pure (99.99 %) feed gases (CH_4 and CO_2) with N_2 gases in a 1:1:3 ratio were introduced into the reactor. A gas hourly space velocity (GHSV) was calculated for the feed gases was $3\times10^5\,h^{-1}$ [40]. The product gas collected from the reactor was analyzed by gas chromatography (GC). The Gas hourly space velocity (GHSV) was maintained at $3x10^5$ h^{-1} during the DRM reaction. The K-type thermocouple was introduced to monitor the temperature in the vicinity of the catalyst bed. The thermocouple was placed above the bed of catalyst for the avoidance of any possible effects of this thermocouple to the catalysts. The desired temperature was maintained before the reaction in the N_2 environment. The feed gases were entered to the reactor by maintain the volumetric flow rates with the help of the mass flow controllers (MFCs) manufactured by the AALBORG Scientific. The produced gases (H_2, CO and unreacted CH_4 and CO_2) was collected with the help of a gas bag that further injected to the gas chromatography (GC, Agilent 6890) to analyze the gas concentration (Fig. 2.7).

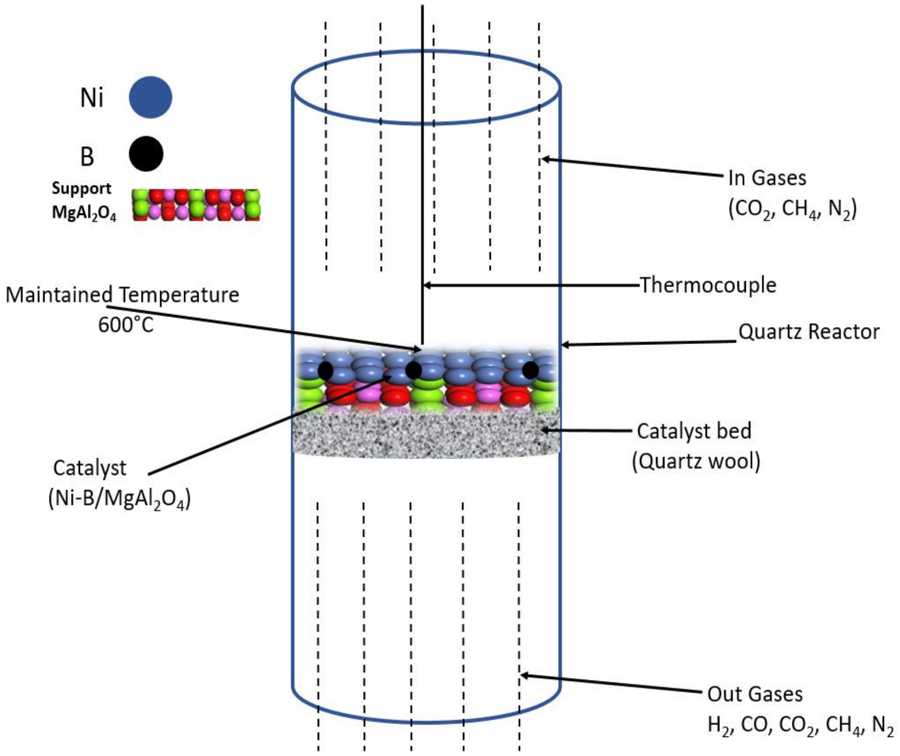

Figure 2.3. A schematic diagram of the catalyst arrangement in the reactor.

2.3.1 Gas hourly space velocity (GHSV):

The GHSV is the volume of gas (typically expressed at standard conditions) entering the reactor per hour per gram of catalyst. The GHSV can be calculated according to the following formula.

$$\text{GHSV} = \left(\frac{\text{Volumetric flow rate of gas feed gas}}{\text{Volume of catalyst}}\right) h^{-1}$$ [37].

2.3.2 Residence time is the ratio of catalyst pallet weight to the molar flow rate of the gases.

$$\text{Residence time} = \left(\frac{\text{Catalyst weight}}{\text{Molar flow rate of the feed gas}}\right) \text{Kg}_{\text{cat}}.\ \text{S mol}^{-1}$$

2.3.3 Conversions of feed gases are defined as the ratio of the number of moles converted to the moles in; it can be calculated as follows.

$$CH_4 \text{ conversion } (\%) = 100 \times \left(\frac{\text{moles } CH_{4_{in}} - \text{moles } CH_{4_{out}}}{\text{moles } CH_{4_{in}}}\right)$$ [39].

CO_2 Conversion (%) = $100 \times \left(\frac{\text{moles } CO_{2_{in}} - \text{moles } CO_{2_{out}}}{\text{moles } CO_{2_{in}}}\right)$ [39].

2.3.4 Yield of syngas:

The of syngas is the ratio of the converted product to the total moles converted.

H_2 yield (%) = $100 \times \left(\frac{\text{moles } H_{2_{out}}}{2 \times \text{moles } CH_{4_{in}}}\right)$ [37].

CO yield (%) = $100 \times \left(\frac{\text{moles } CO_{out}}{\text{moles } CH_{4_{in}} + \text{moles } CO_{2_{in}}}\right)$ [37].

2.3.5 Carbon balance:

The carbon balanced (%) is the total moles of carbon in the product stream to the moles of carbon in the feed.

$$(C_B)\ (\%) = 100 \times \left(\frac{\text{moles } CH_{4_{out}} + \text{moles } CO_{2_{out}} + \text{moles } CO_{out}}{\text{moles } CH_{4_{in}} + \text{moles } CO_{2_{in}}}\right)$$

2.3.6 Turnover frequency (TOF):

The TOF is also calculated for both CH_4 and CO_2 for all the prepared catalysts. The TOF of reactants number of reactant molecules converted over each surface site per second [37, 39, 41].

$$TOF_{CH_4}\ (s^{-1}) = \left(\frac{\text{Flow rate } CH_4}{W_{cat}}\right) * \left(\frac{\text{Conv } CH_4\ (\%)}{100}\right) * \left(\frac{1}{M_S}\right)$$

$$TOF_{CO_2}\ (s^{-1}) = \left(\frac{\text{Flow rate } CO_2}{W_{cat}}\right) * \left(\frac{\text{Conv } CO_2\ (\%)}{100}\right) * \left(\frac{1}{M_S}\right)$$

Where W_{cat} is the weight of the catalyst in g and M_s is the surface metal sites in moles/g calculated from H_2-uptake data from H_2-TPD.

2.3.7 Rate of reactions:

$(-r_a) = \left(\frac{V0 * C_{CH_4} * X_{CH_4}}{W_{cat}}\right)$ mol.s^{-1}.cm^{-3}.

Where V_0= Volumetric flow rate (cm^3.s^{-1}).

W_{cat} = Weight of catalysts.

X_{CH_4}= CH_4 conversion.

C_s is the concentration of reactant (CH_4) entering to the reactor for the reaction mol /cm^3.

$C_s = \frac{P * y_{CH_4}}{RT}$ (mol.cm^{-3}).

Where, P = Pressure (1 atm).

R = Gas constant = 82.06 cm^3 atm/K.mol.

T= Reaction temperature = 773-973 K.

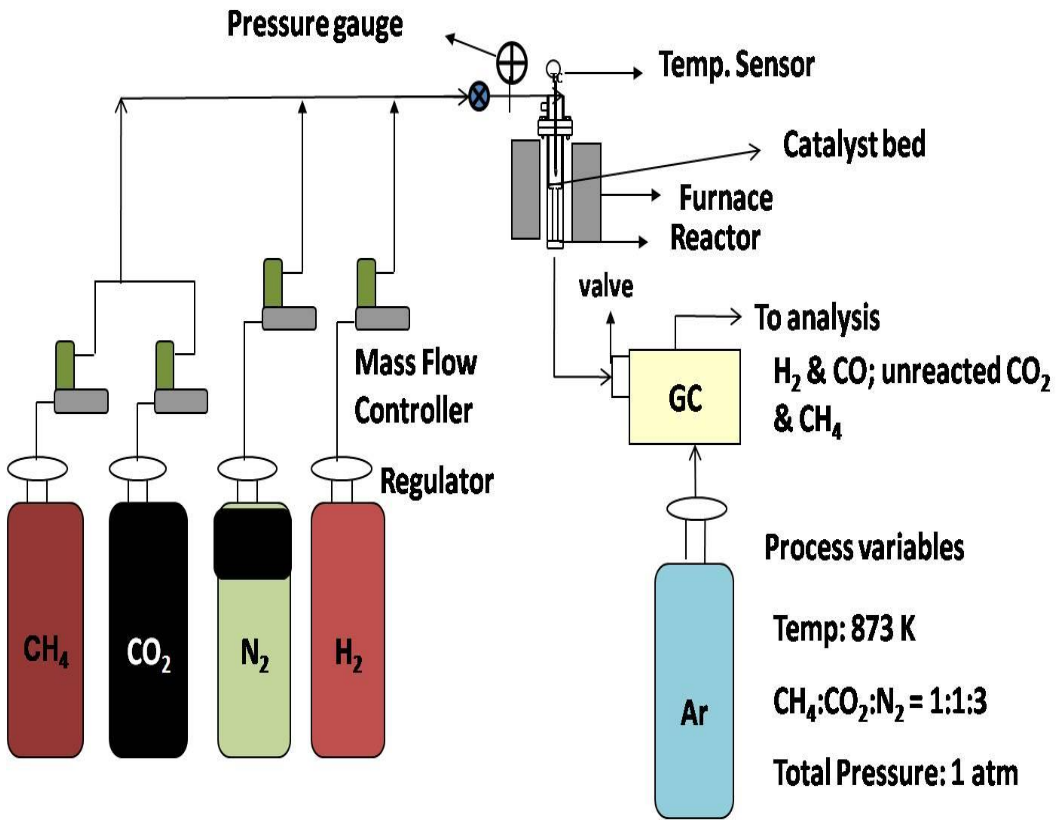

Figure 2.4. A schematic diagram of the setup for the testing of prepared catalyst and kinetics analysis for DRM reaction.

2.4 Computational methods:

The generalized-gradient-approximation (GGA) and Perdew-Burke-Ernzerhof (PBE) exchange-correlation functional were used for electronic structure calculation of the model catalyst under the DFT formalism [119, 120]. The three-layer surface of 75Ni-25Co (111) was established by the optimized bulk 75Ni-25Co, shown by p (2×1) super cell and with a vacuum region of 12 A°. The bottom layer was fixed at the equilibrium bulk position while the top two layers were relaxed. The convergence threshold was set to 1.0×10^{-4} eV/atom for SCF, 1.0×10^{-4} eV/atom for energy with a (4×4×1) Monkhosrst-Pack grid. The effect of spin polarization was considered to calculate the energy of the model surface [121]. The adsorption energy (E_{ads} expressed in eV) was calculated according to the following formulae:

$$E_{ads} = \frac{1}{N_X}(E(X/75Ni - 25Co) - E(75Ni - 25Co) - N_X E_{(X)})$$

Where $(E(X/75Ni - 25Co)$ and $E(75Ni - 25Co)$ are the total energy of the optimized surface of Ni-Co with adsorbate of B /carbon and optimized 75Ni-25Co surface, respectively, $E_{(X)}$ is the energy of free atom of B/carbon and N_X is the number of carbon/B atoms per unit cell [102].

Chapter 3

B-Ni/$MgAl_2O_4$ catalyzed dry reforming of methane: the role of boron to resist the formation of graphitic carbon

This chapter was originally published as "B-Ni/$MgAl_2O_4$ catalyzed dry reforming of methane: the role of boron to resist the formation of graphitic carbon" by MD Shakir, Siddhartha Sengupta, Apurba Sinhamahapatra, Shaomin Liu, Hari Vuthaluru in Fuel (2022), doi.org/10.1016/j.fuel.2022.123950.

3.1 Results and discussion:

The elemental composition was examined for the prepared B(x)-Ni/MA catalyst by the inductively coupled plasma-optical emission spectroscopy (ICP-OES) analysis, and the observed results are shown in Fig. 3.1. The ICP-OES results showed that the Ni amount in all catalysts is between 13.3-14.4 wt.% instead of the aimed 15 wt.%. The amount of B was found to be ~ 0.9, 2.8, and 4.3 wt.% for the catalyst B (1, 3, and 5)-Ni/MA. Although the ICP-OES results indicated a slight decrement in B amount compared to that aimed for, it is confirmed the varying amount of B in the different samples. Further, the BET surface area of the B(x)-Ni/MA catalysts was measured and listed in Table. 3.1. The surface area of the support MA was higher and decreased with increasing Ni and B loading. It has been reported that the decrease in the surface area of the catalysts is due to the blockage of pores [16]

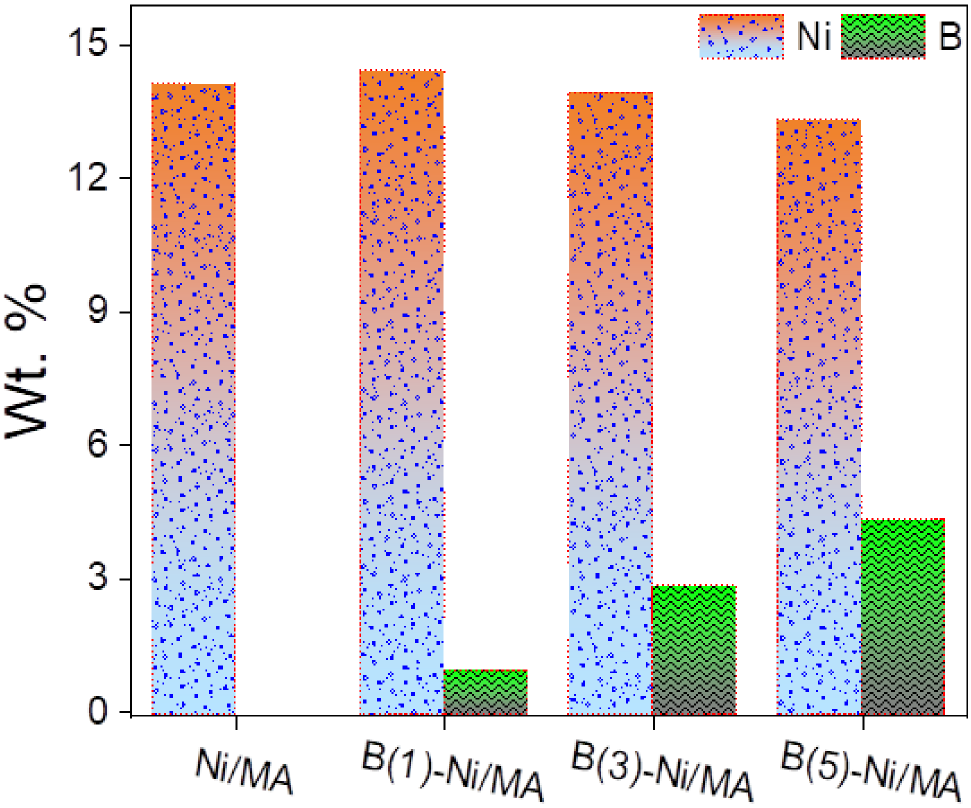

Figure 3.1. ICP-OES analysis results for all B(x)-Ni/MA and Ni/MA catalysts

Table 3.1. Structure properties of the B(x)-Ni/MA catalysts.

Sample	Surface area (m^2/g)
MA	98
Ni/MA	79
B(1)-Ni/MA	76
B(3)-Ni/MA	75
B(5)-Ni/MA	68

The XRD pattern disclosed the phase analysis of the B(x)-Ni/MA catalyst. In Fig. 3.2, the diffraction pattern of MA was observed at 2θ= 31.15 (220), 36.52 (311), 44.08 (400), 58.68 (511), and 65.13° (440) (JCPDS Card No. 77-1203) [33, 122, 123]. The reduction of metal salt in the presence of $NaBH_4$ resulted in the formation of Ni-B species, observed at 2θ = 44.78° (130) (JCPDS No. 17-0335) [124, 125] along with the metallic Ni, identified at the peak position 2θ= 44.4 (111), 51.67 (200) and 76.53° (220) (JCPDS Card No. 04-0850) for the B containing catalysts [126, 127]. In some cases, the weak intensity of Ni peaks could be an indication of the uniform distribution of small-size reduced Ni species over the surface as the incorporation of B restricts the crystal growth [40, 122]. The NiO peak was only observed for the non-B catalyst at 2θ = 62.23 (220) and 79.31° (110) (JCPDS Card No. 47-1049) [39, 40]. No separate peak was identified for any form of B, which is not surprising as it is difficult for boron oxide (BO) to have a crystalline phase [103].

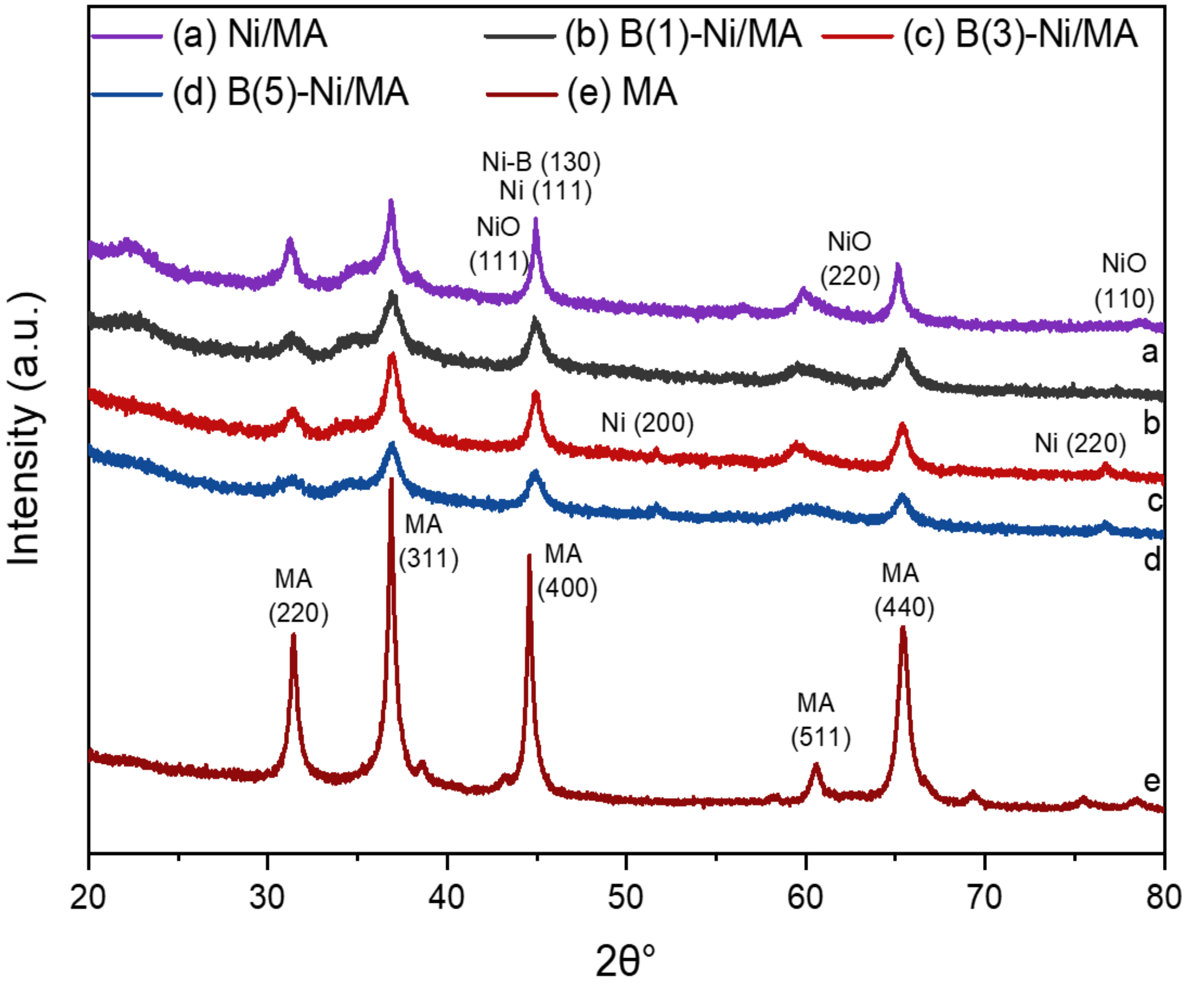

Figure 3.2. XRD of the samples for all B(x)-Ni/MA and Ni/MA catalysts

The change of catalyst reduction behavior of different catalysts was investigated by the H_2-TPR analysis, as shown in Fig. 3.3. For the non-B catalyst, as there was no $NaBH_4$ reduction, the consumptions of H_2 were higher compared to other catalysts. Two clear peaks were observed for H_2 consumption at different temperature ranges, which corresponds to weak and medium metal-support interactions [128, 129]. The peak observed in the range of 300-400°C reflected the reduction of weakly interacted bulk NiO [128, 129]. The H_2 consumption around the temperature range 550-650°C was observed, corresponding to the reduction of smaller surface particles [51, 128]. The peak intensity decreases with increasing the B%, as increasing $NaBH_4$ amount enhanced the extent of reduction of Ni species leading to less consumption of H_2 during TPR suggested SMSI for the B(3)-Ni/MA and B(5)-Ni/MA catalysts demonstrated in Fig. 3.3. Further, to understand the impact of B in catalyst performance, all B(x)-Ni/MA catalysts were tested for DRM.

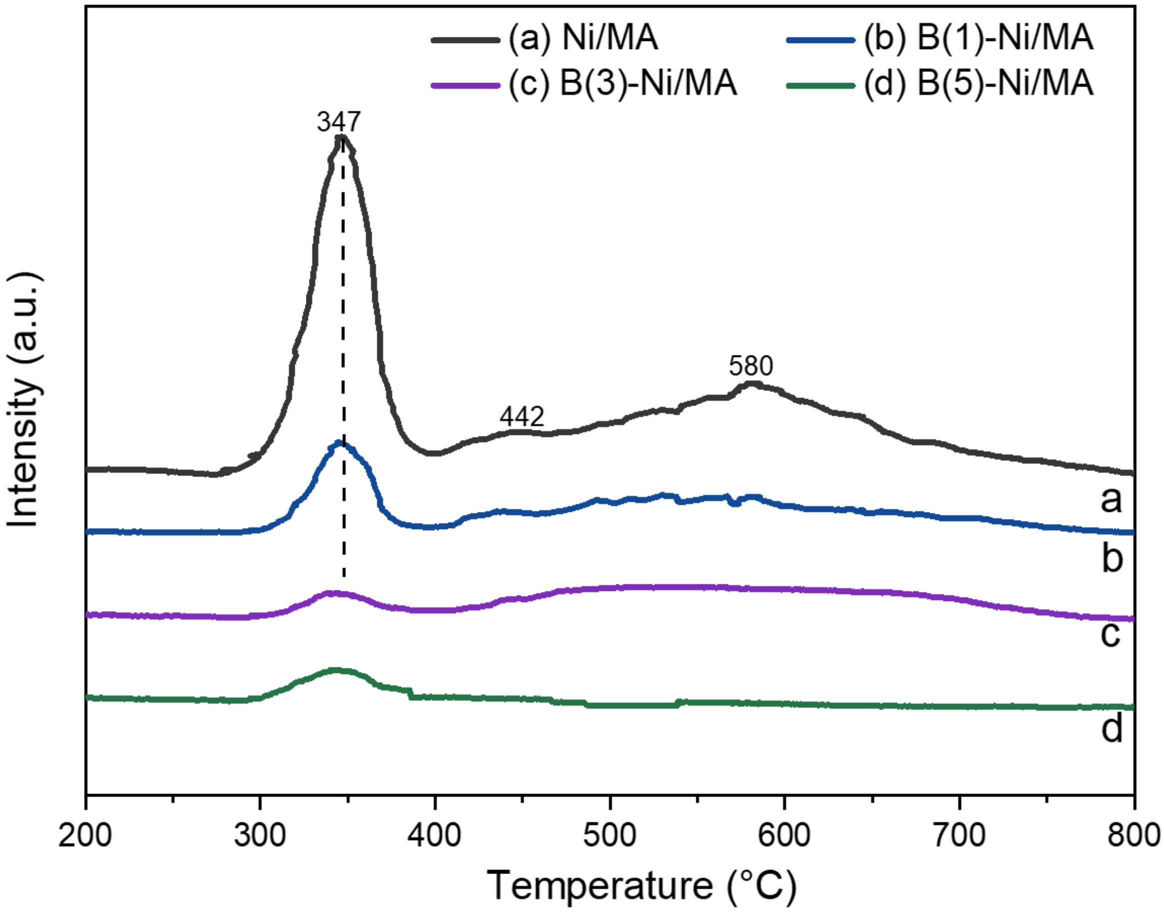

Figure 3.3. H_2-TPR analysis of the samples for all B(x)-Ni/MA and Ni/MA catalysts

Fig. 3.4(a) displays CH_4 conversion with time on stream (TOS) for all catalysts. The minimum CH_4 conversion (%) is observed for the Ni/MA, and the trends indicated a substantial decrement in conversion after 90 min and continued further. The maximum conversion of CH_4 at TOS 90 min was about 17.30% for the B(3)-Ni/MA, which is 3.16 times higher than the non-B catalyst. These differences in conversion persisted throughout the reaction interval. It was also observed that the conversion increased with the amount of B up to 2.8 wt.% and then decreased. Moreover, the decline (%) in CH_4 conversion was also calculated for the catalysts and reported in Fig. 3.4(b). The decline (%) was observed ~5 and ~1.7 times higher for Ni/MA and B(5)-Ni/MA, respectively as compared to B(3)-Ni/MA. The higher decline (%) for B(5)-Ni/MA attributed to poor texture of B over the Ni surface [56, 103]. These results were further compared with the previous studies for B and non-B catalysts are listed in Table. 3.2. The conversion of CH_4 and CO_2 were higher and stable for B-containing catalysts with low , however, some authors reported higher conversion that could be due to the higher reaction temperature and low GHSV [116]. In addition, the turnover frequency of methane (TOF_{CH_4}) was also calculated for the best performing B(3)-Ni/MA and Ni/MA catalysts by using H_2-TPD (Fig. A1) and conversions data, at TOS 30, 120, and 240 min. The calculated TOF_{CH_4} at different time interval was 0.271, 0.311, and 0.289 s^{-1} for B(3)-Ni/MA and 0.129, 0.119 and 0.091 for Ni/MA at TOS 30, 120, and 240 min, respectively.

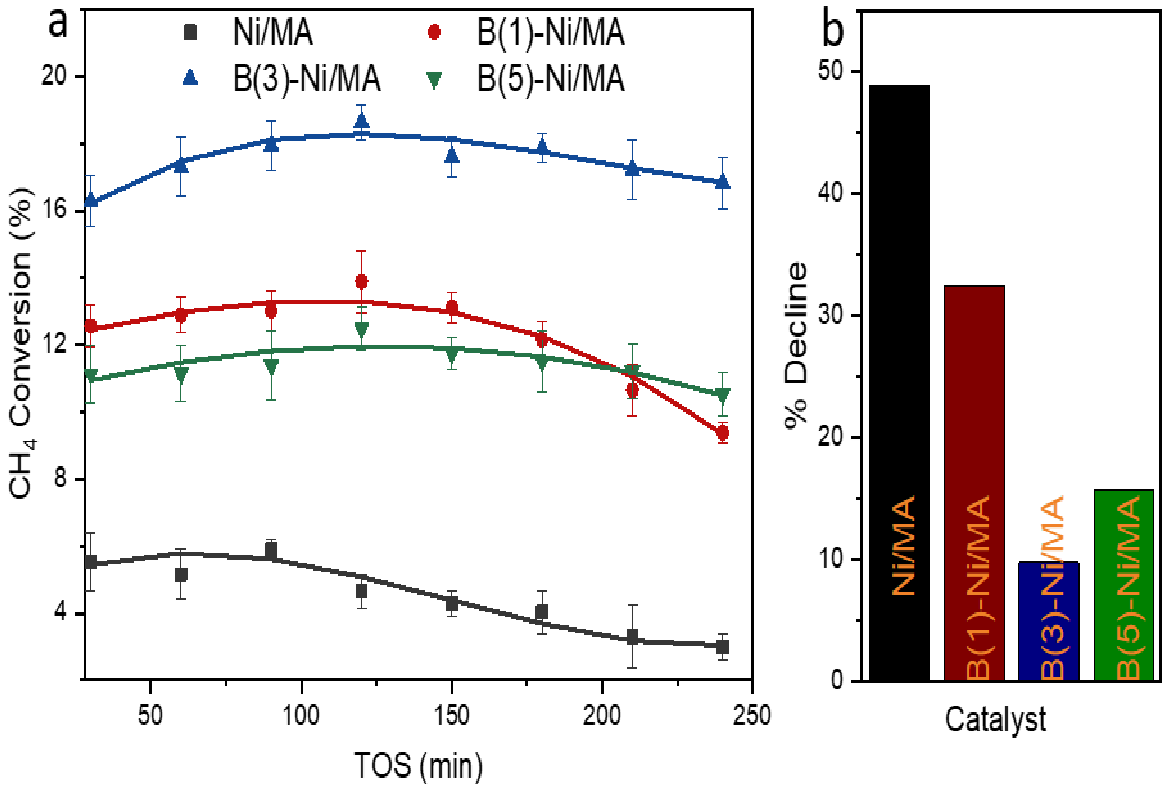

Figure 3.4. The catalytic performances of prepared catalysts in the DRM with GHSV of 3×10^5 h^{-1} (a) CH_4 conversion, (b) Decline (%) for CH_4.

The CO_2 conversion was slightly higher than the CH_4 due to the reverse water gas shift reaction [40]. However, the conversion of CO_2 (%) trend was similar to CH_4 for all the catalysts presented in Fig. 3.5(a). The highest conversion of CO_2 was 29.87%, observed for B(3)-Ni/MA, which was 3.5 times higher than the Ni/MA. Further, the decline (%) in CO_2 conversion was also calculated and reported in Fig. 3.5(b). Similar to CH_4 decline (%), the insignificant decline in CO_2 conversion was observed for the B(3)-Ni/MA compared to non-B Ni/MA catalyst. The H_2-treated non-B Ni/MA was also performed and reported in Fig. A2. Interestingly, the further H_2-reduced non-B catalysts was also significant compared to the B(3)-Ni/MA catalysts. Recently, Rashmi et al. [37] reported a decline in CO_2 conversion by ~56% at TOS 3h in Table. 3.2. Furthermore, the production of syngas (H_2: CO ratio) also demonstrates the performance of the catalyst for DRM [37, 40, 52].

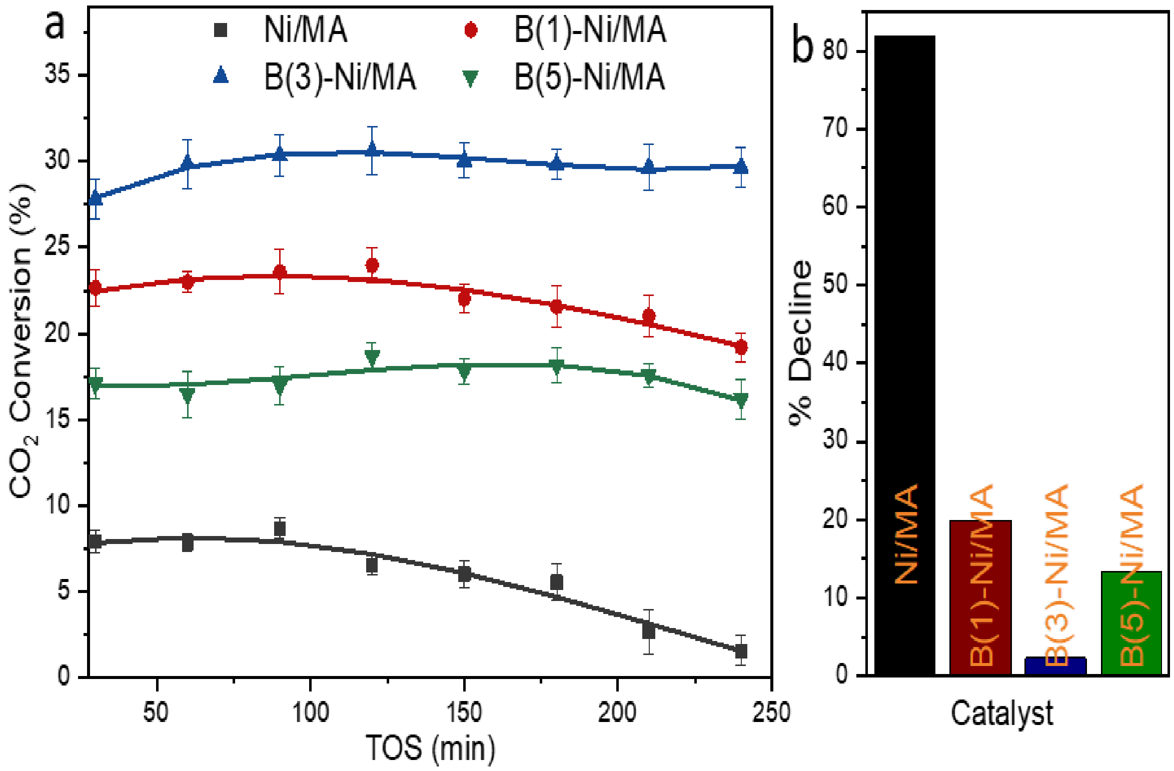

Figure 3.5. The catalytic performances of prepared catalysts in the DRM with GHSV of 3×10^5 h^{-1} (a) CO_2 conversion, (b) Decline (%) for CO_2.

Fig. 3.6 reveals the ratio of produced syngas for all the prepared catalysts. The syngas production also followed a similar trend as CH_4 and CO_2 conversion. It was also noted that the higher B (%) catalyst does not promote conversion further; a possible reason is that the catalyst with higher B (%) has a chance to possess less amount of metallic species the higher amount of Ni-B species resulting in weakening of SMSI leading to lower methane activation [103]. Recently, Zhu et al. [130] suggested that the higher amount of B (%) increases the surface acidity of B-doped CN/SBA catalysts, affecting CO_2 activation. Furthermore, the H_2:CO ratio for B(3)-Ni/MA (~0.6) was higher than that of non-B Ni/MA (~0.3). Previously reported work with Ni/MA catalysts also suggested a similar H_2:CO ratio of ~0.4 at similar reaction conditions [37]. These results suggest that the presence of 3 wt. % B reasonably enhanced the catalyst performance.

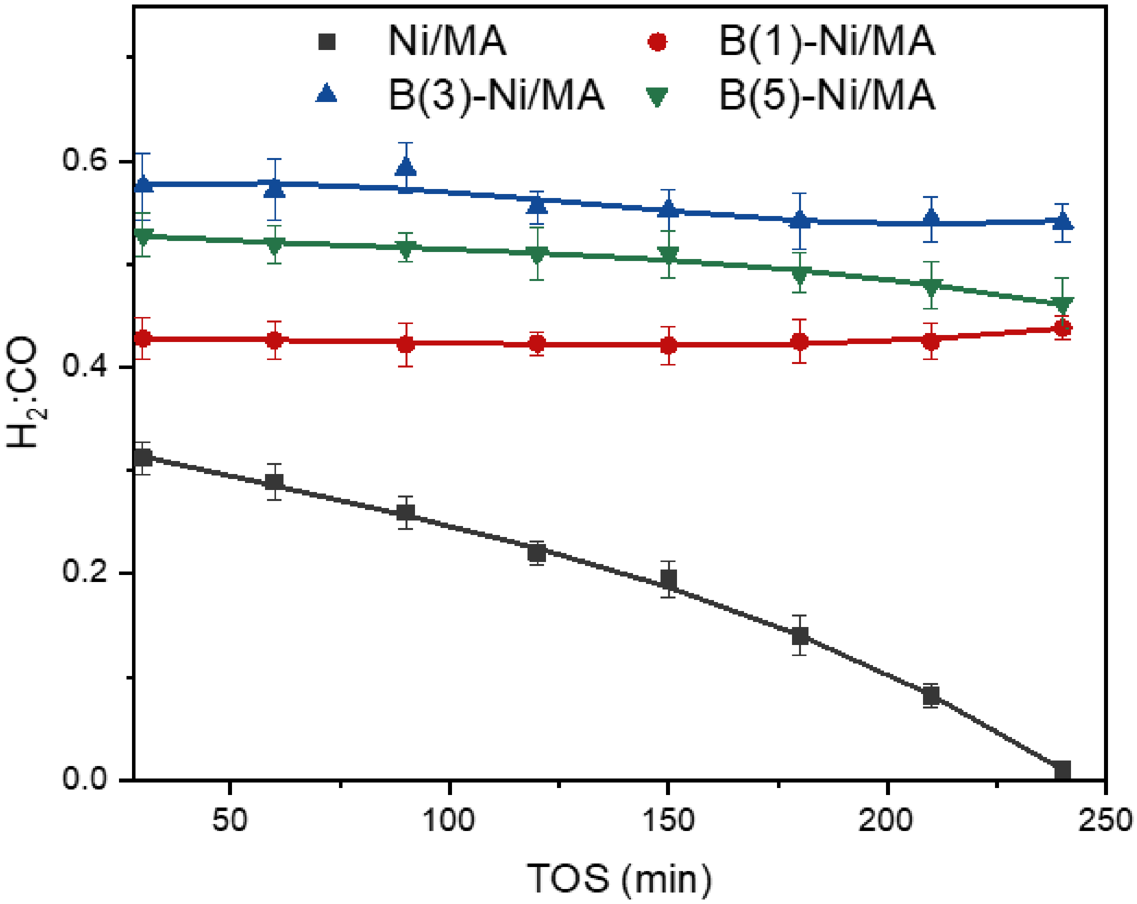

Figure 3.6. The ratio of syngas for the prepared catalysts in the DRM with GHSV of 3×10^5 h^{-1}

Table. 3.2. Comparison of catalyst performance with literature results for DRM.

Catalyst	**Preparation Method**	**Surface area**	**Reaction Condition**		**Conversion (%)**		**Decline (%)**		**C-deposition**	**Ref**
		(m^2 g^{-1})	T (℃)	GHSV	CH_4	CO_2	CH_4	CO_2	(g_C.g_{cat}^{-1})	
B(3)-Ni/MA	$NaBH_4$ reduction	66	600	300000	17.3	29.8	9.7	2.3	0.037	Present work
Pd-Nb 2 Pb-Nb0.5 Pb-Nb 1	IWI	185 183 191	750	60000	83.7 44.2 56.5	90.3 67.8 49.8	6.6 11.3 37.0	5.5 25.5 24.1	0.156 0.084 0.033	[42]
Ni/Al Ni/Ce-Al	Wet impregnation	163 136	860	1200	71.5 72.6	96 96.8	-	-	0.180 0.170	[131]
Ni/ Al_2O_3	IWI	164	600	300000	13.5	-	-	-	0.17	[41]

B-Ni/ Al_2O_3	Wet co-impregnation	196.0	700	30000	55.0	65.0	-	-	0.028	[103]
Ni/$La_{0.46}Sr_{0.34}TiO_3$	Combustion	11.80	700	26400	36.50	43.50	48.15	62.23	-	[132]
NiPt/$Ce_{0.8}Pr_{0.2}O_{2-\delta}$	Sol-gel	13.7	750	30000	68		-	-	0.007	[27]
Ni/MA	IWI	35.98	600	300000	14.1	16.8	48.89	56.92	0.34	[37]
B-Ni/SBA-15	IWI	215.6	800	360000	76.69	83.70	07.23	7.53	-	[56]
B-Co/ZrO_2	$NaBH_4$ and NH_3BH_3	-	750	120000	69.5	-	05.39	-	-	[133]
Ni/MA	Solgel	97.11	600	12000	26.1	32.2	-	-	-	[134]
Ni/MA	Co-pre	95.0	600	180000	35.8	37.2	-	-	-	[17]

Note: IWI- Incipient impregnation method
Co-pre- Co-precipitation method

Further investigation was performed to find the reasons behind the enhancement of catalytic activity. The XPS analysis of B(3)-Ni/MA and Ni/MA was conducted to gain insight into the chemical environments of major elements, and the results are displayed in Fig. 3.7. The survey spectrum revealed peaks of Ni, Mg, Al, O for both B(3)-Ni/MA and Ni/MA catalysts and a sharp peak of B for B(3)-Ni/MA catalyst.

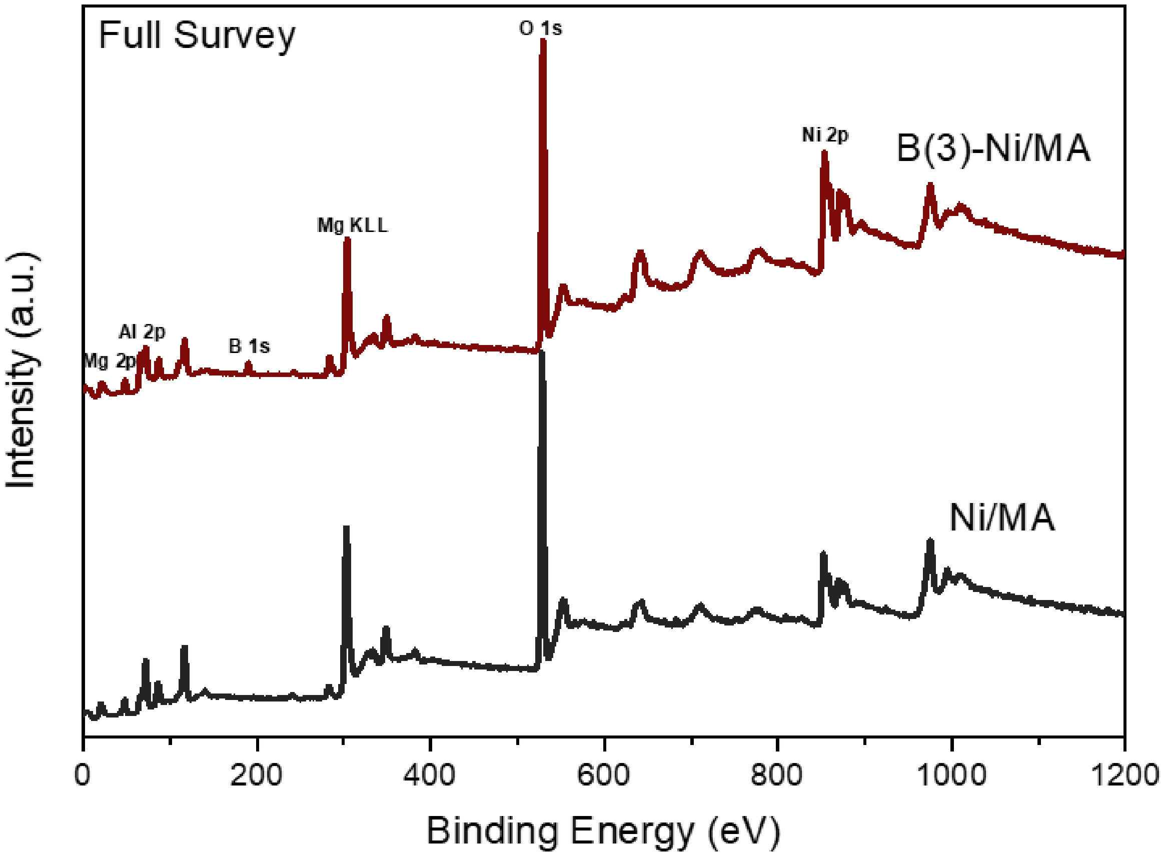

Figure 3.7. XPS analysis of Ni/MA and B(3)-Ni/MA catalysts with a full survey of each element.

Fig. 3.8 shows the XPS spectrum of B(3)-Ni/MA with the specific resolution for Ni 2p. The Ni 2p peaks after deconvolution reflected the presence of $2p_{3/2}$, $2p_{1/2}$ electrons with their corresponding satellite peaks. Peaks position at binding energy (eV) 852.6 and 870. 3 eV were attributed to the presence of Ni $2p_{3/2}$ and Ni $2p_{1/2}$ electrons of Ni-B species, respectively [62, 135]. Similarly, the position of the peaks at binding energy (eV) at 853.5 ($p_{3/2}$) and 872.3 eV ($p_{1/2}$) confirmed the presence of Ni^{2+} along corresponding satellite peaks (Fig. 3.9) [136, 137]. The sample contains Ni-B species and metallic Ni^0 formed during $NaBH_4$ reduction, as indicated in the XRD and TPR profiles. It can be realized that the Ni^{2+} was reduced to Ni^0 by produced syngas during synthesis, and peaks analysis suggested the presence of ~58.29 % Ni and ~41.71 % NiO for B(3)-Ni/MA. The decomposition of $NaBH_4$ in water-ethanol also formed metal hydroxide due to increases of OH^- as the pH of the solution increases [113]. No corresponding peak of Ni^0 was observed for Ni/MA (Fig. 3.9) as there is no reduction of Ni^{2+} to Ni^0 in the absence of $NaBH_4$.

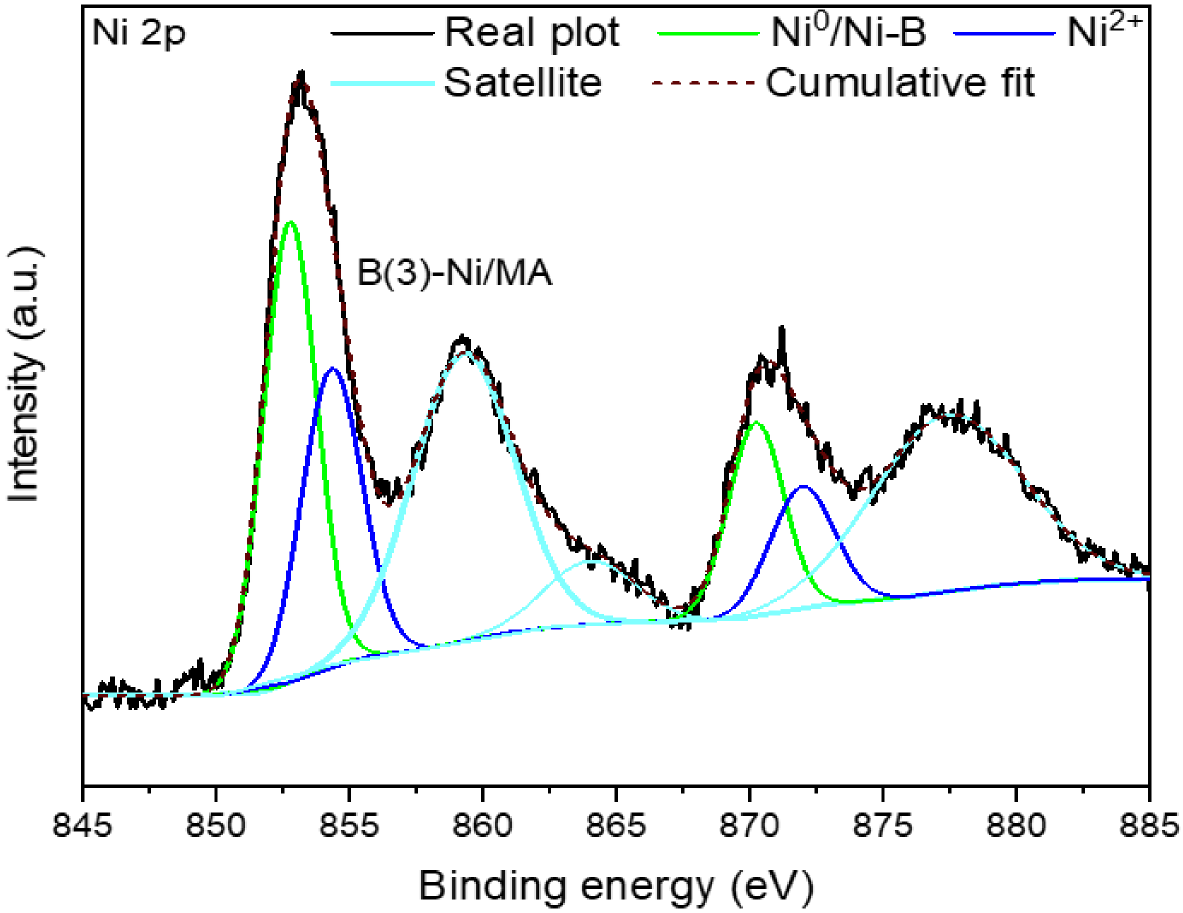

Figure 3.8. XPS analysis of B(3)-Ni/MA for Ni 2p

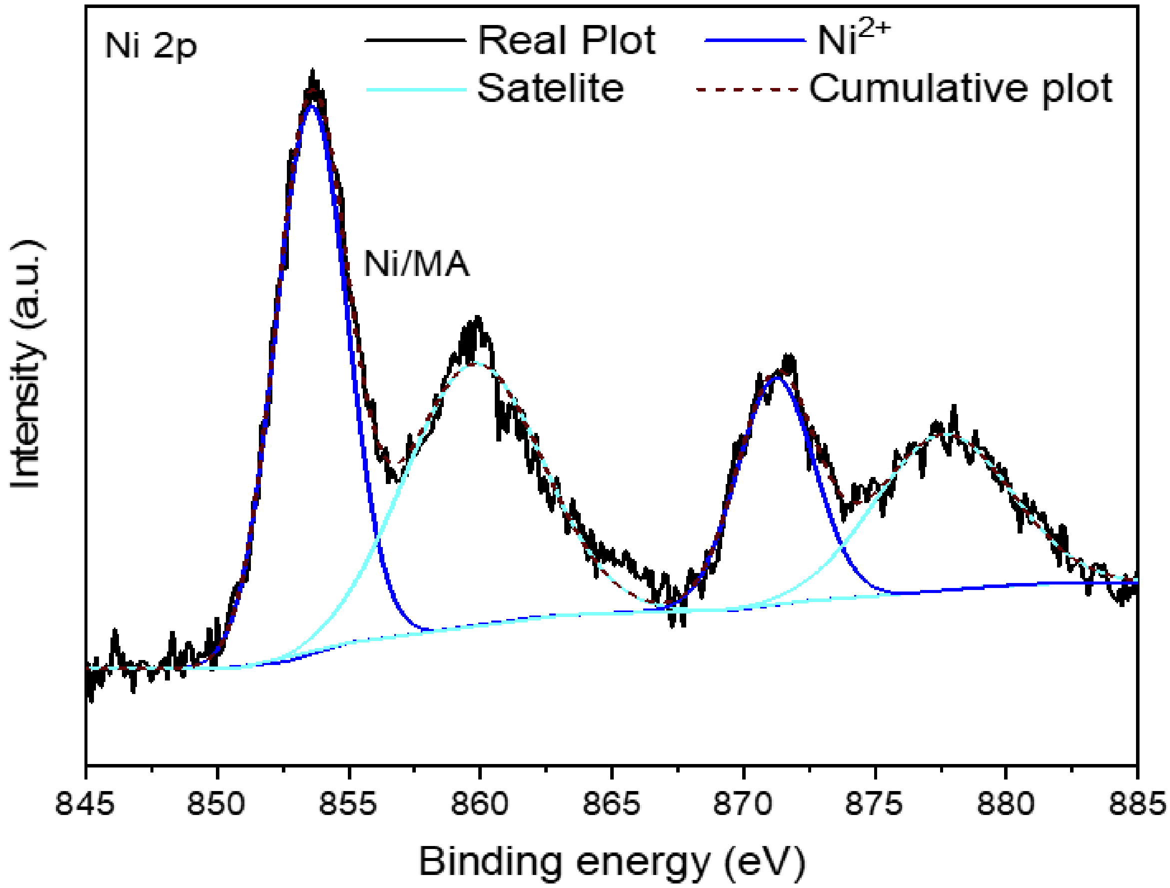

Figure 3.9. XPS analysis of Ni/MA for Ni 2p

The high-resolution core-level XPS spectrum identified the presence of B observed (Fig. 3.10) for B(3)-Ni/MA. The single peak at 189.7 eV appeared because of metal-B interaction due to electron transfer from B to metal, suggesting metal boride-like species formation during $NaBH_4$ reduction [138, 139]. As expected, no peaks of B were identified for non-B catalysts. Moreover, the formation of amorphous borides can be realized as there is no corresponding peak identified in XRD as well

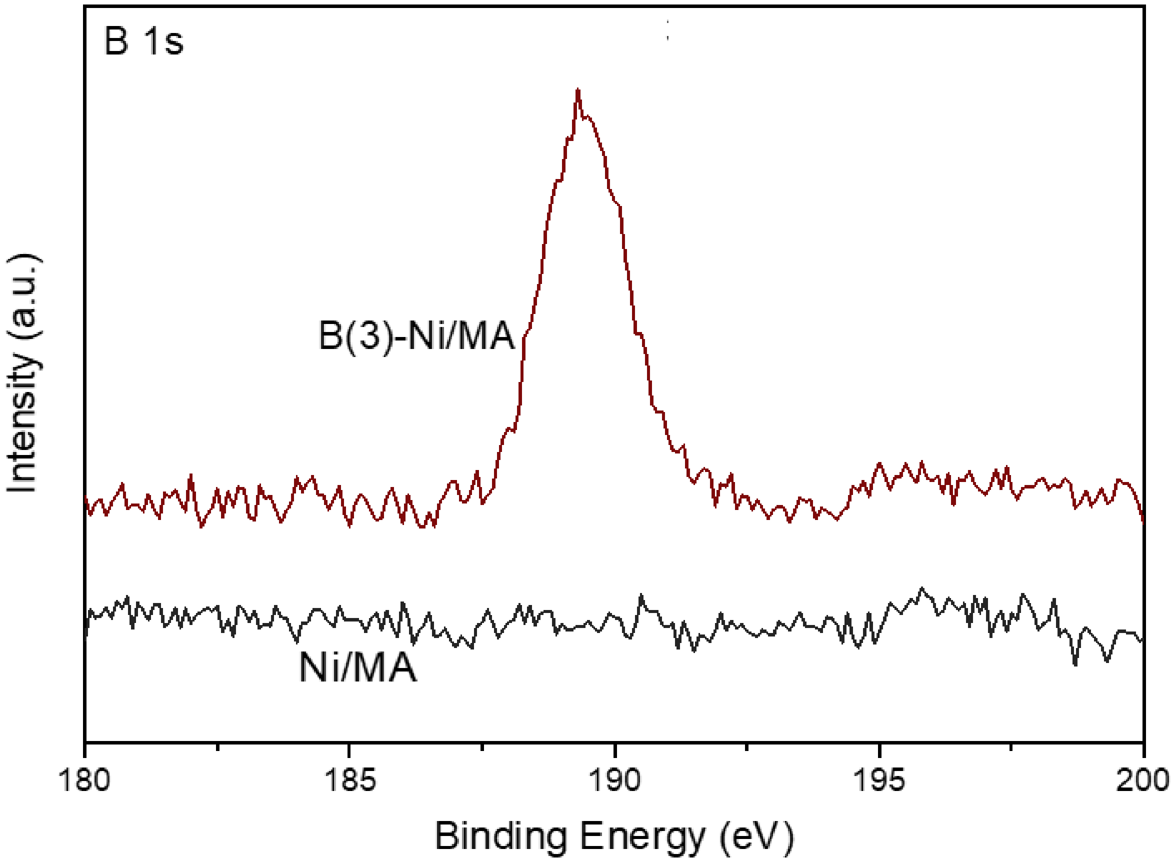

Figure 3.10. XPS analysis of B and non-B Ni/MA catalysts for B 1s

The HR-TEM and HAADF-STEM analysis was also performed for the B(3)-Ni/MA and Ni/MA catalysts reported in Fig. 3.11. A wide range of particle sizes was observed for B(3)-Ni/MA catalyst due to the formation of Ni^0 and Ni-B species in Fig. A3. Comparatively smaller Ni particle size was measured for the B-promoted catalyst with the average particle size around 7 nm, which is 2.3 times lesser than the non-B Ni/MA catalyst represented in Fig. A4. A nano-rod type structure was observed of the Ni^0 and the Ni-B species for the catalyst in Fig. 3.11a, spacing of 0.203 and 0.30 nm were observed that correspond to the Ni^0 (111) and Ni-B species (Fig. 3.11b and c) [140-142]. The formation of Ni_x-B helps enhance the catalytic activity and promotes low catalyst deactivation for DRM, as B exhibits similar chemisorption over the Ni surface.

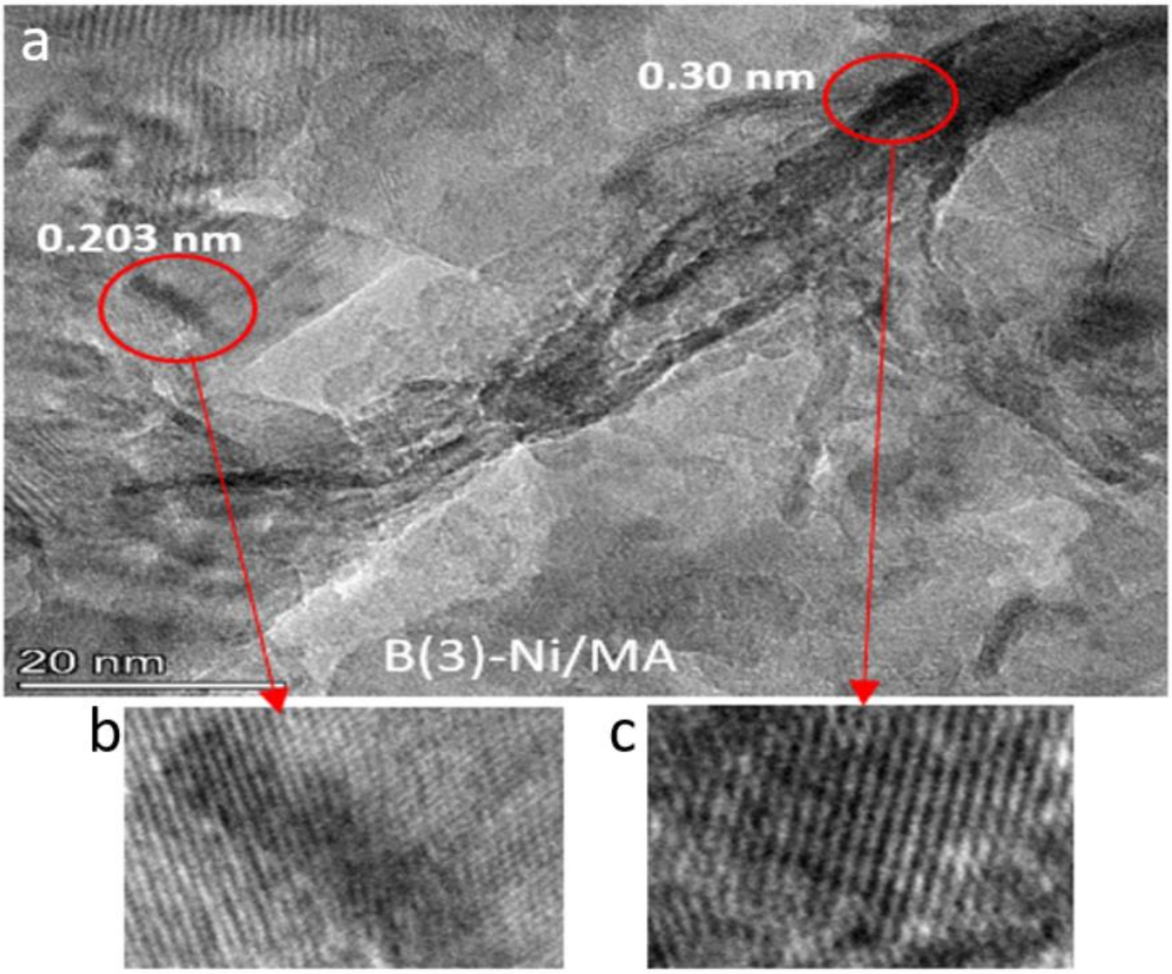

Figure 3.11. HR-TEM image and lattice fringes for B(3)-Ni/MA (a) High resolution image (b) Lattice fringe for Ni^0 and (c) Lattice fringes of Ni-B

The HR-TEM image of the non-B Ni/MA catalyst is presented in Fig A6. The Ni/MA catalyst d-spacing observed about 0.24 and 0.26 nm verifies the presence of NiO and $Ni(OH)_2$ structure (Fig. 3.12a and b), which is in line with the XRD and H_2-TPR results [143, 144]. The Particle size distribution of the Ni/MA catalyst showed in Fig. A7 was about 17.39. Further, the EDS pattern (Fig. A8) of with and without B catalysts was performed to reconfirm the elemental distribution of the catalyst, a sharp peak of Ni, Mg, Al, and O were observed for both catalysts and weak B peak for B(3)-Ni/MA catalyst in Fig. A5. No Na was observed in the EDS analysis, which is in line with the XPS and XRD results.

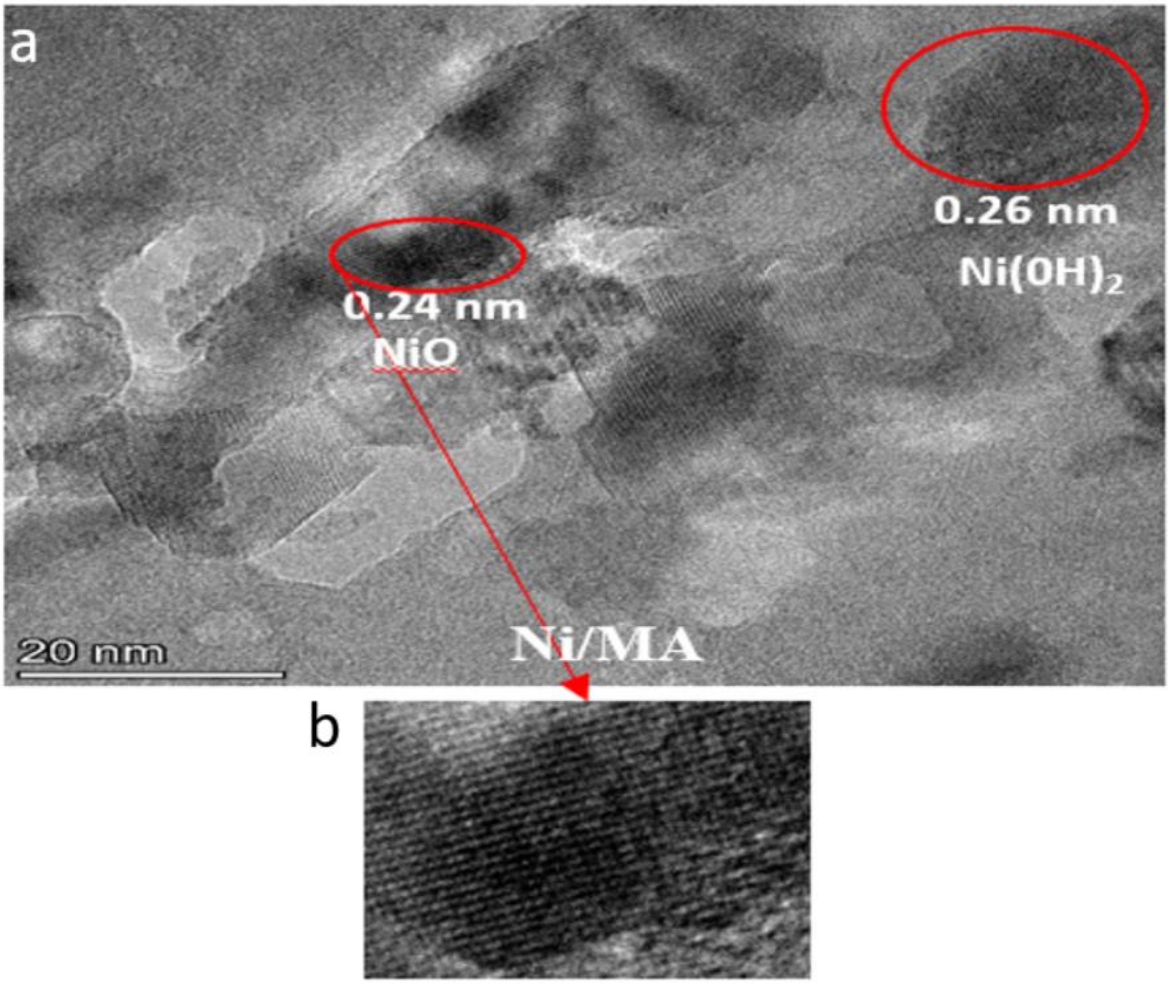

Figure 3.12. HR-TEM image and lattice fringes for Ni/MA (a) High resolution image (b) Lattice fringe for NiO.

Further, the HAADF S-TEM shows the elemental distribution for both catalysts. Fig. 3.13 shows the presence of all elements for B(3)-Ni/MA catalyst with the uniform distribution of B with Ni particle. However, this Ni and B distribution was absent in the Ni/MA catalyst in Fig. 3.14. The presence of support Ni, Mg, Al, and O was observed for both catalysts. These characterization results suggested that the B-containing catalyst prepared by the $NaBH_4$ method appears to be a single-step catalyst reduction method for the preparation of a B-associated Ni-based catalyst for the DRM reaction. It is evidenced that B is bonded with Ni along with the presence of metallic Ni^0. The presence of Ni-B species over the surface restricted the metallic Ni crystal growth leading to smaller particle size and uniform distribution over support. The B-promoted catalyst also revealed remarkable structural differences in particle size distribution compared to the non-B catalyst. The smaller particle size eventually increases the surface-active sites for DRM and the catalytic activity. The same Ni-B species also affected the Ni-

$C_{methane}$ interaction during DRM and reduced carbon formation.

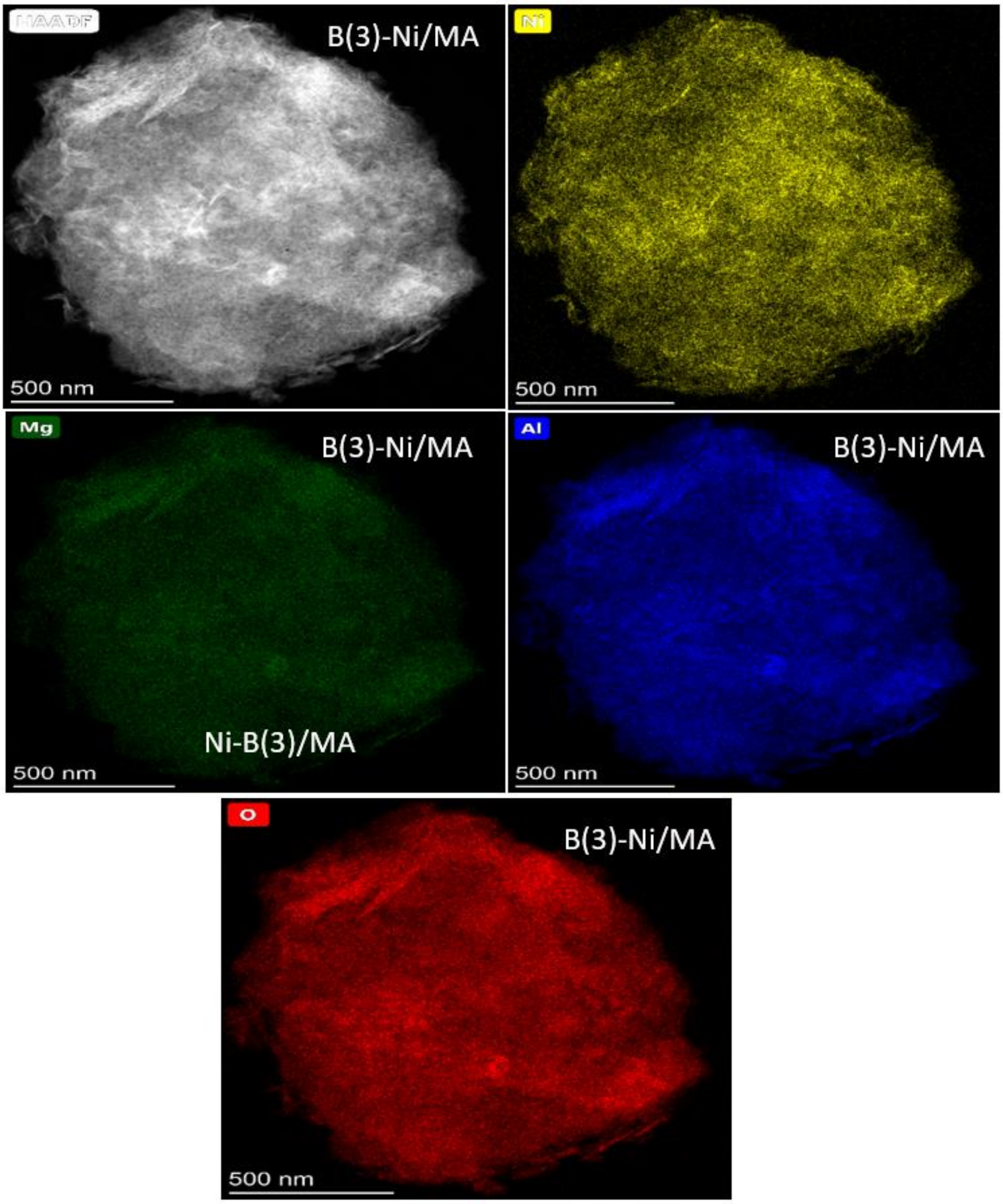

Figure 3.13. STEM HAADF elemental distributions for B(3)-Ni/MA catalyst.

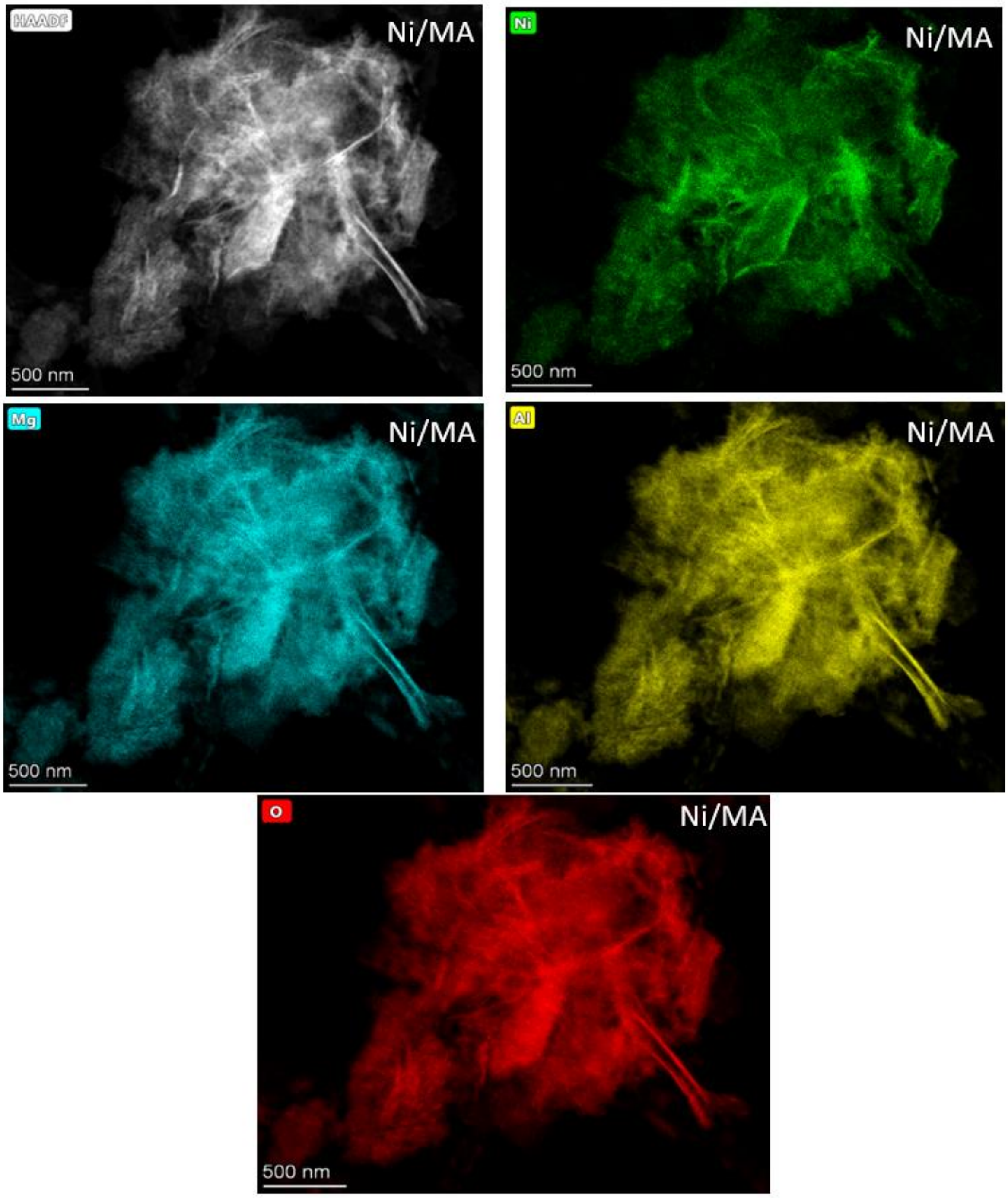

Figure 3.14. STEM HAADF elemental distributions for Ni/MA catalyst.

3.2 Analysis of spent catalysts:

The spent catalysts were characterized by the XRD elemental, Raman, XPS and HR-TEM analysis to analyze the nature of deposited carbon on the catalyst during the DRM. The XRD patterns show the peak of carbon at 2θ ~26.8° for Ni/MA and B(3)-Ni/MA catalysts in Fig. 3.15 [52, 103]. The support MA peaks observed at 2θ= 31.15 (220), 36.52 (311), 44.08 (400), 58.68 (511), and 65.13° (440) (JCPDS Card No. 77-1203) and Ni peaks observed at the peak position 2θ= 44.4 (111), 51.67 (200) and 76.53° (220) (JCPDS Card No. 04-0850) respectively [33, 122, 123]. No Ni oxidation was observed after the reaction.

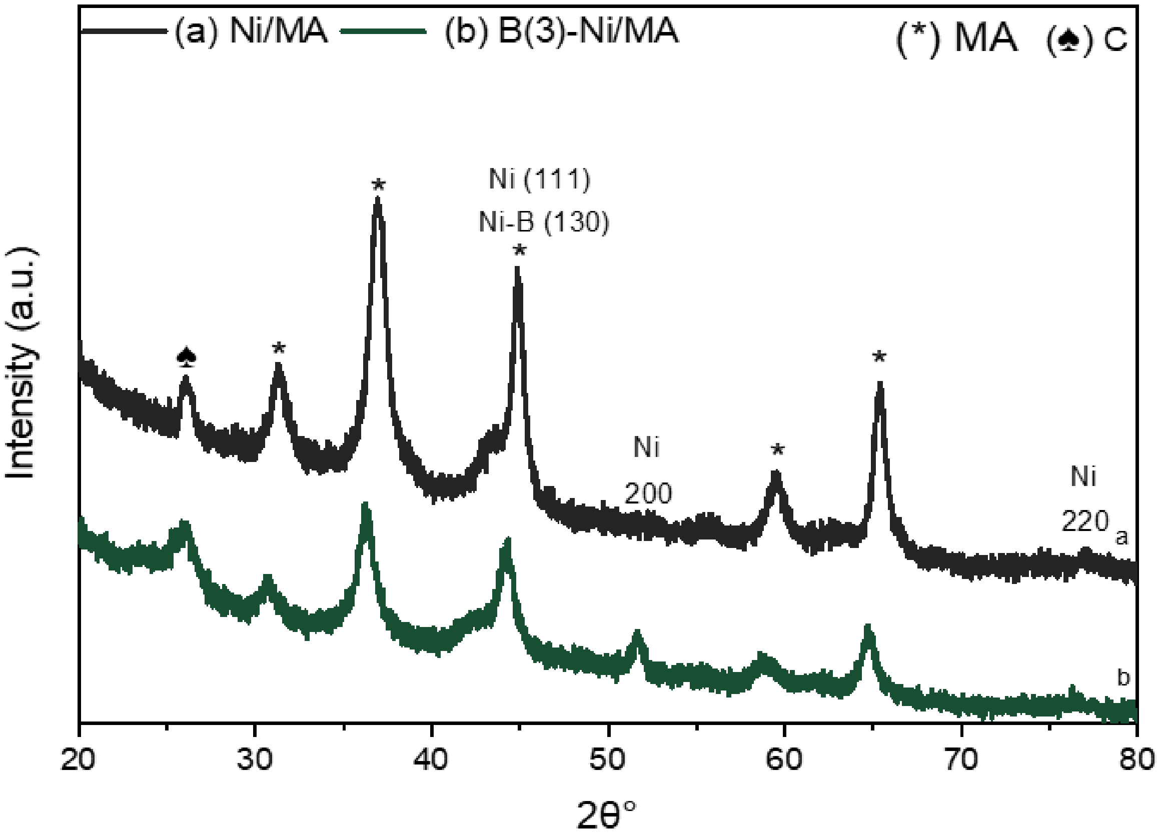

Figure. 3.15. XRD analysis of spent Ni/MA and B(3)-Ni/MA catalysts.

The amount of deposited carbon on the surface of the catalyst after the 4h reaction was measured and presented in Table A1. The carbon content was observed ~ 0.037 ($g_C.g_{cat}^{-1}$) for the B(3)-Ni/MA, which is ~2.4 times lesser than non-B Ni/MA, due to the presence of B and comparatively small size of Ni particle reported in Fig. A8 and 9. The significantly low carbon deposition due to the presence of B and relatively small Ni particle size is in line with the previously reported studies [103]. Recently, Chai et al. [132] also reported that the small size of Ni particles weakened the ability of C formation on the surface of the catalyst listed in Table. 3.2. In addition, the amount of carbon formation was normalized with total methane conversion (assuming methane cracking as the most significant carbon source) in 4h, as the % conversion is varied with different catalysts and the obtained results are presented in Fig. 3.16. Interestingly, the total amount of C was >11 times lesser for B(3)-Ni/MA than non-B Ni/MA (Fig. 3.16).

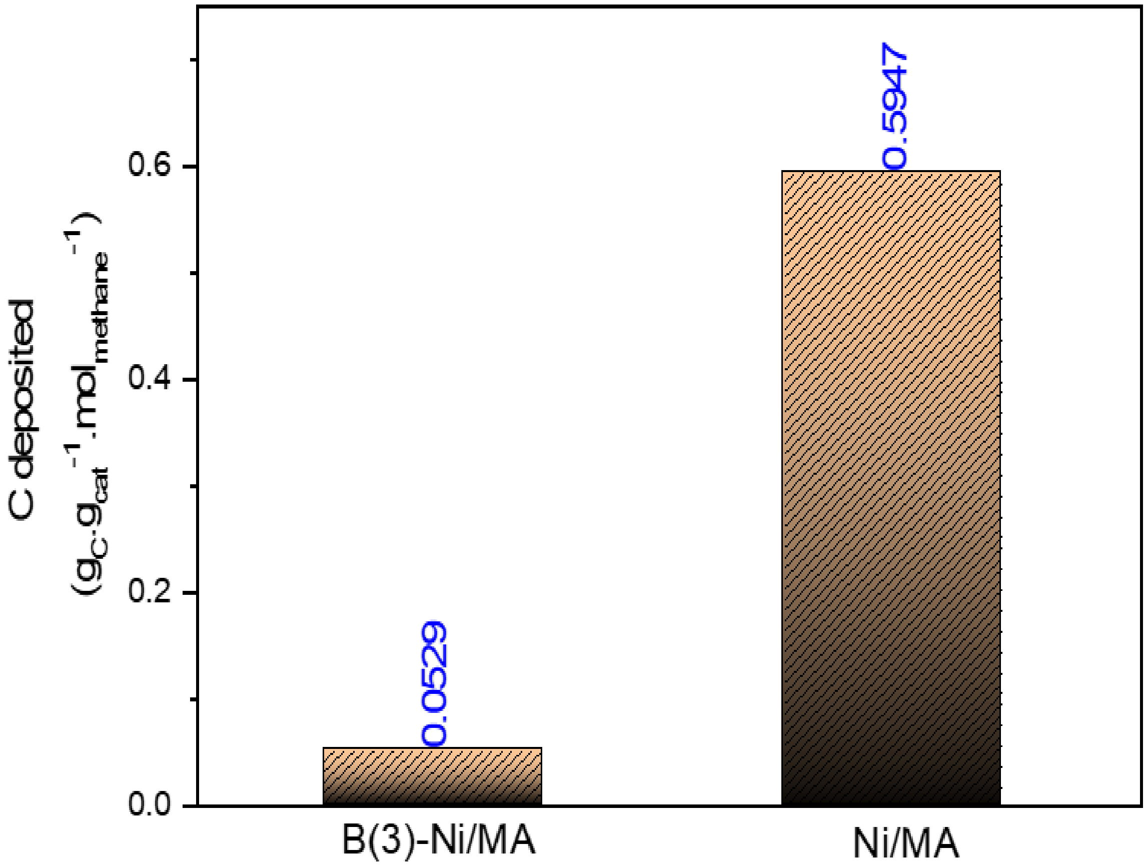

Figure 3.16. Elemental (CHNS/O) analysis of spent Ni/MA and B(3)-Ni/MA catalysts.

The Raman analysis was also performed to examine the characteristics of the deposited carbon. Fig. 3.17 shows the Raman spectra for Ni/MA and B(3)-Ni/MA. Two peaks were observed at about 1310 cm^{-1} for D-band (structural disorder) and 1595 cm^{-1} G-band (Graphitic carbon). The ratio of D-band intensity and G-band intensity (I_D/I_G) estimated the graphitization of the carbon species. The higher values of I_D/I_G for B(3)-Ni/MA (2.95) represent the poor graphitization and the presence of a larger fused carbon ring on the catalyst [129].

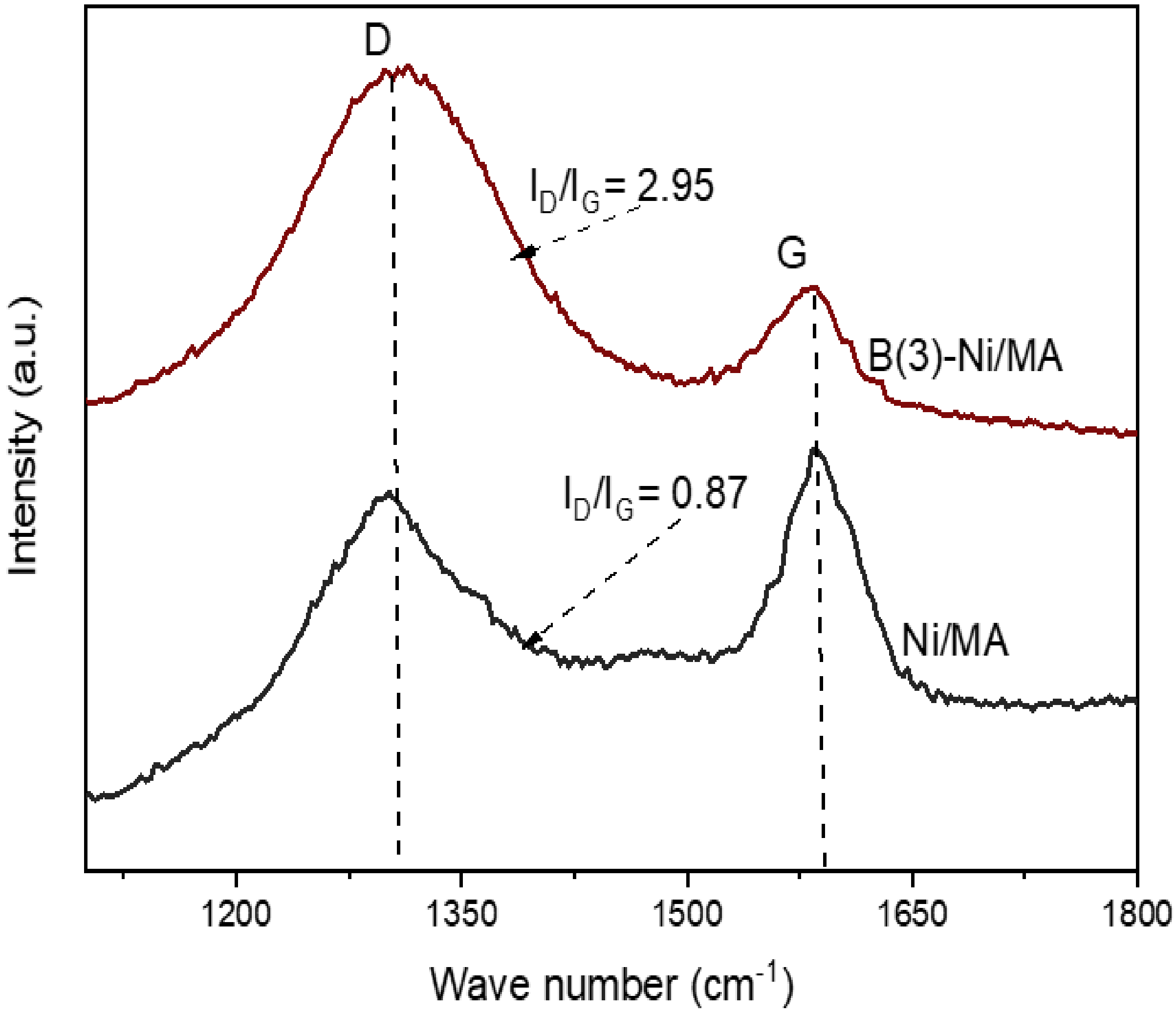

Figure 3.17. Raman Spectroscopy analysis of spent Ni/MA and B(3)-Ni/MA catalysts

The XPS analysis of the spent Ni/MA and B(3)-Ni/MA was also performed to identify the elements' chemical environment changes during DRM. The presence of Ni, Mg, Al, O, and carbon particles was recognized for both B and non-B catalysts, with an additional peak of B for B(3)-Ni/MA catalysts (Fig. 3.18). The sharp peak of B was identified at 189.7 eV in the high-resolution core-level XPS spectrum for the B-containing catalyst and reported in Fig. 3.19. There was no loss of B during the DRM reaction at 600°C, indicating strong interaction of Ni-B species and eliminating the possibilities of elemental B [138]. There was no peak of B in Ni/MA.

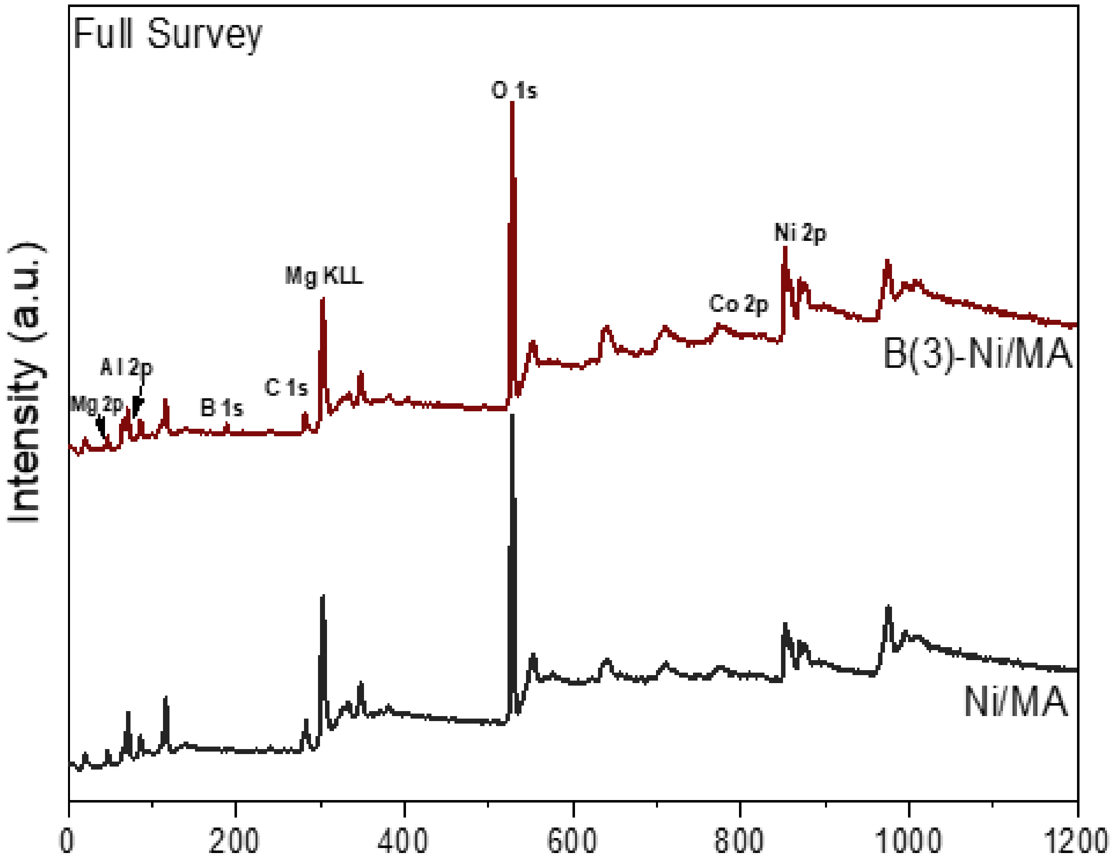

Figure 3.18. XPS analysis of spent Ni/MA and B(3)-Ni/MA catalysts with a full survey of each elements

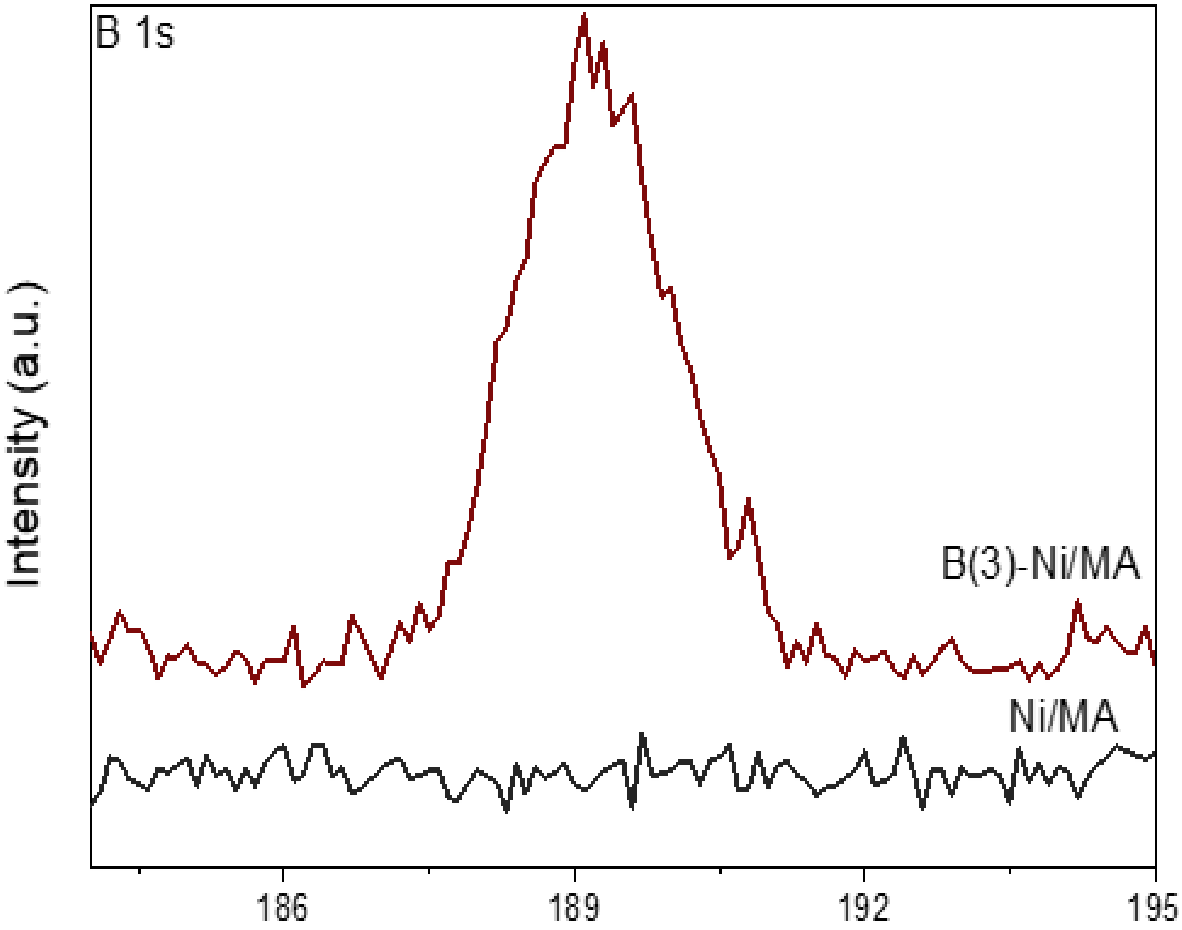

Figure 3.19. XPS B 1s analysis of spent Ni/MA and B(3)-Ni/MA catalysts.

The cumulative fit spectrum of specific resolution for Ni 2p electrons with corresponding satellite peaks for B(3)-Ni/MA is represented in Fig. 4.20. A sharp Ni^0 peak was identified at binding energy 852.6 and 870.3 eV (Fig. 3.20) suggested that the metallic state remained unoxidized during DRM. While, for Ni/MA, the Ni^{2+} corresponding to NiO was identified at 853.5 eV ($p_{3/2}$) along with the peaks of metallic Ni at binding energy 852.6 eV (Fig. 3.21). The result suggested the partial reduction of NiO by produced syngas during DRM [136, 137].

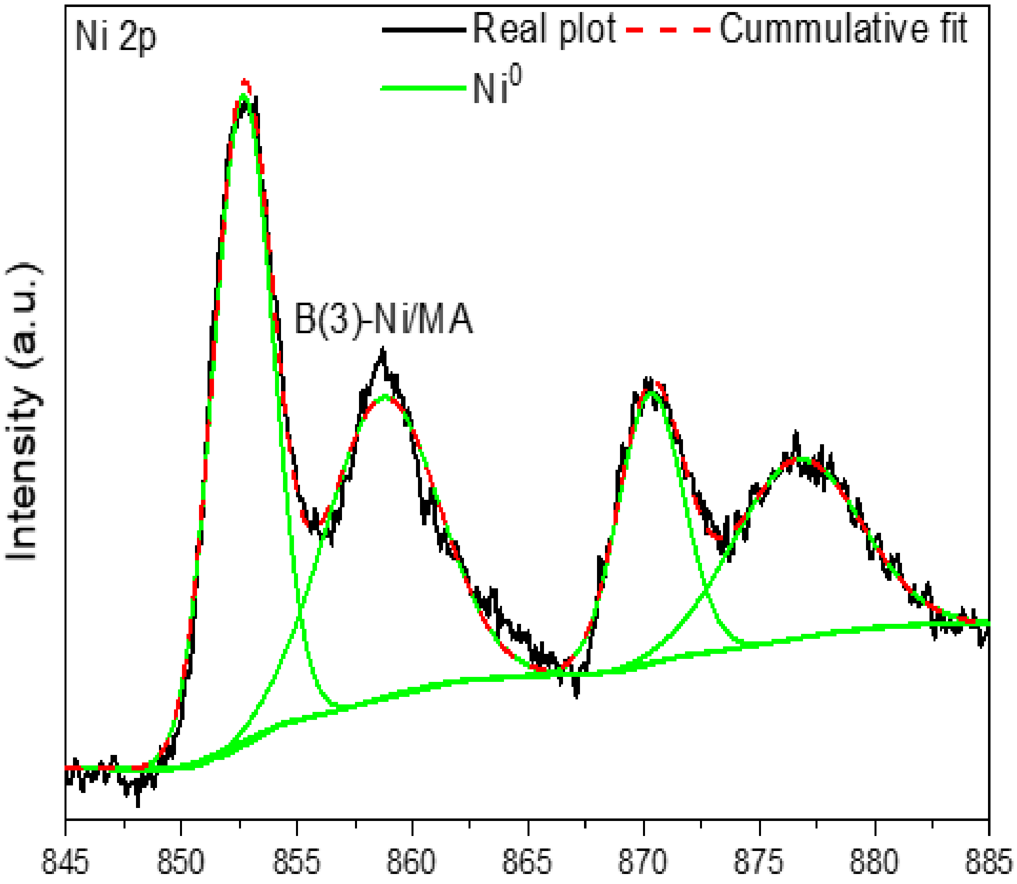

Figure 3.20. XPS analysis of spent B(3)-Ni/MA catalyst for the Ni 2p elemental distributions.

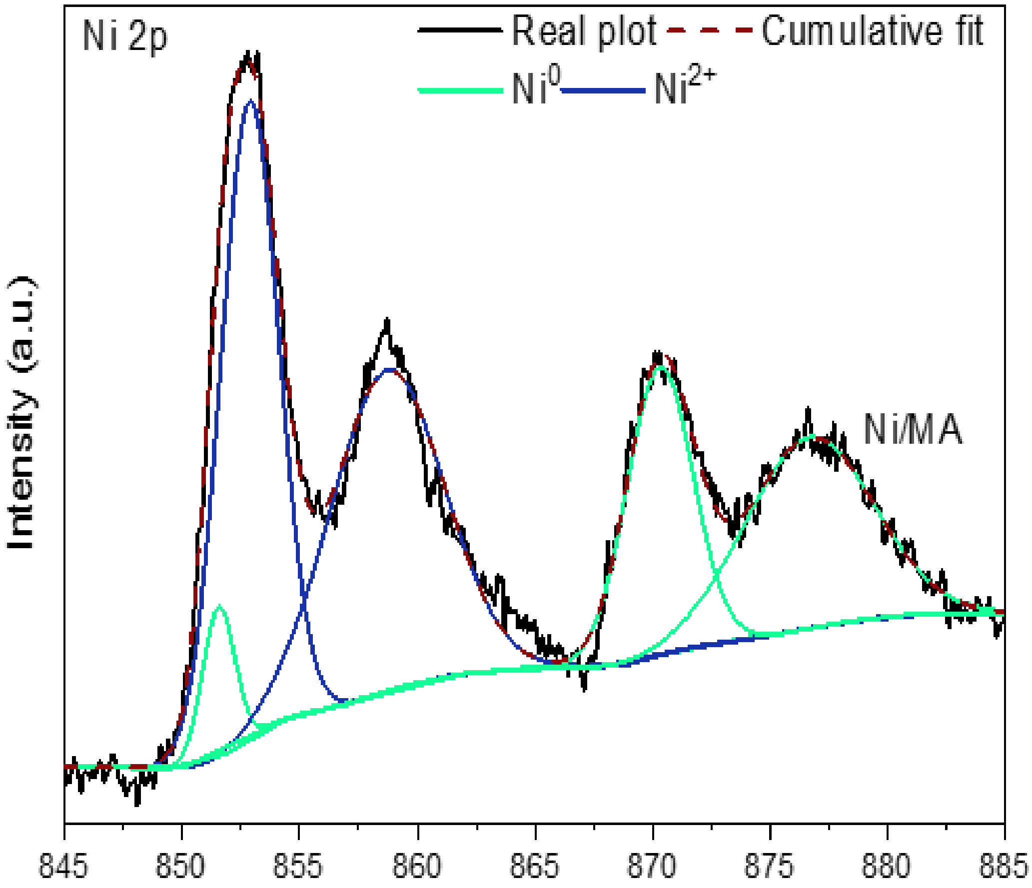

Figure 3.21. XPS analysis of spent non-B Ni/MA catalyst for the Ni 2p elemental distributions

Furthermore, the C-1s peak was observed for the spent catalysts (Fig. 3.22), confirming the formation of carbon during DRM. Three carbon peaks observed that correspond to sp^2 (graphitic), sp^3 (non-graphitic), and oxygenated carbon species were identified at 284.6, 285.9 and 289.3 eV (Fig. 3.22) [48, 145]. However, for the Ni/MA, the graphitic carbon was 2.3 times higher than B(3)-Ni/MA (Fig. 3.23) [146-148]. The results evidenced low graphitic carbon deposition for the B(3)-Ni/MA, which is in line with the Raman analysis, explaining the higher catalytic performance in DRM. For further insightful analysis, HR-TEM of the spent catalysts was carried out (Fig. A9). The presence of graphitic structure observed for Ni/MA catalyst in Fig. A9. However, a nanotube-like structure was observed for B(3)-Ni/MA (Fig. A10) that could be oxygenated and non-graphitic, as shown by Raman XPS analysis [77]. The particle size determination of catalysts suggested a comparatively bigger Ni particle formed after the reaction than the fresh catalyst due to the possible agglomeration and carbon deposition. However, the particle size growth for spent-Ni/MA (increases from 17 to 29 nm) was ~3 times higher than the spent-B(3)-Ni/MA (increases from 7 to 11nm), indicating the presence of B restricted the agglomeration along with carbon deposition and avoided decrement in catalytic activity.

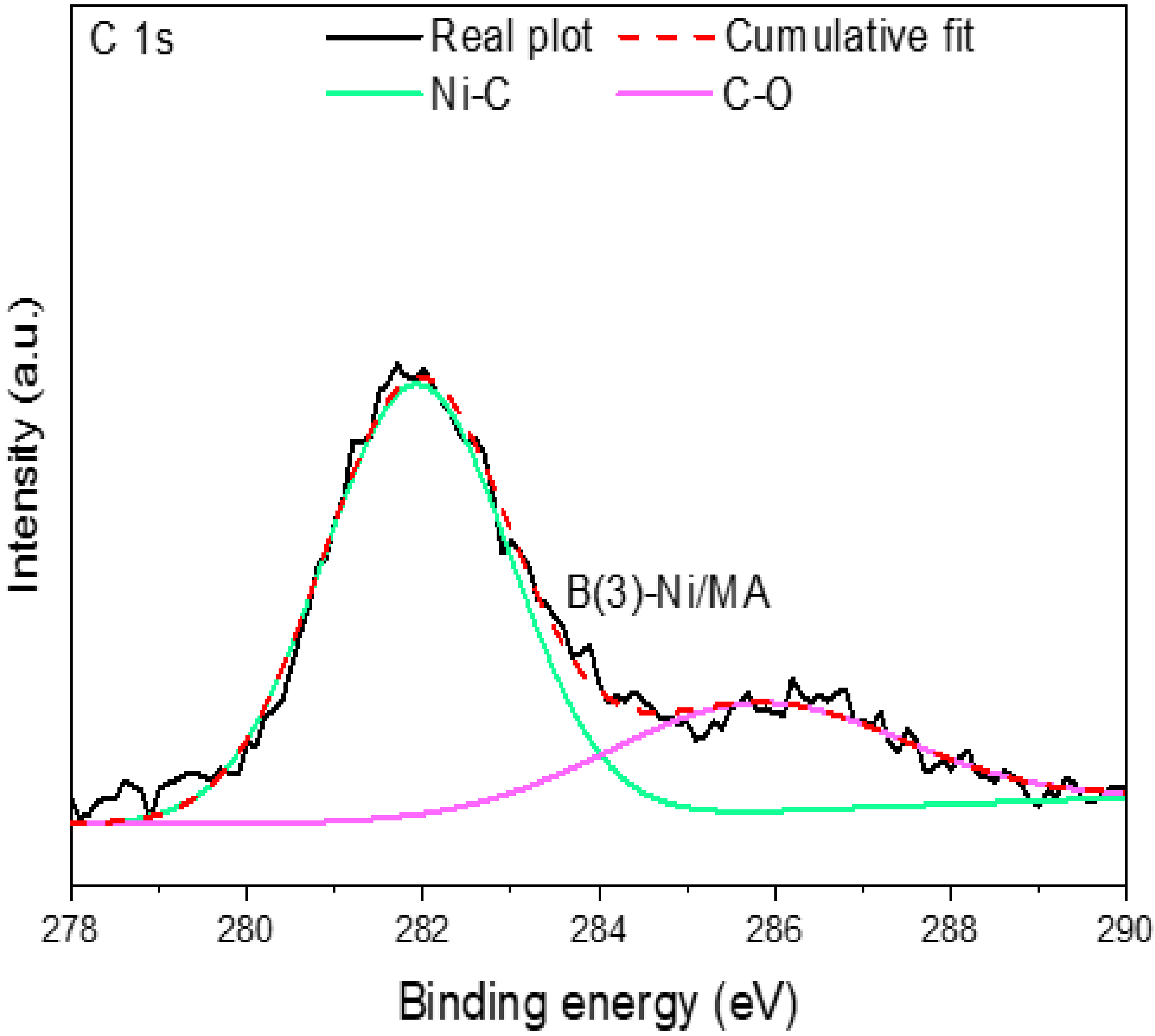

Figure 3.22. XPS analysis of spent B(3)-Ni/MA catalyst for the C 1s elemental distributions.

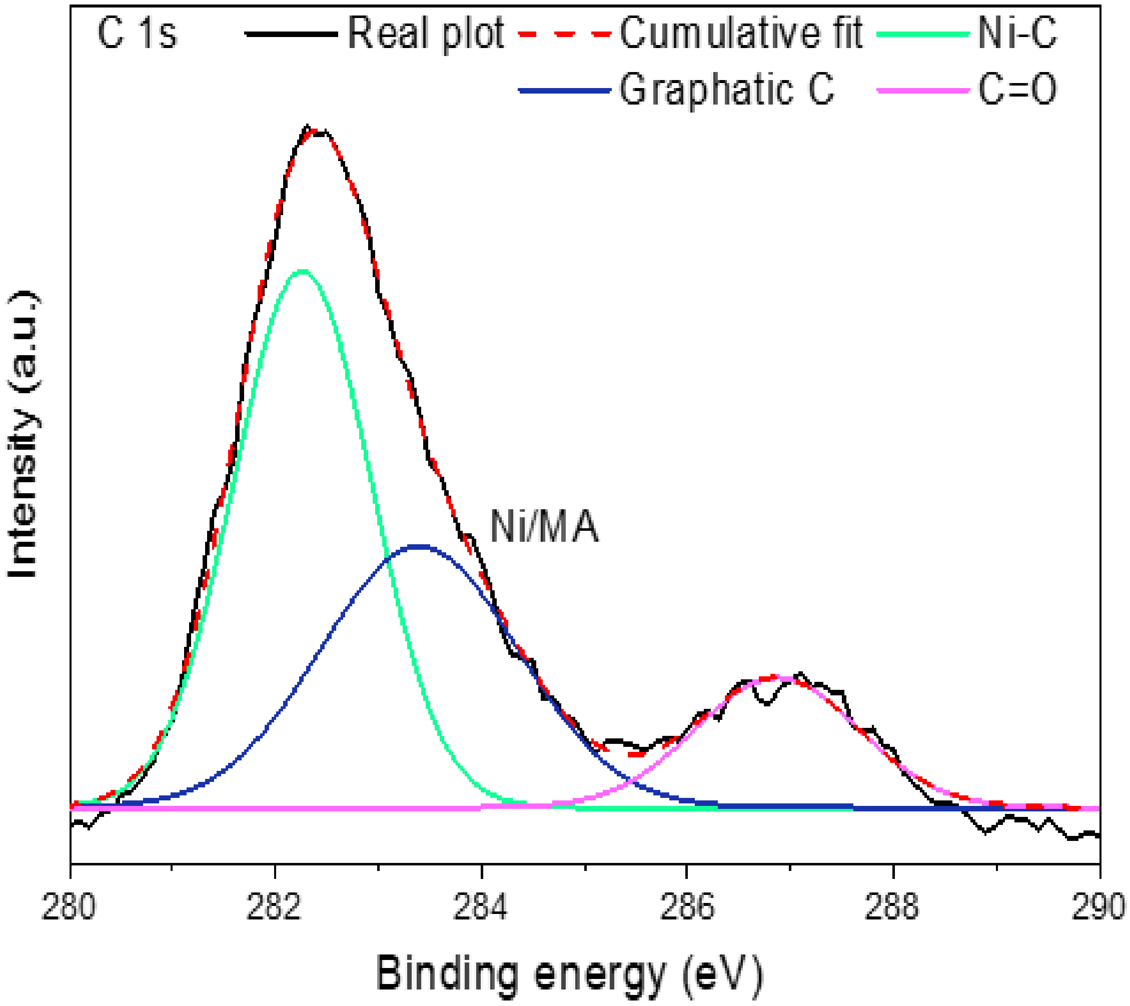

Figure 3.23. XPS analysis of spent B(3)-Ni/MA catalyst for the C 1s elemental distributions

3.3 Role of boron:

A series of B-containing B(x)-Ni/MA catalysts were synthesized by the $NaBH_4$ reduction method appears as a one-step catalyst preparation method as $NaBH_4$ plays two crucial roles - doping of B and reduction Ni-salt to Ni^0 and Ni-B. The detailed investigations of the catalysts confirmed the presence of metallic Ni and Ni-B species. It is also realized that smaller particle size (~7 nm) for the B-containing catalyst than the non-B Ni/MA (17 nm). It is generally accepted that the smaller Ni size helps enhance catalyst performance and suppress the deactivation of the catalysts for DRM, an optimized size of 6-9 nm suggested in a number of reported studies [103, 149, 150]. The B(x)-Ni/MA catalysts tested for the DRM reaction, which further revealed catalyst with 3 wt.% B showed excellent performance among the prepared catalyst with 2.61 times higher $\mathrm{TOF}_{\mathrm{CH_4}}$ compared to the non-B catalyst. The decline in conversion was also insignificant, about ~9.7% for the B(3)-Ni/MA catalyst compared to the Ni/MA catalyst (~49%). The drop in non-B (Ni/MA) catalyst conversion was also reported in the recent literature listed in Table 3.2. Extremely low C deposition was observed over the catalyst surface due to the B at the subsurface sites of Ni surfaces that block C diffusion into nickel lattice as B and C both exhibits similar chemisorption on Ni surface, as suggested by Xu et al. [105]. Interestingly, the Raman analysis disclosed the nature of deposited carbon over the catalyst surface and suggested a graphitic (carbon) free catalyst for the B(3)-Ni/MA catalyst compared to non-B Ni/MA catalyst due to higher values of I_D/I_G value that further verified by the XPS analysis of the spent catalysts. The retainment of B after the DRM was also revealed by XPS analysis of spent catalysts, which means B was successfully seated at the subsurface site that possessed difficulty for the resilient carbon to form over the surface. B-containing catalyst helps to control the surface acidity of the catalysts and improve the metal–support interactions for the DRM [103, 151, 152].

3.4 Outcomes:

The current study shows enhancement of catalyst performance by adding B by the one-step $NaBH_4$ catalyst reduction method for the DRM reaction. The catalyst preparation method using $NaBH_4$ appears to be the prime source of dispersing B on Ni-based catalyst and a straightforward way for reducing metal salts. The B(x)-Ni/MA catalysts enhanced the conversion of CH_4 and CO_2 and promoted graphitic free DRM reaction. The maximum conversion was CH_4: 18.75% and CO_2: 30.61% for B(3)-Ni/MA catalyst and the corresponding $\mathrm{TOF}_{\mathrm{CH_4}}$was 0.31 s^{-1} which is 2.61 times higher compared to non-B catalyst. Interestingly, the deposition of resilient graphitic carbon for the B catalyst was significantly lower (~11 times) than the non-B catalyst. It was found that the presence of B facilitated the formation of Ni-B species along with metallic Ni (reduced by $NaBH_4$), controlled the particle size and stabilized the metallic state, and influenced the Ni-C interaction leading to the advancement in catalytic performance and diminution in deactivation.

Chapter 4

NaBH$_4$ assisted synthesis of B-(Ni-Co)/MgAl$_2$O$_4$ nanostructure for catalytic dry reforming of methane

This chapter is published with title ''NaBH$_4$ assisted synthesis of B-(Ni-Co)/MgAl$_2$O$_4$ nanostructure for catalytic dry reforming of methane'' by MD Shakir, Manohar Prasad, Koustav Ray, Siddhartha Sengupta, Apurba Sinhamahapatra, Shaomin Liu, Hari Vuthaluru in ACS applied nano material.

4.1 Results & discussion:

4.1.1 Compositional and structural analysis:

The prepared catalysts [B-Ni/MA, B-(75Ni-25Co)/MA, B-(50Ni-50Co)/MA, B-(25Ni-75Co)/MA and B-100-Co/MA] were characterized by using ICP-OES to find out the elemental composition as shown in Table. 4.1. The results showed ~14 wt.% of total metal content, and the ratio of Ni/Co as 2.94, 1.03, and 0.35 for B-(75Ni-25Co)/MA, B-(50Ni-50Co)/MA, B-(25Ni-75Co)/MA respectively. The B content ranges from 2.4 to 2.8 wt %, that confirmed the presence of B and $NaBH_4$ acted as source for B. As $NaBH_4$ is highly reducing agent so it is very important to evaluate the reduction behavior of the catalysts prepared by the $NaBH_4$ reduction method. The H_2-TPR analysis was performed for all $NaBH_4$ assisted B-containing catalysts reported in Fig. 4.1. Generally three peaks is expected in the H_2-TPR profile for non-reducing synthesis method for Ni-Co/MA catalysts reported in the previous studies, A similar H_2-TPR profile were observed for the non-B 75Ni25Co/MA (Fig. B1), which attributes to the weak, medium and strong interaction of metal-oxide (MO) and support reducibility behavior of the catalyst [37, 51, 129]. However, the $NaBH_4$ reduced Ni-rich catalysts showed only two H_2 consumption peaks which corresponds to the reduction of weak and medium interacted MO [37, 51, 128, 129]. The H_2 consumption observed at a lower temperature (300-350°C) is attributed to the reduction of the bulk metal oxide (MO) cluster, which has a weak interaction with the support [128, 129, 153]. The H_2 consumption at 430-450°C is observed due to the medium interaction of the metal oxide with the support [51, 129]. Interestingly, reduction of MO at higher temperature (>600°C) was not observed for Ni-rich $NaBH_4$ reduced catalyst that represents the reduction of MO during the synthesis of catalysts. However, a high temperature peak (647.6°C) was observed for monometallic B-Co/MA catalyst suggested comparatively poor reduction of MO [51, 128]. The H_2 -TPR profile of the bimetallic catalysts displayed dissimilarities compared to the monometallic catalysts also suggesting the co-existence of Ni and Co. Further, the degree of reduction (DOR) of the catalysts was also calculated from H_2-TPR profile reported in Table. 4.1. A comparatively low DOR was observed for bimetallic catalysts indicating a greater extent of reduction of catalyst prepared by $NaBH_4$ reduction method. The BET surface area of all catalysts [B-Ni/MA, B-(75Ni-25Co)/MA, B-(50Ni-50Co)/MA, B-(25Ni-75Co)/MA and B-100-Co/MA] was also performed and listed in Table. 4.1. The surface area of bi-metallic catalyst was almost similar ~70 m^2/g, whereas the surface area for monometallic B-Co/MA catalyst was higher that could be due to poor dispersion of

Co over the support surface. However, the catalysts surface area is not directly relatable to the reactivity of catalysts for DRM reported in previous studies [16].

Table 4.1. Structural properties of the MA supported and metal loaded B-containing catalysts.

Sample	**Composition [a] (wt %)**			**Surface area [b] (m^2/g)**	**Degree of reduction [c] (%)**	**Active sites [d] (mmol/g)**
	Ni	Co	B			
B-Ni/MA	13.76	-	2.75	75.59	21	0.143
B-(75Ni 25Co)/MA	10.89	3.71	2.68	69.98	19	0.165
B-(50Ni 50Co)/MA	6.79	6.58	2.80	70.29	16	0.156
B-(25Ni 75Co)/MA	3.87	11.14	2.62	69.67	16	0.112
B-Co/MA	-	13.98	2.45	74.01	29	0.138

[a] ICP- OES; [b] BET, [c] H_2-TPR; [d] H_2-TPD

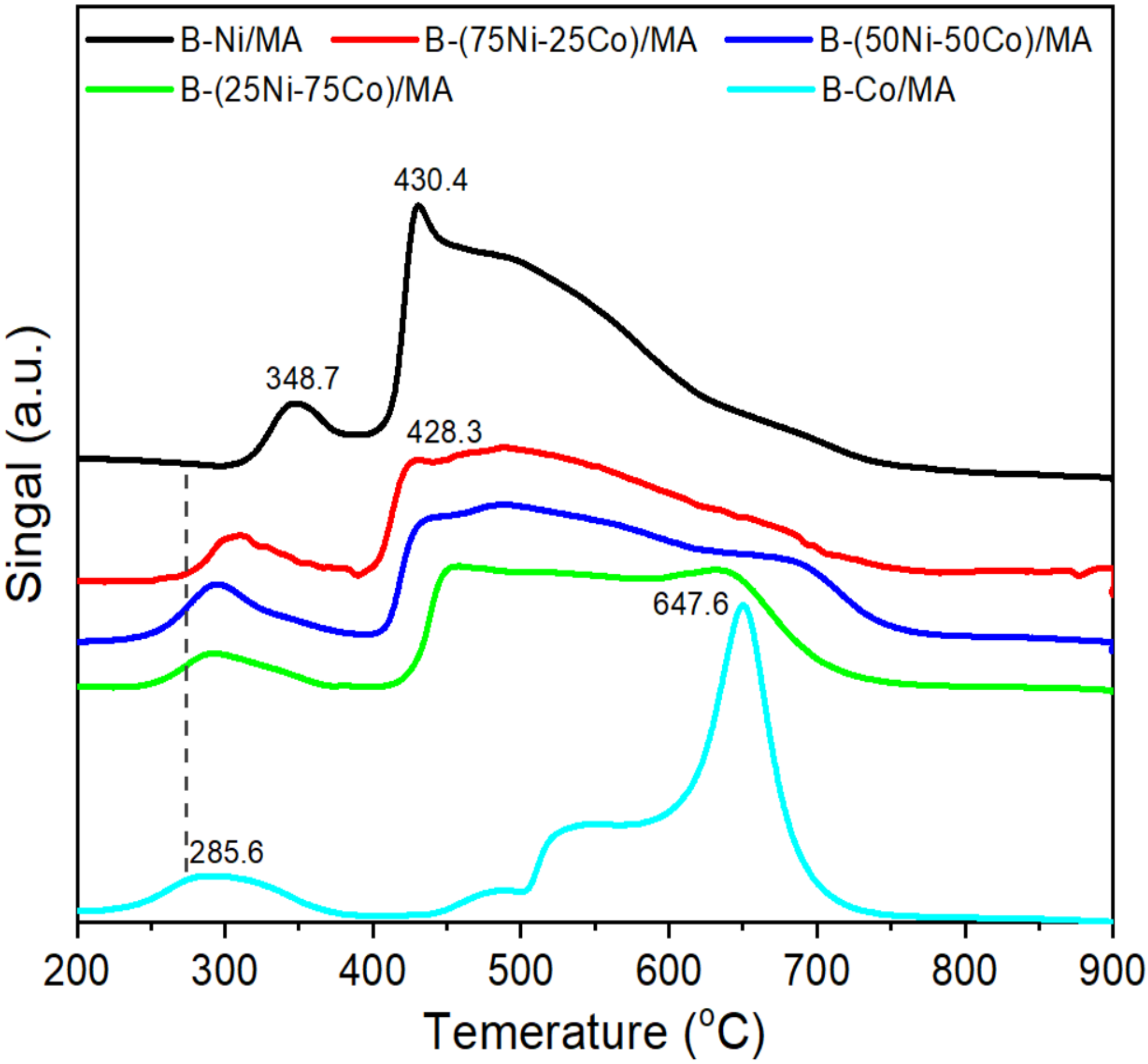

Figure 4.1. H_2-TPR profiles of as-prepared samples by the $NaBH_4$ reduction method.

The XRD analysis was performed for $NaBH_4$ reduced as-prepared catalyst (Without any heat treatment) and N_2 treatment catalysts (Fig. 4.2). The peaks for support MA were observed at 2θ: 31.34, 36.80, 44.85, 59.40, and 65.34° corresponding to JCPDS Card No. 77-1203 in Fig. B2 [33, 99, 122]. The peaks related to Ni/Co species was not so prominent for as-prepared catalysts (Fig. 4.2a) due to poor crystallinity of Ni/Co.

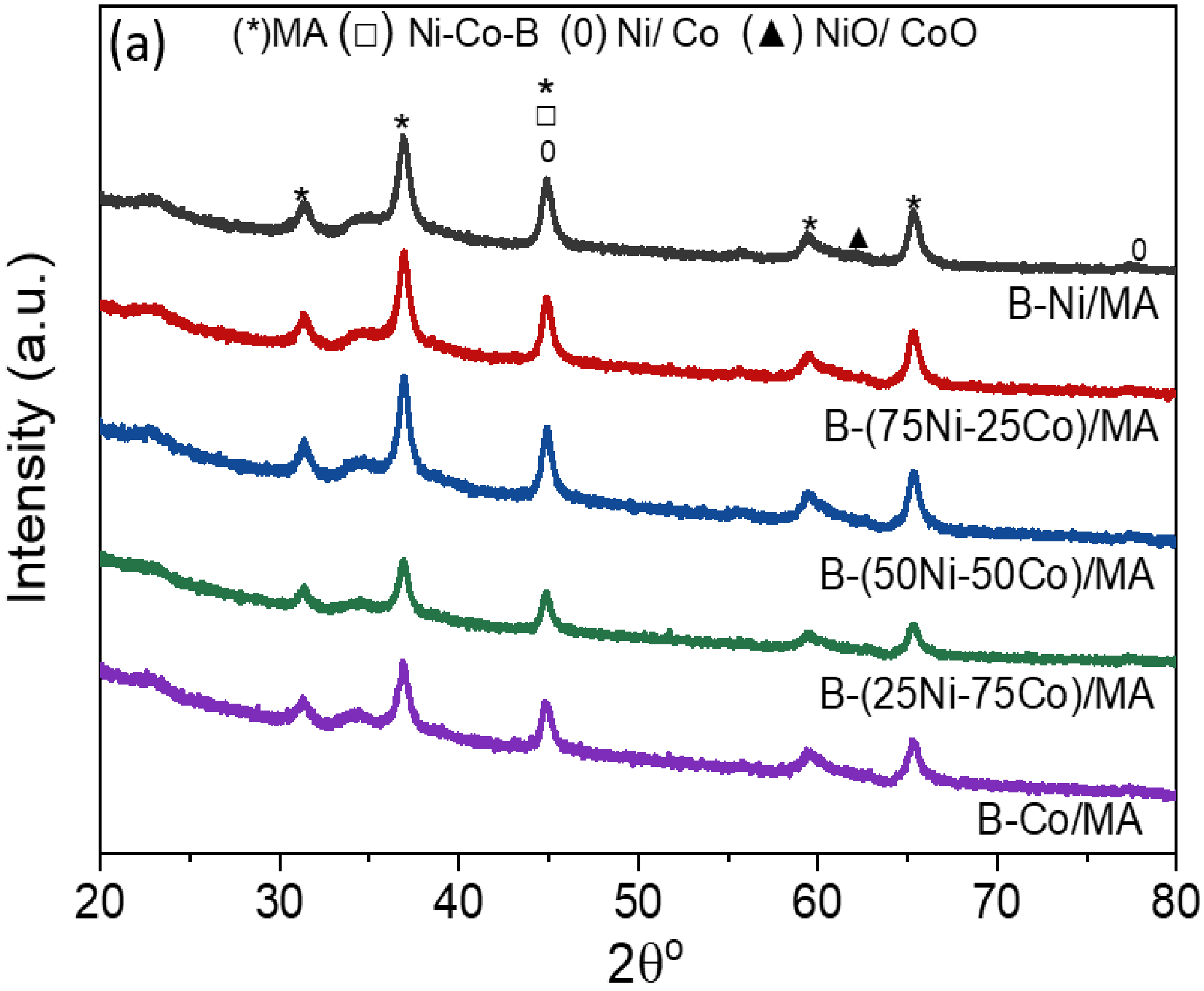

Figure 4.2a. XRD pattern of $NaBH_4$ reduced catalysts as-prepared catalysts without any further treatment for B-Ni/MA, B-(75Ni-25Co)/MA, B-(50Ni-50Co)/MA, B-(25Ni-75Co)/MA and B-100-Co/MA catalysts.

Fig. 5.2b they appeared after annealing at 600°C in N_2 environment. The peak at $2\theta = 77.30°$ were observed for the metallic-Ni (JCPDS Card No. 04-0850) for B-Ni/MA, B-(75Ni-25Co)/MA, B-(50Ni-50Co)/MA, B-(25Ni-75Co)/MA and B-100-Co/MA catalysts and observed same for non-B catalyst in Fig. S2 [40, 99, 122]. The formation of B-Ni, B-Co and B-Ni-Co was also observed at $2\theta = 44.78°$ (JCPDS No. 17-0335) represents the presence of B in form of Ni and Co boride which is in-line with the previous studies reported for the catalysts synthesized by the $NaBH_4$ reduction methods [124, 125, 154]. A weak peak at $2\theta = 62.21°$ (JCPDS Card No. 47-1049) was indicated for the presence of NiO or CoO due to the partial reduction of the catalysts during the synthesis by the $NaBH_4$ reduction method [39, 40, 99]. However, no separate peak of Co was appeared for bimetallic catalysts due to the multi-peaks overlapping [37, 40, 51]. However, the oxide phase of B which is B_2O_3 were also not identified in XRD profile that generally appears at 2θ = 27.4 and 39.8° which suggested difficulty of the formation of the amorphous glassy phase of B compounds [103, 155, 156].

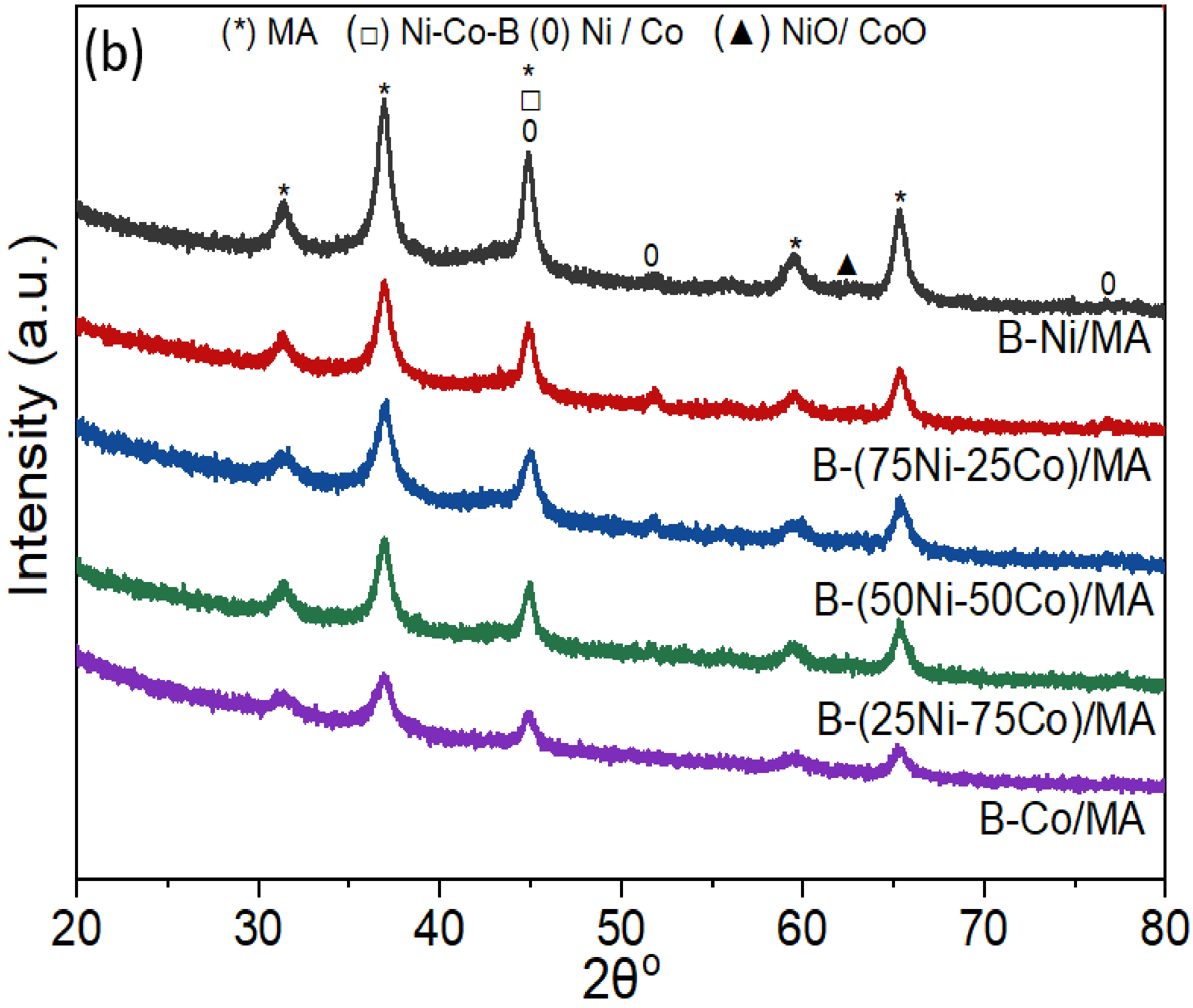

Figure 4.2b. XRD pattern of $NaBH_4$ reduced catalysts as-prepared catalysts after N_2 treatment at 600°C for B-Ni/MA, B-(75Ni-25Co)/MA, B-(50Ni-50Co)/MA, B-(25Ni-75Co)/MA and B-100-Co/MA catalysts.

The XPS analysis was performed for both B and non-B (75Ni-25Co)/MA catalysts to gain insight into the chemical environment of the elements like Mg, Al, Ni, Co, O and B. Fig. 4.3 shows full survey XPS spectrum indicating the presence of Mg, Al, Ni, Co and O for both catalyst B and non-B catalysts. Additionally, a sharp B peak were also observed for the B-(75Ni-25Co)/MA catalyst in Fig. 4.4 showed a high-resolution core-level XPS spectrum of B 1s. The peak at 189.4 eV suggested the interaction of metal-B, which is in line with the XRD analysis that revealed the formation of Ni-Co-B at 2θ = 44.78° (Fig. 4.2b) and reported studies about the formation of metal-boride by $NaBH_4$ method [111, 157-161]. There was no oxidizing (B_2O_3) or alloy B formation which generally appears at BE 188.1 and 192.5 eV [162].

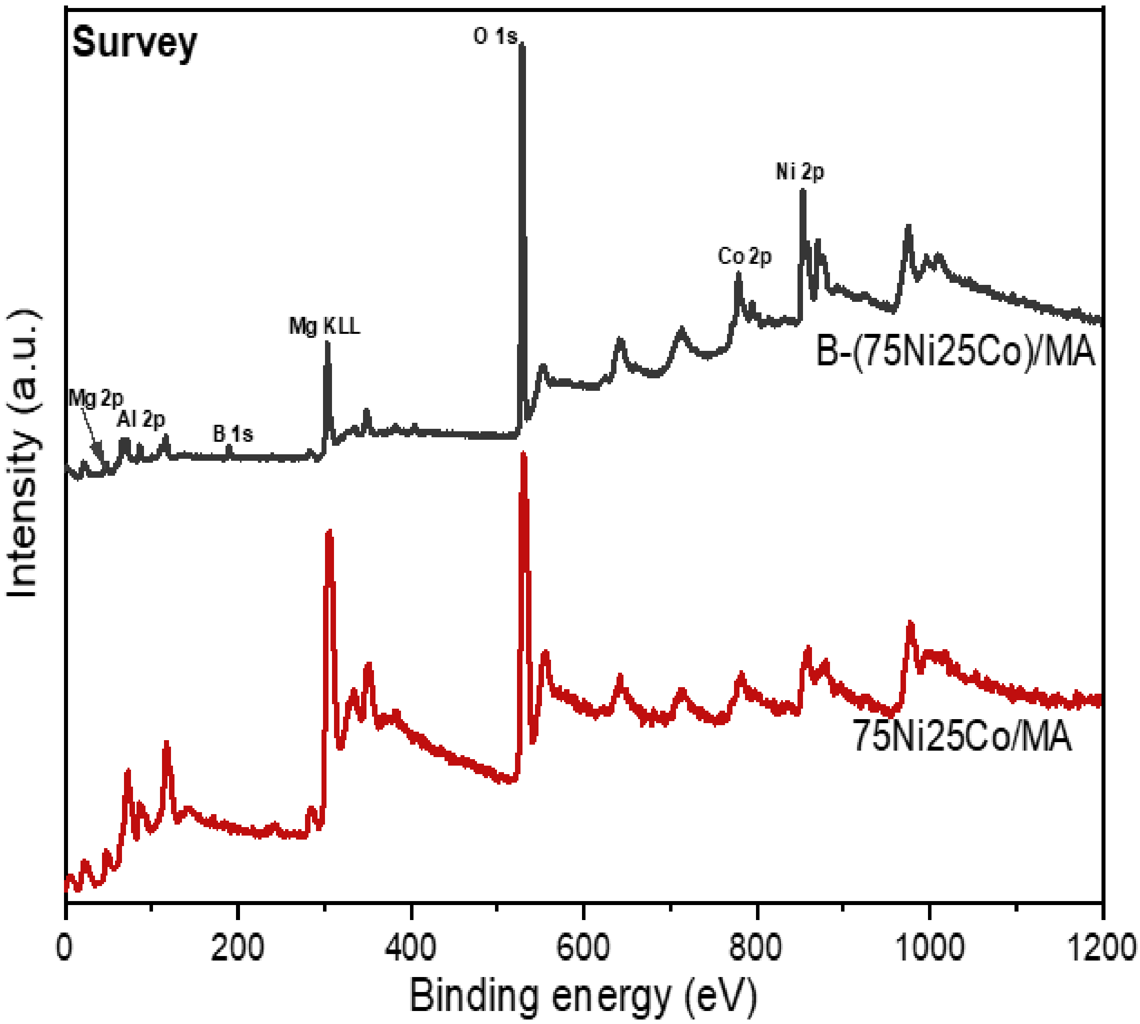

Figure 4.3. XPS analysis of B-(75Ni-25Co)/MA and non-B 75Ni-25Co/MA catalysts with a full survey of each element.

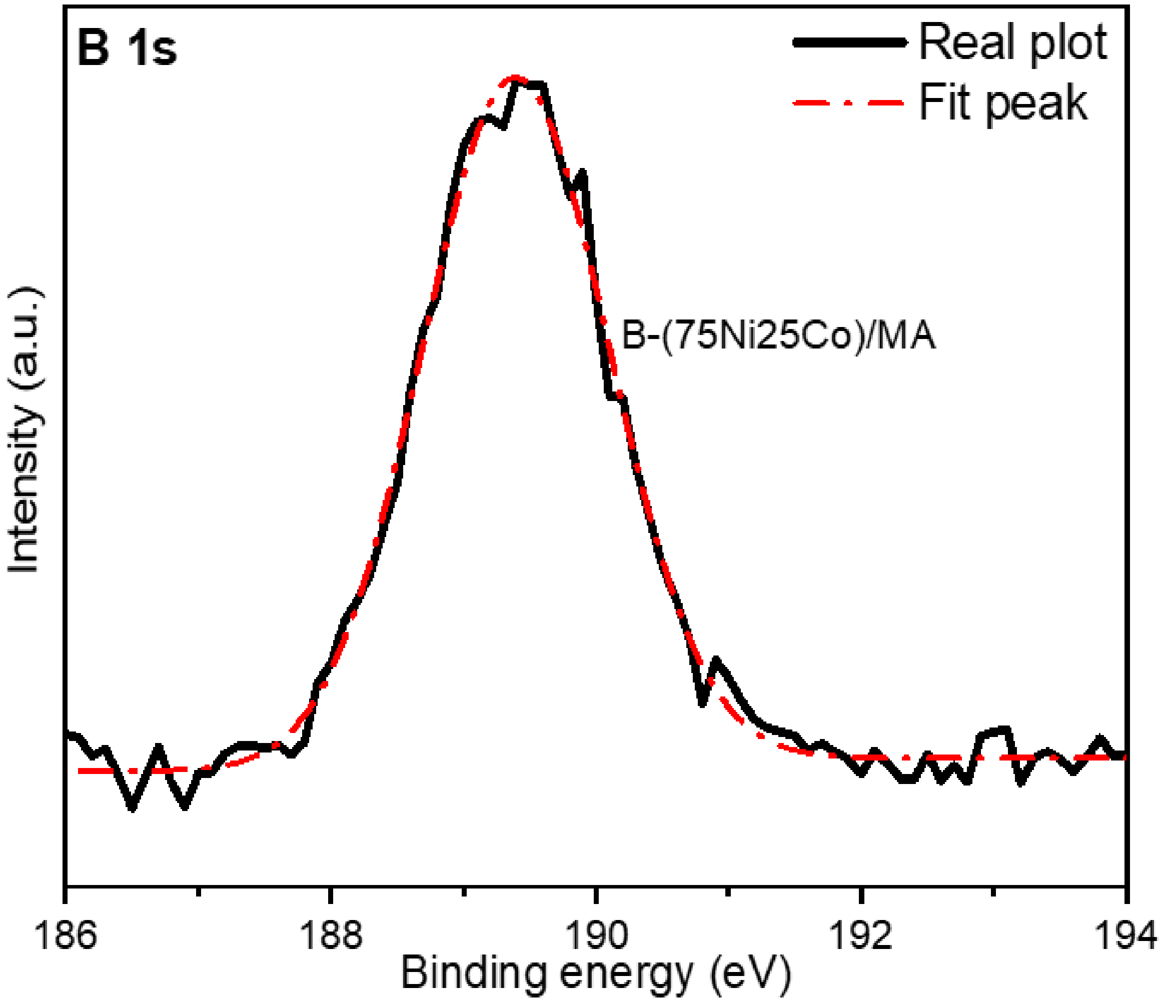

Figure 4.4. XPS analysis of B-(75Ni-25Co)/MA catalysts for B 1s.

The high-resolution core-level Ni 2p XPS spectrum for B (Fig. 4.5) and non-B (Fig. 4.6) showed multiple peaks after deconvolution, including peaks for $2p_{3/2}$, $2p_{1/2}$ electrons, and corresponding satellite peaks. The observed peaks for both B and non-B catalyst at binding energy 852.7 and 870. 4 eV with a split-split coupling of 17.7 eV, were attributed to Ni $2p_{3/2}$ and Ni $2p_{1/2}$ electron, respectively of metallic state of mixed Ni-Co-B [136, 137, 162]. However, the peaks observed at 853.4 ($p_{3/2}$) and 872.4 eV ($p_{1/2}$) for B-catalyst confirmed the Ni^{2+}, which is in-line with the previous studies [162]. A strong presence of corresponding satellite peaks was also recorded for Ni^0 and Ni^{2+}.

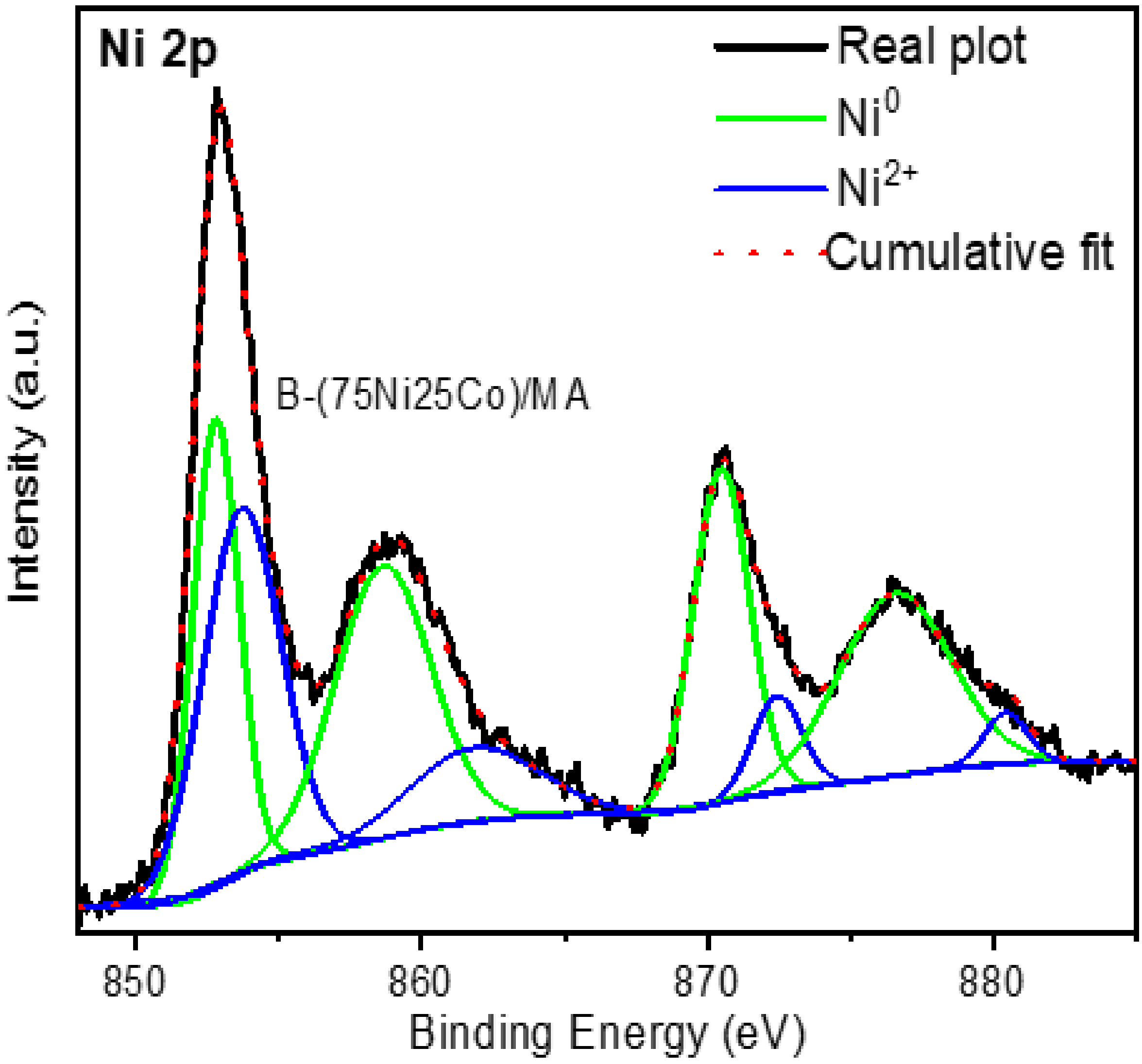

Figure 4.5. XPS analysis of B-(75Ni-25Co)/MA catalysts for Ni 2p.

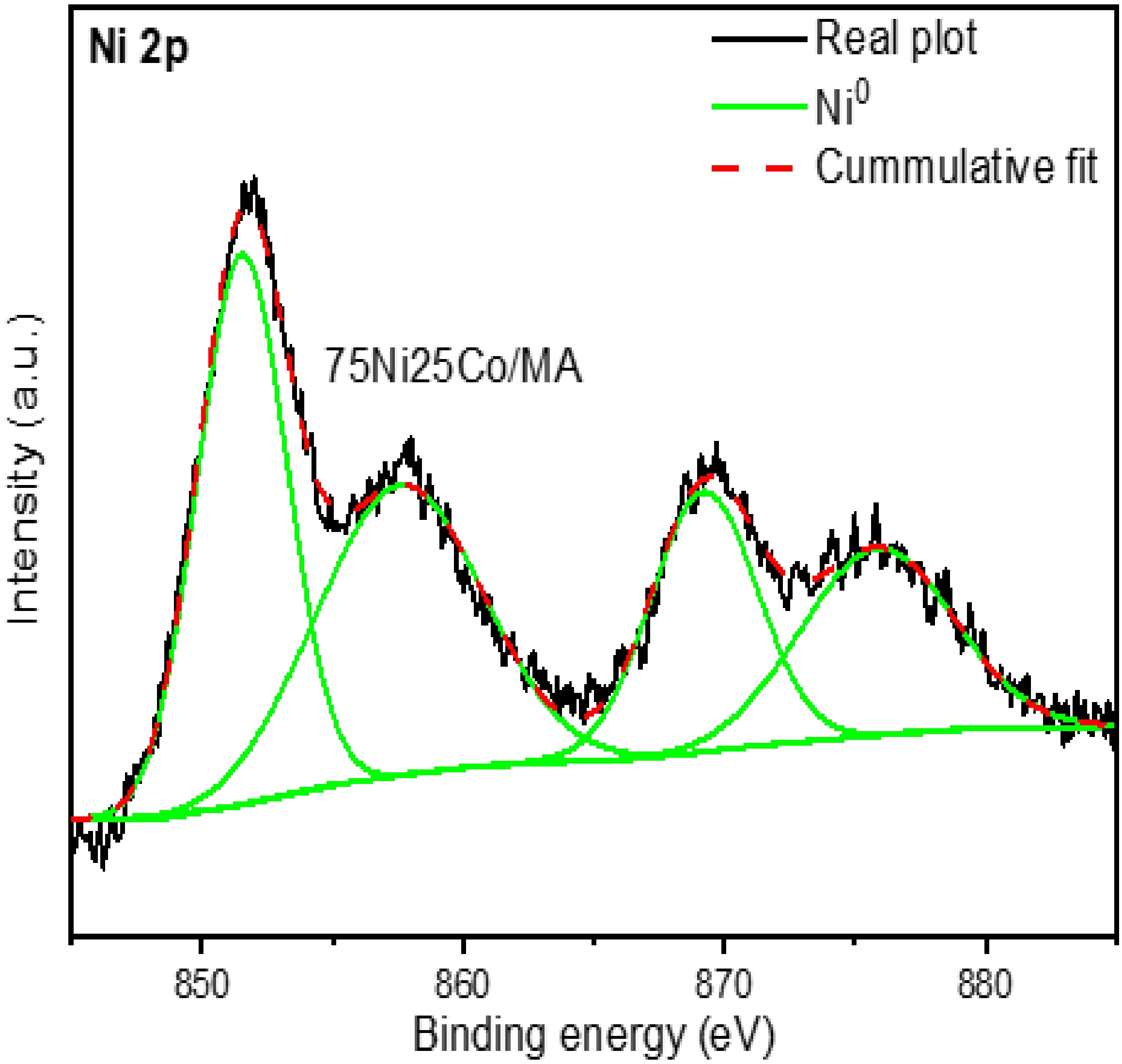

Figure 4.6. XPS analysis of non-B 75Ni-25Co/MA catalysts for Ni 2p.

Further, the high-resolution core-level Co 2p XPS spectrum for B (Fig. 4.7) and non-B (Fig 4.8) catalysts. It also confirmed the metallic Co ($2p_{3/2}$:778.0 and $2p_{1/2}$:794.0 eV) for both B and non-B catalysts and Co^{2+} ($2p_{3/2}$: 779.2, $2p_{3/2}$:799.1 eV) for B catalyst [162]. As conclusion, the surface composition of nano-particle B-(75Ni-25Co)/MA catalyst contains metallic M^0 and M^{2+} formed Metal-B interaction. The catalyst prepared by one-step $NaBH_4$ reduction method appears promising method for reduction of metal salt to metal and incorporates B. The above XPS analysis is in line with the XRD and H_2-TPR analysis.

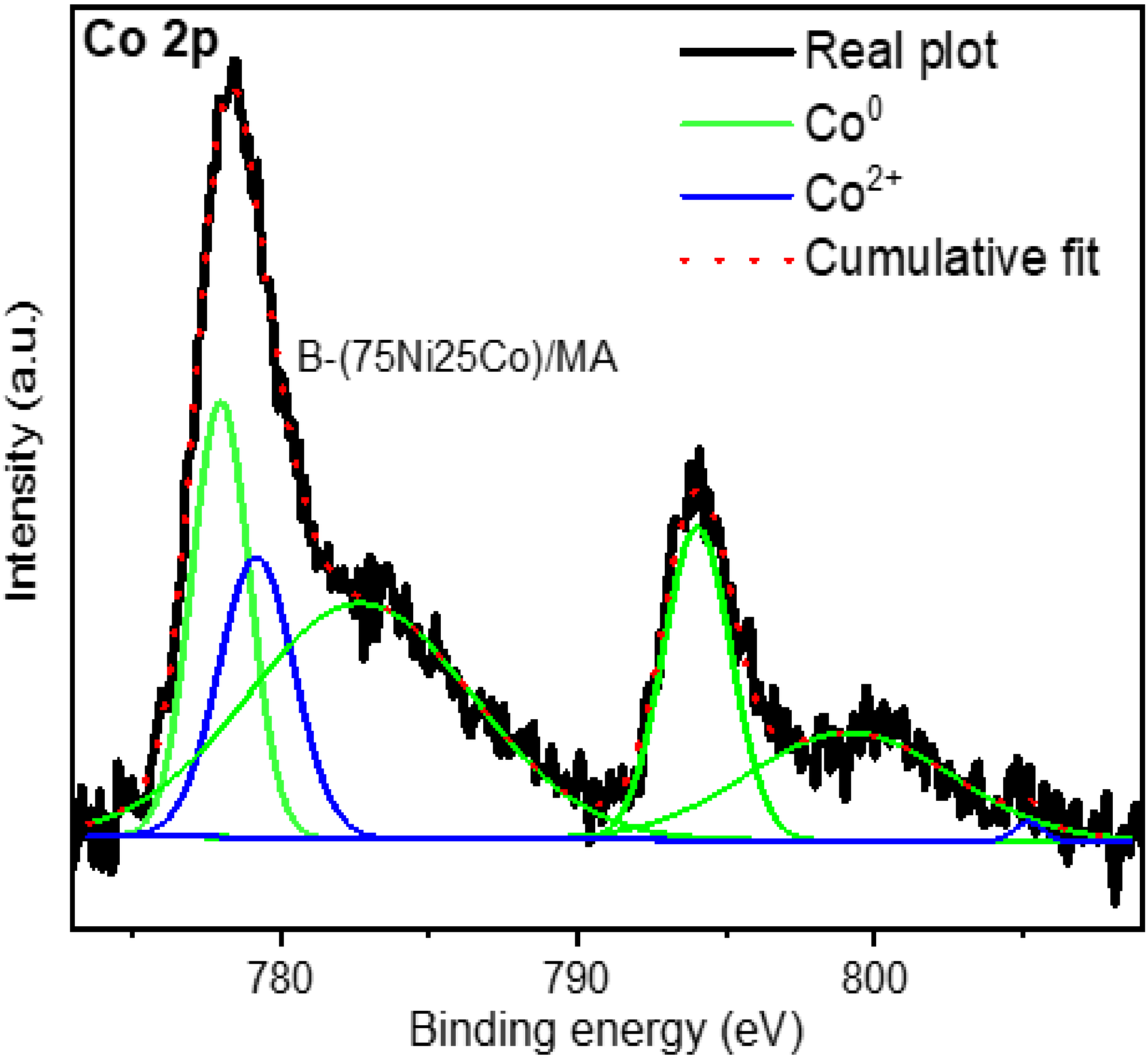

Figure 4.7. XPS analysis of B-(75Ni-25Co)/MA catalysts for Co 2p.

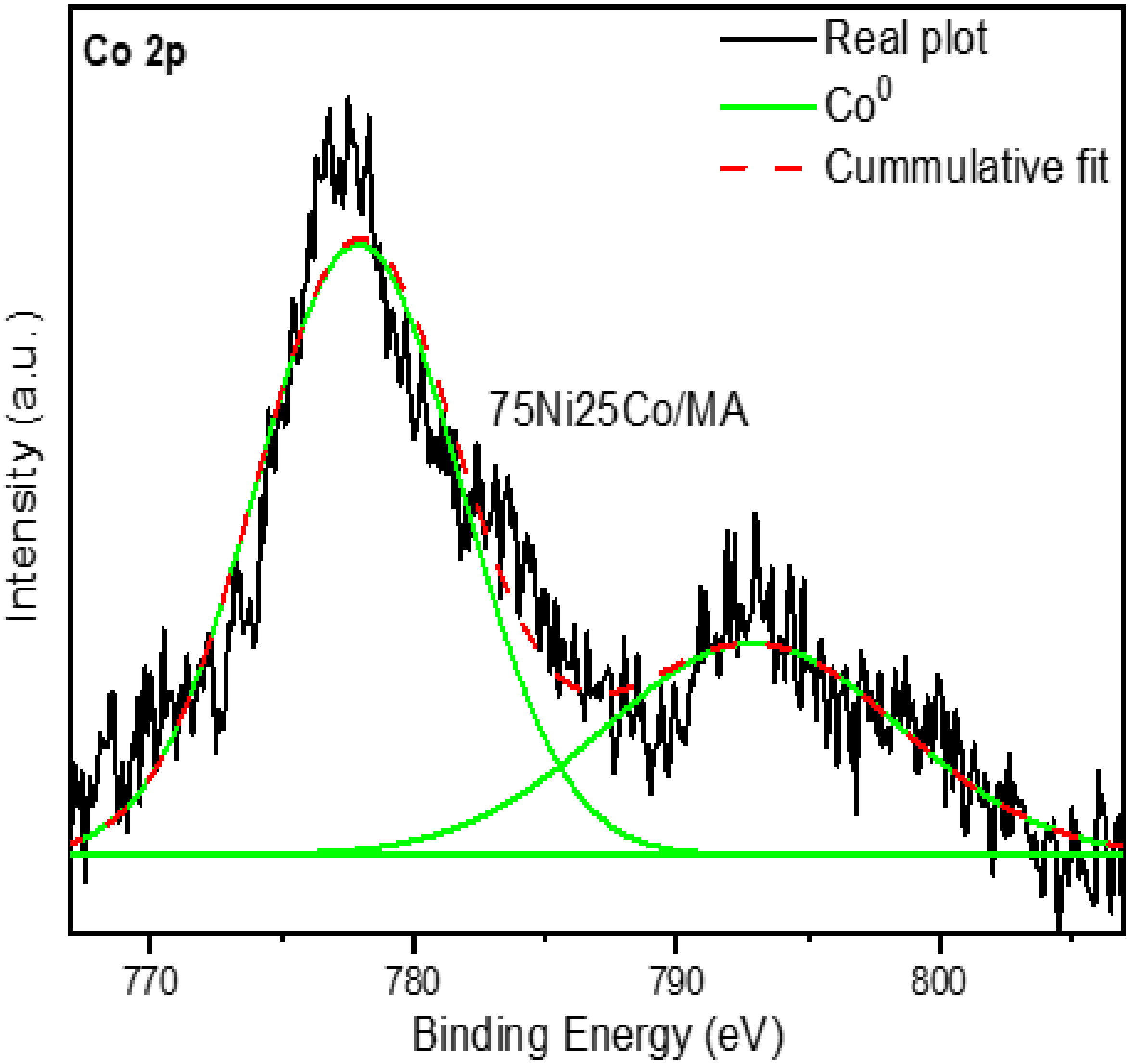

Figure 4.8. XPS analysis of non-B 75Ni-25Co/MA catalysts for Co 2p.

4.1.2 Morphological analysis:

The HR-TEM analysis was performed for the N_2 treated B-(75Ni-25Co)/MA catalyst (Fig. 5.9). A nano rod-type Ni-Co-B grafted on the two-dimensional flakes of support MA were observed with the metallic Ni-Co and Ni-Co-B species. The higher magnified image (Fig. B3) revealed the presence of the metal nano-rods type structure with average size ~ 6-7 nm. Further, the lattice fringes of the metal and support was clearly observed. The d-spacing 0.21, 0.203 and 0.30 nm that attributed to presence of alloy Ni-Co and Ni-Co-B species [140-142]. The B interacted with number of Ni-Co nanospacies and form B-$(Ni\text{-}Co)_x$, same observation reported in the previous studies [114, 141, 163-165]

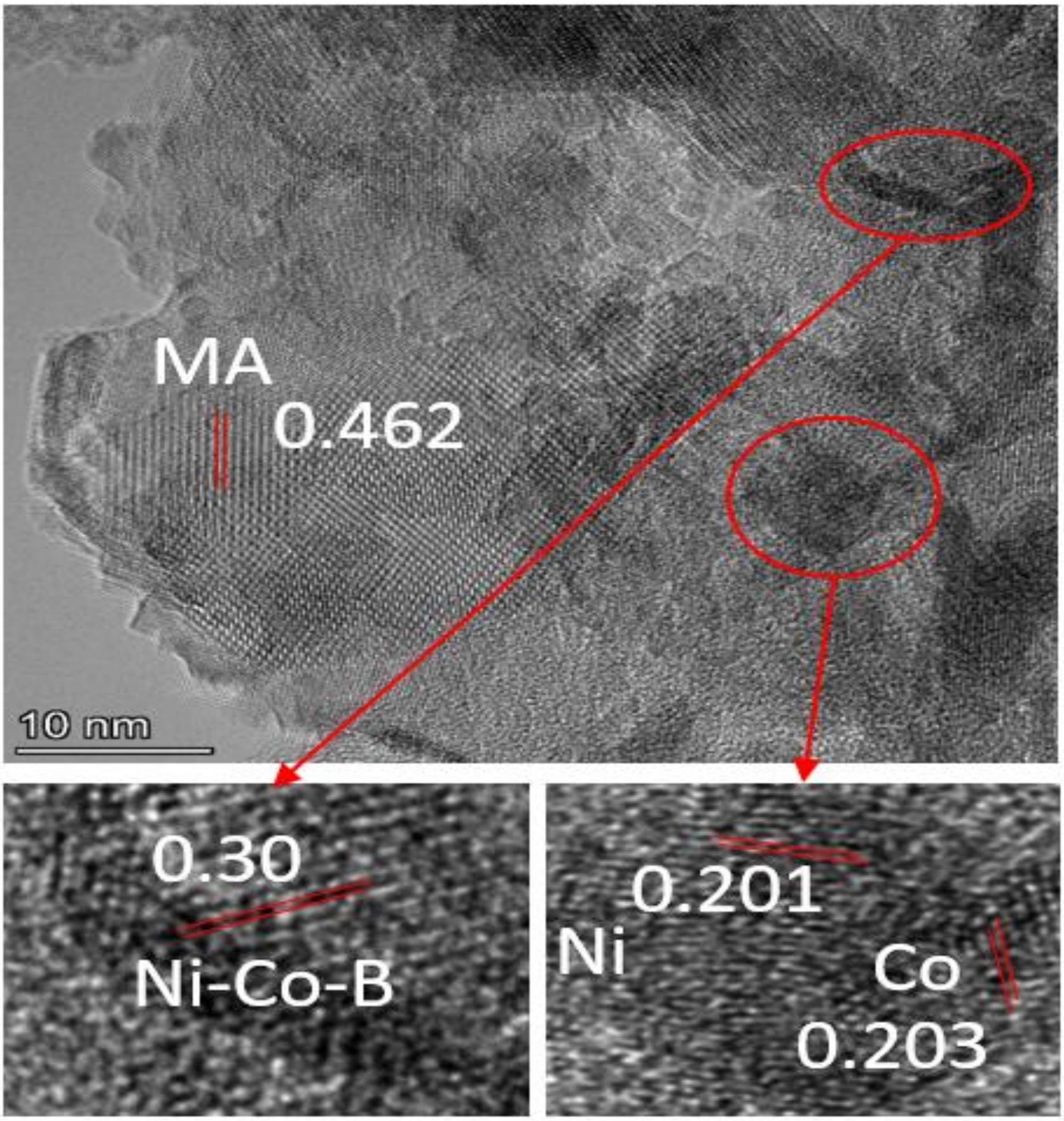

Figure 4.9. HR-TEM image and lattice fringes for B-(75Ni-25Co)/MA catalysts with the lattice fringes of Ni, Co and Ni-Co-B along with the support MA.

Fig. 4.10a represents the EDS analysis of the catalyst that also confirmed the presence of Ni, Co, Mg, Al, O and B with a zoomed B spectrum (Fig. 4.10b). The EDS compositional analysis results are in line with the ICP-OES analysis of the catalyst within ±1% (Table. B2). The SAED pattern displays the bright dots and dotted rings corresponding to metal and MA support, respectively (Fig. 4.10c) [30]. It has been reported that the nano-rods offers a higher number of surface-active metal sites for the catalytic reaction [122, 166].

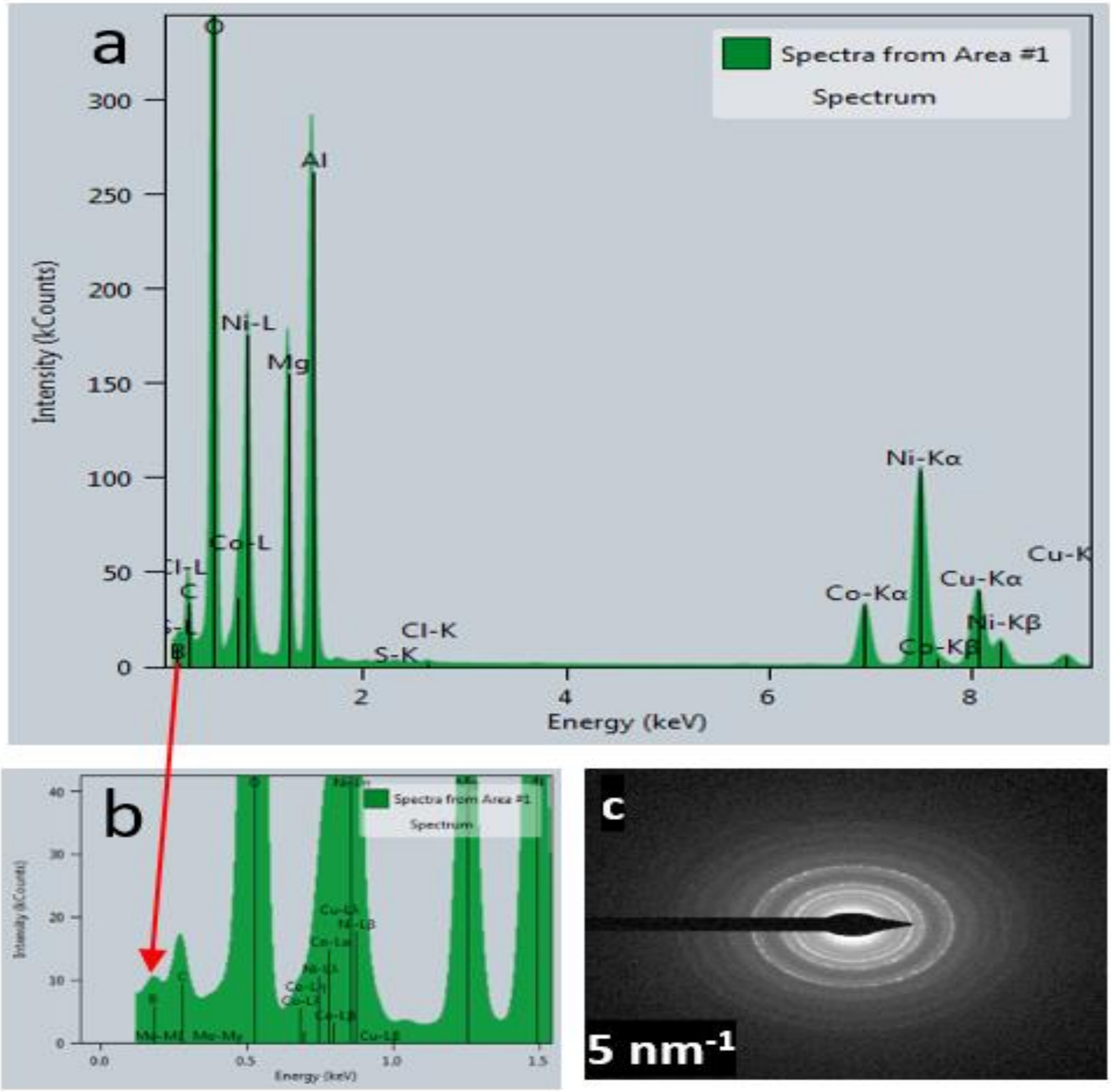

Figure 4.10. (a) ESD profile (b) Zoomed image and (c) SAED pattern of B-(75Ni-25Co)/MA catalyst.

The elemental mapping using HAADF S-TEM analysis for catalyst represented in Fig. 4.11. A clear distribution of individual particle was observed for the B-(75Ni-25Co)/MA catalyst prepared by the one-step $NaBH_4$ reduction method.

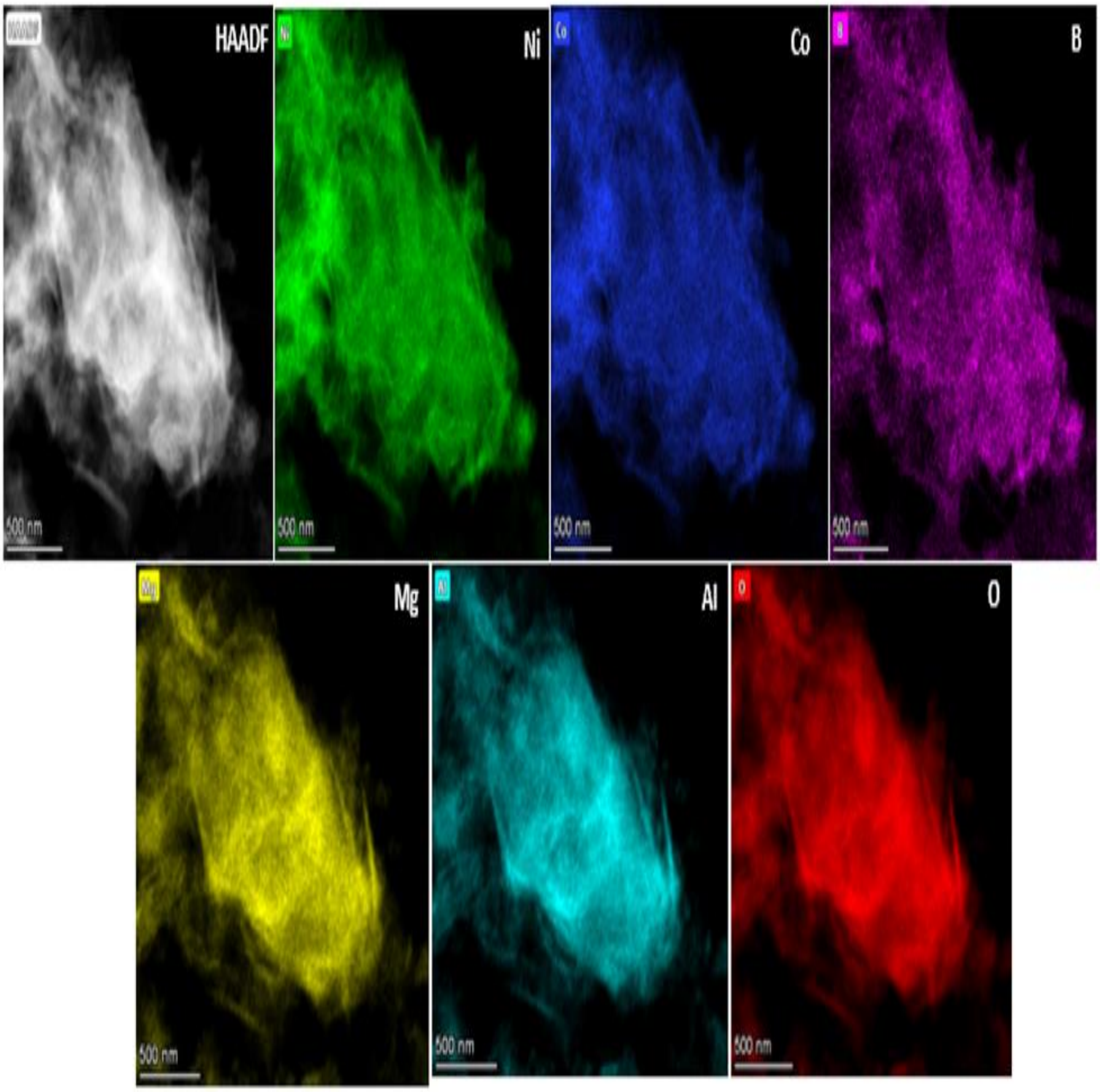

Figure 4.11. S-TEM HAADF elemental distribution of B-(75Ni-25Co)/MA catalyst.

4.1.3 H_2-Temperature programmed desorption (H_2-TPD) and metal dispersion:

The prepared catalysts [B-Ni/MA, B-(75Ni-25Co)/MA, B-(50Ni-50Co)/MA, B-(25Ni-75Co)/MA and B-100-Co/MA] were also characterized by H_2-TPD shown in Fig. 4.12. The H_2 desorption profile followed similar trends for all catalysts. Two major peaks were observed for all the B containing catalysts, a lower temperature peak observed at ~100-135°C and a higher temperature peak at ~600°C. The bimetallic catalysts showed a broader and intense peak for physisorbed H_2 compared to the monometallic catalysts suggested a higher ability of H_2 adsorption due to the addition of second metal and presence of more metallic content in the bimetallic catalysts.

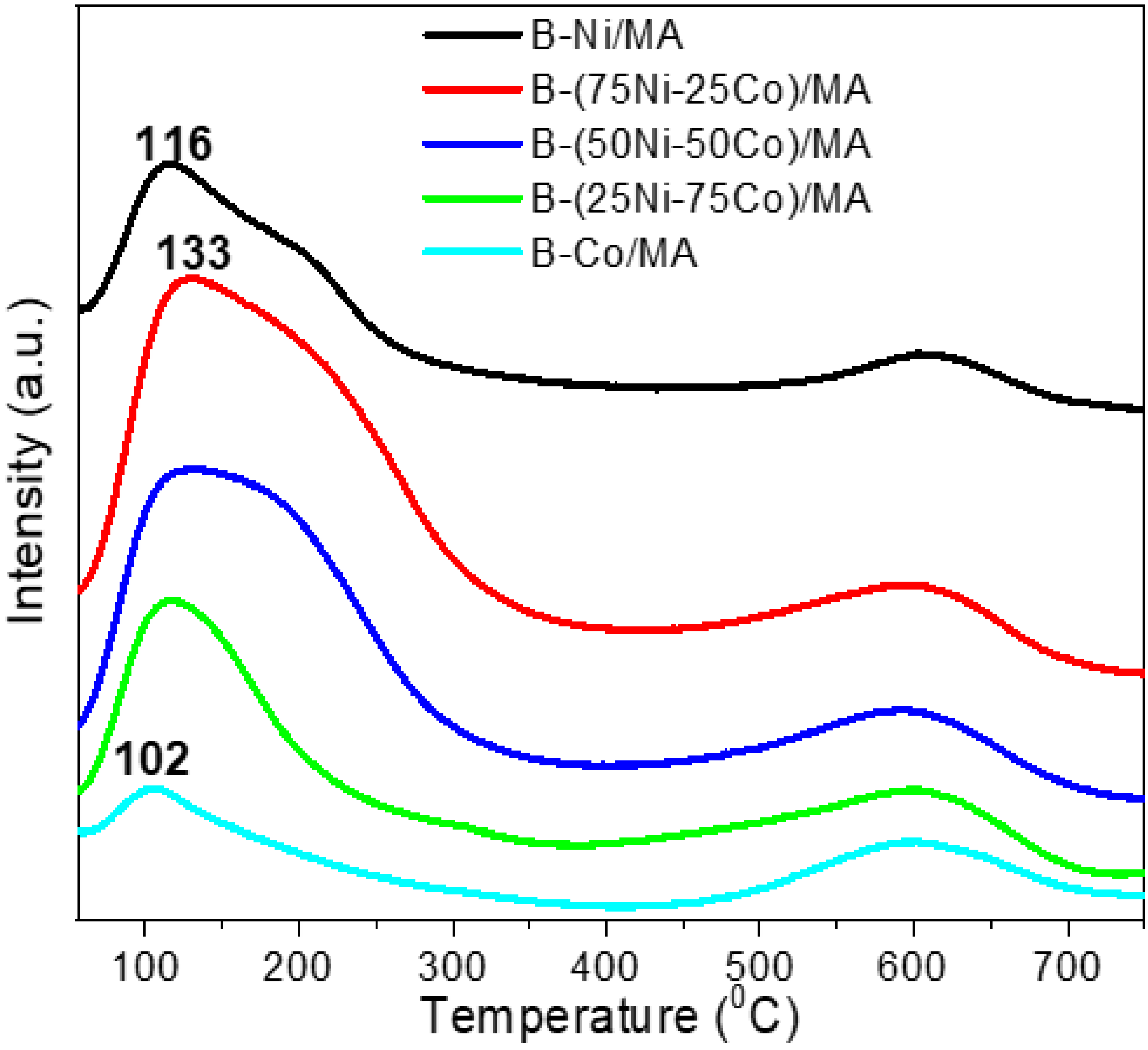

Figure 4.12. H_2-TPD profile of B-Ni/MA, B-(75Ni-25Co)/MA, B-(50Ni-50Co)/MA, B-(25Ni-75Co)/MA and B-Co/MA catalysts.

The H_2-uptake from the H_2-TPD were also calculated and listed in Table. B1. The metal dispersion (%) from this H_2-uptake presented in Fig. 4.13. The maximum metal dispersion was 6.46% for B-(75Ni-25Co)/MA, which is ~1.52 times higher compared to the previous work for non-B similar 75Ni-25Co/MA catalyst reported by Kumari et al. [37] was ~4 times higher from the Ni/MA catalyst reported by N Hadian et al. [17]. Furthermore, the metal dispersion was observed decreased with increasing Co content for the bimetallic catalysts. Similar results were also reported for Ni-Co/Al_2O_3 catalyst [37, 41]. The higher metal dispersion for B-(75Ni-25Co)/MA could result from the synergic effect of Co addition in a particular ratio of Ni/Co = 3 and the presence of B. In addition, the active sites of the catalyst were also calculated from the H_2-TPD profile and reported in Table. 4.1. The trend of metal active sites was in line with the metal dispersion with highest value of 0.165 mmol/g for B-(75Ni-25Co)/MA catalyst.

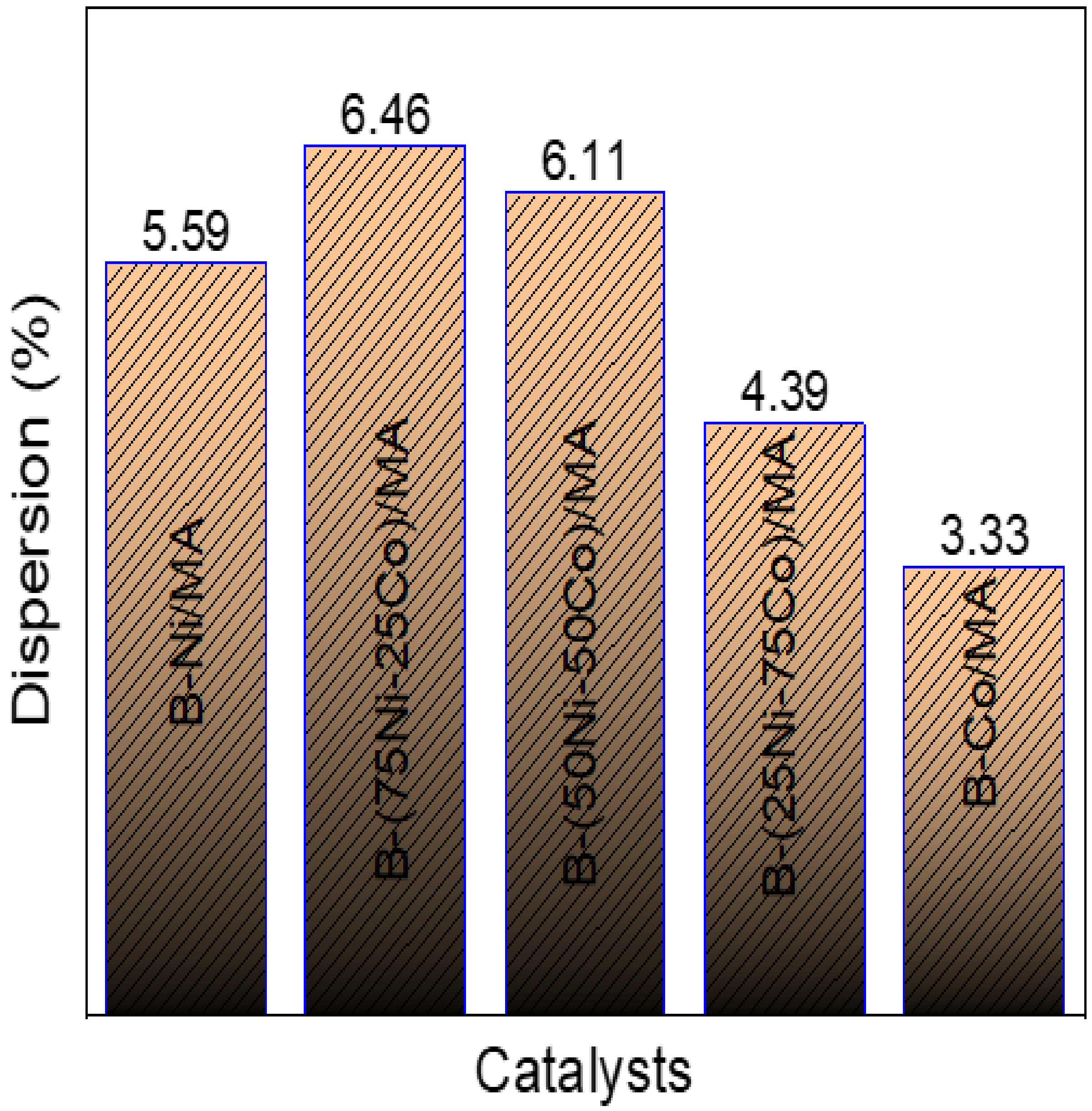

Figure 4.13. Metal dispersion (%) of B-Ni/MA, B-(75Ni-25Co)/MA, B-(50Ni-50Co)/MA, B-(25Ni-75Co)/MA and B-100-Co/MA catalysts.

4.1.4 Catalytic activity:

Fig. 4.14 shows CH_4 conversion with time on stream (TOS). The highest conversion observed for the B-(75Ni-25Co)/MA, which initially increases in the first hour and then shows a nominal decrease up to 4 h. Initially, the CH_4 conversion for B-(75Ni-25Co)/MA was 19.82%, which was ~1.21 times higher than the conversion observed for B-Ni/MA catalyst. The difference in conversion almost remains unaltered throughout the reaction TOS 240 min. It was also observed that the addition of Co is beneficial in terms of conversion specifically for Ni/Co ratio 3. Interestingly, all the B containing catalysts showed an insignificant decline in conversion throughout the reaction. For further understanding, the non-B 75Ni-25Co/MA was also studied, and almost similar initial conversion was witnessed. However, it decreases continuously with TOS, which suggested a strong influence of B that was incorporated during $NaBH_4$ reduction method in terms of consistent conversion throughout reaction period. Further, a prolonged TOS 24 h reaction was performed to observe the catalysts deactivation of the catalyst and compared it with the non-B 75Ni-25Co/MA catalyst. Fig. 4.14a/ shows the CH_4 conversion decreased dramatically for non-B catalyst around 18% over the reaction period 24 h while B-containing catalyst was showing only 4% decline in the same reaction period. This reaction result verifies the theoretical (DFT) work that the B-containing catalysts can effectively block carbon diffusion into nickel lattice, mainly by lowering the E_{ads} of C [104].

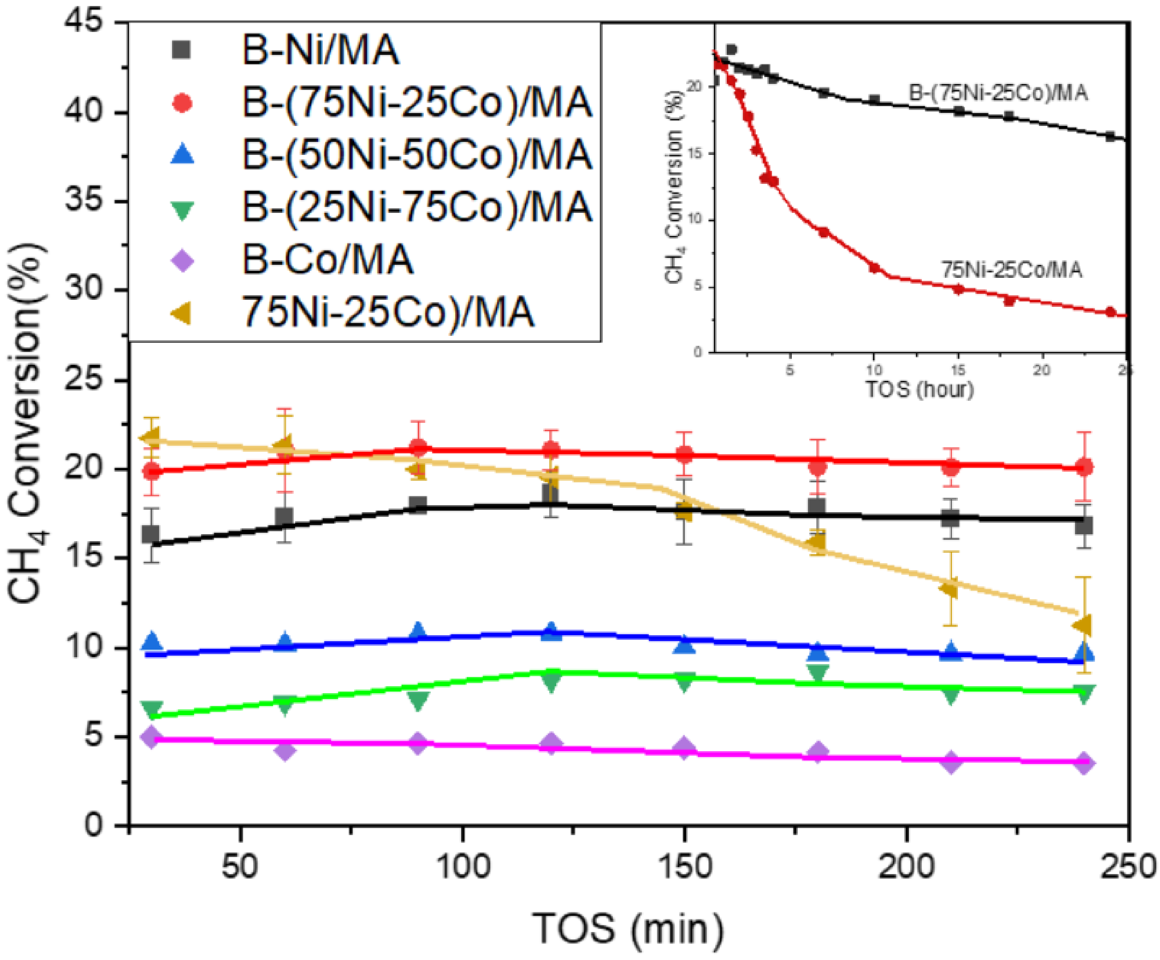

Figure 4.14. (a) The CH_4 conversion with TOS of prepared catalysts in the DRM with GHSV of 3×10^5 h^{-1} for B-Ni/MA, B-(75Ni-25Co)/MA, B-(50Ni-50Co)/MA, B-(25Ni-75Co)/MA, B-100-Co/MA and non-B 75Ni-25Co/MA catalysts (a/) Long reaction for B-(75Ni-25Co)/MA and non-B 75Ni-25Co/MA catalysts.

Fig. 4.15 represents the CO_2 conversion profile for different catalysts and follows a similar trend to that of CH_4 conversion. However, CO_2 conversion always observed higher than CH_4 due to reverse water gas shift reactions which is in line with the previous reported works [37, 40, 41]. The CO_2 conversion was 33.47% for B-(75Ni-25Co)/MA was higher than that of the B-Ni/MA catalyst. In the case of a long reaction, the decline in CO_2 conversion for B-(75Ni-25Co)/MA catalyst was only around 5% whereas the decline for non-B catalyst was around 26% in Fig. 4.15b$^{/}$. Additionally, the turnover frequency (TOF) for CH_4 and CO_2 was also calculated for B-(75Ni-25Co)/MA using H_2-TPD and conversions data. The calculated TOF_{CH_4} at different time interval is 0.280 ± 0.012, 0.299± 0.022, and 0.284 ± 0.010 s^{-1} at TOS 30, 90, and 240 min, respectively. Similarly, the calculated TOF_{CO_2} at different time interval is 0.471 ± 0.028, 0.480 ± 0.039, 0.474 ± 0.027 s^{-1}at TOS 30, 90, and 240 min, respectively. These values are close to the previously reported TOF_{DRM} for Ni-Co/MA catalyst at TOS of 30 min (0.27 for 100Ni/MA and 0.41 for 75Ni-25Co/MA) but unlike the present work, it declines significantly over the reaction period [37].

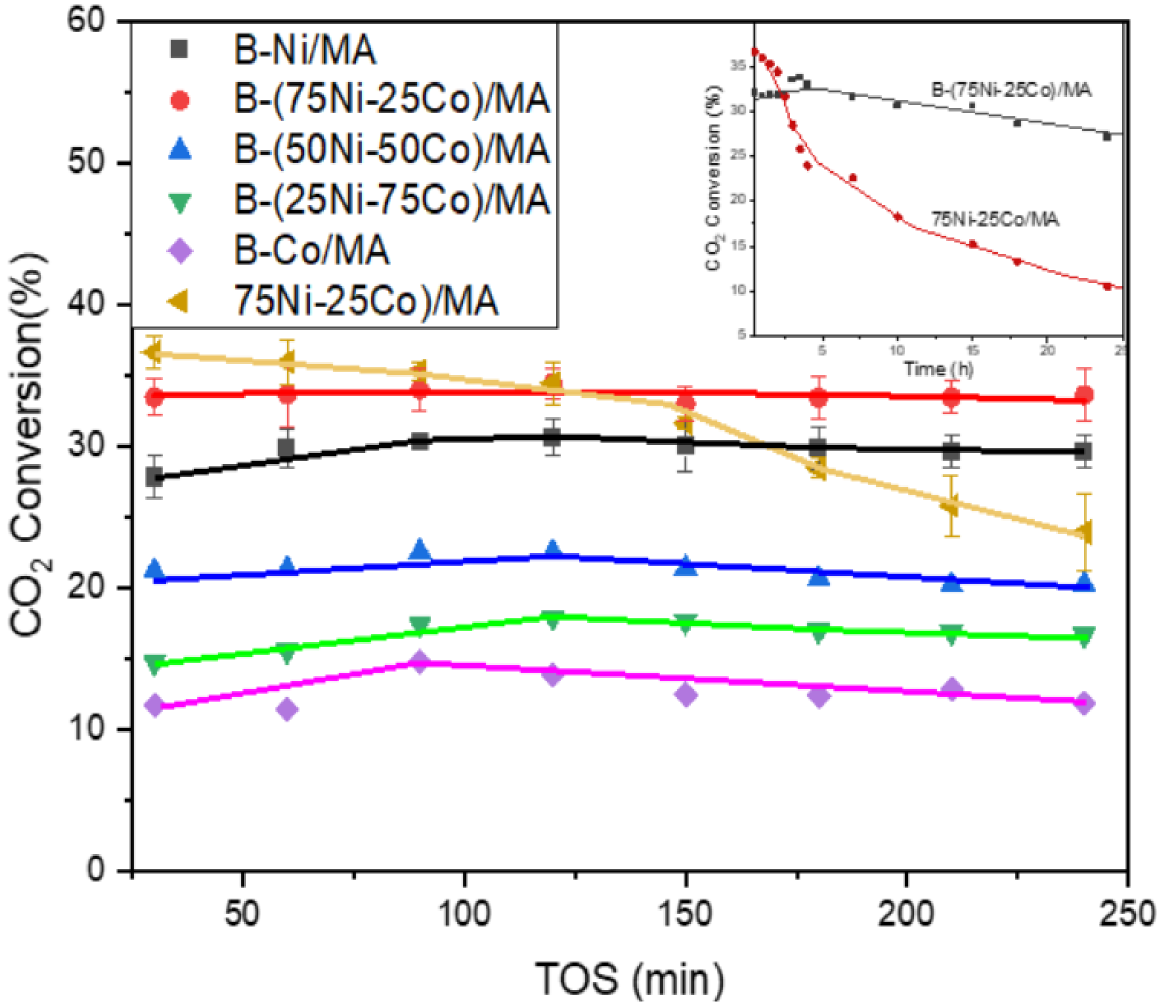

Figure 4.15. The CO_2 conversion with TOS of prepared catalysts in the DRM with GHSV of 3×10^5 h^{-1}

for B-Ni/MA, B-(75Ni-25Co)/MA, B-(50Ni-50Co)/MA, B-(25Ni-75Co)/MA, B-100-Co/MA and non-B 75Ni-25Co/MA catalysts (b$^{/}$) Long reaction for B-(75Ni-25Co)/MA and non-B 75Ni-25Co/MA catalysts

The ratio of produced H_2 and CO is also important to study different catalysts for DRM [37, 40, 41, 52]. Fig. 4.16 shows the produced syngas ratio (H_2: CO) for the B and non-B 75Ni-25Co/MA catalysts. The H_2: CO ratio followed a similar trend as that of the conversions (CH_4 and CO_2). It was observed that the Co catalysts is facilitating CO formation while Ni was favouring hydrogen formation. For the bimetallic catalysts, the ratio of Ni/Co decides production of syngas ratio and Ni/Co = 3 ratio catalyst [B-(75Ni-25Co)/MA catalyst] provides a maximum H_2 formation with a ratio of 0.62 with CO. further, the B and non-B 75Ni-25Co/MA catalysts was also analyzed for long TOS 24h reaction period that follows the similar trend as conversions (CH_4 and CO_2) in Fig. 4.16c$^{/}$. The decline in produced syngas was significant for 75Ni-25Co)/MA catalysts which was ~2.61 times than the B-containing [B-(75Ni-25Co)/MA] catalyst. Further the carbon balance (C_B) was calculated to verify the activity test and products formation. The C_B (%) was 96.13% for B-Ni/MA, 95.31% for B-(75Ni25Co)/MA, 95.69% for B-(50Ni50Co)/MA, 96.23% for B-(25Ni75Co)/MA, and 96.79% for B-Co-B/MA catalysts. The low value of C_B (%) was observed for B-(75Ni25Co)/MA catalyst due to the higher CH_4 conversion. Ray et al. [76] also reported the more affinity towards the CH_4 and favoured CO disproportion reaction are the causes of the poor carbon balance.

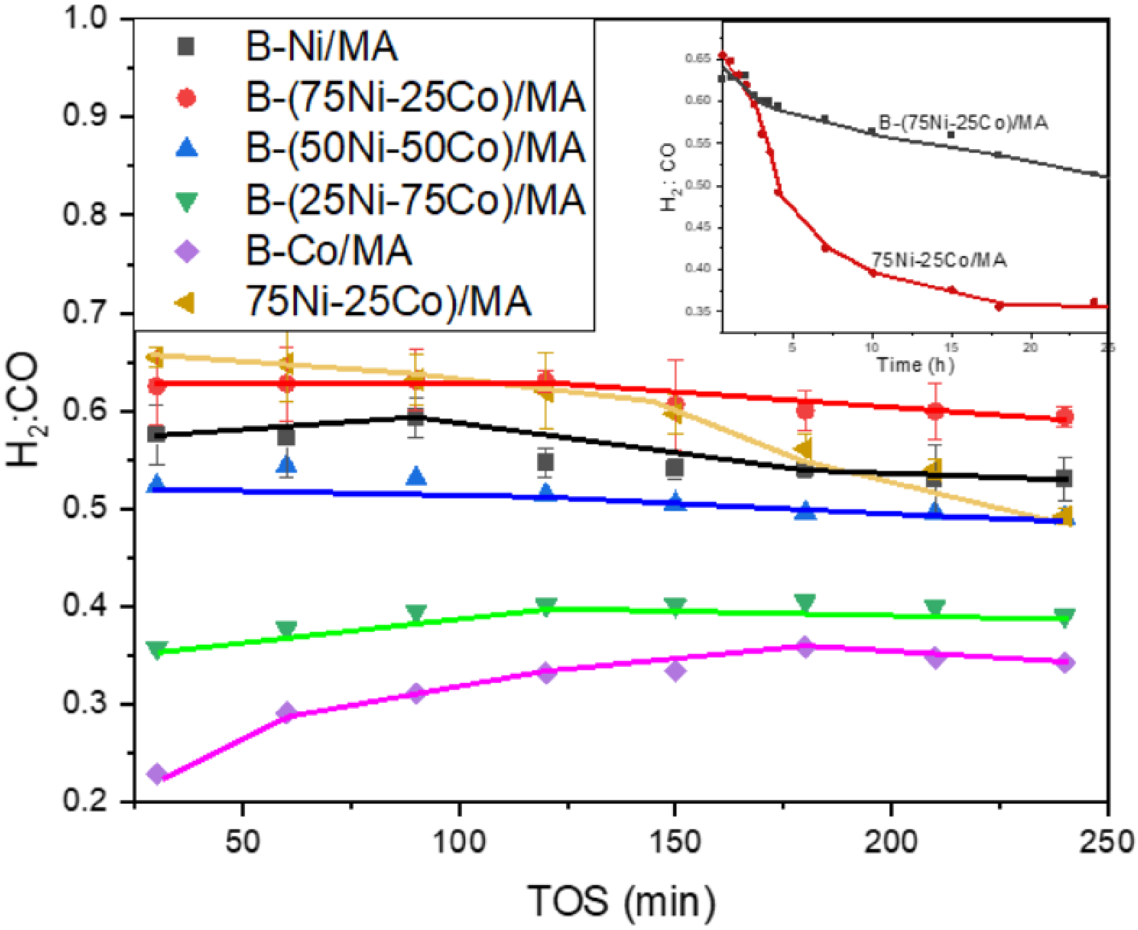

Figure 4.16. The H_2:CO ratio with TOS of prepared catalysts in the DRM with GHSV of 3×10^5 h^{-1} for B-Ni/MA, B-(75Ni-25Co)/MA, B-(50Ni-50Co)/MA, B-(25Ni-75Co)/MA, B-100-Co/MA and non-B 75Ni-25Co/MA catalysts (c$'$) Long reaction for B-(75Ni-25Co)/MA and non-B 75Ni-25Co/MA catalysts.

4.1.5 Analysis of used catalysts:

The spent catalysts were characterized by the XRD, ICP-OES, elemental analysis, and Raman spectroscopy to analyze the deposited carbon on the catalyst during the reaction. In Fig. 4.17, the XRD patterns indicate carbon formation at 2θ ~26.8° [52, 103, 153]. However, no peak for carbon was observed for Co rich catalysts [B-(25Ni-75Co)/MA and B-Co-B/MA] due to their low methane conversions. Further, the absence of MO peaks suggested no oxidation of metallic species during the reaction. The composition of B was identified by the ICP-OES analysis of the spent catalysts and observed that there was no loss of B during the reaction.

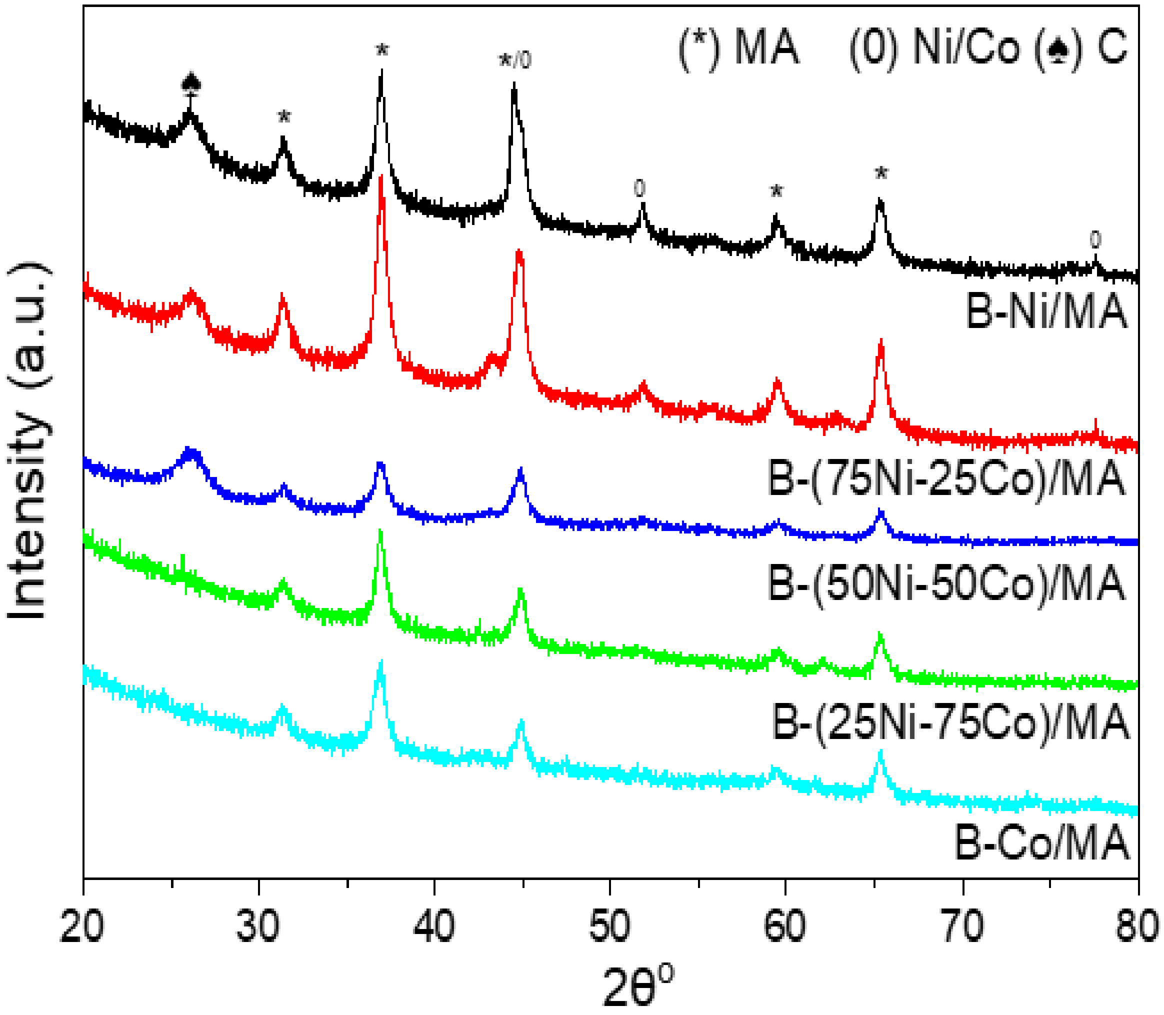

Figure 4.17. XRD pattern of spent catalysts for B-Ni/MA, B-(75Ni-25Co)/MA, B-(50Ni-50Co)/MA, B-(25Ni-75Co)/MA and B-Co/MA catalysts.

The amount of deposited carbon on the catalysts surface were also calculated and presented in Fig. B4. It was observed that the carbon content is higher with Ni-rich catalysts and lower with

Co-rich catalysts. The maximum carbon deposited on the catalyst with Ni: Co ratio 3:1. The results suggested that in presence B, carbon deposition is linearly related to conversions. In addition to that the produced carbon during DRM was normalized with the total mole methane converted (assuming methane cracking as the most significant carbon source) presented in Fig. 4.18. The total amount of C was ~2.8 times higher for non-B 75Ni-75Co/MA than the B containing B-(25Ni-75Co)/MA catalyst.

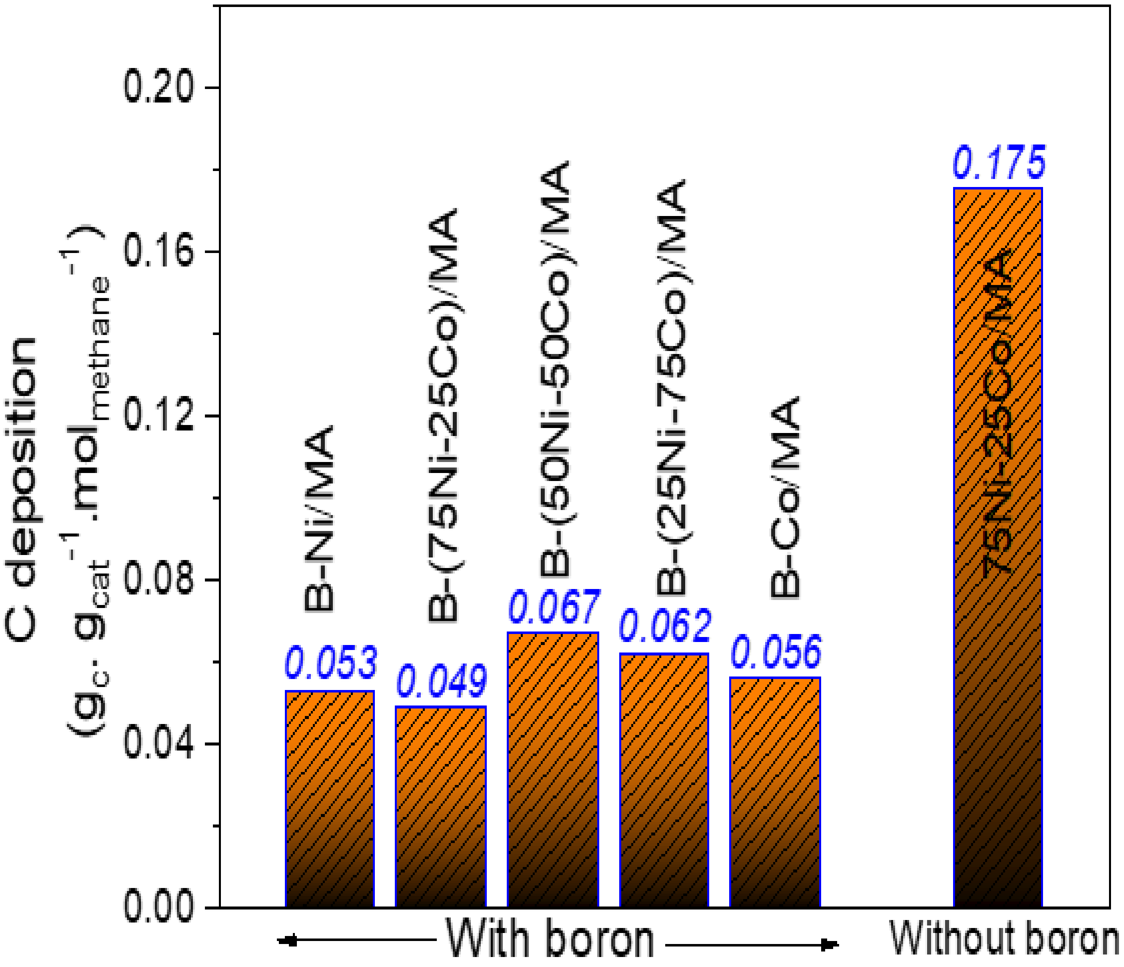

Figure 4.18. Amount of carbon deposition of spent catalysts normalize with the methane produced for B-Ni/MA, B-(75Ni-25Co)/MA, B-(50Ni-50Co)/MA, B-(25Ni-75Co)/MA, B-100-Co/MA and traditional non-B 75Ni-25Co/MA catalysts.

The Raman spectroscopy (Fig. 4.19) of B-containing catalysts exhibited two peaks at ~ 1310 cm^{-1} and 1595 cm^{-1} for D-band (attributes to structural disorders) and G-band (attributes to C-C stretching vibrations of pair of sp^2 carbon) [40, 167-169]. The intensity ratio of the *D* and *G* bands (I^D/I^G) estimates the degree of disorder in the formed carbon species [40, 167-169]. The highest value of I^D/I^G was observed as 3.17 for B-(75Ni-25Co)/MA, and it decreases with Co amount. The higher value indicates poor graphitization of the formed carbon on the spent catalyst due to the presence of B and 3:1 Ni:Co ratio [129]. The TEM image of spent B-(75Ni-25Co)/MA shows carbon nanotube formation (Fig. B5).

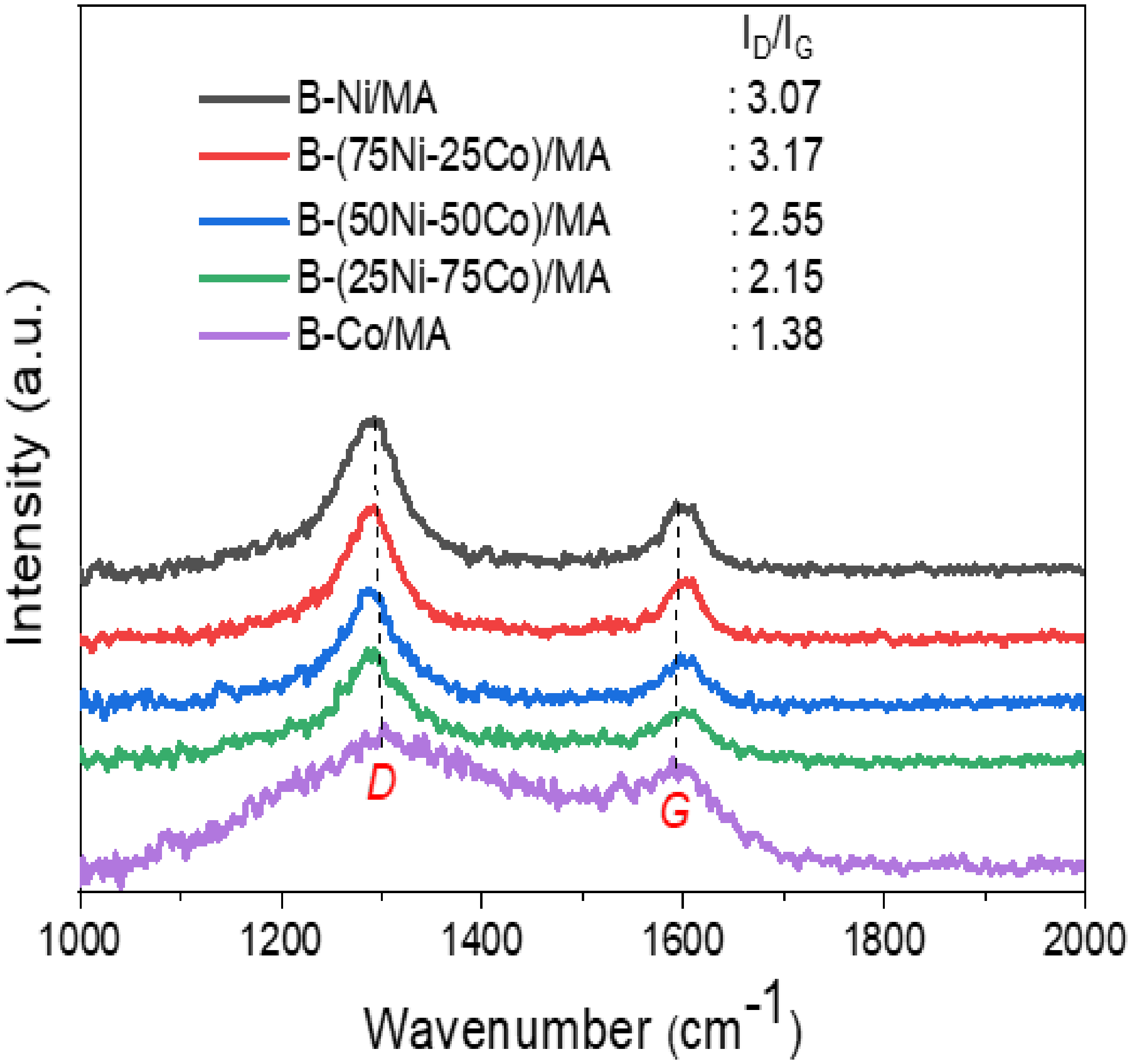

Figure 4.19. Raman analysis of B-Ni/MA, B-(75Ni-25Co)/MA, B-(50Ni-50Co)/MA, B-(25Ni-75Co)/MA and B-100-Co/MA catalysts.

4.2 Density Functional Theory (DFT) Calculations:

The effect of B on the surface of 75Ni25Co catalyst was evaluated by the DFT calculations to provide a theoretical insight. The adsorption energy (E_{ads}) of C at various sites and their effects with the presence of B atom at different sites were calculated for the 75Ni-25Co catalyst. The carbon atom was adsorbed at the twofold bridge, threefold FCC hollow, and HCP hollow sites (Fig. B6), and the calculated E_{ads} was tabulated in Table. 5.2. The E_{ads} of carbon (E_{ads} C) at the HCP hollow and FCC hollow sites are around -6.913 eV and -6.816 eV, which are in line with the previously reported value of -6.861 eV (-662 kJ/mol) and -6.789 eV (-655 kJ/mol) respectively [102].

Further, B was kept fixed at HCP hollow site on the surface of 75Ni-25Co, and C adsorbed at other possible sites. It is clear from Table. 4.2 that E_{ads} C at various sites is decreased to around 0.5 eV in the presence of B. Interestingly, the decrement of E_{ads} energy denotes weaker C adsorption in the presence of B [21]. On the other hand, the values of E_{ads} C for different sites in the presence of surface B decreased more relative to the values of E_{ads} C in the presence of B at the subsurface, which denotes weaker C adsorption at surface [21]. Additionally, the E_{ads} B at HCP hollow site, FCC hollow site, and subsurface are -5.908, -6.178, and -6.443 eV, respectively, indicating subsurface is the preferred site for adsorption of B as compared to surface HCP hollow site [102]. Thus, adding a small amount of B may effectively block these sites for carbon and force carbon atoms to remain on the 75Ni-25Co catalyst surface for the reaction, consequently preventing the coking.

Table 4.2. The adsorption energy of carbon at different sites in the absence and presence of B.

C adsorption site		**E_{ads} C (eV)**		
		absence of B	**presence of B at HCP hollow site**	**presence of B at the subsurface**
Twofold bridge site	**between Ni-Co**	-6.871	-6.344	- 6.660
	between Ni-Ni	-6.913	-6.578	- 6.677
HCP hollow site		-6.913	-6.333	-6.677
FCC hollow site		-6.816	-6.706	-6.925

4.3 Effect of B and Ni: Co ratio:

The characterization of the catalysts confirmed the presence of rod-like metallic Ni-Co alloy and metal borides on MA flakes. The metal dispersion (%) from H_2-TPD also suggested a definite improvement in metal dispersion for the prepared catalysts in the presence of B, compared to the non-B catalyst. The observed trend of the metal dispersion was also reported previously [37]. The H_2-TPR and XPS plot confirmed the reduction of the catalyst by using $NaBH_4$, and the DOR (16 %) demonstrated the formation of the M^{2+} and M-B interaction. The DRM reaction results revealed that the catalysts prepared by $NaBH_4$ treatment enhanced the performance. The results evidenced that the Ni: Co ratio of 3:1 influenced the conversion, and B controlled the formation of carbon. Further, a DFT study also reveals that the presence of B (Ni:Co =3:1) significantly reduces the catalyst deactivation as the presence of B lowers the adsorption energy (E_{ads}) of C by ~0.5eV, which is in line with the previous theoretical work [104]. Usually, blocking the surface site may decrease methane activation. However, in this study, B facilitates methane activation by increasing the exothermicity of CH_4 dissociation [133]. The inclusion of B into the catalyst matrix leads to advancements in multiple aspects like a greater extent of reduction, higher metallic dispersion, stabilize the metallic state, activation of the reactants, and lower carbon deposition. B also stabilizes the metallic state by decreasing the possibility of metal oxidation during the reaction as it helps to maintain the amounts of formed C and O at the surface [133].

4.4 Outcomes:

The present study developed B-containing Ni-Co bimetallic catalyst, which offered a steady conversion of CH_4 and CO_2 for the DRM with a reasonable H_2:CO ratio. The catalyst was prepared by a unique and one-step method that uses $NaBH_4$ as a critical reagent for metal salts reduction and as a B source. The developed catalyst's performance was better than the catalyst prepared without using $NaBH_4$ in reactivity and resistance towards carbon deposition. Also, the severe H_2 reduction step during preparation was not required for the developed catalyst, which is often used traditionally. The maximum $\mathrm{TOF}_{\mathrm{CH}_4}$ and $\mathrm{TOF}_{\mathrm{CO}_2}$ were found to be 0.299 and 0.480 $s^{-1,}$ respectively for catalysts containing 10.89 wt% of Ni, 3.71 wt% of Co, and 2.68 wt% of B [(B-(75Ni-25Co)/MA], which were 1.50 and 1.17 times higher than the similar non-B catalyst. Interestingly, the carbon deposition was found to be extremely low (~3.57 times lesser than the non-B) and of non-graphitic nature. B also helps in hindering the formation of carbon on the catalyst surface. Furthermore, the DFT calculation also revealed the adsorption energy ($\mathrm{E}_{\mathrm{ads}}$) of C on (Ni-Co =3:1) catalyst significantly reduces the deactivation of Ni-based catalysts with B's presence by ~0.5eV. Besides the importance of B inclusion, the study also realizes that a particular metallic ratio (Ni-Co =3:1) is also crucial for the supported bimetallic catalyst to achieve maximum activity and stability for DRM. Finally, the present study provides a new strategy to perform carbon-free DRM without compromising the activity.

Chapter 5

Synergistic effect of $NaBH_4$ followed by H_2 reduction towards advancement of catalytic activity of B-(75Ni25Co)/ $MgAl_2O_4$ for dry reforming of methane

This manuscript is ready to communicate in journal “Synergistic effect of $NaBH_4$ *followed by* H_2 *reduction towards advancement of catalytic activity of (75Ni25Co)-B/*$MgAl_2O_4$ *for dry reforming of methane” by MD Shakir, Siddhartha Sengupta, Apurba Sinhamahapatra, Shaomin Liu, Hari Vuthaluru.*

5.1 Results and discussion:

5.1.1 Composition and structural analysis:

The prepared B-containing (B-(75Ni25Co)/MA)) catalysts were further reduced and compared with as-prepared catalysts to change in performce after H_2-treatment at 600°C. Both catalysts were characterized by ICP-OES to identify the elemental composition of metals and boron showed in Table 5.1. As expected, the composition of Ni and Co were around ~14 wt% for both as-prepared and further catalysts. The amount of B content were also observed similar ~2.65 for both catalysts that confirmed the dispersion of B on the catalyst and $NaBH_4$ acted as a source. Further, the reduction effect and degree of reduction for both further reduced and as-prepared catalysts were revealed by the H_2-TPR analysis. In Fig 5.1 the reduction profile showed two different temperature peaks crossponded to the H_2-consumption corresponds to weak and medium metal-supported interactions [51, 128, 129]. The peak observed at temperature (300-350°C) represents the reduction of weakly supported interacted bulk metal oxide (MO) [128, 129, 153]. The H_2 consumption at 430-450°C was observed for the medium interacted MO with support [51, 114, 129]. Eventually, no peak observed for high temperature (>500°C) region, which represents the reduction of smaller surface particles due to the reduction of the catalyst during preparation. As catalysts were pre-reduced with H_2 for further reduced catalyst, the TPR profile was observed as expected low-intensity peaks. These results suggested absence of MO as it converted to M^0 due to additional H_2-reduction step . Further, the degree of reduction (DOR) revealed about the reducibility of the catalyst for both catalysts presented in Table 5.1. A comparatively low degree of reduction was observed for H_2-reduced catalysts indicating a greater extent of reduction compared to the as-prepared catalyst due to the additional H_2-reduction step.

Table 5.1. Structural properties of the support MA and metal-loaded B-containing catalysts.

Sample	Surface Area (m^2/g)	Pore Volume (cm^3/g)	Pore Size (nm)	Composition (wt %)			Degree of reduction (%)	Metal dispersion (%)
				Ni	Co	B		
H_2-reduced	62.31	0.1522	10.315	10.66	3.62	2.65	3.56	7.11
As prepared	69.98	0.1059	11.3821	10.89	3.71	2.68	19.87	6.46

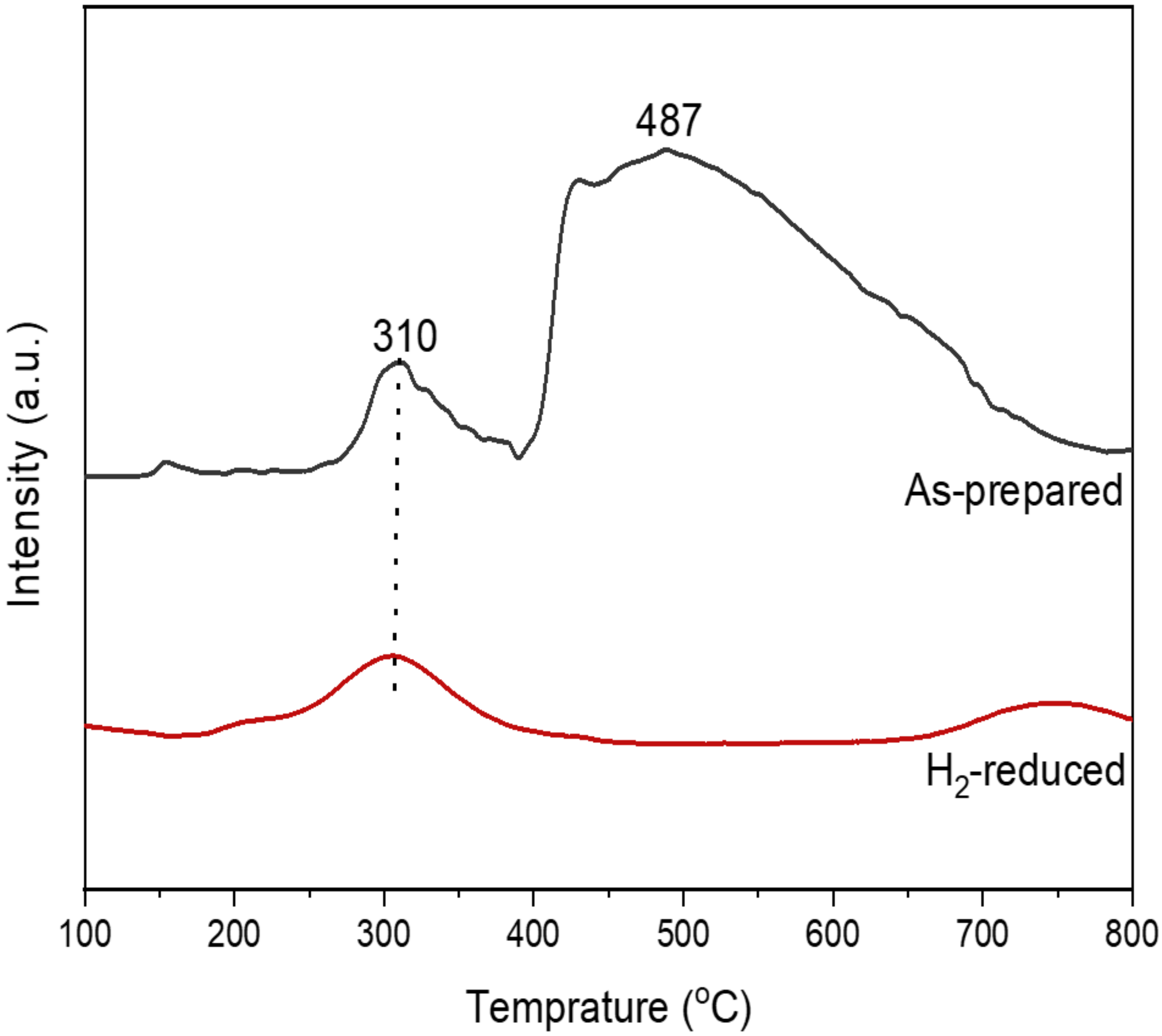

Figure 5.1. H_2-TPR analysis of as-prepared and H_2-reduced B-(75Ni25Co)/MA catalysts.

The XRD analysis of B-(75Ni25Co)/MA catalyst was performed for the N_2-treated and H_2-reduced (Fig. 5.2). For support (MA) peaks were observed for both catalyst at 2θ: 31.34, 36.80, 44.85, 59.40, and 65.34° corresponding to JCPDS Card No. 77-1203[33, 99, 122]. Whereas the peaks related to Ni/Co species are not observed to be so sharp for N_2-Treated catalyst due to low crystallinity; however, they appeared so prominent for H_2-treated catalyst, and peaks appeared at 2θ = 44.78°and 77.30° corresponding metallic-Ni/Co (JCPDS Card No. 04-0850) [40, 99, 122]. For. However, no separate peak was evident for cobalt due to multi-peak overlapping [37, 40, 51]. A weak peak at 2θ =62.21° observed for the N_2-treated catalyst reflected the presence of NiO or CoO due to the partial reduction of the catalyst during the synthesis by the $NaBH_4$ reduction method (JCPDS Card No. 47-1049)[39, 40, 99]. This result was in line with obtained TPR data. There was no BO or metal-boride peak observed, which suggested the amorphous formation phase of boron compounds [103]. The surface areas of N_2-treated and H_2-reduced B-(75Ni-25Co)/MA catalyst were also determined by Brunauer–Emmett–Teller (BET) analysis Table 6.1. The surface area of support MA was 86.70 (m^2/g), which is more than the metallic B-(75Ni25Co)/MA catalyst that is because of the dispersion of active components in the pores of support [12]. The surface area of the N_2-treated was 69.98, which is ~1.12 times more than the catalyst was H_2-reduced catalyst due to the partial reduction and presence of NiO. However, further H_2-reduced catalysts have higher M^0 with a DOR of 3.56%.

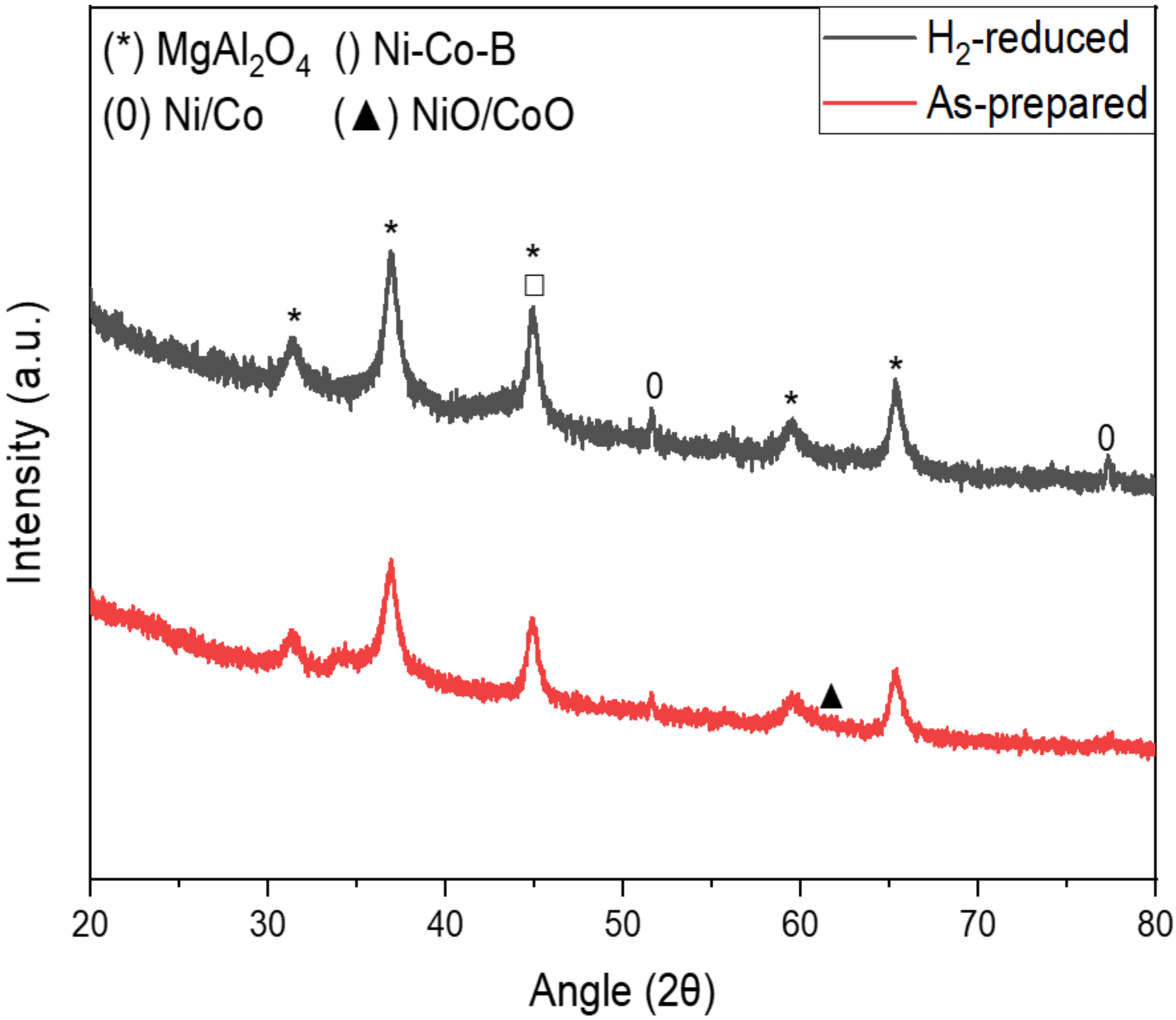

Figure 5.2. XRD analysis of as-prepared and H_2-reduced B-(75Ni25Co)/MA catalysts

5.1.2 XPS Analysis:

The XPS analysis for as-prepared and H_2-reduced B-(75Ni25Co)/MA catalyst to observe the elemental distribution of major existing elements. Fig. 5.3 shows the full XPS survey spectrum in which the presence of Mg, Al, Ni, Co, O, and B can be very clearly seen. [113]. The high-resolution XPS spectrum for B particle showed in Fig. 5.4. A single peak observed at binding energy 189.4 eV reflects the metal-B interaction by $NaBH_4$ treatment and formed metal boride. General BO peak appears at ~187.2 and ~192.5 eV, which is the absence in the plot, and a strong peak at 189.4 eV is observed for elemental B [138, 139].

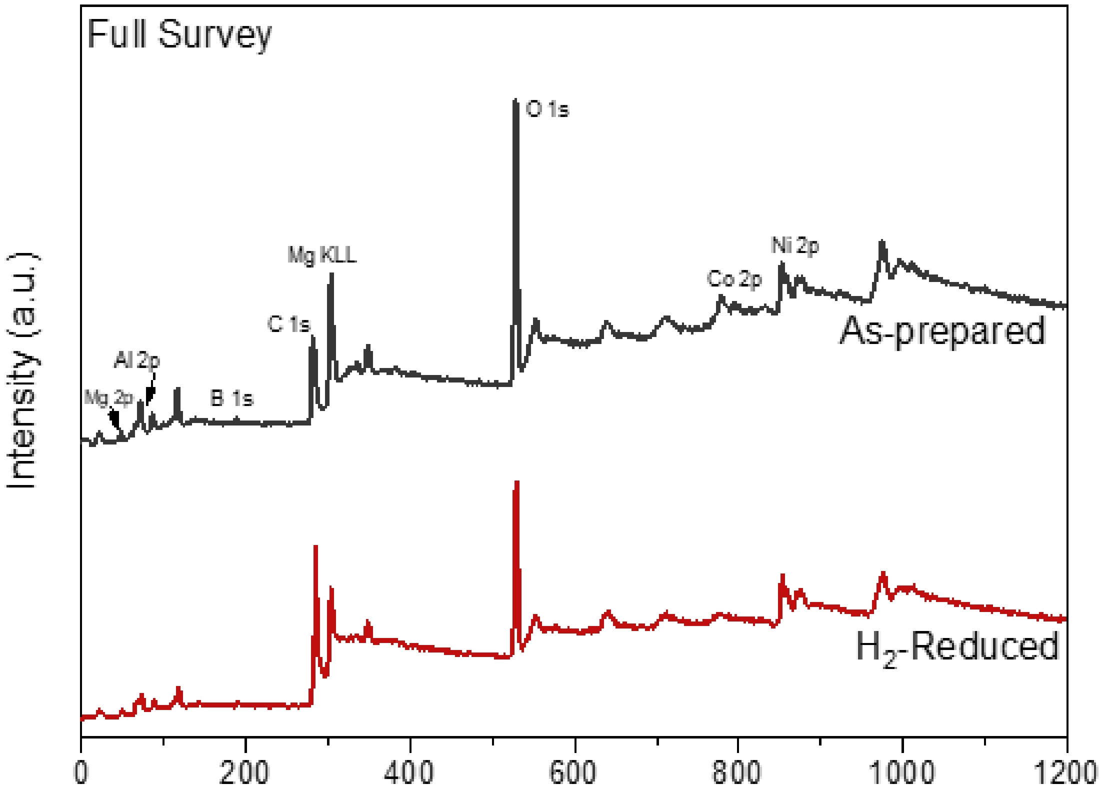

Figure 5.3. XPS analysis of as-prepared and further H_2-reduced B-(75Ni-25Co)/MA catalysts with a full survey of each element

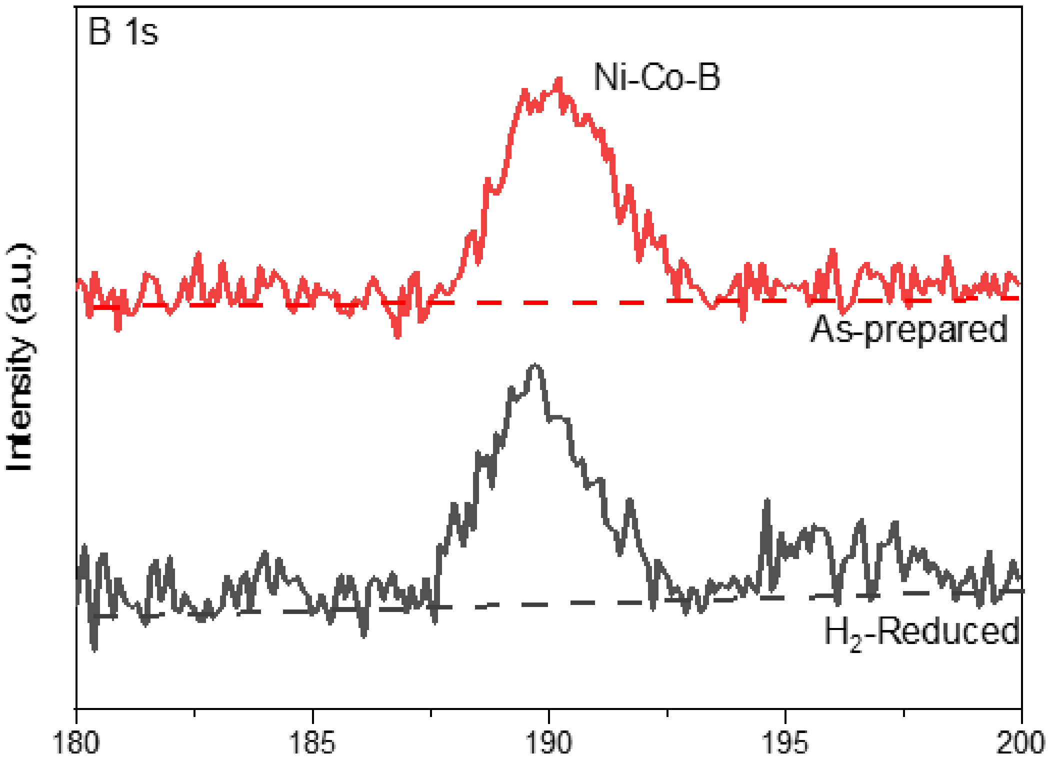

Figure 5.4. B 1s XPS spectrum of as-prepared and further H_2-reduced B-(75Ni-25Co)/MA catalysts.

The specific resolution of dominated metal (Ni 2p) XPS spectrum for as-prepared and H_2-reduced B-(75Ni25Co)/MA catalysts showed in Fig 5.5 (a and b). The multiple peaks after deconvolution were observed as Ni $2p_{3/2}$ and $2p_{1/2}$ and corresponding satellite peaks. Fig 5.5a showed Ni 2p spectrum for as-prepared B-(75Ni25Co)/MA catalyst, the peaks observed at 852.7 and 870. 4 eV attributed to the presence of Ni $2p_{3/2}$ and Ni $2p_{1/2}$ respectively of Ni metallic [136, 137]. Whereas the peaks observed at 853.4 ($p_{3/2}$) and 872.4 eV ($p_{1/2}$) reported the presence of the Ni^{2+} of NiO along with the corresponding satellite peaks [136, 137]. However, the further H_2-reduced B-(75Ni25Co)/MA catalyst showed only metallic Ni peaks at binding energy 852.7 and 870. 4 eV in Fig. 5.5b, which is in-line with the H_2-TPR and XRD analysis.

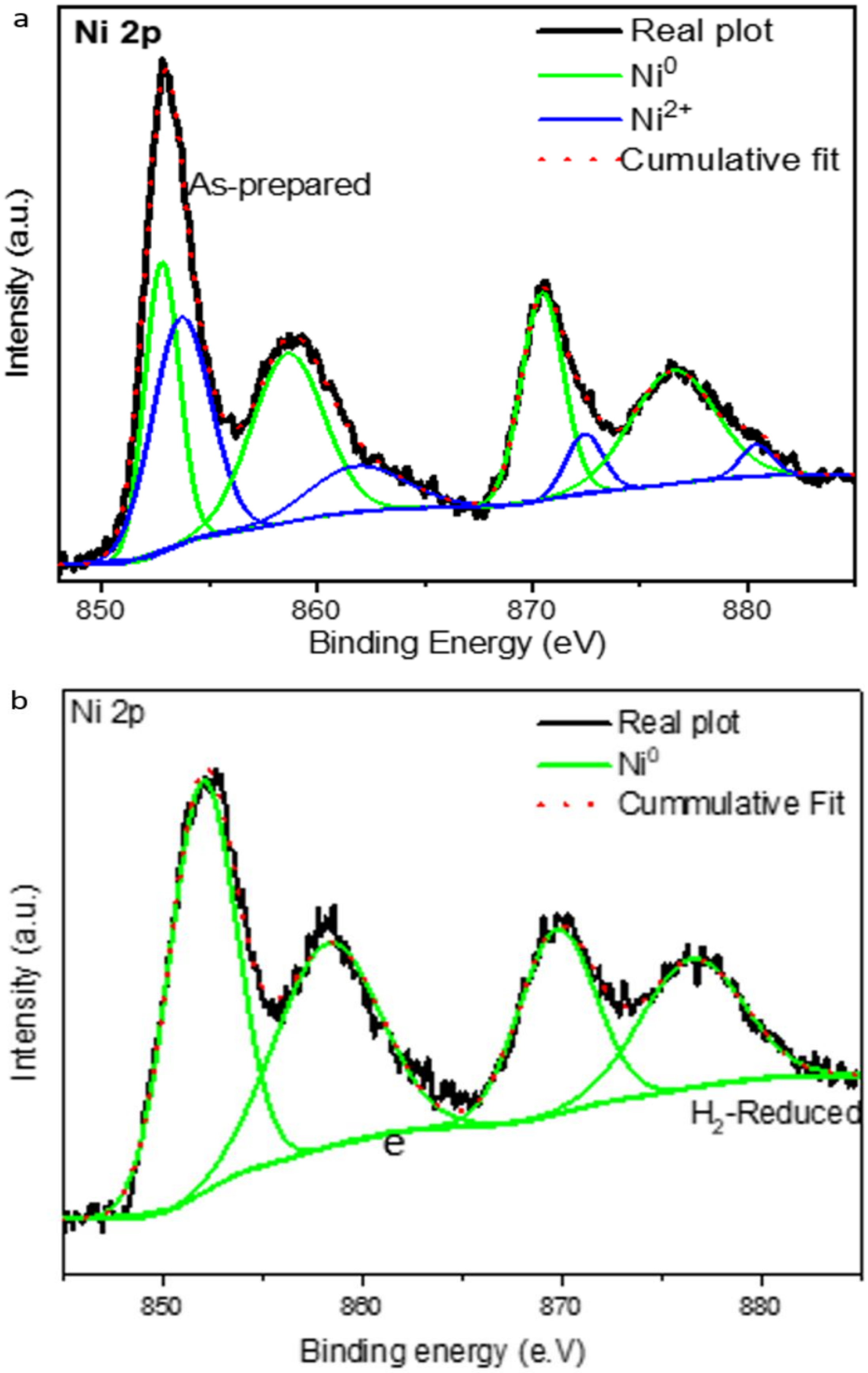

Figure 5.5. Ni 2p XPS spectrum of B-(75Ni-25Co)/MA catalysts (a) as-prepared and (b) Further H_2-reduced catalysts

Further, the core-level Co 2p XPS spectrum showed in Fig. 6.6 (a and b) for as-prepared and H_2-reduced B-(75Ni25Co)/MA catalysts. The spectrum confirmed the presence of metallic Co ($2p_{3/2}$:778.3 and $2p_{1/2}$:794.1 eV) and Co^{2+} ($2p_{3/2}$: 779.4, $2p_{3/2}$:799.3 eV) of CoO for as-prepared catalysts in Fig. 5.6a [170]. However, the further reduced catalyst showed the metallic peak Co^0 Fig. 5.6b. Hence it is evident that the complete reduction of metals (Ni and Co) phase for further reduced catalysts. The above analytical characterization techniques showed there are distinct physiochemical properties for as-prepared and further H_2-reduced B-(75Ni25Co)/MA catalysts. The impact of these changes was further analyzed by their catalyst activity performance.

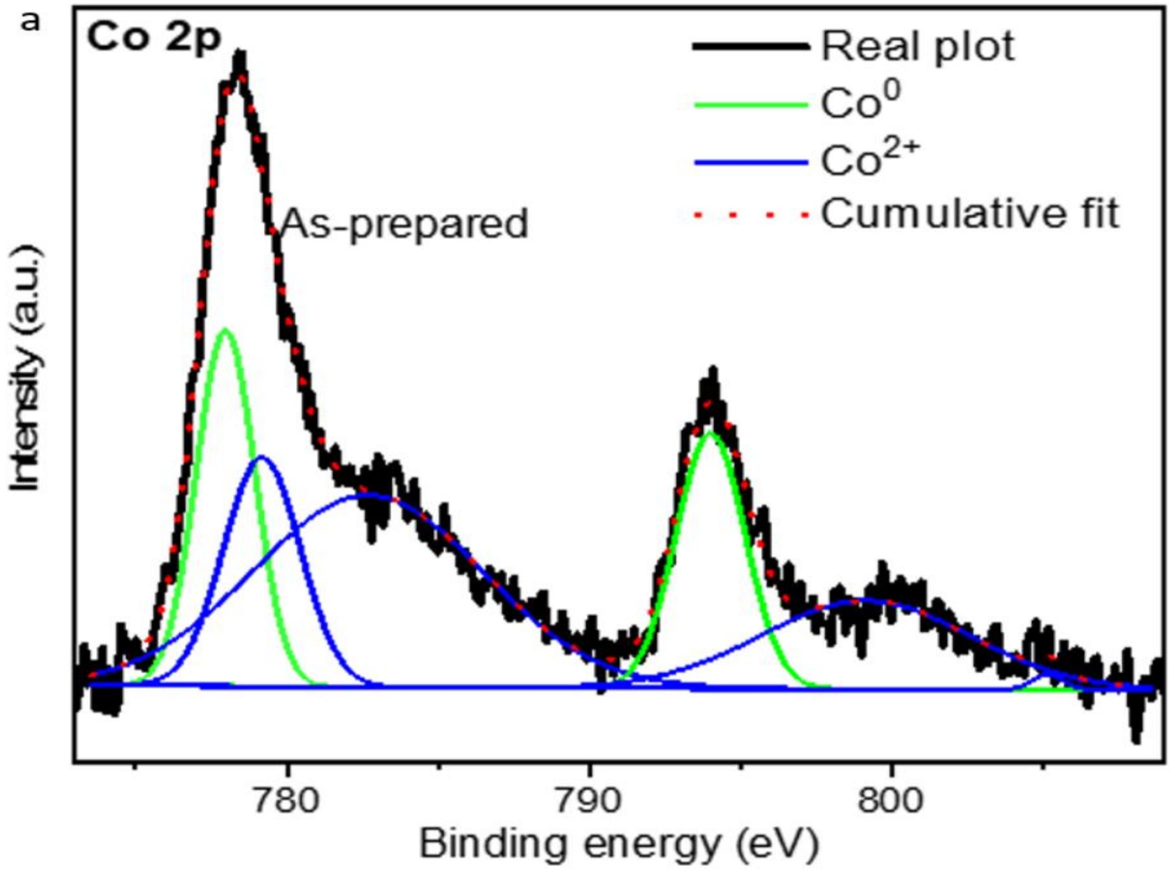

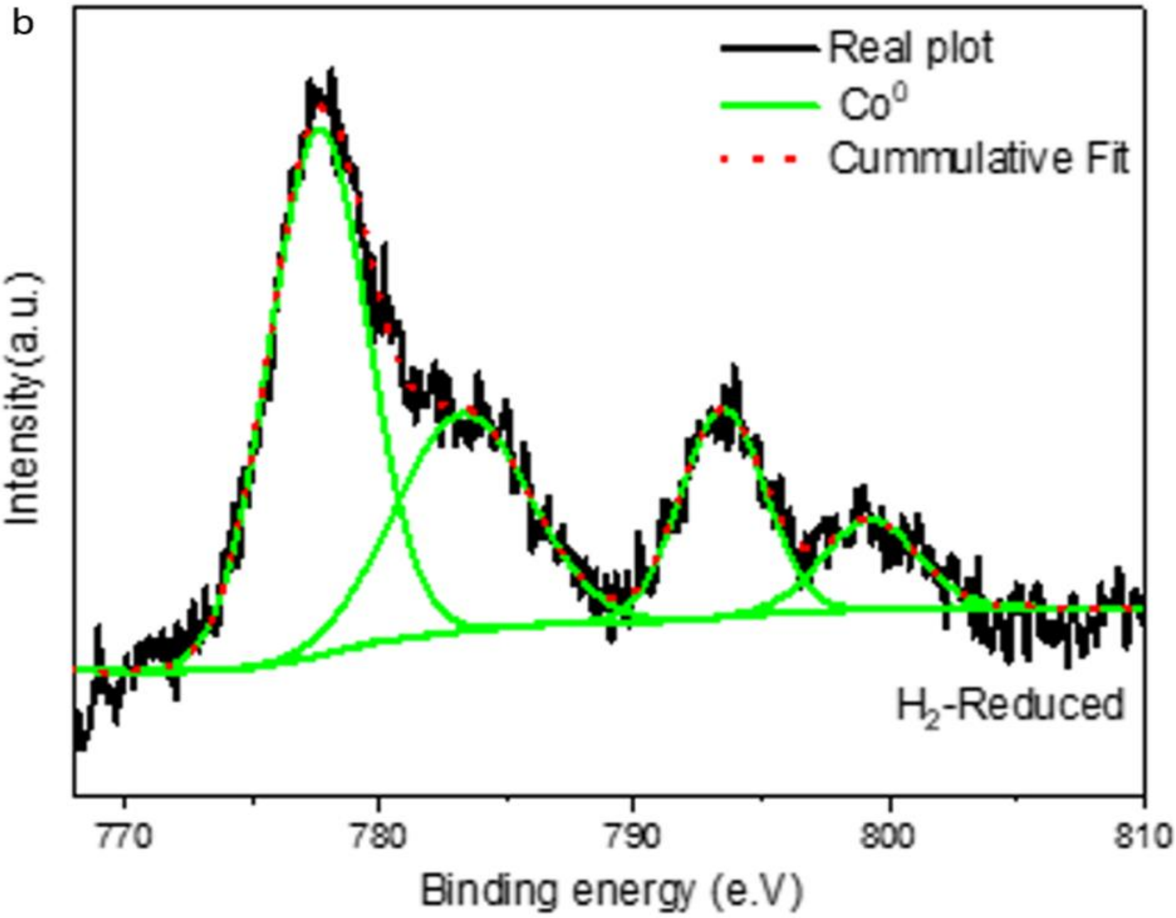

Figure 5.6. Co 2p XPS spectrum of B-(75Ni-25Co)/MA catalysts (a) as-prepared and (b) Further H_2-reduced catalysts.

5.1.3 Catalytic activity:

The DRM was performed with the as-prepared and H_2-reduced B-(75Ni25Co)/MA catalyst in a fixed-bed reactor at 600°C and atmospheric pressure with a GHSV of 3×10^5 h^{-1} to evaluate the activity of the catalyst. The Mears' and Weisz-Prater criteria were used for this reaction data and observed there are no effects of any internal and external mass transfer under these reaction conditions (Table. D1-D2) [37, 118]. Moreover, the equilibrium conversion (CH_4:53% and CO_2:63%) is less than that of reported conversions of CH_4 and CO_2 under similar conditions [37, 171]. A 24 h long reaction was performed for both catalysts; the sample was collected every 30min from the reactor to analyze the conversion using gas chromatography (GC). Fig 5.7 shows CH_4 conversion with time for both as-prepared and H_2-reduced B-(75Ni-25Co)/MA catalyst. The highest conversion pattern was observed for the H_2-reduced, which is obvious as we observed from the characterization of the catalyst that the further reduction helps to improve the dispersion and more Ni^0/Co^0 metallic form. In the beginning, the conversion of the H_2-reduced catalyst shows 30.45%, which is around 1.48 times higher than the as-prepared catalyst. After 24h of reaction completion, the H_2-reduced conversion dropped by ~15 %, while the as-prepared catalyst dropped only by 4% throughout the reaction period, this could be due to the deposition of C on Ni^0 site for H_2-reduced catalysts compared to the as-prepared catalysts.

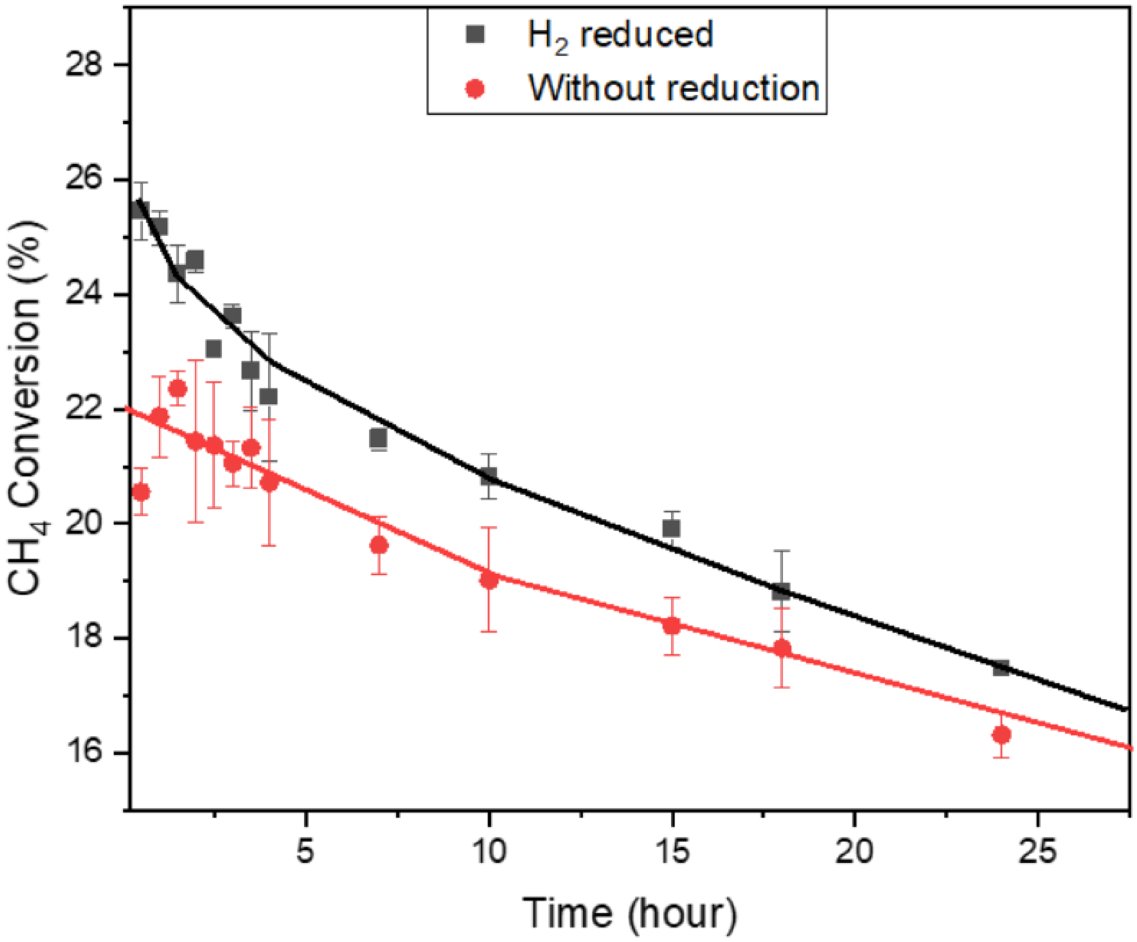

Figure 5.7. The CH_4 conversion of H_2-reduced and as-prepared B-(75Ni-25Co)/MA catalysts in the DRM at 600°C and GHSV of 3×10^5 h^{-1} with time.

Fig 5.8 represents the CO_2 conversion of both as-prepared and H_2-reduced B-(75Ni25Co)/MA catalyst and follows a similar trend to CH_4 conversion. The CO_2 conversions of both catalysts were higher compared to the CH_4 conversions due to the reverse water gas shift reaction (RWGS) [1, 2]. The initial conversion of CO_2 for H_2-reduced was higher (42.24%) compared to the as-prepared catalyst (32.47%). However, the decline in conversion was more for H_2-reduced by around 2.4 times at the end of the reaction.

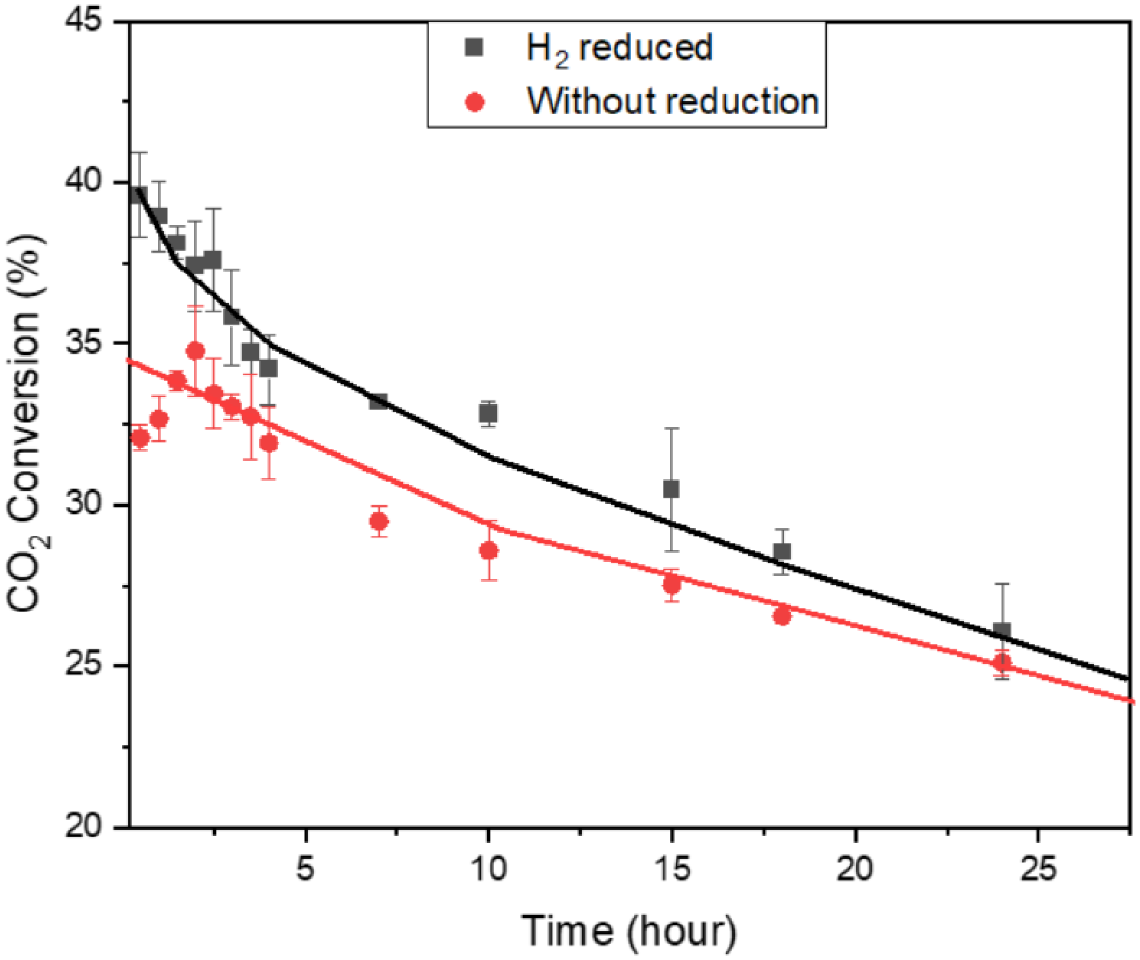

Figure 5.8. The CO_2 conversion of H_2-reduced and as-prepared B-(75Ni-25Co)/MA catalysts in the DRM at 600°C and GHSV of 3×10^5 h^{-1} with time.

The produced H_2 and CO ratio plays a vital role in the identification of catalyst performance. Fig. 5.9 shows H_2: CO ratio for both catalysts. It is seen that the H_2: CO ratio for all catalysts is less than one due to the reverse water gas shift reaction (RWGS) reaction, which consumed H_2. The further H_2-reduced catalyst produced a higher value of 0.88 at the very beginning, while the as-prepared catalyst was 0.6251. However, there was a slight increment in the ratio was observed for the as-prepared catalyst in the initial 2h then it dropped to 0.512. The drop in syngas was higher for further reduced catalyst, around 0.35, while the drop in as-prepared catalyst was only around 0.11. Further, the $\mathrm{TOF}_{\mathrm{CH}_4}$was also calculated based on methane conversion represented in Fig. 5.10. The $\mathrm{TOF}_{\mathrm{CH}_4}$ of H_2-reduced catalysts was higher compared to the as-prepared catalyst. The difference in $\mathrm{TOF}_{\mathrm{CH}_4}$was about 0.0612, which gradually decreased with time, and was about 0.0181 at 24h of the reaction period. This reaction result represents that the further reduction helps to increase the conversion and syngas ratio due to the presence of M^0 compared to as-prepared catalysts at the beginning of the DRM, but for a long reaction, both catalysts showed similar results afterward 5h of reaction period.

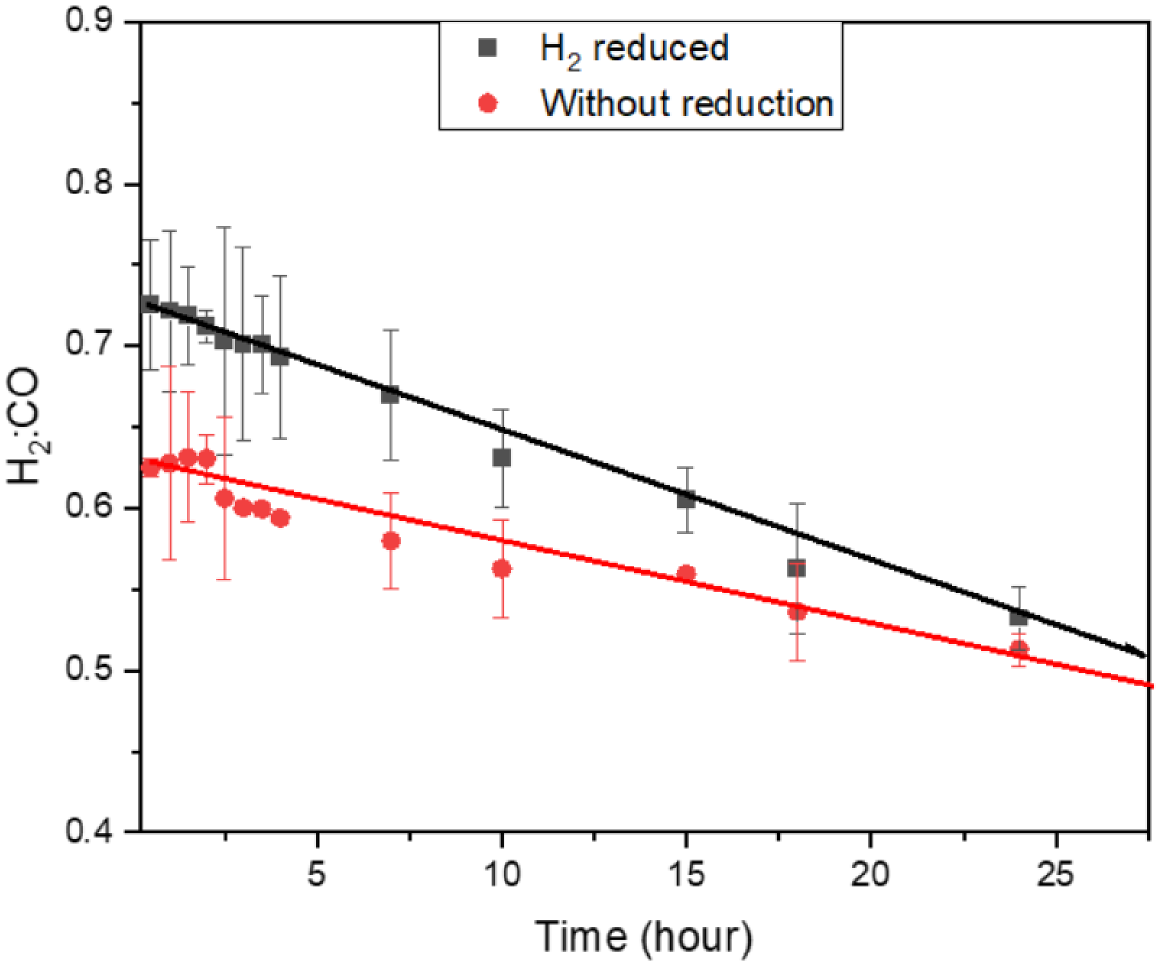

Figure 5.9. H_2: CO ratio of H_2-reduced and as-prepared B-(75Ni-25Co)/MA catalysts in the DRM at 600°C and GHSV of 3×10^5 h^{-1} with time.

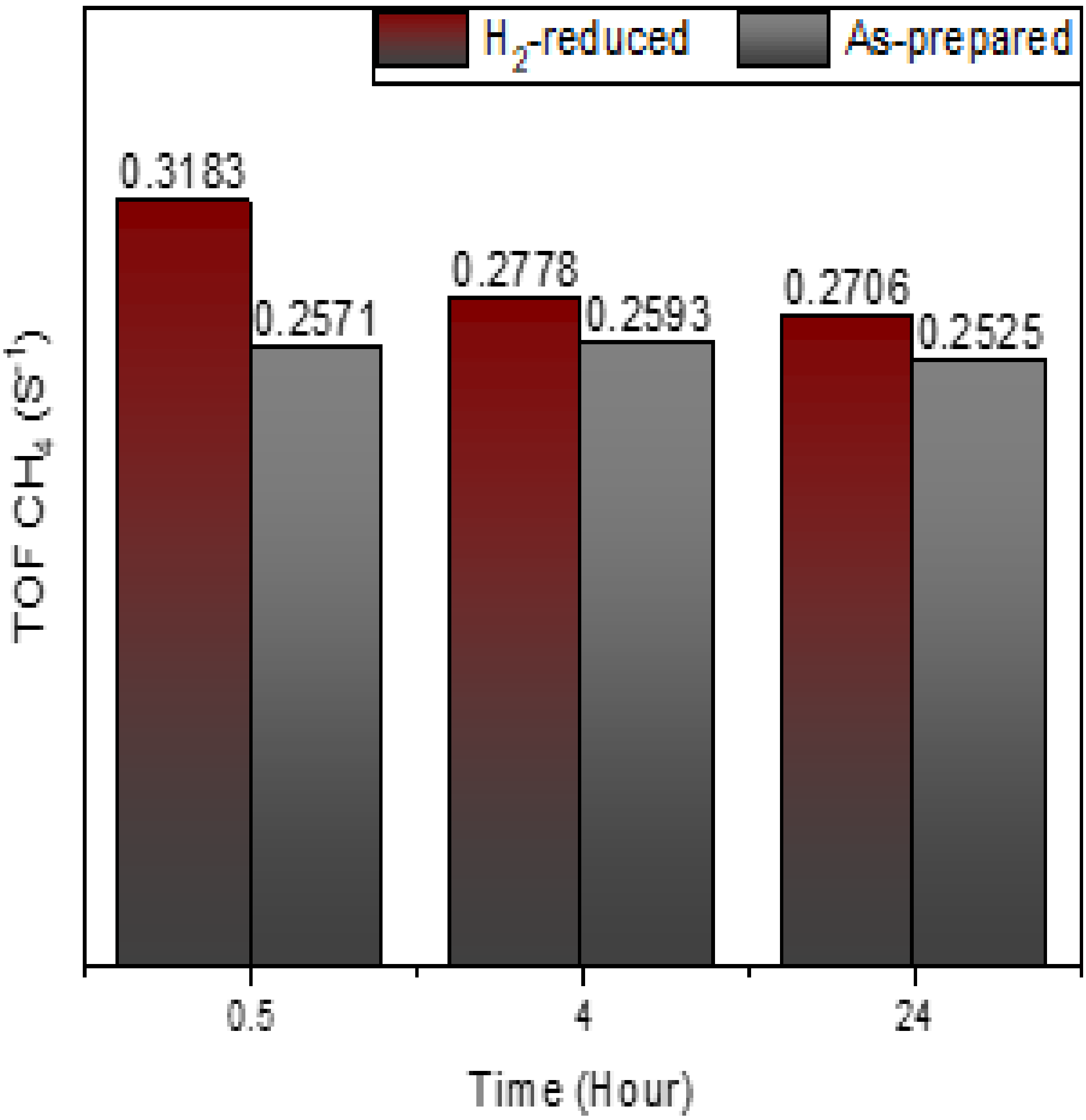

Figure 5.10. Variation of turnover frequency of methane at different for as-prepared and further H_2-reduced B-(75Ni-25Co)/MA catalysts

5.1.4 Analysis of spent catalysts:

The catalyst after the reaction was also characterized by Raman and elemental analysis to study the catalyst deactivation during the reaction due to the deposition of carbon. Fig. 5.11 represents the Raman analysis of spent catalysts of as-prepared and further reduced B-(75Ni-25Co)/MA catalysts. The I_D/I_G was similar for further reduced catalysts compared to the as-prepared catalysts, with a higher value ~3 suggested there was no graphitic carbon in the spent catalysts. Further, the elemental analysis of spent catalysts for both as-prepared and further reduced catalysts was also performed. Fig C1 showed the presence of C ($g_c.g_{cat}^{-1}$) was 0.409 for the further reduced catalyst which is 2.7 times higher than the without H_2-reduced catalyst. Interestingly, the amount of catalysts was observed to be similar when normalized with the produced methane ($g_c.g_{cat}^{-1}$.moles CH_4 converted^{-1}) in Fig. 5.12, which represents the further H_2-reduction step was not provided any additional advantage to limit the carbon deposition.

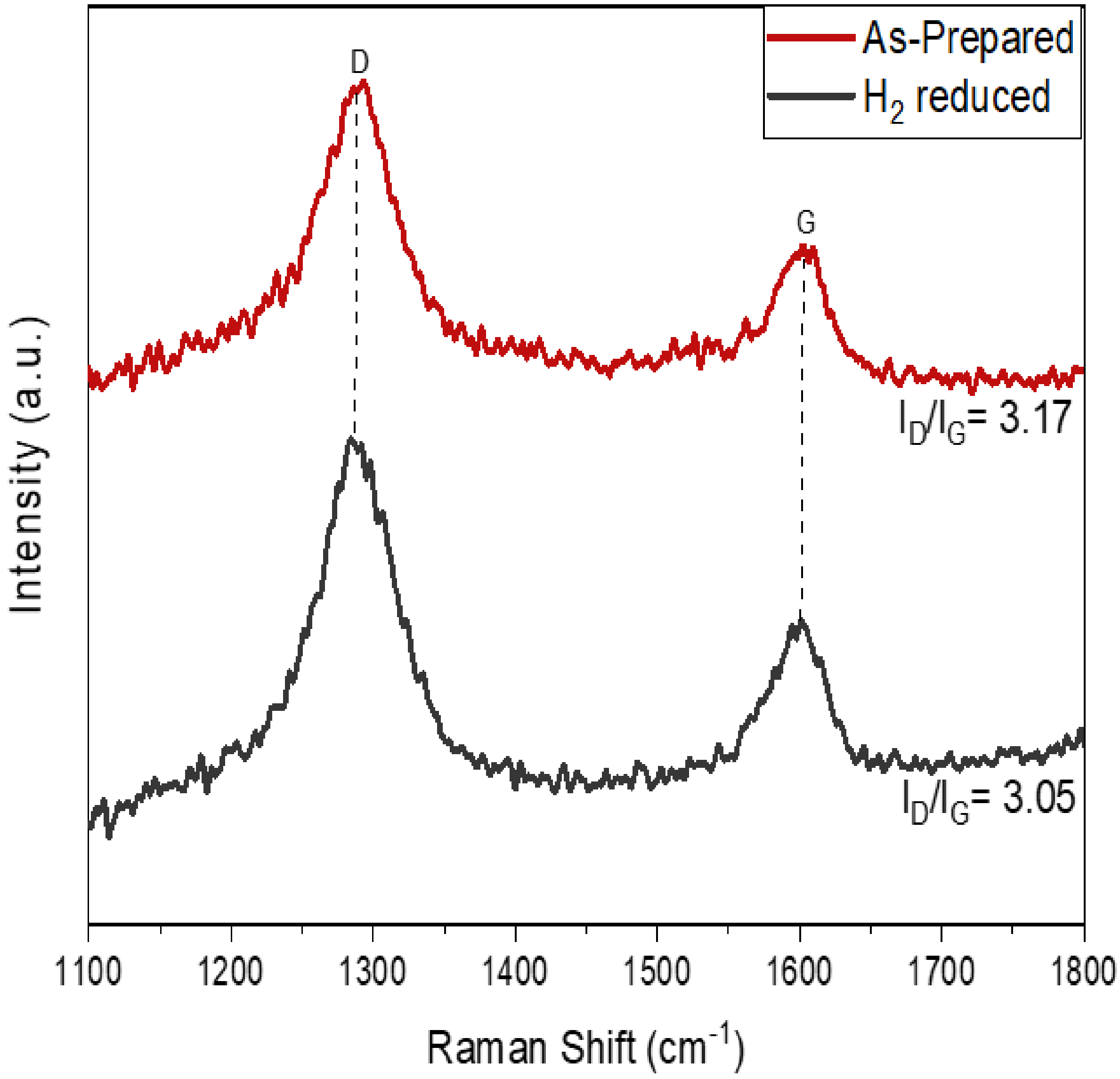

Figure 5.11. Raman analysis for spent as-prepared and further H_2-reduced B-(75Ni-25Co)/MA catalysts

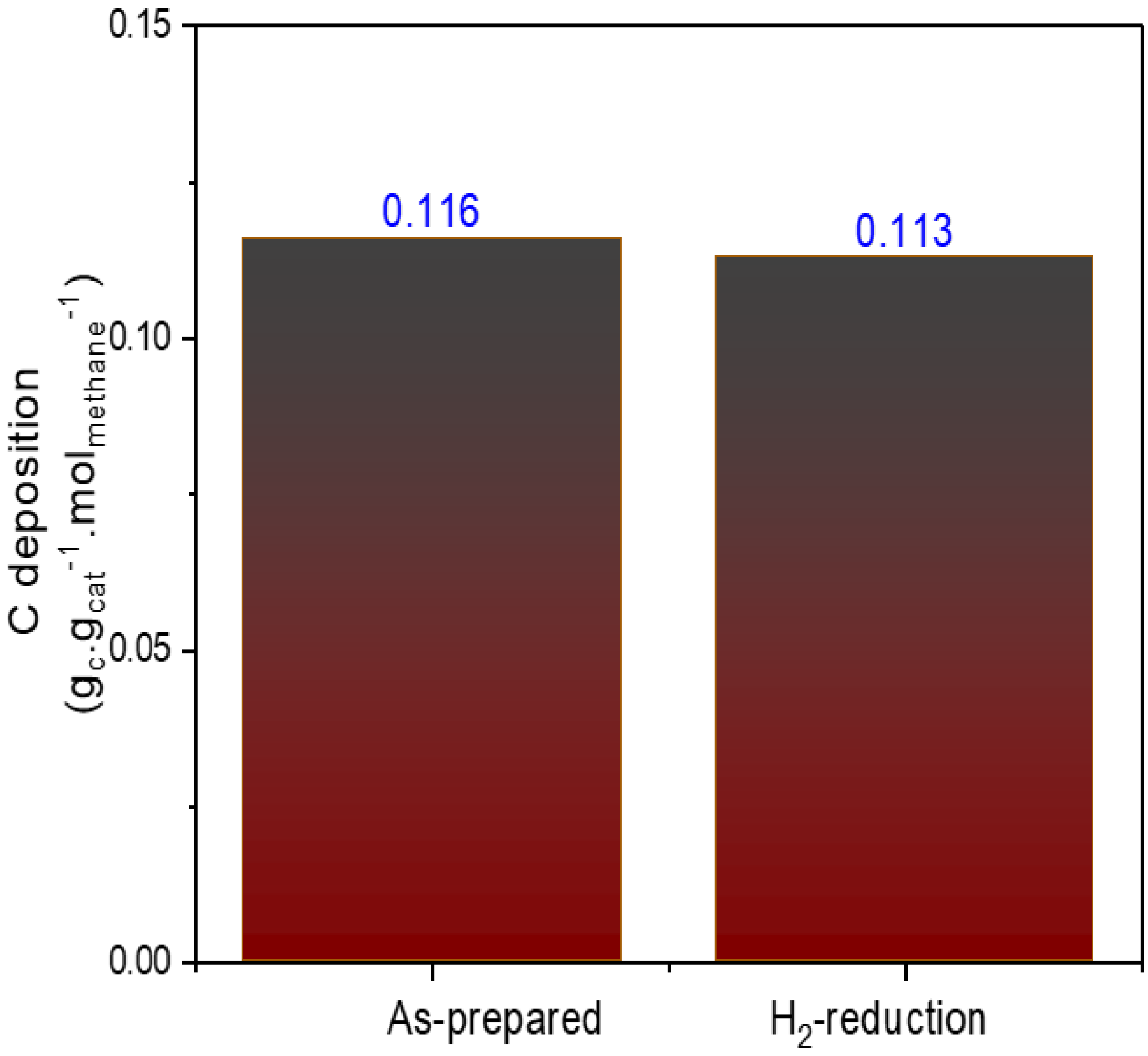

Figure 5.12. Analysis of carbon deposited by elemental analyzer for spent as-prepared and further H_2-reduced B-(75Ni-25Co)/MA catalysts.

5.2 Outcomes:

The DRM was studied over 15 % bimetallic B-(75Ni25Co)/MA supported catalyst over the support MA with further H_2-reduced catalyst and as-prepared catalyst to observe its impact on the reaction performance and also on the deactivation of the catalyst over a long reaction time. From the characterization of both catalysts using XRD, it was observed that sharp peaks of Ni in the H_2-reduced catalyst. However, there was a peak of NiO for the as-prepared catalyst with two peaks of Ni also observed in H_2-TPR with a high degree of reduction compared to the H_2-reduced catalyst. XPS measurements also revealed the exact scenario of the elements with Ni 2p $_{(3/2)}$ and Ni 2p $_{(1/2)}$ for NiO and Ni^0 as-prepared catalyst, while Ni^0 was observed for further reduced catalyst. Most interestingly, the reaction result reveals that the further reduction of the catalyst improves the catalyst performance in terms of CH_4 & CO_2 conversion, H_2: CO ratio, and TOF. However, the carbon deposition was similar for both as-prepared and further reduced catalysts.

Chapter 6

A comparative kinetics and carbon deposition analysis for single-step $NaBH_4$ assisted boron and non-boron $75Ni25Co/MgAl_2O_4$ catalysts

6.1 Results and discussion:

The kinetic analysis of catalysts was investigated for both the boron and non-B 75Ni25Co/MA catalysts. As the conversions of feed gases (CH_4 and CO_2) are the function of temperature as showed in Fig. 6.1. The conversion of CH_4 was observed linearly increased with the temperature for both catalysts. However, the conversion of B-containing catalysts was higher compared to the non-B catalysts, these conversion differences between the two catalysts was well maintianed for all the tempratures (773-973K) . The B-(75Ni25Co)/MA catalysts conversion was ~ 3.9 at 773K, that was ~1.12 times higher than the non-B 75Ni25Co/MA catalysts. However, this factor was slightly increased with the temperature and was ~ 1.21 at 973K.

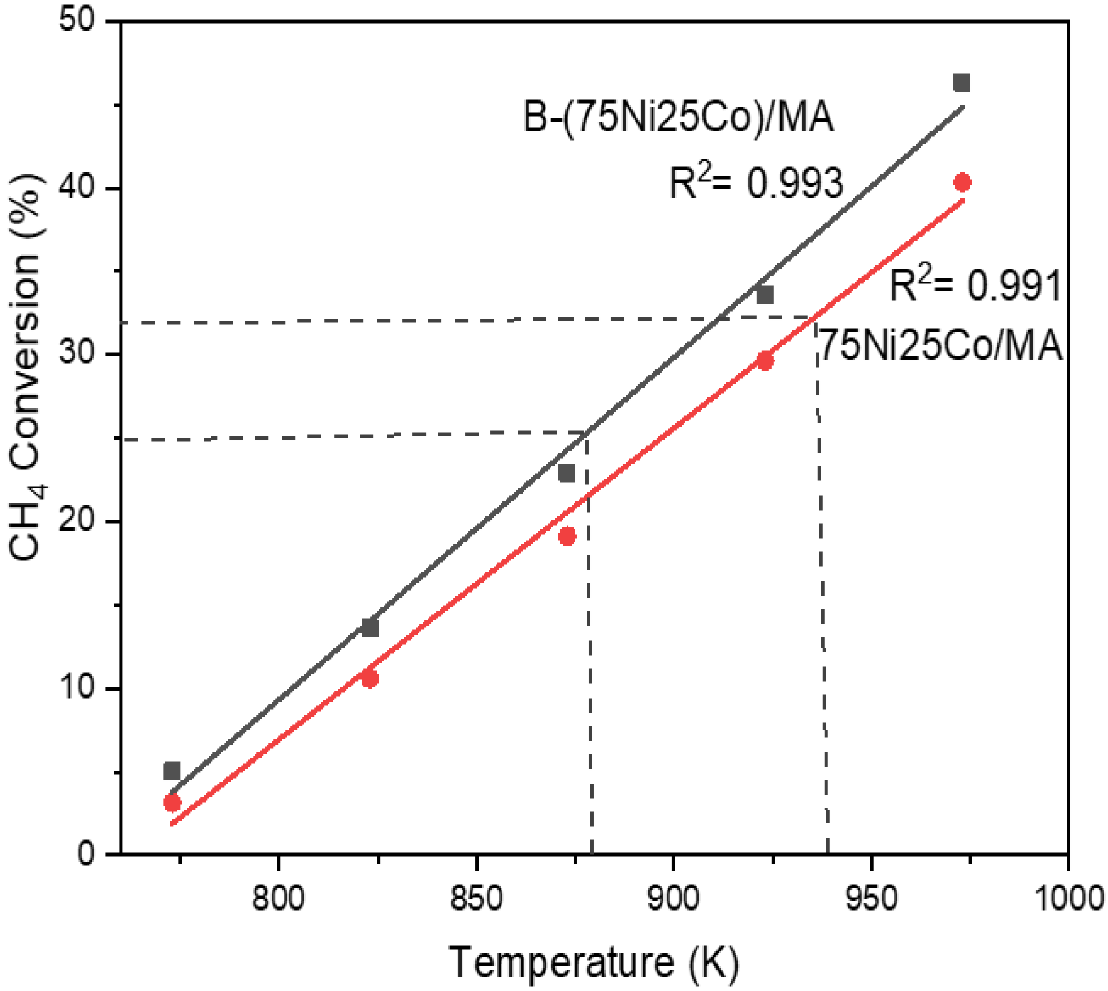

Figure 6.1. The conversion of methane with temperature for B and non-B catalysts.

The CO_2 conversion for both B and non-B 75Ni25Co/MA catalysts was observed in Fig. 6.2. The CO_2 conversion increased linearly for both catalysts, with a higher conversion for B-containing catalysts than for the non-B catalysts. The B-(75Ni25Co)/MA conversion was ~ 6.7 at 773K, which was 1.13 times higher than the non-B 75Ni25Co/MA catalysts; the factor slightly increased with the temperature and was ~ 1.18 at 973K. These conversions data revealed that the B-containing catalysts enhanced the performance of the catalyst for higher temperatures compared to the non-B catalysts.

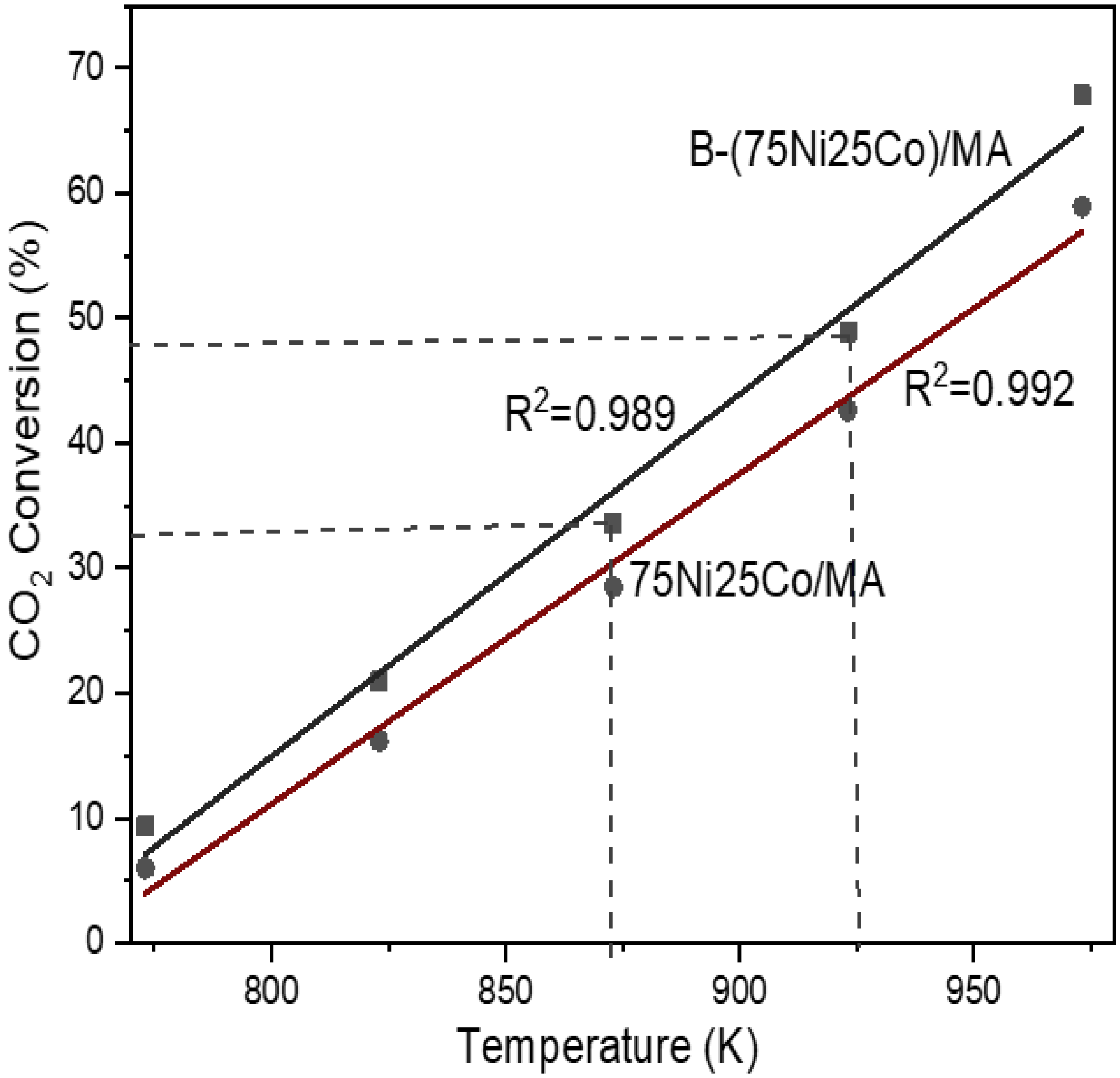

Figure 6.2. Carbon dioxide conversion with temperature for B and non-B catalysts

Furthermore, the rate of reaction was calculated for both B and non-B catalysts. The reaction rate was increased with the temperature for both catalysts. However, the reaction rate for the B-containing catalyst was slightly higher than for the non-B catalysts. This calculated rate of reaction was further used to plot the temperature profile to calculate the apparent activation energy.

Table 6.1. Change of concentration and rate of CH_4 with temperature for with and without B catalyst.

Temperature (K)	**Concentration (mol.cm^{-3}) x (10^{-5})**	**Rate (mol s^{-1}cm^{-3}) x (10^{-5})**	
		B-(75Ni25Co)/MA	**75Ni25Co/MA**
773	5.04	4.48	4.22
823	4.74	9.55	7.23
873	4.47	15.32	13.68
923	4.22	26.51	25.52
973	4.01	30.09	29.94

The slope of the rate of reaction versus inverse temperature plot gives activation energy (E) and gas constant (R) ratio. The rate of reaction for methane conversion for both B and non-B 75Ni25Co/MA catalysts showed in Fig 6.3. A linear decline in the rate of reaction was observed with temperature for both B and non-B catalysts, and a straight line was observed for both catalysts with an insignificant difference. Further, the activation energy calculated from the plot was ~66.67 kJ/mol for B-(75Ni25Co)/MA catalysts. However, the activation energy of the non-B catalyst was slightly higher ~66.94. In addition, the activation energy for CO_2 was also calculated from the rate of reaction versus temperature plot for both B and non-B catalysts. However, the low values of activation energy of carbon dioxide were obtained compared to methane, which could be due to the strong affinity of the CO_2 with the oxides showed in Fig. 6.4. Similar to the CH_4 trend, the CO_2 rate versus temperature plot linearly declined with temperature for both catalysts. The activation energy was calculated as ~55.20 kJ/mol for B-(75Ni25Co)/MA catalysts, slightly lower than the non-B 75Ni25Co/MA catalyst. The low values of activation energy of carbon dioxide were obtained due to the strong affinity of CO_2 with the oxides. These results conclude that the B modification improves the catalyst performance without lowering its activation energy. Further, the effect of internal-external mass transfer was also evaluated by Mear's Criteria suggesting the generated reaction data is in a kinetic regime (Table. D1-D2).

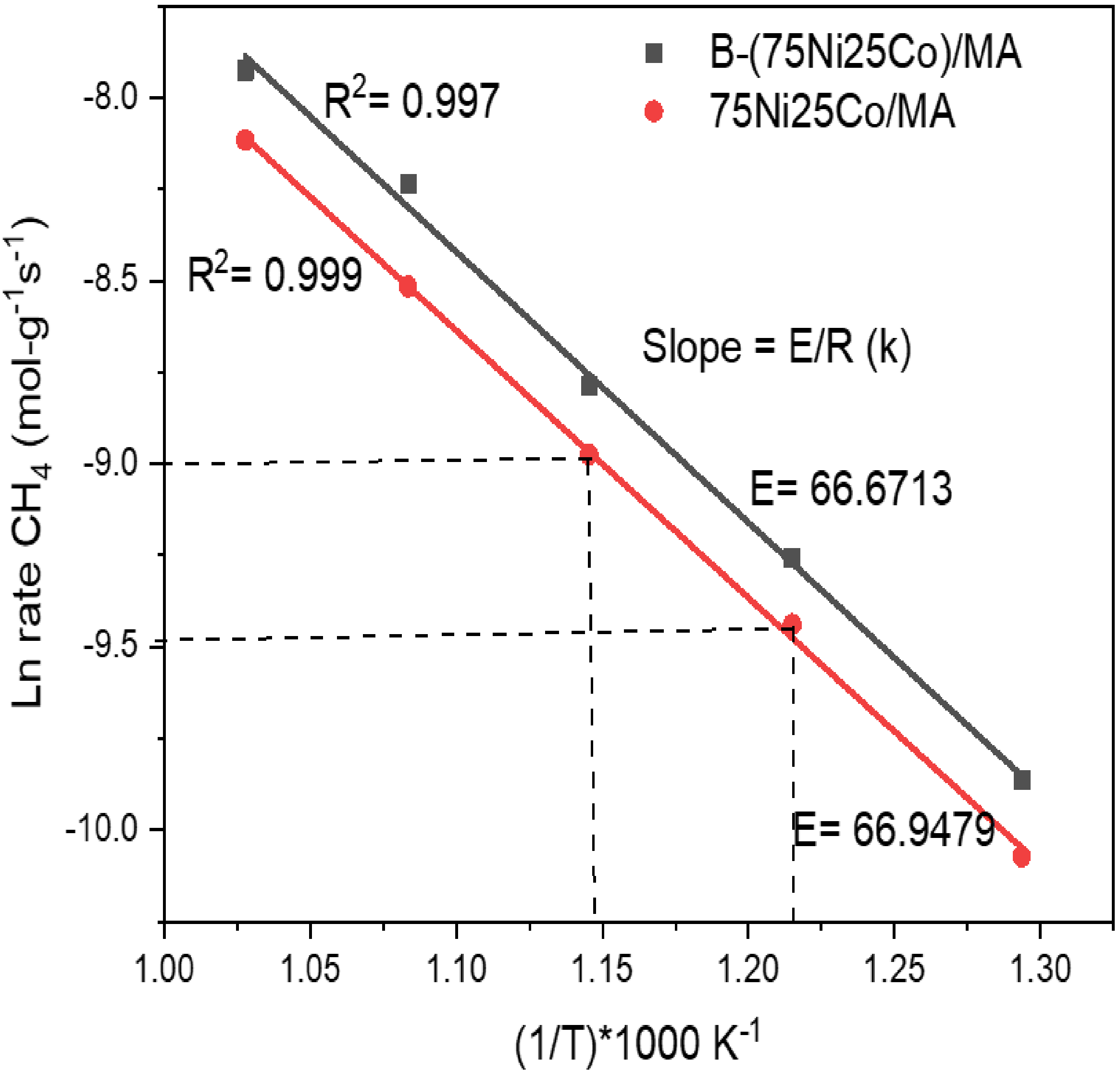

Figure 6.3. The rate of reaction for methane verses temperature for B and non-B catalysts.

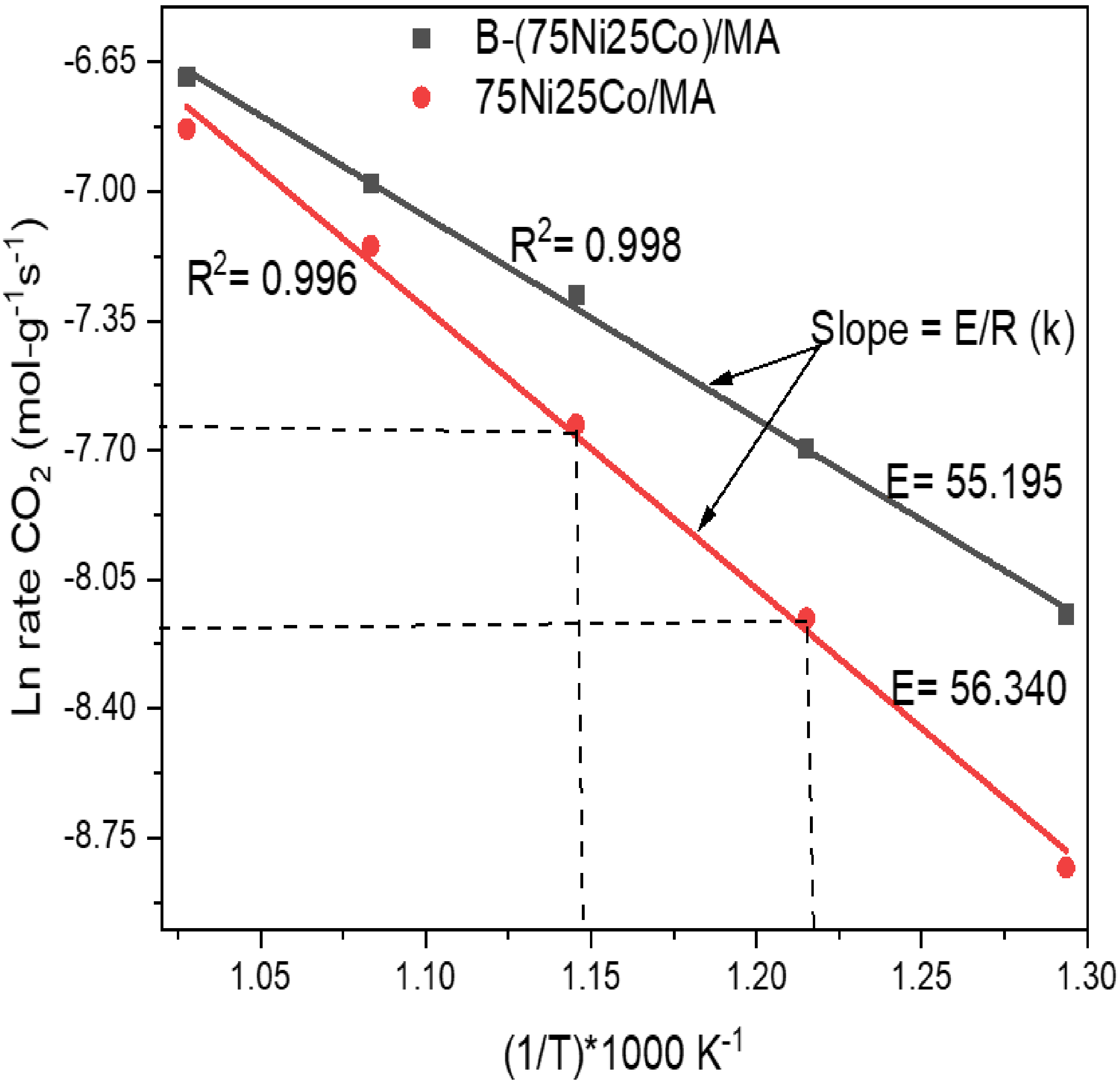

Figure 6.4. The rate of reaction for carbon dioxide versus temperature for B and non-B catalysts.

The obtained activation energy for both B and non-B catalysts was further compared with the previously reported catalysts in Table 6.2. Recently, Zhang et al. [8] reported the activation energy of methane as 69.40 kJ/mol for Ni-Co/Al-Mg-O catalysts at the higher temperature range of 923-1023K. Another study by Qiao et al. [14] with Ni/CeMgAl catalyst showed an activation energy of 65.52 kJ/mol in 773 -873K. Gallego et al. [174] studied the activation energy of samples Ni/La_2O_3 catalyst at the temperature range of 893-963K and reported higher activation energy than Ni/CeMgAl and Ni-Co/Al-Mg-O catalyst. Nandini et al. [175] reported lower activation energy for 13.5Ni-2K/10CeO_2- Al_2O_3 catalyst for the temperature range of 873-1073K. The traditional DRM catalyst Ni/γ-Al_2O_3 shows impressive lower activation energy of 50.90 kJ/mol for the temperature range of 773-973K. The recent study by Kumari et al. [37] reported the activation energy of 59.16 kJ/mol for the 75Ni25Co/MA catalyst. However, the catalysts' activation energy depends on many factors such as the active metal sites, support, another metal, synthesis procedure, operating conditions, reactants ratios, and the promoters such as B [1].

Table 6.2. Compared activation energy data obtained from reported work at different temperatures with the current study for with and without B catalyst.

Source	Catalyst	Temperature Range (K)	Activation energy of CH_4 (kJ/mol)	References
Current work	B-(75Ni25Co)/MA	823-923	66.67	-
Current work	(75Ni25Co)/MA	823-923	66.94	-
Zhang et al.	Ni-Co/Al-Mg-O	923-1023	69.4	[172]
Qiao et al.	$Ni_{15}CeMgAl$	773-873	65.5	[173]
Zhang et al.	Ni/γ-Al_2O_3	773-973	50.9	[24]
Gallego et al.	Ni/La_2O_3	773-973	70.0	[174]
Lemonidou et al.	Ni/CaO/Al_2O_3	893-963	106.7	[71]
Nandini et al.	13.5Ni-2K/10CeO_2-Al_2O_3	873-1073	46.1	[175]
Kumari et al.	75Ni25Co/MA	823-923	59.16	[37]

6.1.1 Analysis of spent catalysts:

The spent catalysts were characterized by the ICP-OES and elemental CHNS analysis for both

B and non-B catalysts at different temperatures in Table 6.3. The composition of Ni, Co, and B was identified by the ICP-OES analysis, and it was observed that the metal-contained B-containing catalysts were not significantly dropped after the DRM reaction. However, the lowest value is ~ 9.89 wt. % was observed at 773K since the higher carbon deposition for DRM at a lower temperature. This trend was similar for both Ni and Co. interestingly, the B wt. % remained the same for all temperatures, showing strong B-Ni-Co interaction that resisted catalysts from the deactivation. However, the Ni and Co wt. % was observed to be lower than the B-containing catalysts due to the deactivation of catalysts during the dry reforming reaction. Further, the amount of deposited carbon was evaluated by the elemental analysis for both B and non-B catalysts listed in Table 6.3. The amount of carbon deposition was increased with the temperature for both catalysts. However, the carbon deposition was ~5.72 times higher for non-B catalysts than the B-containing catalysts at 773K. At the higher temperature, the carbon deposition for non-B catalysts was ~4.63 times higher than the B-containing catalyst. The lower carbon deposition for B-containing catalysts was observed due to the fact that the B effectively sited on the subsurface site of metals where generally carbon used to occupy, resulting the deactivation of catalysts shown in Fig. 6.5.

Table 6.3. Compositions and elemental analysis of spent B and non-B catalysts at different temperatures for DRM reactions.

Temperature (K)	**ICP-OES analysis (Wt %)**					**Elemental analysis ($g_c*g_{cat}^{-1}$)**	
	B-(75Ni25Co)/MA			**75Ni25Co/MA**		**B-(75Ni25Co)/MA**	**75Ni25Co/MA**
	Ni	**Co**	**B**	**Ni**	**Co**		
773	9.89	3.48	2.44	8.14	2.69	0.046	0.262
823	10.11	3.51	2.41	8.11	2.61	0.040	0.224
873	10.23	3.54	2.43	8.69	2.97	0.037	0.196
923	10.53	3.58	2.45	9.26	3.08	0.026	0.148
973	10.62	3.62	2.44	9.89	3.18	0.019	0.087

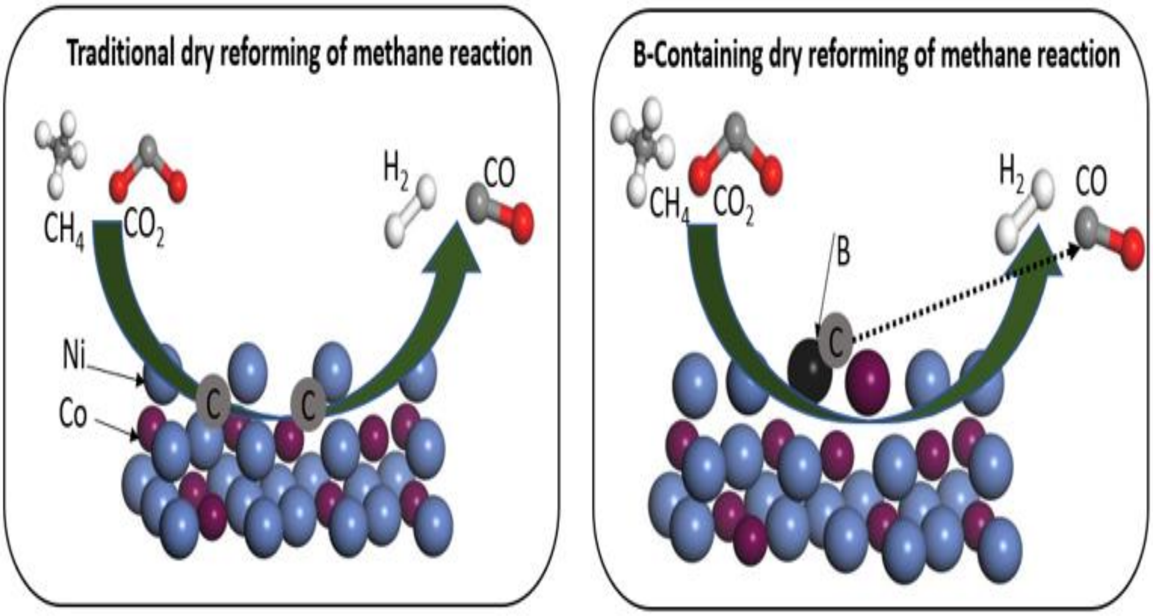

Figure 6.5. A mechanistic representation of bimetallic 75Ni-25Co/MA catalysts for traditional and $NaBH_4$ assisted single-step B-containing catalysts for DRM.

6.2 Outcomes:

The present study developed a kinetic study for the B and non-B bimetallic 75Ni-25Co/MA catalysts for the temperature range from 773-973 K. The conversion of CH_4 and CO_2 linearly increased with increasing temperature. The concentration and rate of reaction for CH_4 and CO_2 were also calculated from conversion and reported to increase with temperature. However, the reaction rate was comparatively higher for the B-containing catalyst than for the non-B catalyst. Further, the calculated activation energy revealed the B-containing catalysts had low activation energy compared to the non-B catalysts. The spent catalysts were characterized by the ICP-OES and elemental analysis. The loss of metal (Ni and Co) was insignificant compared to the non-B catalysts. Interestingly, the retainment of B was observed in spent catalysts at all temperatures. The carbon deposition was extremely low ~5.8 times lesser than the non-B catalysts. In-depth study suggested that the presence of a small amount of B helps a catalyst to achieve good B-metal dispersion and stable metallic species. Finally, the present study provides a new strategy to perform carbon-free DRM with B-containing catalysts for the temperature range of 773-973K without compromising the activity.

Chapter 7

Conclusions and recommendations

7.1 Conclusions:

The current study concludes the enhancement of catalyst performance with doping of a small amount of B on Ni-based catalyst surfaces by the single-step $NaBH_4$ reduction method for the DRM reactions. The catalyst preparation method using $NaBH_4$ appears to be the prime source of dispersing B on Ni-based catalysts and a straightforward way for reducing metal salts. The B(x)-Ni/MA catalysts enhanced the conversion of CH_4 and CO_2 and promoted graphitic-free DRM reaction. The maximum conversion was 2.8 wt. % B-containing B-Ni/MA catalyst and the corresponding $\mathrm{TOF_{CH_4}}$was 0.31 s^{-1}, which was 2.61 times higher than the non-B Ni/MA catalyst. Interestingly, the deposition of resilient graphitic carbon for the B catalyst was significantly lower (~11 times) than for the non-B catalyst. It was found that the presence of B (~2.8 wt.%) facilitated the formation of Ni-B species along with metallic Ni (reduced by $NaBH_4$), controlled the particle size and stabilized the metallic state, and influenced the Ni-C interaction leading to the advancement in catalytic performance and diminution in deactivation.

The developed one-step $NaBH_4$ method for the B (2.8 wt.%) containing Ni-Co bimetallic catalysts offered a steady conversion of CH_4 and CO_2 for the DRM with a reasonable H_2:CO ratio. The B-modified catalyst's performance was better than the catalyst prepared by the traditional impregnation method in terms of reactivity and resistance toward carbon deposition. Additionally, the severe H_2 reduction step during preparation was not required for the developed catalyst, which is traditionally used. The in-depth study suggests that the presence of a small amount of B helps a catalyst to achieve good B-metal dispersion and stable metallic species. The lattice spacing and the elemental distribution confirmed the presence of Ni, Co, and Ni-Co-B. The maximum $\mathrm{TOF_{CH_4}}$ and $\mathrm{TOF_{CO_2}}$ were found to be 0.299 and 0.480 $s^{-1,}$ respectively, for catalysts containing 10.89 wt% of Ni, 3.71 wt% of Co, and 2.68 wt% of B [(B-(75Ni-25Co)/MA], which were 1.50 and 1.17 times higher than the similar non-B catalyst. Interestingly, the carbon deposition was extremely low (~5 times lesser than the non-B) and of non-graphitic nature. B also helps in hindering the formation of carbon on the catalyst surface. The amount of deposited carbon was 0.039 g/g_{cat}^{-1} for the developed catalyst, while 0.106 g/g_{cat}^{-1} for the catalyst that does not contain B. Besides the importance of B inclusion, the study also realizes that a particular metallic ratio (Ni-Co =3:1) is also crucial for the supported bimetallic catalyst to achieve maximum activity and stability for DRM. Additionally, the DFT calculation also revealed the adsorption energy ($\mathrm{E_{ads}}$) of C on (Ni-Co =3:1) catalyst significantly reduces the deactivation of Ni-based catalysts with B's presence by ~0.5eV. Thus, adding a small amount of B may effectively block these sites for carbon and force carbon atoms to remain on the 75Ni-25Co catalyst surface for the reaction, consequently preventing the coking

The bimetallic B-(75Ni25Co)/MA catalyst was further reduced with H_2 to observe the effect on the DRM reaction compared with the as-prepared B-(75Ni25Co)/MA catalyst. A complete reduction of catalysts (degree of reduction of 3.56 %) was observed for further H_2-reduced catalyst along with the enhancement of the metal dispersion. A sharp peak of M^0 was observed in the XRD spectrum for the further H_2-reduced catalyst. However, there was a peak of M^0 and MO peak present for the as-prepared catalyst. For more clarity, the XPS analysis revealed the exact scenario of the elements with Ni 2p (3/2) and Ni 2p (1/2) for NiO and Ni0 for the as-prepared catalyst while only Ni0 was observed for further H_2-reduced catalyst that was in line with the XRD and H_2-TPR results. Interestingly the reaction result reveals that further H_2-reduction improves the catalyst performance in terms of conversion and H_2: CO ratio at the initial phase of the reaction. However, the difference in conversion and produced H_2: CO ratio was similar to the as-prepared catalyst at TOS 24h. In addition, the $\mathrm{TOF}_{\mathrm{CH_4}}$ was also comparable for both catalysts after 4h of the reaction period, suggested the further H_2-reduction of $NaBH_4$ reduced B-(75Ni25Co)/MA catalysts showed high conversions only at the initial phase of reaction and became same as as-prepared catalysts after 4-5h of reaction. The characterizations of spent catalysts suggested graphitic-free DRM after 24h; the amount of deposited carbon was similar for both further H_2-reduced and as-prepared B-(75Ni25Co)/MA deposition with normalization with the methane conversion. Furthermore, a kinetic study for the B and non-B bimetallic 75Ni-25Co/MA catalysts suggested that the conversion of CH_4 and CO_2 linearly increased with increasing temperature. The concentration and rate of reaction for CH_4 and CO_2 were also calculated from conversion and reported to increase with temperature. However, the reaction rate was comparatively higher for the B-containing catalyst than for the non-B catalyst. Further, the calculated activation energy was observed to be the same for both catalysts. The spent catalysts were characterized by the ICP-OES and elemental analysis. The loss of metal (Ni and Co) was insignificant compared to the non-B catalysts. Interestingly, the retainment of B was observed in spent catalysts at all temperatures. The carbon deposition was extremely low ~5.8 times lesser than the non-B catalysts. The in-depth study suggests that the presence of a small amount of B helps a catalyst to achieve good B-metal dispersion and stable metallic species. Finally, the present study provides a new strategy to perform carbon-free DRM with B-containing catalysts for the temperature range of 773-973K without compromising the activity.

7.2 Recommendations:

The present study developed a novel catalyst preparation method for low-deactivated graphitic-carbon-free DRM reaction pathways. The catalyst synthesis by the $NaBH_4$ reduction method appears to be a promising single-step method of doping B on the surface of Ni-based catalysts. ~ 2.8 wt % of B showed as an optimum amount for 15 wt % of metal-containing catalysts. Additionally, the bimetallic 3:1 ratio B-containing B-(75Ni-25Co)/MA catalyst appeared as the best-performing catalyst with low carbon deposition for DRM. Based on current outcomes and as this method has not been used extensively used so for the future work the recommendations are as follows.

- Nowadays, peroxide catalysts have been used to solve the catalyst deactivation issue. However, the preparation of catalysts is too complicated, and losses of metallic elements are very often, so it would be interesting to observe the effect

- It would be interesting to observe the effect of traditional promoters such as Ca and Mg on the surface of the B-(75Ni-25Co)/MA catalyst. However, the amount of promoters should be very optimum to prevent the active site of Ni particles.

- The oxygen storage support, such as ceria and zirconia-based support, can use to effect on DRM

- The catalysts can be used for other reforming processes, such as steam reforming of methane and partial oxidation of methane. Additionally, the mixed steam and dry reforming (Bi-reforming) of methane reaction is another way to produce syngas. The present B-(75Ni-25Co)/MA catalyst could show some exciting results as the H_2 and CO ratio can expect to be higher compared to the DRM.

- In terms of theoretical studies, it would be worthwhile to develop a kinetic model using simulation tools can be developed to observe the effect of B-(75Ni-25Co)/MA catalyst at different reaction conditions such as temperature, pressure, feed ratio, GHSV, reactor size, bed height, particle size and inert gas (N_2 and He).

References:

[1] Khandekar ML, Murty TS, Chittibabu P. The Global Warming Debate: A Review of the State of Science. pure and applied geophysics 2005;162(8):1557-86.

[2] Abdulrasheed A, Jalil AA, Gambo Y, Ibrahim M, Hambali HU, Shahul Hamid MY. A review on catalyst development for dry reforming of methane to syngas: Recent advances. Renewable and Sustainable Energy Reviews 2019;108:175-93.

[3] Al-Mamoori A, Krishnamurthy A, Rownaghi AA, Rezaei F. Carbon Capture and Utilization Update. Energy Technology 2017;5(6):834-49.

[4] Zabula W. Summary for Policymakers of IPCC Special Report on Global Warming of 1.5°C approved by government. 2018.

[5] Alfonso S, Gesto M, Sadoul B. Temperature increase and its effects on fish stress physiology in the context of global warming. Journal of Fish Biology 2021;98(6):1496-508.

[6] McCarthy MP, Best MJ, Betts RA. Climate change in cities due to global warming and urban effects. Geophysical Research Letters 2010;37(9).

[7] Rogelj J, den Elzen M, Höhne N, Fransen T, Fekete H, Winkler H, et al. Paris Agreement climate proposals need a boost to keep warming well below 2 °C. Nature 2016;534(7609):631-9.

[8] Peters GP, Andrew RM, Boden T, Canadell JG, Ciais P, Le Quéré C, et al. The challenge to keep global warming below 2 °C. Nature Climate Change 2013;3(1):4-6.

[9] Nogueira LM, Yabroff KR, Bernstein A. Climate change and cancer. CA: a cancer journal for clinicians 2020;70(4):239-44.

[10] Jang W-J, Shim J-O, Kim H-M, Yoo S-Y, Roh H-S. A review on dry reforming of methane in aspect of catalytic properties. Catalysis Today 2019;324:15-26.

[11] Kallio P, Pásztor A, Akhtar MK, Jones PR. Renewable jet fuel. Current Opinion in Biotechnology 2014;26:50-5.

[12] Wang J-h, Mamkhezri J, Khezri M, Karimi MS, Khan YA. Insights from European nations on the spatial impacts of renewable energy sources on CO2 emissions. Energy Reports

2022;8:5620-30.

[13] Snyder CS, Bruulsema TW, Jensen TL, Fixen PE. Review of greenhouse gas emissions from crop production systems and fertilizer management effects. Agriculture, Ecosystems & Environment 2009;133(3):247-66.

[14] Iddphonce R, Wang J. Investigation of CO2 and CH4 competitive adsorption during enhanced shale gas production. Journal of Petroleum Science and Engineering 2021;205:108802.

[15] Elsayed NH, Roberts NRM, Joseph B, Kuhn JN. Low temperature dry reforming of methane over Pt–Ni–Mg/ceria–zirconia catalysts. Applied Catalysis B: Environmental 2015;179:213-9.

[16] Guo J, Lou H, Zhao H, Chai D, Zheng X. Dry reforming of methane over nickel catalysts supported on magnesium aluminate spinels. Applied Catalysis A: General 2004;273(1):75-82.

[17] Hadian N, Rezaei M, Mosayebi Z, Meshkani F. CO2 reforming of methane over nickel catalysts supported on nanocrystalline MgAl2O4 with high surface area. Journal of Natural Gas Chemistry 2012;21(2):200-6.

[18] Karemore AL, Sinha R, Chugh P, Vaidya PD. Mixed reforming of methane over Ni–K/CeO2–Al2O3: Study of catalyst performance and reaction kinetics. International Journal of Hydrogen Energy 2021;46(7):5223-33.

[19] Wang Z, Cheng Y, Shao X, Veder J-P, Hu X, Ma Y, et al. Nanocatalysts anchored on nanofiber support for high syngas production via methane partial oxidation. Applied Catalysis A: General 2018;565:119-26.

[20] Wen J, Xie Y, Ma Y, Sun H, Wang H, Liu M, et al. Engineering of surface properties of Ni-CeZrAl catalysts for dry reforming of methane. Fuel 2022;308:122008.

[21] Wong Y, Halim HH, Khairudin NF, Pham TN, Putra SEM, Hamamoto Y, et al. Dry Reforming of Methane on Cobalt Catalysts: DFT-Based Insights into Carbon Deposition Versus Removal. The Journal of Physical Chemistry C 2021;125(40):21902-13.

[22] Zhang G, Liu J, Xu Y, Sun Y. A review of CH4CO2 reforming to synthesis gas over Ni-based catalysts in recent years (2010–2017). International Journal of Hydrogen Energy

2018;43(32):15030-54.

[23] Zhang J, Wang H, Dalai AK. Development of stable bimetallic catalysts for carbon dioxide reforming of methane. Journal of Catalysis 2007;249(2):300-10.

[24] Zhang M, Cheng D-g, Zhang Y-p. Carbon dioxide reforming of methane over a novel Ni/Al2O3 catalysts. Prepr Pap-Am Chem Soc, Div Fuel Chem 2004;49(1):188.

[25] Theofanidis SA, Galvita VV, Poelman H, Marin GB. Enhanced Carbon-Resistant Dry Reforming Fe-Ni Catalyst: Role of Fe. ACS Catalysis 2015;5(5):3028-39.

[26] Torrez-Herrera JJ, Korili SA, Gil A. Recent progress in the application of Ni-based catalysts for the dry reforming of methane. Catalysis Reviews 2021:1-58.

[27] Vasiliades MA, Damaskinos CM, Kyprianou KK, Kollia M, Efstathiou AM. The effect of Pt on the carbon pathways in the dry reforming of methane over Ni-Pt/Ce0.8Pr0.2O2-δ catalyst. Catalysis Today 2020;355:788-803.

[28] Vasiliades MA, Makri MM, Djinović P, Erjavec B, Pintar A, Efstathiou AM. Dry reforming of methane over 5wt% Ni/Ce1-xPrxO2-δ catalysts: Performance and characterisation of active and inactive carbon by transient isotopic techniques. Applied Catalysis B: Environmental 2016;197:168-83.

[29] Abbas SZ, Dupont V, Mahmud T. Kinetics study and modelling of steam methane reforming process over a NiO/Al2O3 catalyst in an adiabatic packed bed reactor. International Journal of Hydrogen Energy 2017;42(5):2889-903.

[30] Braga AH, de Oliveira DC, Taschin AR, Santos JBO, Gallo JMR, C. Bueno JM. Steam Reforming of Ethanol Using Ni–Co Catalysts Supported on MgAl2O4: Structural Study and Catalytic Properties at Different Temperatures. ACS Catalysis 2021;11(4):2047-61.

[31] Guo J, Xie C, Lee K, Guo N, Miller JT, Janik MJ, et al. Improving the Carbon Resistance of Ni-Based Steam Reforming Catalyst by Alloying with Rh: A Computational Study Coupled with Reforming Experiments and EXAFS Characterization. ACS Catalysis 2011;1(6):574-82.

[32] Hallajbashi N, Shahraki BH, Asemani M. Multilateral Analysis of Pressure and Temperature Effects on Steam Methane Reforming Reaction. Petroleum Science and Technology 2012;30(21):2264-72.

[33] Katheria S, Gupta A, Deo G, Kunzru D. Effect of calcination temperature on stability and activity of Ni/MgAl2O4 catalyst for steam reforming of methane at high pressure condition. International Journal of Hydrogen Energy 2016;41(32):14123-32.

[34] Nguyen HM, Pham GH, Ran R, Vagnoni R, Pareek V, Liu S. Dry reforming of methane over Co–Mo/Al2O3 catalyst under low microwave power irradiation. Catalysis Science & Technology 2018;8(20):5315-24.

[35] Nguyen HM, Pham GH, Tade M, Phan C, Vagnoni R, Liu S. Microwave-Assisted Dry and Bi-reforming of Methane over M–Mo/TiO2 (M = Co, Cu) Bimetallic Catalysts. Energy & Fuels 2020.

[36] Nguyen HM, Sunarso J, Li C, Pham GH, Phan C, Liu S. Microwave-assisted catalytic methane reforming: A review. Applied Catalysis A: General 2020;599.

[37] Kumari R, Sengupta S. Catalytic CO2 reforming of CH4 over MgAl2O4 supported Ni-Co catalysts for the syngas production. International Journal of Hydrogen Energy 2020.

[38] Das T, Sengupta S, Deo G. Effect of calcination temperature during the synthesis of Co/Al2O3 catalyst used for the hydrogenation of CO2. Reaction Kinetics, Mechanisms and Catalysis 2013;110(1):147-62.

[39] Ray K, Sengupta S, Deo G. Reforming and cracking of CH 4 over Al 2 O 3 supported Ni, Ni-Fe and Ni-Co catalysts. Fuel Processing Technology 2017;156:195-203.

[40] Sengupta S, Deo G. Modifying alumina with CaO or MgO in supported Ni and Ni–Co catalysts and its effect on dry reforming of CH4. Journal of CO2 Utilization 2015;10:67-77.

[41] Sengupta S, Ray K, Deo G. Effects of modifying Ni/Al2O3 catalyst with cobalt on the reforming of CH4 with CO2 and cracking of CH4 reactions. International Journal of Hydrogen Energy 2014;39(22):11462-72.

[42] Ballesteros-Plata D, Infantes-Molina A, Rodríguez-Castellón E, Cauqui MA, Yeste MP. Improving noble metal catalytic activity in the dry reforming of methane by adding niobium. Fuel 2022;308:121996.

[43] Ray K, Bhardwaj R, Singh B, Deo G. Developing descriptors for CO2 methanation and CO2 reforming of CH4 over Al2O3 supported Ni and low-cost Ni based alloy catalysts. Phys

Chem Chem Phys 2018;20(23):15939-50.

[44] Binte Mohamed DK, Veksha A, Lim T-T, Lisak G. Hydrogen bromide in syngas: Effects on tar reforming, water gas-shift activities and sintering of Ni-based catalysts. Applied Catalysis B: Environmental 2021;280:119435.

[45] Hadian N, Rezaei M. Combination of dry reforming and partial oxidation of methane over Ni catalysts supported on nanocrystalline MgAl2O4. Fuel 2013;113:571-9.

[46] Bae JW, Kang S-H, Lee Y-J, Jun K-W. Synthesis of DME from syngas on the bifunctional Cu–ZnO–Al2O3/Zr-modified ferrierite: Effect of Zr content. Applied Catalysis B: Environmental 2009;90(3):426-35.

[47] Wang Y, Wang W-l, Chen Y-x, Zheng J-j, Li R-f. Synthesis of dimethyl ether from syngas using a hierarchically porous composite zeolite as the methanol dehydration catalyst. Journal of Fuel Chemistry and Technology 2013;41(7):873-80.

[48] Shi Y, Xiang Z, Deng J, Nan J, Zhang B. Synthesis Pd/biomass-based carbon microsheet composite for efficient dehydrogenation from formic acid. Materials Letters 2019;237:61-4.

[49] Steinhauer B, Kasireddy MR, Radnik J, Martin A. Development of Ni-Pd bimetallic catalysts for the utilization of carbon dioxide and methane by dry reforming. Applied Catalysis A: General 2009;366(2):333-41.

[50] Vakili R, Gholami R, Stere CE, Chansai S, Chen H, Holmes SM, et al. Plasma-assisted catalytic dry reforming of methane (DRM) over metal-organic frameworks (MOFs)-based catalysts. Applied Catalysis B: Environmental 2020;260:118195.

[51] Movasati A, Alavi SM, Mazloom G. Dry reforming of methane over CeO2-ZnAl2O4 supported Ni and Ni-Co nano-catalysts. Fuel 2019;236:1254-62.

[52] Wolfbeisser A, Sophiphun O, Bernardi J, Wittayakun J, Föttinger K, Rupprechter G. Methane dry reforming over ceria-zirconia supported Ni catalysts. Catalysis Today 2016;277:234-45.

[53] Wang Z, Hu X, Dong D, Parkinson G, Li C-Z. Effects of calcination temperature of electrospun fibrous Ni/Al2O3 catalysts on the dry reforming of methane. Fuel Processing Technology 2017;155:246-51.

[54] Wang Z, Shao X, Larcher A, Xie K, Dong D, Li C-Z. A study on carbon formation over

fibrous NiO/CeO2 nanocatalysts during dry reforming of methane. Catalysis Today 2013;216:44-9.

[55] Arora S, Prasad R. An overview on dry reforming of methane: strategies to reduce carbonaceous deactivation of catalysts. RSC Advances 2016;6(110):108668-88.

[56] Singh S, Nguyen TD, Siang TJ, Phuong PTT, Huy Phuc NH, Truong QD, et al. Boron-doped Ni/SBA-15 catalysts with enhanced coke resistance and catalytic performance for dry reforming of methane. Journal of the Energy Institute 2020;93(1):31-42.

[57] Zhang S, Ying M, Yu J, Zhan W, Wang L, Guo Y, et al. NixAl1O2-δ mesoporous catalysts for dry reforming of methane: The special role of NiAl2O4 spinel phase and its reaction mechanism. Applied Catalysis B: Environmental 2021;291.

[58] Zhu M, Song Y, Chen S, Li M, Zhang L, Xiang W. Chemical looping dry reforming of methane with hydrogen generation on Fe2O3/Al2O3 oxygen carrier. Chemical Engineering Journal 2019;368:812-23.

[59] Zhang Q, Zhang T, Shi Y, Zhao B, Wang M, Liu Q, et al. A sintering and carbon-resistant Ni-SBA-15 catalyst prepared by solid-state grinding method for dry reforming of methane. Journal of CO2 Utilization 2017;17:10-9.

[60] Walter JC, Zurawski A, Montgomery D, Thornburg M, Revankar S. Sodium borohydride hydrolysis kinetics comparison for nickel, cobalt, and ruthenium boride catalysts. Journal of Power Sources 2008;179(1):335-9.

[61] Aly M, Fornero EL, Leon-Garzon AR, Galvita VV, Saeys M. Effect of Boron Promotion on Coke Formation during Propane Dehydrogenation over Pt/γ-Al2O3 Catalysts. ACS Catalysis 2020;10(9):5208-16.

[62] Biswas S, Lee H-Y, Prasad M, Sharma A, Yu J-S, Sengupta S, et al. Black TiO2–x Nanoparticles Decorated with Ni Nanoparticles and Trace Amounts of Pt Nanoparticles for Photocatalytic Hydrogen Generation. ACS Applied Nano Materials 2021;4(5):4441-51.

[63] Egelske BT, Keels JM, Monnier JR, Regalbuto JR. An analysis of electroless deposition derived Ni-Pt catalysts for the dry reforming of methane. Journal of Catalysis 2020;381:374-84.

[64] C.H.Bartholomew, R.B.Pannell. The stoichiometry of hydrogen and carbon monoxide chemisorption on alumina- and silica-supported nickel. Journal of Catalysis 1980;65(2):390-401.

[65] Ozdogan SZ, Gochis PD, Falconer JL. Carbon and carbon monoxide hydrogenation on nickel: Support effects. Journal of Catalysis 1983;83(2):257-66.

[66] Fujimoto K, Kameyama M, Kunugi T. Hydrogenation of adsorbed carbon monoxide on supported platinum group metals. Journal of Catalysis 1980;61(1): 7-14.

[67] Raupp GB, Dumesic JA. Effect of varying titania surface coverage on the chemisorptive behavior of nickel. Journal of Catalysis 1985;95(2):587-601.

[68] Shibiao R, Jinheng Q, Chunyan W, Bolian X, Yining F, Yi C. Influence of Nickel Salt Precursors on the Hydrogenation Activity of Ni/γ-Al2O3 Catalyst. Chinese Journal of Catalysis 2007;28(7):651–6.

[69] Wu H, Pantaleo G, La Parola V, Venezia AM, Collard X, Aprile C, et al. Bi- and trimetallic Ni catalysts over Al2O3 and Al2O3-MOx (M=Ce or Mg) oxides for methane dry reforming: Au and Pt additive effects. Applied Catalysis B: Environmental 2014;156-157:350-61.

[70] Hao Z, Zhu Q, Jiang Z, Hou B, Li H. Characterization of aerogel Ni/Al2O3 catalysts and investigation on their stability for CH4-CO2 reforming in a fluidized bed. Fuel Processing Technology 2009;90(1):113-21.

[71] Lemonidou AA, Vasalos IA. Carbon dioxide reforming of methane over 5 wt.% Ni/CaO-Al2O3 catalyst. Applied Catalysis A: General 2002;228(1):227-35.

[72] Luisetto I, Sarno C, De Felicis D, Basoli F, Battocchio C, Tuti S, et al. Ni supported on γ-Al2O3 promoted by Ru for the dry reforming of methane in packed and monolithic reactors. Fuel Processing Technology 2017;158:130-40.

[73] Morales Anzures F, Salinas Hernández P, Mondragón Galicia G, Gutiérrez Martínez A, Tzompantzi Morales F, Romero Romo MA, et al. Synthetic gas production by dry reforming of methane over Ni/Al2O3–ZrO2 catalysts: High H2/CO ratio. International Journal of Hydrogen Energy 2021;46(51):26224-33.

[74] Ocsachoque M, Pompeo F, Gonzalez G. Rh–Ni/CeO2–Al2O3 catalysts for methane dry

reforming. Catalysis Today 2011;172(1):226-31.

[75] Ocsachoque M, Quincoces CE, González MG. Effect of rh addition on activity and stability over NI/γ-AL2o3 catalysts during methane reforming with CO2. In: Bellot Noronha F, Schmal M, Falabella Sousa-Aguiar E, editors. Studies in Surface Science and Catalysis. Elsevier; 2007, p. 397-402.

[76] Ray D, Reddy PMK, Subrahmanyam C. Ni-Mn/γ-Al2O3 assisted plasma dry reforming of methane. Catalysis Today 2018;309:212-8.

[77] Romeo E, Saeys M, Monzón A, Borgna A. Carbon nanotube formation during propane decomposition on boron-modified Co/Al2O3 catalysts: A kinetic study. International Journal of Hydrogen Energy 2014;39(31):18016-26.

[78] Ay H, Üner D. Dry reforming of methane over CeO2 supported Ni, Co and Ni–Co catalysts. Applied Catalysis B: Environmental 2015;179:128-38.

[79] Han K, Yu W, Xu L, Deng Z, Yu H, Wang F. Reducing carbon deposition and enhancing reaction stability by ceria for methane dry reforming over Ni@SiO2@CeO2 catalyst. Fuel 2021;291:120182.

[80] Pappacena A, Razzaq R, de Leitenburg C, Boaro M, Trovarelli A. The Role of Neodymium in the Optimization of a Ni/CeO2 and Ni/CeZrO2 Methane Dry Reforming Catalyst. Inorganics 2018;6(2).

[81] Zhang R-j, Xia G-f, Li M-f, Wu Y, Nie H, Li D-d. Effect of support on the performance of Ni-based catalyst in methane dry reforming. Journal of Fuel Chemistry and Technology 2015;43(11):1359-65.

[82] Chatla A, Abu-Rub F, Prakash AV, Ibrahim G, Elbashir NO. Highly stable and coke-resistant Zn-modified Ni-Mg-Al hydrotalcite derived catalyst for dry reforming of methane: Synergistic effect of Ni and Zn. Fuel 2022;308:122042.

[83] Vasiliades MA, Djinović P, Davlyatova LF, Pintar A, Efstathiou AM. Origin and reactivity of active and inactive carbon formed during DRM over Ni/Ce0.38Zr0.62O2-δ studied by transient isotopic techniques. Catalysis Today 2018;299:201-11.

[84] Khajenoori M, Rezaei M, Meshkani F. Dry reforming over CeO 2 -promoted Ni/MgO nano-

catalyst: Effect of Ni loading and CH 4 /CO 2 molar ratio. Journal of Industrial and Engineering Chemistry 2015;21:717-22.

[85] Jing QS, Fei JH, Lou H, Mo LY, Zheng XM. Effective reforming of methane with CO2 and O2 to low H2/CO ratio syngas over Ni/MgO–SiO2 using fluidized bed reactor. Energy Conversion and Management 2004;45(20):3127-37.

[86] Rouibah K, Barama A, Benrabaa R, Guerrero-Caballero J, Kane T, Vannier R-N, et al. Dry reforming of methane on nickel-chrome, nickel-cobalt and nickel-manganese catalysts. International Journal of Hydrogen Energy 2017;42(50):29725-34.

[87] Shin SA, Noh YS, Hong GH, Park JI, Song HT, Lee K-Y, et al. Dry reforming of methane over Ni/ZrO 2 -Al 2 O 3 catalysts: Effect of preparation methods. Journal of the Taiwan Institute of Chemical Engineers 2018;90:25-32.

[88] San-José-Alonso D, Juan-Juan J, Illán-Gómez MJ, Román-Martínez MC. Ni, Co and bimetallic Ni–Co catalysts for the dry reforming of methane. Applied Catalysis A: General 2009;371(1-2):54-9.

[89] Fan M-S, Abdullah AZ, Bhatia S. Utilization of Greenhouse Gases through Dry Reforming: Screening of Nickel-Based Bimetallic Catalysts and Kinetic Studies. ChemSusChem 2011;4(11):1643-53.

[90] Song Z, Wang Q, Guo C, Li S, Yan W, Jiao W, et al. Improved Effect of Fe on the Stable NiFe/Al2O3 Catalyst in Low-Temperature Dry Reforming of Methane. Industrial & Engineering Chemistry Research 2020;59(39):17250-8.

[91] Dai C, Zhang S, Zhang A, Song C, Shi C, Guo X. Hollow zeolite encapsulated Ni–Pt bimetals for sintering and coking resistant dry reforming of methane. Journal of Materials Chemistry A 2015;3(32):16461-8.

[92] Singha RK, Shukla A, Sandupatla A, Deo G, Bal R. Synthesis and catalytic activity of a Pd doped Ni–MgO catalyst for dry reforming of methane. Journal of Materials Chemistry A 2017;5(30):15688-99.

[93] Estephane J, Aouad S, Hany S, El Khoury B, Gennequin C, El Zakhem H, et al. CO2 reforming of methane over Ni–Co/ZSM5 catalysts. Aging and carbon deposition study.

International Journal of Hydrogen Energy 2015;40(30):9201-8.

[94] Gonzalez-delaCruz VM, Pereñiguez R, Ternero F, Holgado JP, Caballero A. In Situ XAS Study of Synergic Effects on Ni–Co/ZrO2 Methane Reforming Catalysts. The Journal of Physical Chemistry C 2012;116(4):2919-26.

[95] Zhang X, Yang C, Zhang Y, Xu Y, Shang S, Yin Y. Ni–Co catalyst derived from layered double hydroxides for dry reforming of methane. International Journal of Hydrogen Energy 2015;40(46):16115-26.

[96] Chang J-S, Hong D-Y, Li X, Park S-E. Thermogravimetric analyses and catalytic behaviors of zirconia-supported nickel catalysts for carbon dioxide reforming of methane. Catalysis Today 2006;115(1-4):186-90.

[97] Gould TD, Montemore MM, Lubers AM, Ellis LD, Weimer AW, Falconer JL, et al. Enhanced dry reforming of methane on Ni and Ni-Pt catalysts synthesized by atomic layer deposition. Applied Catalysis A: General 2015;492:107-16.

[98] Ay H, Üner D. Dry reforming of methane over CeO 2 supported Ni, Co and Ni–Co catalysts. Applied Catalysis B: Environmental 2015;179:128-38.

[99] Jalali R, Nematollahi B, Rezaei M, Baghalha M. Mesoporous nanostructured Ni/MgAl2O4 catalysts: Highly active and stable catalysts for syngas production in combined dry reforming and partial oxidation. International Journal of Hydrogen Energy 2019;44(21):10427-42.

[100] Xu J, Zhou W, Li Z, Wang J, Ma J. Biogas reforming for hydrogen production over nickel and cobalt bimetallic catalysts. International Journal of Hydrogen Energy 2009;34(16):6646-54.

[101] C.H.Bartholomew, R.J.Farrauto. Fundamentals industrial catalytic processes. 2005.

[102] Xu J, Saeys M. Improving the coking resistance of Ni-based catalysts by promotion with subsurface boron. Journal of Catalysis 2006;242(1):217-26.

[103] Fouskas A, Kollia M, Kambolis A, Papadopoulou C, Matralis H. Boron-modified Ni/Al2O3 catalysts for reduced carbon deposition during dry reforming of methane. Applied Catalysis A: General 2014;474:125-34.

[104] Xu J, Saeys M. First principles study of the coking resistance and the activity of a boron

promoted Ni catalyst. Chemical Engineering Science 2007;62(18):5039-41.

[105] Xu J, Chen L, Tan KF, Borgna A, Saeys M. Effect of boron on the stability of Ni catalysts during steam methane reforming. Journal of Catalysis 2009;261(2):158-65.

[106] Saeys M, Tan KF, Chang J, Borgna A. Improving the stability of cobalt Fischer-Tropsch catalysts by boron promotion. Industrial and Engineering Chemistry Research 2010;49(21):11098-100.

[107] Saeys XJaM. Coking Mechanism and Promoter Design for Ni-Based Catalysts: a First Principles Study. *The 2005 Annual Meeting (Cincinnati, OH)*

Cincinnati, OH. AIChe; 2005.

[108] Chen L, Lu Y, Hong Q, Lin J, Dautzenberg FM. Catalytic partial oxidation of methane to syngas over Ca-decorated-Al2O3-supported Ni and NiB catalysts. Applied Catalysis A: General 2005;292:295-304.

[109] Saeys M, Tan KF, Chang J, Borgna A. Improving the Stability of Cobalt Fischer−Tropsch Catalysts by Boron Promotion. Industrial & Engineering Chemistry Research 2010;49(21):11098-100.

[110] Tan KF, Chang J, Borgna A, Saeys M. Effect of boron promotion on the stability of cobalt Fischer-Tropsch catalysts. Journal of Catalysis 2011;280(1):50-9.

[111] Geng J, Jefferson DA, Johnson BFG. Exploring the Structural Complexities of Metal–Metalloid Nanoparticles: The Case of Ni·B as Catalyst. Chemistry – A European Journal 2009;15(5):1134-43.

[112] Xu D, Wang H, Guo Q, Ji S. Catalytic behavior of carbon supported Ni–B, Co–B and Co–Ni–B in hydrogen generation by hydrolysis of KBH4. Fuel Processing Technology 2011;92(8):1606-10.

[113] Furusawa T, Shirasu M, Sugiyama K, Sato T, Itoh N, Suzuki N. Preparation of Ru/ZrO2 Catalysts by NaBH4 Reduction and Their Catalytic Activity for NH3 Decomposition To Produce H2. Industrial & Engineering Chemistry Research 2016;55(50):12742-9.

[114] Shakir MD, Sengupta S, Sinhamahapatra A, Liu S, Vuthaluru H. B-Ni/MgAl2O4 catalyzed dry reforming of methane: The role of boron to resist the formation of graphitic carbon. Fuel

2022;320:123950.

[115] Pakhare D, Spivey J. A review of dry (CO2) reforming of methane over noble metal catalysts. Chemical Society Reviews 2014;43(22):7813-37.

[116] Ayoub M, Chong CC, Zamir A, Cheng YW, Farrukh S, Naqvi SR, et al. Effects of operating parameters for dry reforming of methane: A short review. E3S Web Conf 2021;287:04015.

[117] Habibi N, Arandiyan H, Rezaei M. Mesoporous MgO·Al2O3 nanopowder-supported meso–macroporous nickel catalysts: a new path to high-performance biogas reforming for syngas. RSC Advances 2016;6(35):29576-85.

[118] Fogler HS. Elements of chemical reaction engineering. PHI, India; 2006.

[119] Perdew JP, Burke K, Ernzerhof M. Generalized Gradient Approximation Made Simple. Physical Review Letters 1996;77(18):3865-8.

[120] Clark SJ, Segall MD, Pickard CJ, Hasnip PJ, Probert MIJ, Refson K, et al. First principles methods using CASTEP. Zeitschrift für Kristallographie - Crystalline Materials 2005;220(5-6):567-70.

[121] Prasad M, Ray K, Sinhamahapatra A, Sengupta S. Ni/CexZr1-xO2 catalyst prepared via one-step co-precipitation for CO2 reforming of CH4 to produce syngas: role of oxygen storage capacity (OSC) and oxygen vacancy formation energy (OVFE). Journal of Materials Science 2022:1-18.

[122] Li G, Cheng H, Zhao H, Lu X, Xu Q, Wu C. Hydrogen production by CO2 reforming of CH4 in coke oven gas over Ni–Co/MgAl2O4 catalysts. Catalysis Today 2018;318:46-51.

[123] Zhu Y, Zhang S, Chen B, Zhang Z, Shi C. Effect of Mg/Al ratio of NiMgAl mixed oxide catalyst derived from hydrotalcite for carbon dioxide reforming of methane. Catalysis Today 2016;264:163-70.

[124] Guo J, Fan S-b, Gao X-h, Ma Q-x, Zhang J-l, Zhao T-s. Study on catalytic performance of Co-Ni-B/SBA-15 for hydroformylation of 1-octene. Journal of Fuel Chemistry and Technology 2021;49(7):945-51.

[125] Schaefer ZL, Ke X, Schiffer P, Schaak RE. Direct Solution Synthesis, Reaction Pathway Studies, and Structural Characterization of Crystalline Ni3B Nanoparticles. The Journal of

Physical Chemistry C 2008;112(50):19846-51.

[126] Zhang Z, Zhao G, Li W, Zhong J, Xie J. Key properties of Ni/CeAlO3-Al2O3/SiC-foam catalysts for biogas reforming: Enhanced stability and CO2 activation. Fuel 2022;307:121799.

[127] He Q, Kang X, Fu F, Ren M, Liao F. The Synthesis of rGO/Ni/Co Composite and Electrochemical Determination of Dopamine. Journal of Inorganic and Organometallic Polymers and Materials 2020;30(11):4269-77.

[128] Mizuno SCM, Braga AH, Hori CE, Santos JBO, Bueno JMC. Steam reforming of acetic acid over MgAl2O4-supported Co and Ni catalysts: Effect of the composition of Ni/Co and reactants on reaction pathways. Catalysis Today 2017;296:144-53.

[129] Zhang Z, Hu X, Zhang L, Yang Y, Li Q, Fan H, et al. Steam reforming of guaiacol over Ni/Al2O3 and Ni/SBA-15: Impacts of support on catalytic behaviors of nickel and properties of coke. Fuel Processing Technology 2019;191:138-51.

[130] Zhu J, Diao T, Wang W, Xu X, Sun X, Carabineiro SAC, et al. Boron doped graphitic carbon nitride with acid-base duality for cycloaddition of carbon dioxide to epoxide under solvent-free condition. Applied Catalysis B: Environmental 2017;219:92-100.

[131] Bereketidou OA, Goula MA. Biogas reforming for syngas production over nickel supported on ceria–alumina catalysts. Catalysis Today 2012;195(1):93-100.

[132] Chai Y, Fu Y, Feng H, Kong W, Yuan C, Pan B, et al. A Nickel-Based Perovskite Catalyst with a Bimodal Size Distribution of Nickel Particles for Dry Reforming of Methane. ChemCatChem 2018;10(9):2078-86.

[133] Al Abdulghani AJ, Park J-H, Kozlov SM, Kang D-C, AlSabban B, Pedireddy S, et al. Methane dry reforming on supported cobalt nanoparticles promoted by boron. Journal of Catalysis 2020;392:126-34.

[134] Zarei M, Meshkani F, Rezaei M. Preparation of mesoporous nanocrystalline Ni-MgAl2O4 catalysts by sol-gel combustion method and its applications in dry reforming reaction. Advanced Powder Technology 2016;27(5):1963-70.

[135] Masa J, Sinev I, Mistry H, Ventosa E, de la Mata M, Arbiol J, et al. Ultrathin High Surface

Area Nickel Boride (NixB) Nanosheets as Highly Efficient Electrocatalyst for Oxygen Evolution. Advanced Energy Materials 2017;7(17):1700381.

[136] Patel N, Fernandes R, Guella G, Miotello A. Nanoparticle-assembled Co-B thin film for the hydrolysis of ammonia borane: A highly active catalyst for hydrogen production. Applied Catalysis B: Environmental 2010;95(1-2):137-43.

[137] Xu J, Chen L, Tan K, Borgna A, Saeys M. Effect of boron on the stability of Ni catalysts during steam methane reforming. Journal of Catalysis 2009;261(2):158-65.

[138] Wang M, Li H, Wu Y, Zhang J. Comparative studies on the catalytic behaviors between the Ni–B amorphous alloy and other Ni-based catalysts during liquid phase hydrogenation of acetonitrile to ethylamine. Materials Letters 2003;57(19):2954-64.

[139] Kukula P, Gabova V, Koprivova K, Trtik P. Selective hydrogenation of unsaturated nitriles to unsaturated amines over amorphous CoB and NiB alloys doped with chromium. Catalysis Today 2007;121(1):27-38.

[140] Ding X, Wang X, Song W, Wei X, Zhu J, Tang Y, et al. Synergism of 1D/2D boride/MXene nanosheet heterojunctions for boosted overall water splitting. New Journal of Chemistry 2021;45(46):21905-11.

[141] Xu X, Deng Y, Gu M, Sun B, Liang Z, Xue Y, et al. Large-scale synthesis of porous nickel boride for robust hydrogen evolution reaction electrocatalyst. Applied Surface Science 2019;470:591-5.

[142] Kim B, Das G, Kim J, Yoon HH, Lee DH. Ni-Co-B nanoparticle decorated carbon felt by electroless plating as a bi-functional catalyst for urea electrolysis. Journal of Colloid and Interface Science 2021;601:317-25.

[143] Li Y, Zhang W, Li H, Yang T, Peng S, Kao C, et al. Ni-B coupled with borate-intercalated Ni(OH)2 for efficient and stable electrocatalytic and photocatalytic hydrogen evolution under low alkalinity. Chemical Engineering Journal 2020;394:124928.

[144] Huo F, Shen Y-A, He S, Zhang K, Nishikawa H. Fabrication of NiO/ZrO2 nanocomposites using ball milling-pyrolysis method. Vacuum 2021;191:110370.

[145] Lesiak B, Kövér L, Tóth J, Zemek J, Jiricek P, Kromka A, et al. C sp2/sp3 hybridisations in

carbon nanomaterials – XPS and (X)AES study. Applied Surface Science 2018;452:223-31.

[146] Kovács GJ, Bertóti I, Radnóczi G. X-ray photoelectron spectroscopic study of magnetron sputtered carbon–nickel composite films. Thin Solid Films 2008;516(21):7942-6.

[147] Chen X, Wang X, Fang D. A review on C1s XPS-spectra for some kinds of carbon materials. Fullerenes, Nanotubes and Carbon Nanostructures 2020;28(12):1048-58.

[148] Gong X, Liu Y, Wang Y, Xie Z, Dong Q, Dong M, et al. Amino graphene oxide/dopamine modified aramid fibers: Preparation, epoxy nanocomposites and property analysis. Polymer 2019;168:131-7.

[149] Kim J-H, Suh DJ, Park T-J, Kim K-L. Effect of metal particle size on coking during CO2 reforming of CH4 over Ni–alumina aerogel catalysts. Applied Catalysis A: General 2000;197(2):191-200.

[150] San-José-Alonso D, Juan-Juan J, Illán-Gómez MJ, Román-Martínez MC. Ni, Co and bimetallic Ni–Co catalysts for the dry reforming of methane. Applied Catalysis A: General 2009;371(1):54-9.

[151] Wu JCS, Chou H-C. Bimetallic Rh–Ni/BN catalyst for methane reforming with CO2. Chemical Engineering Journal 2009;148(2):539-45.

[152] Ni J, Chen L, Lin J, Kawi S. Carbon deposition on borated alumina supported nano-sized Ni catalysts for dry reforming of CH4. Nano Energy 2012;1(5):674-86.

[153] Li B, Yuan X, Li B, Wang X. Impact of pore structure on hydroxyapatite supported nickel catalysts (Ni/HAP) for dry reforming of methane. Fuel Processing Technology 2020;202:106359.

[154] Wu Z, Mao X, Zi Q, Zhang R, Dou T, Yip ACK. Mechanism and kinetics of sodium borohydride hydrolysis over crystalline nickel and nickel boride and amorphous nickel–boron nanoparticles. Journal of Power Sources 2014;268:596-603.

[155] Tran BH, Tieu K, Wan S, Zhu H, Cui S, Wang L. Understanding the tribological impacts of alkali element on lubrication of binary borate melt. RSC Advances 2018;8(51):28847-60.

[156] Guo X, Rao L, Wang P, Zhang L, Wang Y. Synthesis of Porous Boron-Doped Carbon Nitride: Adsorption Capacity and Photo-Regeneration Properties. International Journal of

Environmental Research and Public Health 2019;16(4):581.

[157] Singh PK, Das T. Generation of hydrogen from NaBH4 solution using metal-boride (CoB, FeB, NiB) catalysts. International Journal of Hydrogen Energy 2017;42(49):29360-9.

[158] Chen X, Yu Z, Wei L, Zhou Z, Zhai S, Chen J, et al. Ultrathin nickel boride nanosheets anchored on functionalized carbon nanotubes as bifunctional electrocatalysts for overall water splitting. Journal of Materials Chemistry A 2019;7(2):764-74.

[159] Jeong SU, Cho EA, Nam SW, Oh IH, Jung UH, Kim SH. Effect of preparation method on Co–B catalytic activity for hydrogen generation from alkali NaBH4 solution. International Journal of Hydrogen Energy 2007;32(12):1749-54.

[160] Geng J, Jefferson DA, Johnson BFG. The unusual nanostructure of nickel–boron catalyst. Chemical Communications 2007(9):969-71.

[161] Liu Y-C, Huang C-Y, Chen Y-W. Hydrogenation of p-chloronitrobenzene on Ni–B Nanometal Catalysts. Journal of Nanoparticle Research 2006;8(2):223-34.

[162] Li H, Wu Y, Zhang J, Dai W, Qiao M. Liquid phase acetonitrile hydrogenation to ethylamine over a highly active and selective Ni–Co–B amorphous alloy catalyst. Applied Catalysis A: General 2004;275(1):199-206.

[163] Wang D, Gong W, Zhang J, Han M, Chen C, Zhang Y, et al. Encapsulated Ni-Co alloy nanoparticles as efficient catalyst for hydrodeoxygenation of biomass derivatives in water. Chinese Journal of Catalysis 2021;42(11):2027-37.

[164] Shu R, Wu Y, Li X, Zhang J, Wan Z, Li N. Fabrication of yolk-shell NiCo alloy@C composites derived from trimetallic metal–organic frameworks as light-weight and high-performance electromagnetic wave absorbers. Composites Part A: Applied Science and Manufacturing 2021;147:106451.

[165] Mustapić M, Horvat J, Hossain MS, Sun Z, Skoko Ž, Mitchell DRG, et al. Novel synthesis of superparamagnetic Ni–Co–B nanoparticles and their effect on superconductor properties of MgB2. Acta Materialia 2014;70:298-306.

[166] Saha S, Ganguly S, Banerjee D, Kargupta K. Novel bimetallic graphene–cobalt–nickel (G–Co–Ni) nano-ensemble electrocatalyst for enhanced borohydride oxidation. International

Journal of Hydrogen Energy 2015;40(4):1760-73.

[167] Liu D, Quek XY, Cheo WNE, Lau R, Borgna A, Yang Y. MCM-41 supported nickel-based bimetallic catalysts with superior stability during carbon dioxide reforming of methane: Effect of strong metal–support interaction. Journal of Catalysis 2009;266(2):380-90.

[168] Korup O, Schlögl R, Horn R. Carbon formation in catalytic partial oxidation of methane on platinum: Model studies on a polycrystalline Pt foil. Catalysis Today 2012;181(1):177-83.

[169] Han YK, Ahn C-I, Bae J-W, Kim AR, Han GY. Effects of Carbon Formation on Catalytic Performance for CO2 Reforming with Methane on Ni/Al2O3 Catalyst: Comparison of Fixed-Bed with Fluidized-Bed Reactors. Industrial & Engineering Chemistry Research 2013;52(37):13288-96.

[170] Mondal A, Biswas S, Srishti, Kumar A, Yu J-S, Sinhamahapatra A. Sub 10 nm CoO nanoparticle-decorated graphitic carbon nitride for solar hydrogen generation via efficient charge separation. Nanoscale Advances 2020;2(10):4473-81.

[171] García-Diéguez M, Herrera C, Larrubia MÁ, Alemany LJ. CO2-reforming of natural gas components over a highly stable and selective NiMg/Al2O3 nanocatalyst. Catalysis Today 2012;197(1):50-7.

[172] Zhang J, Wang H, Dalai AK. Kinetic Studies of Carbon Dioxide Reforming of Methane over Ni−Co/Al−Mg−O Bimetallic Catalyst. Industrial & Engineering Chemistry Research 2009;48(2):677-84.

[173] Qiao Z, Wang Z, Zhang C, Yuan S, Zhu Y, Wang J, et al. PVAm–PIP/PS Composite Membrane with High Performance for CO2/N2 Separation. AIChE Journal 2013;59(1):215-28.

[174] Sierra Gallego G, Batiot-Dupeyrat C, Barrault J, Mondragón F. Dual Active-Site Mechanism for Dry Methane Reforming over Ni/La2O3 Produced from LaNiO3 Perovskite. Industrial & Engineering Chemistry Research 2008;47(23):9272-8.

[175] Nandini A, Pant KK, Dhingra SC. Kinetic study of the catalytic carbon dioxide reforming of methane to synthesis gas over Ni-K/CeO2-Al2O3 catalyst. Applied Catalysis A: General 2006;308:119-27.

Publications:

- Paper published with tittle “B-Ni/$MgAl_2O_4$ catalyzed dry reforming of methane: the role of boron to resist the formation of graphitic carbon” by MD Shakir, Siddhartha Sengupta, Apurba Sinhamahapatra, Shaomin Liu, Hari Vuthaluru in Fuel journal.

- Paper (1st revision submitted) with tittle $NaBH_4$ assisted one-step synthesis of bi-metallic B-Ni-Co/$MgAl_2O_4$ catalysts for the dry reforming of methane reaction” by MD Shakir, Manohar Prasad, Koustav Ray, Siddhartha Sengupta, Apurba Sinhamahapatra, Shaomin Liu, Hari Vuthaluru in ACS applied nano material journal.

- The prepared manuscript is ready to submit in journal with tittle “Synergistic effect of $NaBH_4$ followed by H_2 reduction towards advancement of catalytic activity of (75Ni25Co)-B/$MgAl_2O_4$ for dry reforming of methane” by MD Shakir, Siddhartha Sengupta, Apurba Sinhamahapatra, Shaomin Liu, Hari Vuthaluru.

Conferences:

- International conference CHEMECA 2021, Australia, **Oral presentation**. Topic Effect of B prompted on Ni-Co bimetallic $Ce_{0.6}Zr_{0.4}O_2$ catalyst

- ACS Spring 2021 **Poster Presentation**. Topic: Enhancement of catalyst performance by doping B over the Ni, Co, Ni-Co $CeZrO_2$ for dry reforming of methane reaction.

- 12th International Conference on Applied Energy (ICAE2020), the United Nations Conference Centre (UNCC) International Bangkok: **Oral Presentation**: Synthesis of boron-containing Ni, Co, Ni-Co/$MgAl_2O_4$ catalyst for dry reforming of methane

- International Conference on Material for the Millennium (MatCon-2021), **Oral presentation**, “Enhancement of catalyst performance by doping B over the Ni, Co for dry reforming of methane reaction”.

- CHEMCON, ‘17 Organized by IICHE India, **Oral presentation**, Conference presentation on “Synthesis of suitable Catalyst for CO2 Utilization”.

Appendix A:

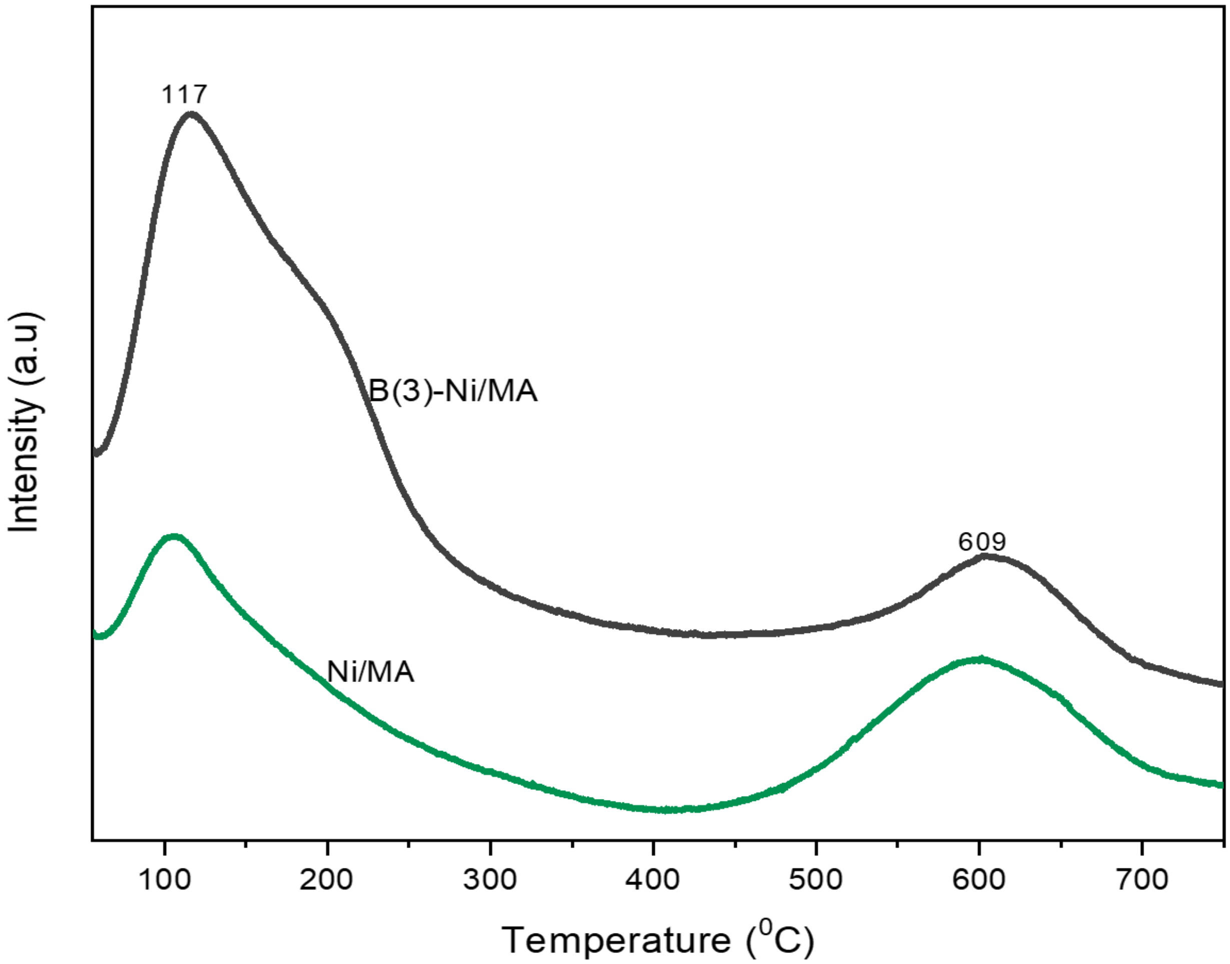

Figure A1. H_2-TPD analysis of Ni/MA and B(3)-Ni/MA

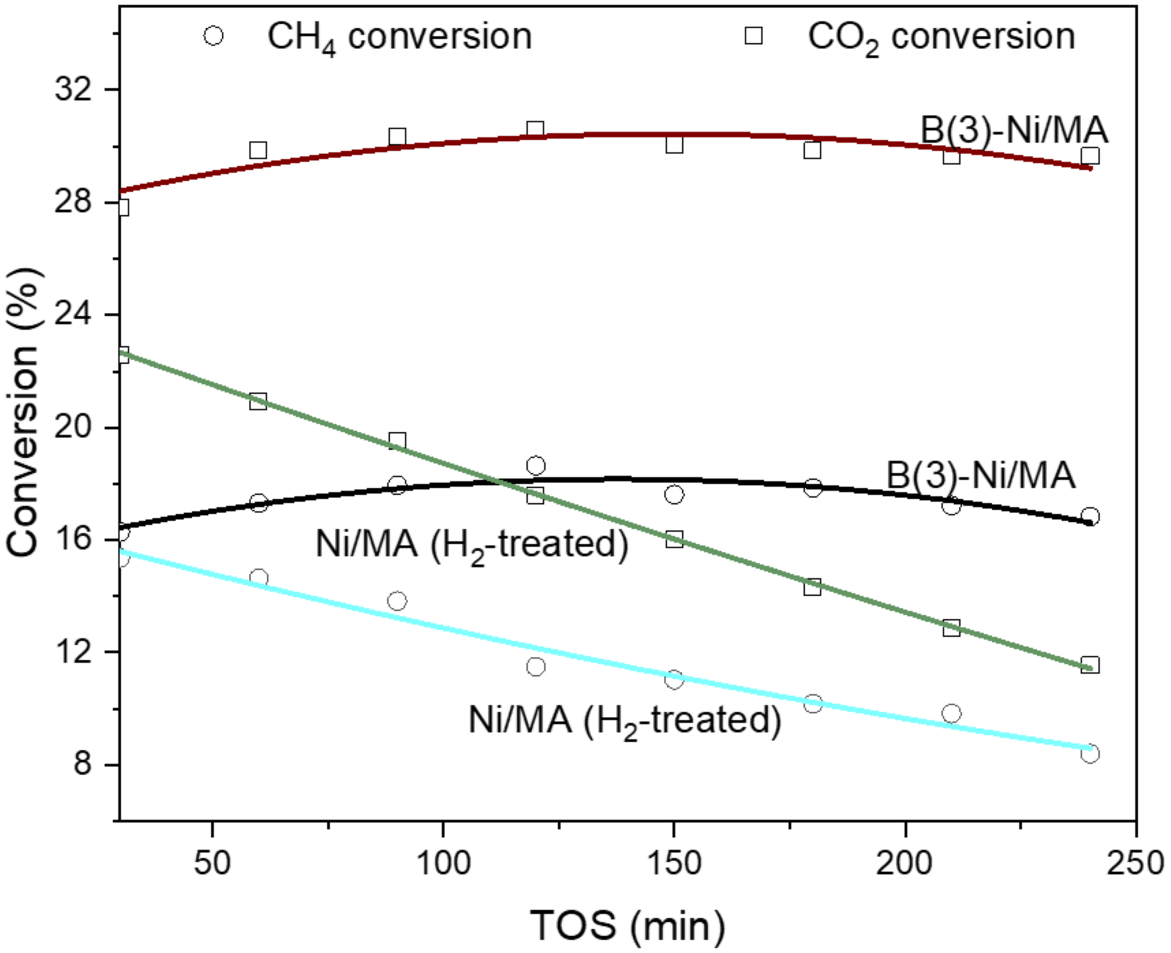

Figure A2. The catalytic performances of H_2-treated Ni/MA catalyst for DRM

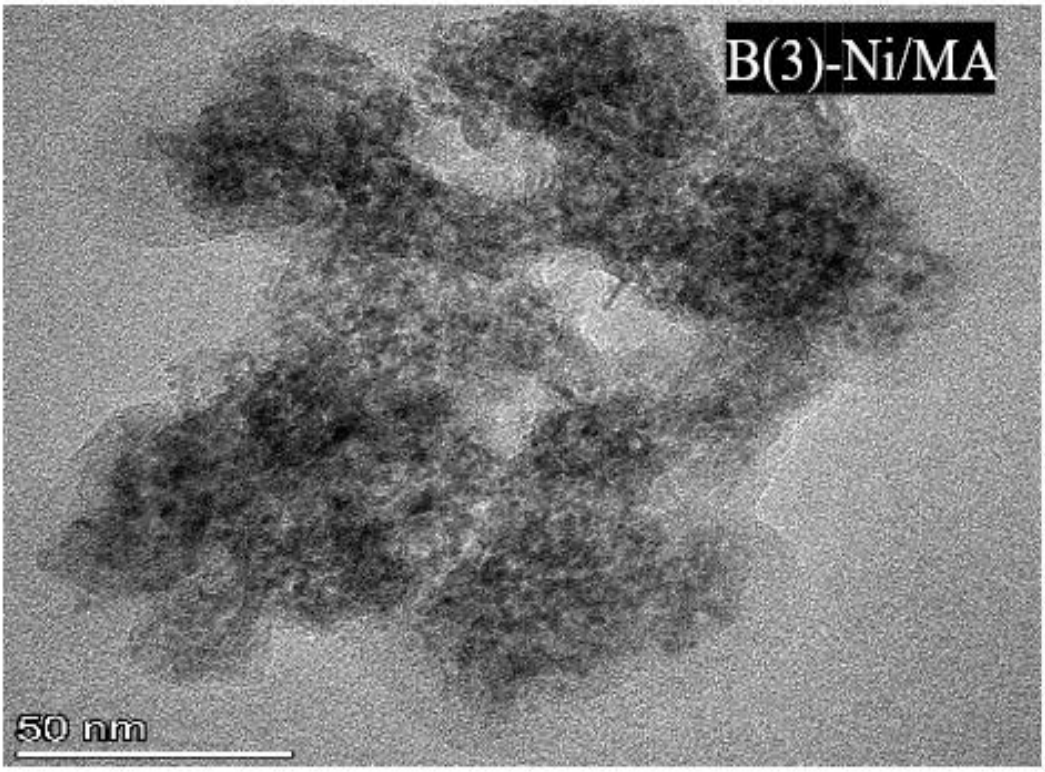

Figure A3. HR-TEM analysis for B(3)-Ni/MA catalyst

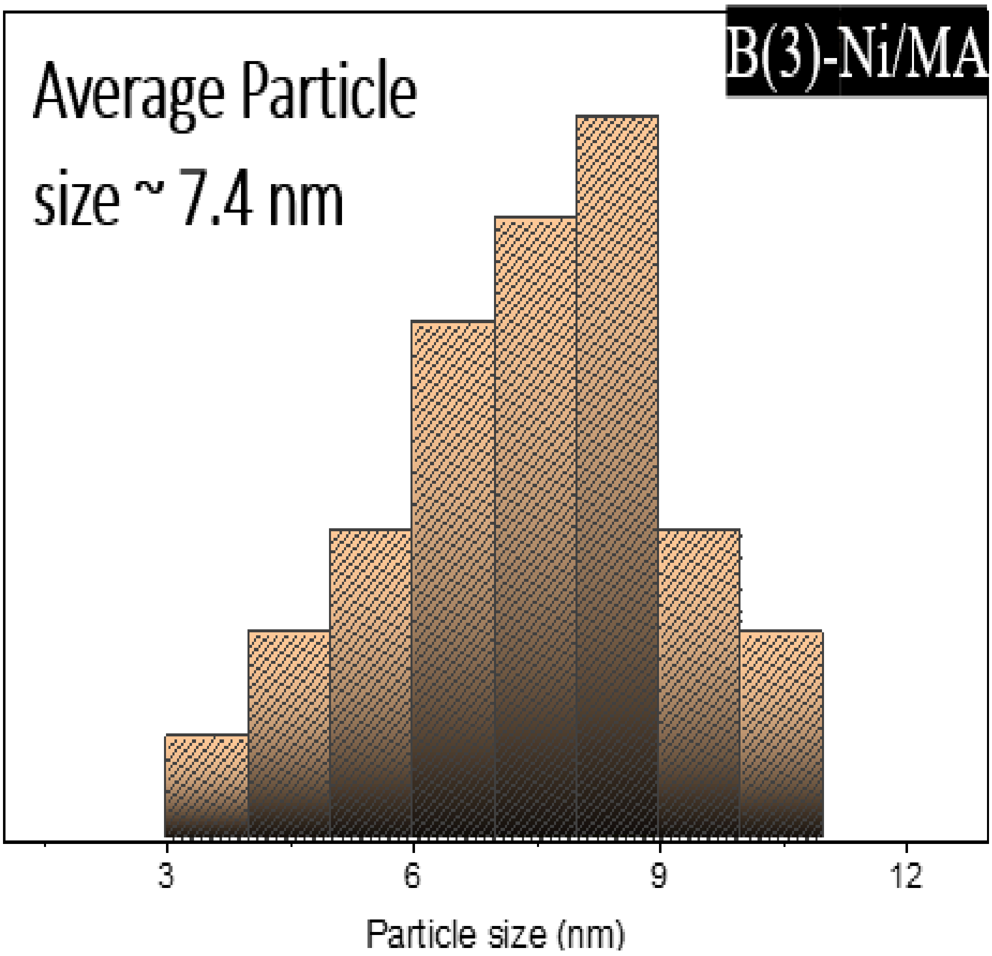

Figure A4. Particle size distribution of B(3)-Ni/MA catalyst

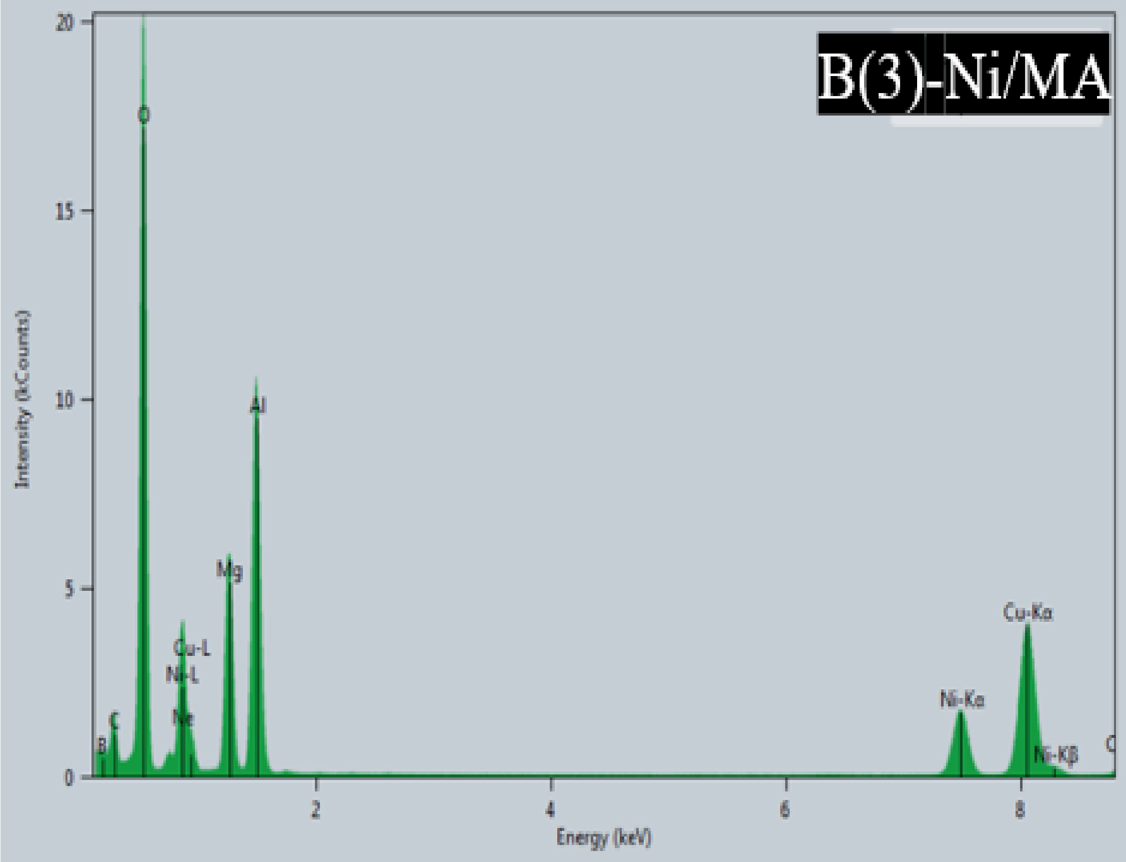

Figure A5. EDS analysis of B(3)-Ni/MA catalyst

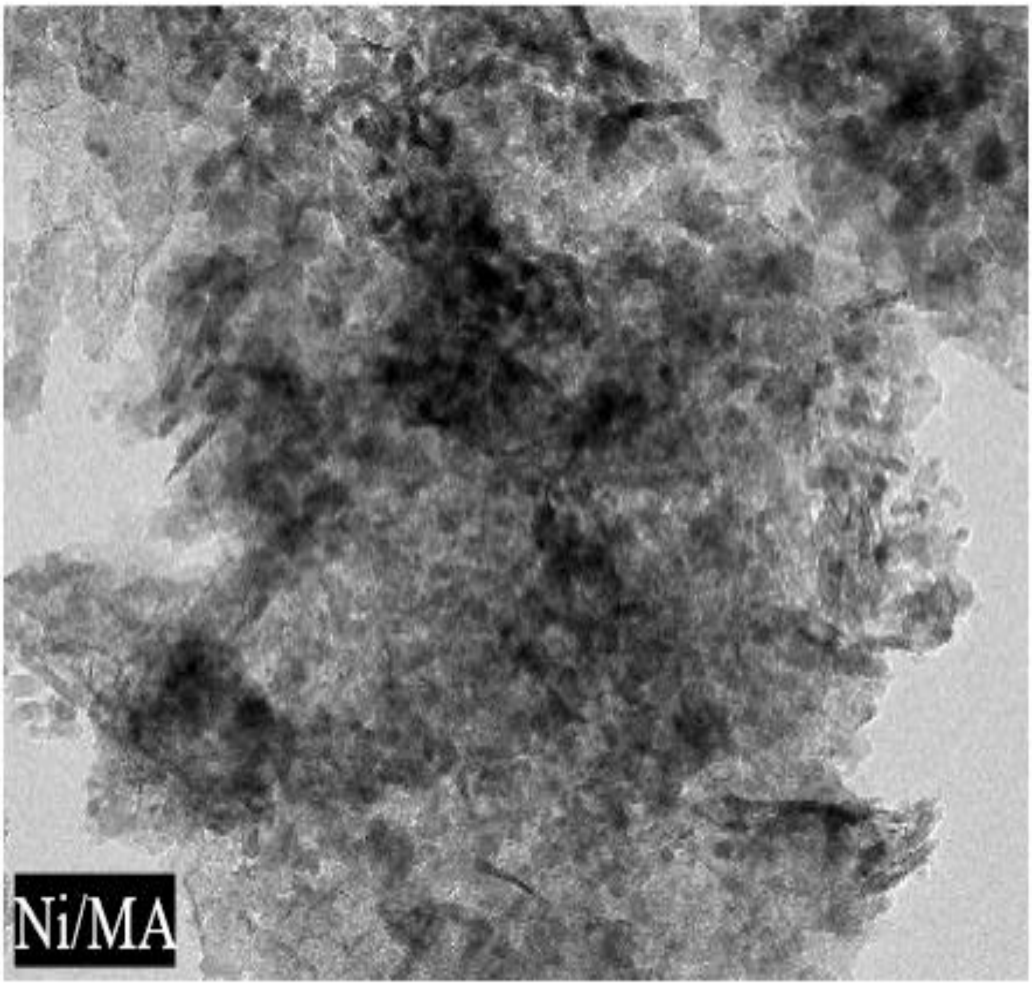

Figure A6. HR-TEM analysis for Ni/MA catalyst

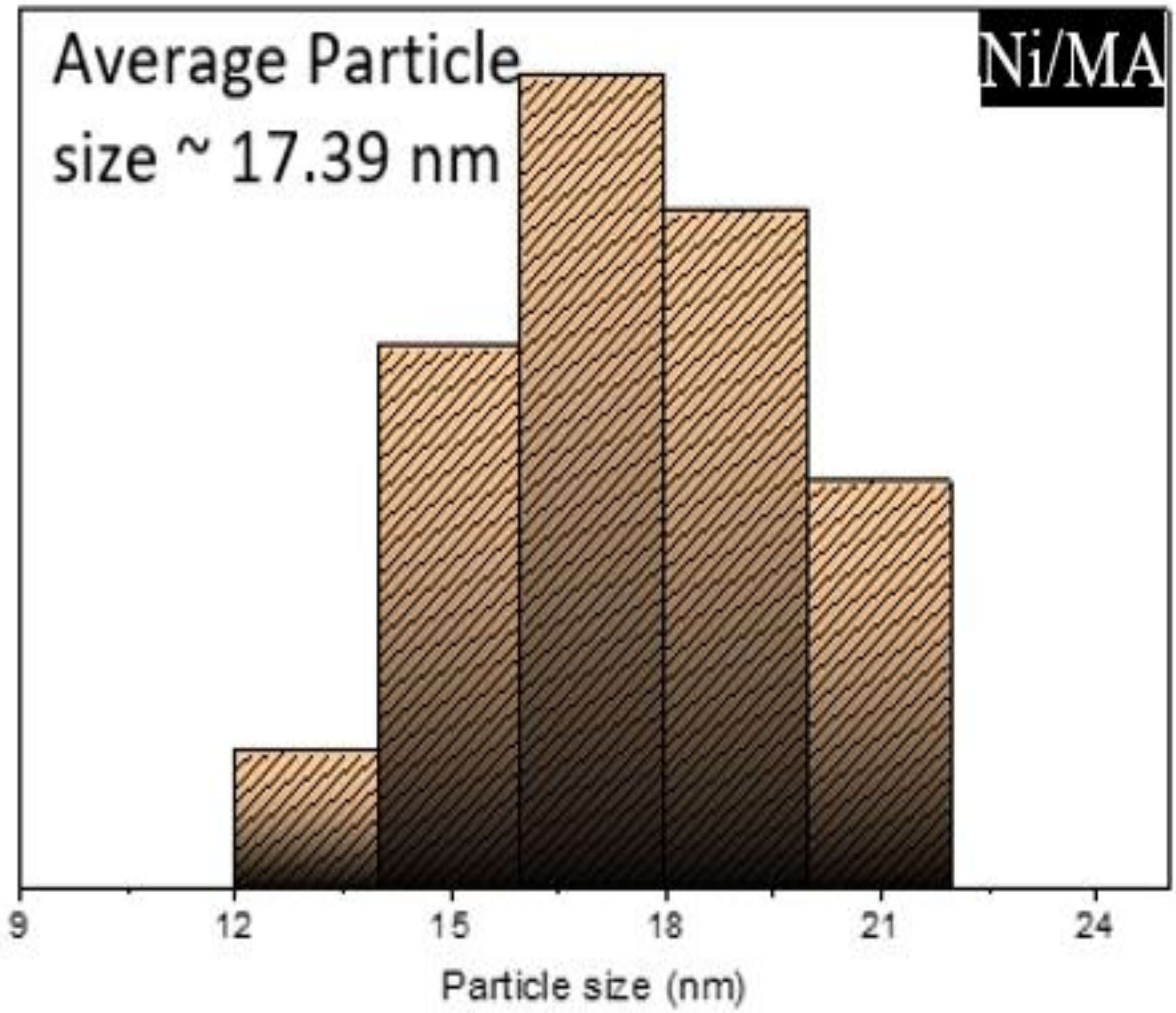

Figure A7. Particle size distribution of Ni/MA catalyst

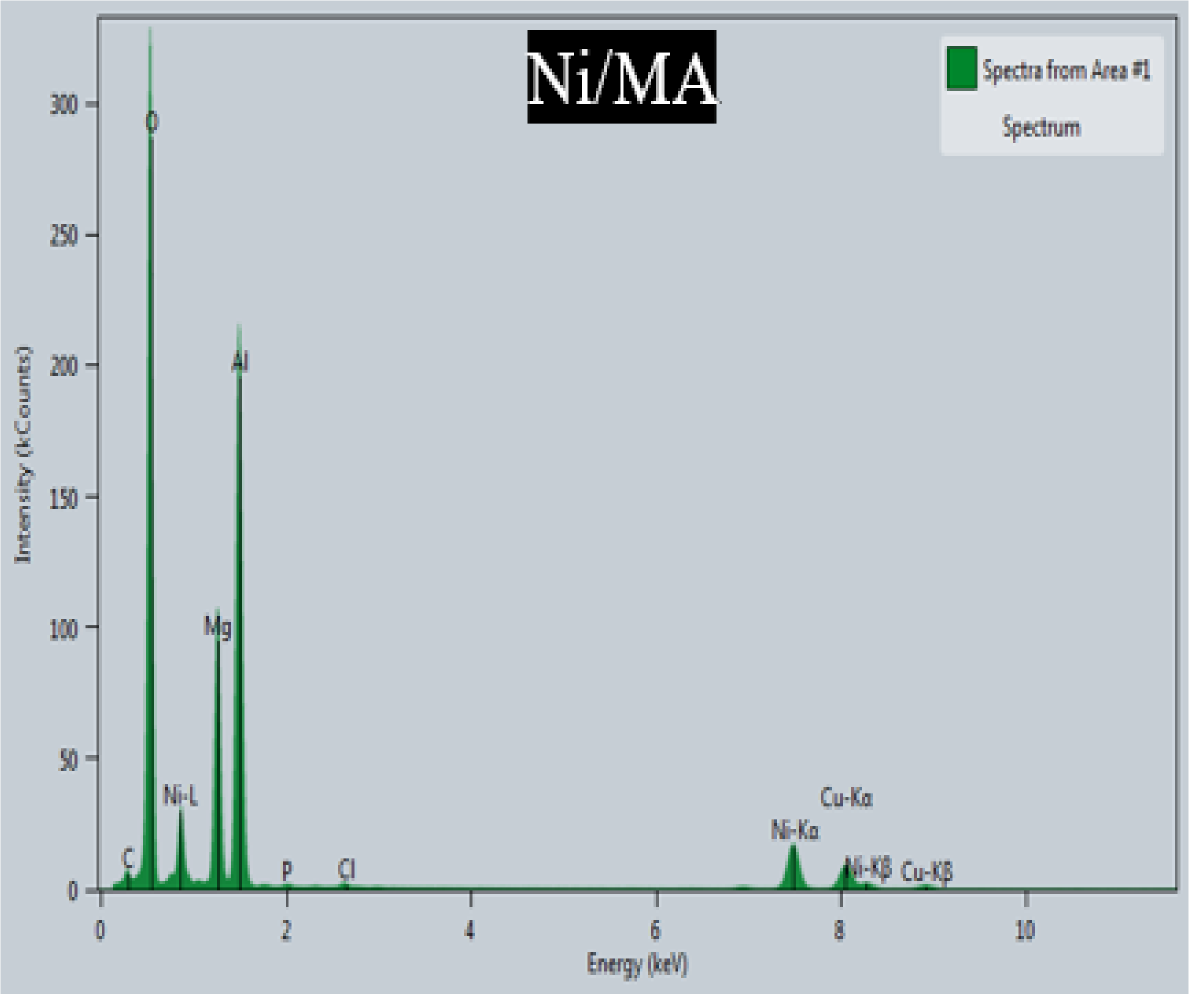

Figure A8. HRTEM-EDS analysis of Ni/MA catalyst

Table A1. Analysis of carbon deposition on spent B and non-B catalyst.

Catalyst	Total carbon deposition measured ($g_C g_{cat}^{-1}$)	Carbon deposition with respect to the methane conversion($g_C g_{cat}^{-1} mol_{methane}^{-1}$)
Ni/MA	0.089	0.595
Ni/MA (H_2 treated)	0.105	0.275
B(3)-Ni/MA	0.037	0.053
B(5)-Ni/MA	0.034	0.076

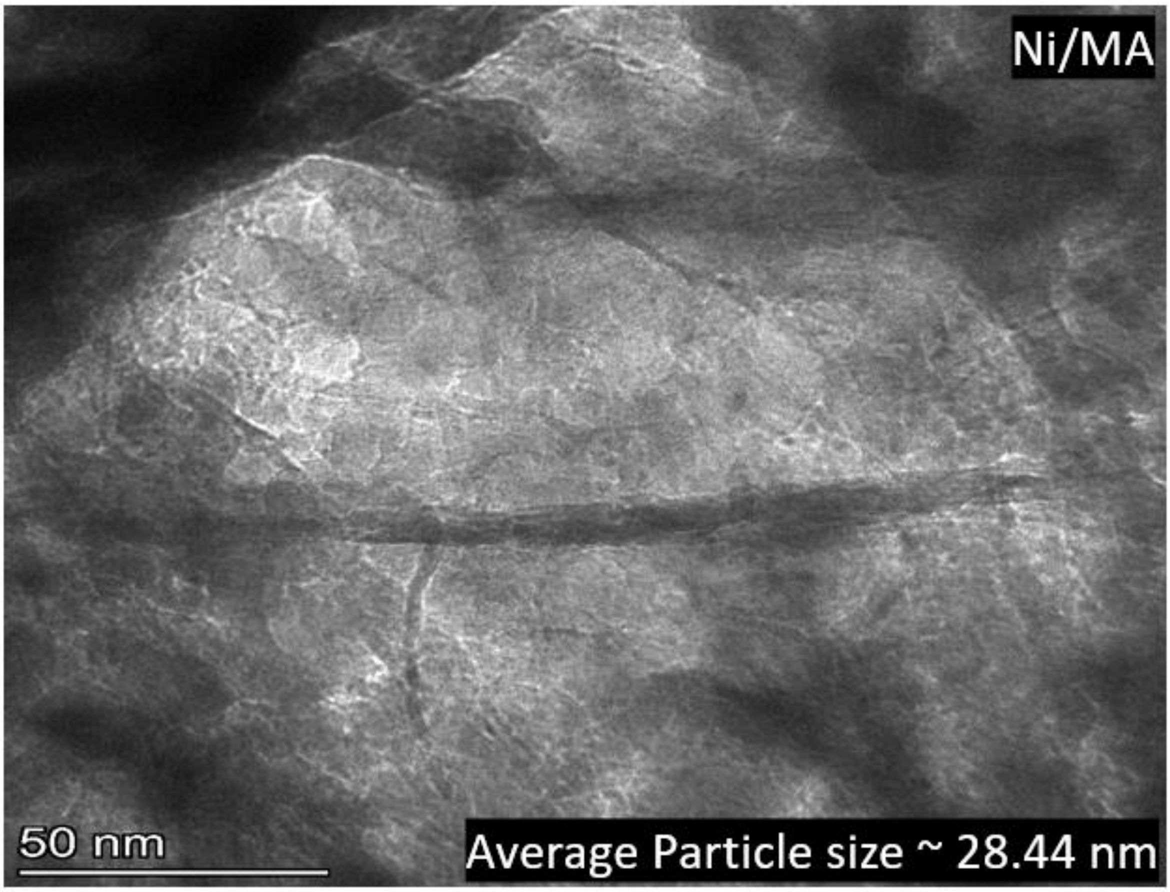

Figure A9. HR-TEM analysis of spent Ni/MA catalyst

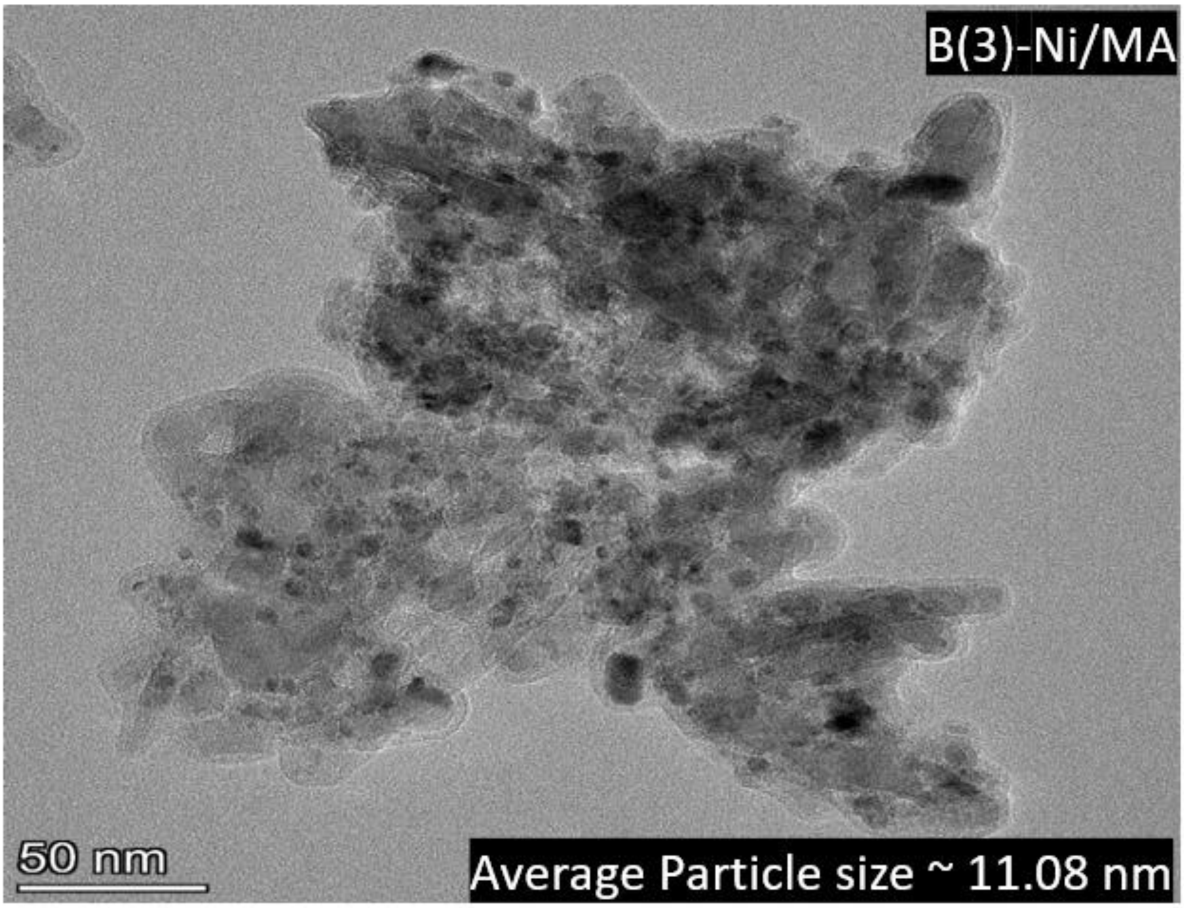

Figure A10. HR-TEM analysis of spent B(3)-Ni/MA catalyst

Appendix B:

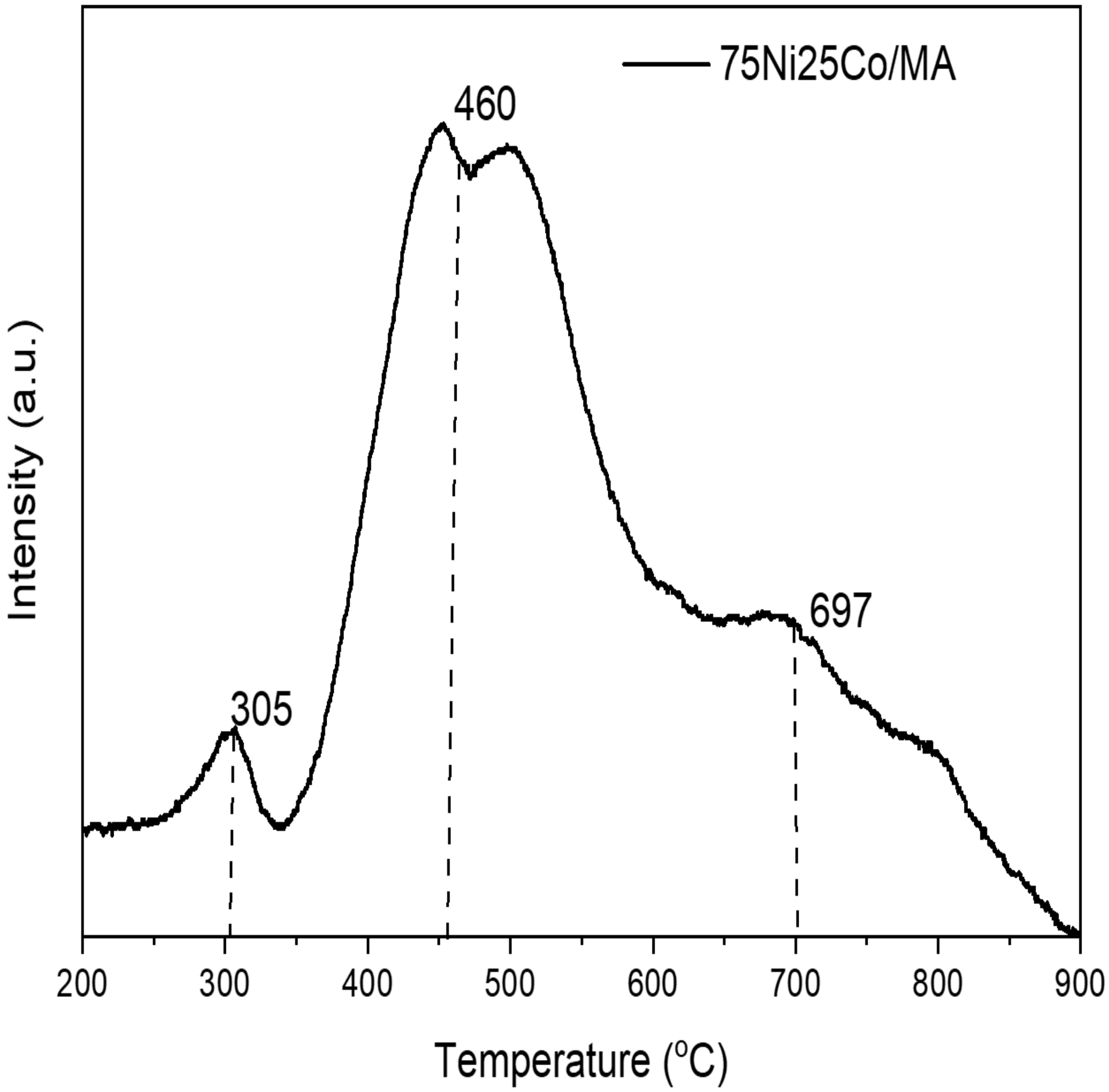

Figure B1. H_2-TPR profile of non-B 75Ni25Co/MA catalyst

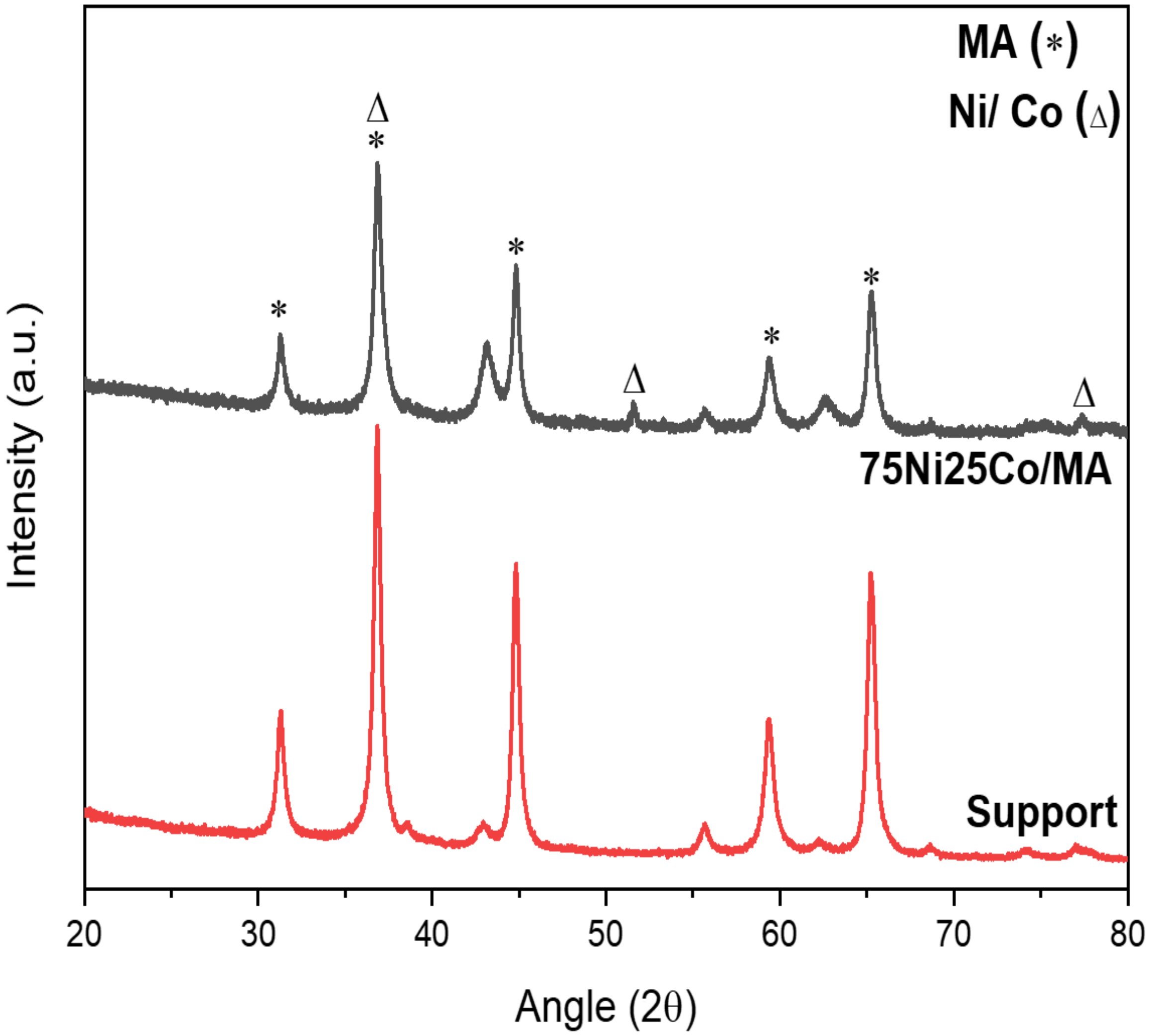

Figure B2. XRD pattern of Support MA and non-B 75Ni25Co/MA

Table B1. Metallic ratio and H_2-TPD for the boron-containing catalysts

Sample	**Ni: Co**	**H_2-uptake (μmol/ g)**
B-Ni/MA	-	143
B-(75Ni25Co)/MA	3:1	165
B-(50Ni50Co)/MA	1:1	156
B-(25Ni75Co)/MA	1:3	112
B-Co/MA	-	85

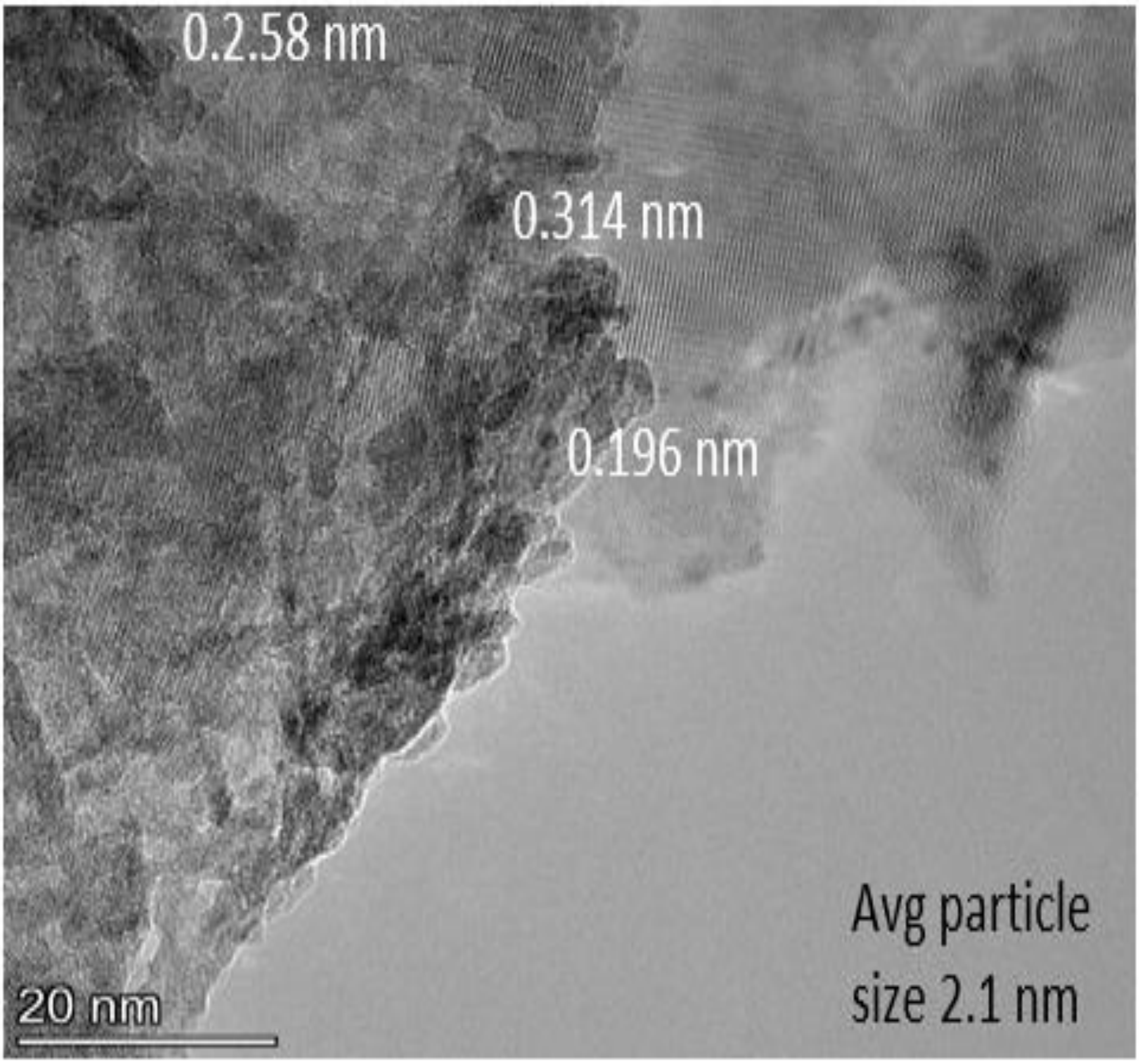

Figure B3. HR-TEM analysis of B-(75Ni25Co)/MA catalyst.

Table B2. The elemental composition of B-(75Ni25Co)/MA catalyst using ICP-OES and EDS analysis

Element	ICP-OES (wt. %)	TEM-EDS (wt. %)
Ni	10.89	9.95
Co	3.71	3.23
B	2.68	1.02

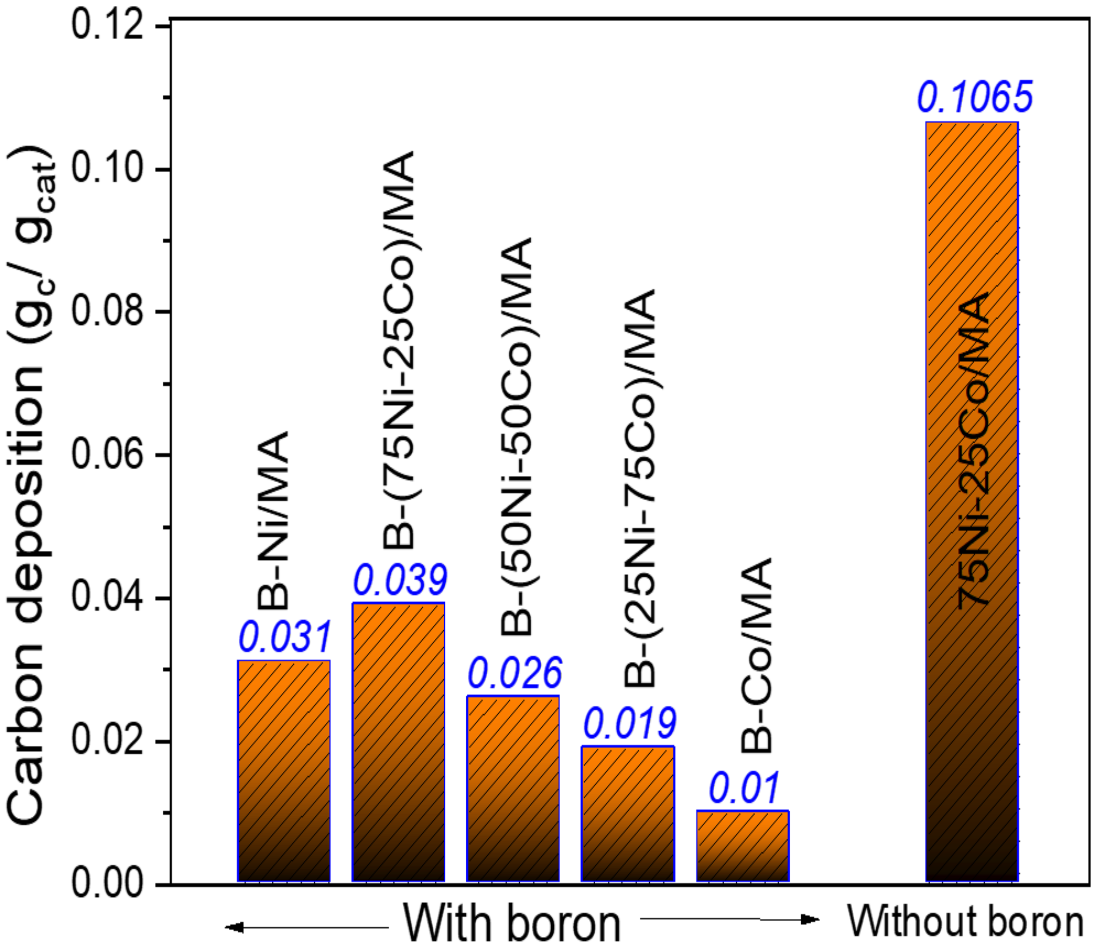

Figure B4. Elemental analysis of B and non-B catalysts

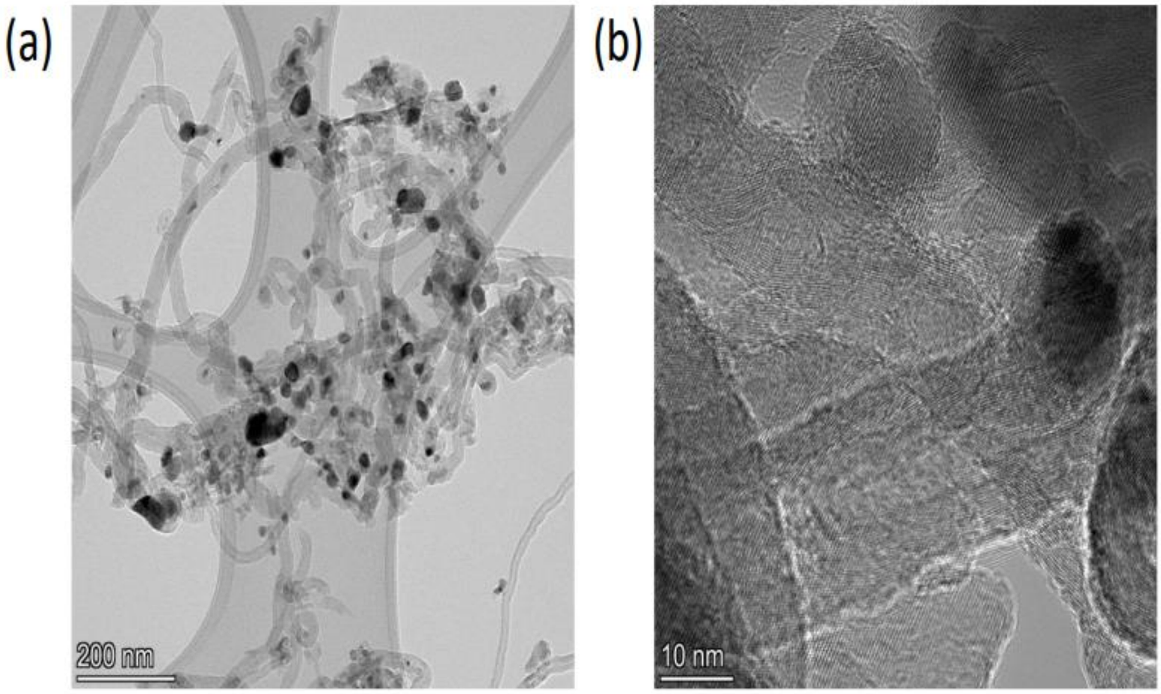

Figure B5. TEM images of spent B-(75Ni-25Co)/MA (a) Particle distribution (b) High resolution image

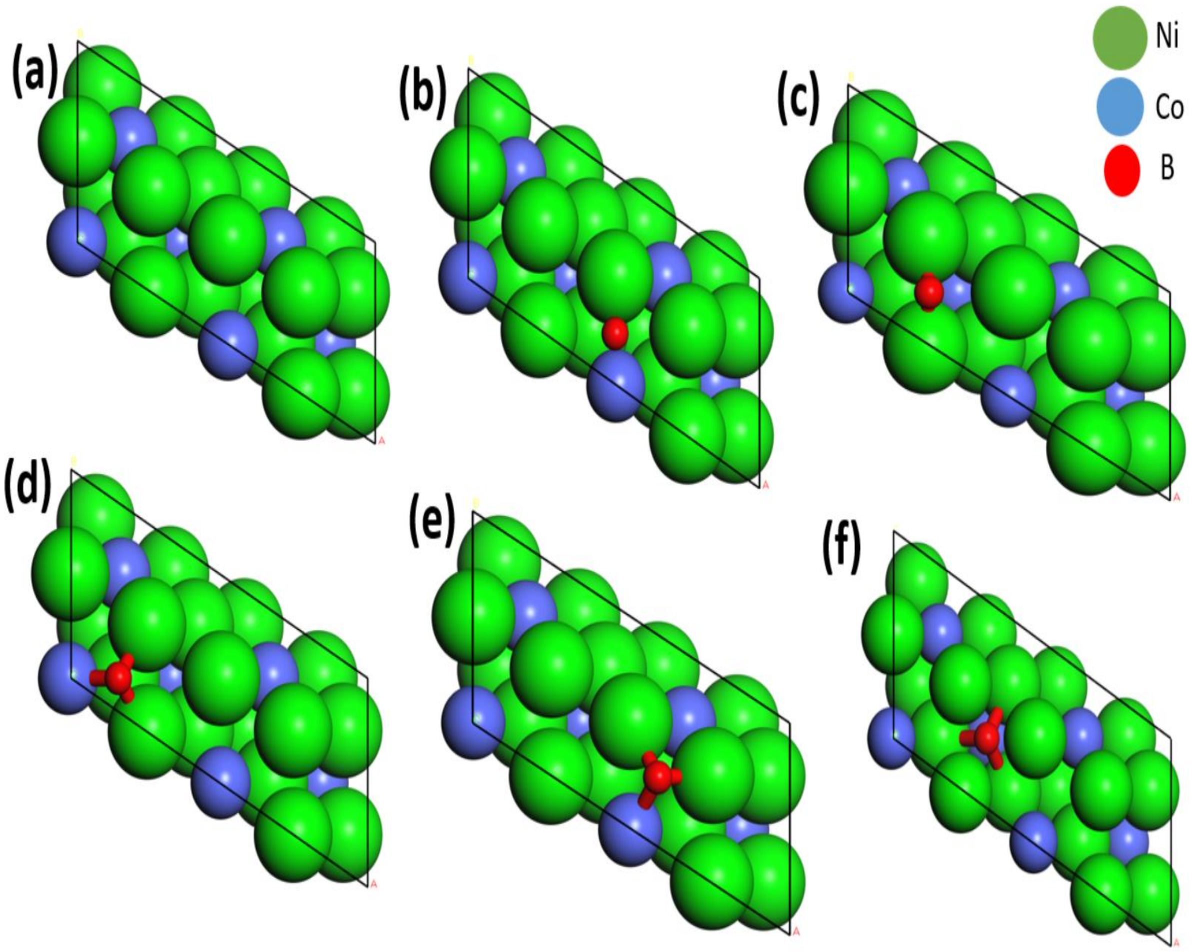

Figure B6. (a) Pristine 75Ni-25Co , (b) Twofold bridge site (between Ni-Co), (c) Twofold bridge site (between Ni-Ni), (d) HCP hollow site, (e) FCC hollow site (f) Subsurface site

Appendix C:

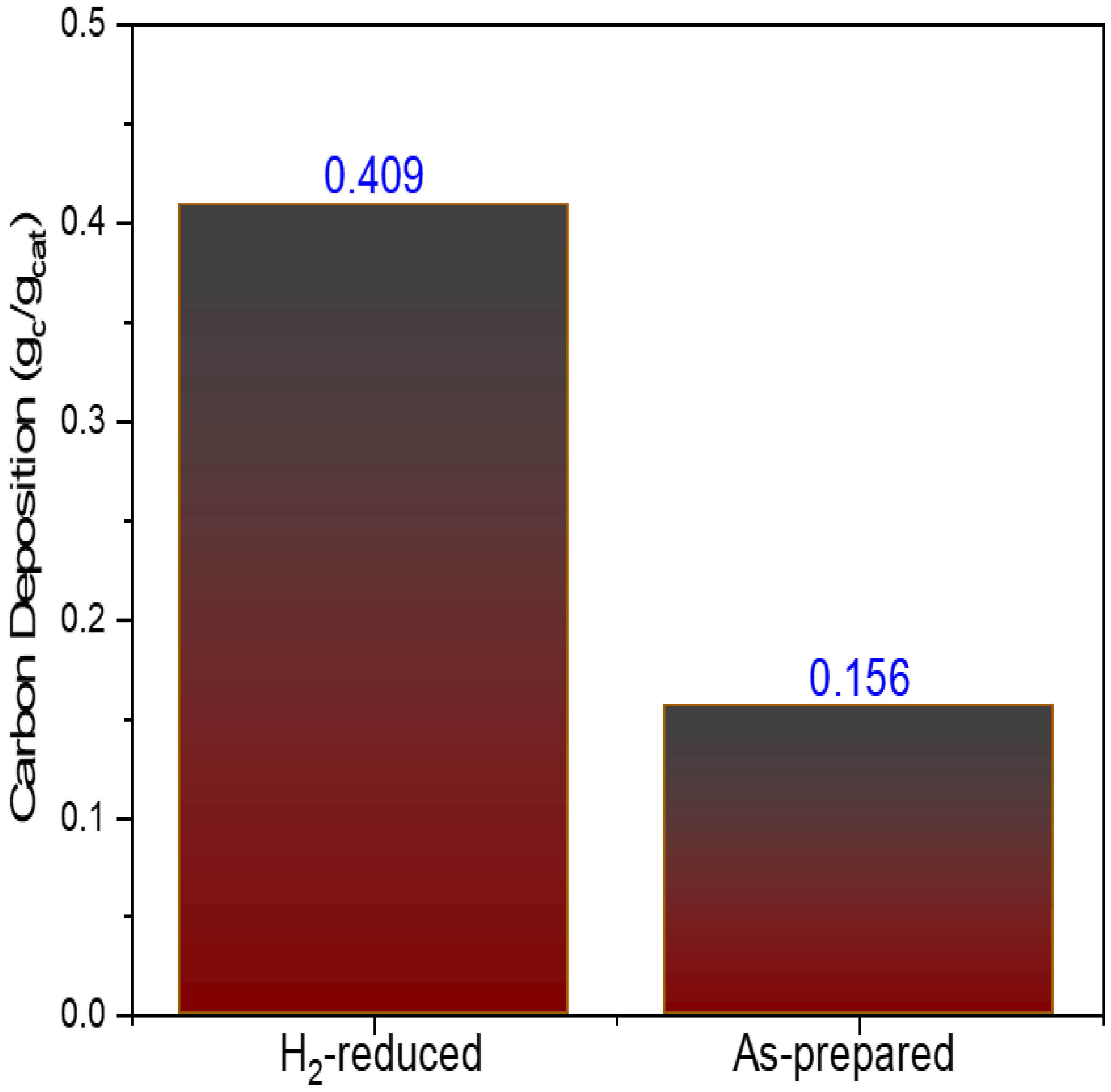

Figure C1. Elemental analysis of spent as-prepared and further reduced catalysts

Appendix D:

D1. Mear’s Criterion for intra-particle transport (Inside particle)

$$\left(\frac{\mathbf{r_a} * \left(\mathbf{r_p}^2\right)}{\mathbf{C_c}\ \ \mathbf{D_e}}\right) < \left(\frac{1}{\mathbf{n} - \boldsymbol{\beta}\Upsilon}\right)$$

Presented calculations are based on criteria equations from Mear’s D.E. Ind. Eng. Chem.

Where β is the maximum temperature difference that exists within the particle can be calculated as follows

$$\beta = \left(\frac{(-\Delta H) * De * Cs}{\lambda * Ts}\right)$$

($-\Delta H_{298k}$) is the heat of chemical reaction for dry reforming reaction (eq. 4) in kJ/mol reported $247*10^3$ J/mol

- C_s is the concentration of reactant (CH_4) entering to the reactor for the reaction mol /cm^3.
- r_a is the rate of reaction calculated as mol.$s^{-1}cm^{-3}$.

$r_a = V_0 * C_{CH_4} * X_{CH_4} / W_{cat}$

Table. D1. Mear’s intra-particle calculation

Temperature (K)	**75Ni25Co-B**		**75Ni25Co**	
	$\frac{\mathbf{r_a} * (\mathbf{r_p}^2)}{\mathbf{C_c}\ \mathbf{D_e}}$	$\left(\frac{1}{\mathbf{n}-\boldsymbol{\beta}\Upsilon}\right)$	$\frac{\mathbf{r_a} * (\mathbf{r_p}^2)}{\mathbf{C_c}\ \mathbf{D_e}}$	$\left(\frac{1}{\mathbf{n}-\boldsymbol{\beta}\Upsilon}\right)$
773	$4.4526*10^{-4}$	2.0362	$2.136*10^{-3}$	2.0162
823	$4.4539*10^{-4}$	2.0359	$2.131*10^{-3}$	2.0159
873	**$4.4559*10^{-4}$**	**2.0354**	**$2.125*10^{-3}$**	**2.0154**
923	$4.4576*10^{-4}$	2.0344	$2.119*10^{-3}$	2.0144
973	$4.4597*10^{-4}$	2.0338	$2.082*10^{-3}$	2.0138

Hence $\left(\frac{\mathbf{r_a} * (\mathbf{r_p}^2)}{\mathbf{C_c}\ \mathbf{D_e}}\right) < \left(\frac{1}{\mathbf{n}-\boldsymbol{\beta}\Upsilon}\right)$

D2. Mears Criterion for inter-particle transport (Outside particle):

Mass transfer limitations can be neglected if the Mears Criterion is satisfied.

$$\left(\frac{(-\boldsymbol{r}_{\mathbf{A}}{'}) * \ \mathbf{r}_{\mathbf{p}} * \ \boldsymbol{n}}{\boldsymbol{k}_{\mathbf{c}} \ \ \boldsymbol{C}_{\mathbf{Ab}}}\right) < \mathbf{0.15}$$

The above equation is based on criteria equations from Mear's D.E. Ind. Eng. Chem.

k_c is the mass transfer coefficient between gas and particle, cm/sec. The mass transfer coefficient can be calculated by using Sherwood number as follows $k_c = Sh*D_e/d_p$

Sherwood number (Sh) represents the mass transfer coefficient for transport from gas interphase to a swarm of catalyst particles, $\mathbf{Sh = 2.0 + 0.61*Re^{0.5}Sc^{0.33}}$

- The Reynolds number is defined as Re = D*u*ρ/μ, where D is the reactor diameter, u is the average flow velocity, ρ is the density of the gas and μ is the dynamic viscosity of the gas.

D = 2.5 (cm)

$\rho = 0.2156*10^{-6}$(kg/cm^3)

μ = 0.000000315 (kg/cm.s)

Re= 0.00504

Sc= 104.23

$Sh = 2.0+ 0.61* 2.450^{0.5} *104.2^{0.33} = 2.000349$

$k_c = Sh*D_e/d_p = 2.14$ cm/sec

Inter-particle transport

$$\left(\frac{(-r_{\mathrm{A}}{'}) * \ \mathrm{r}_{\mathrm{p}} * \ n}{k_{\mathrm{c}} \ \ C_{\mathrm{Ab}}}\right) < 0.15$$

Table D2. Mear's inter-particle calculation

Temperature (K)	$\frac{(-\boldsymbol{r}_{\mathbf{A}}{'}) * \ \mathbf{r}_{\mathbf{p}} * \ \boldsymbol{n}}{\boldsymbol{k}_{\mathbf{c}} \ \ \boldsymbol{C}_{\mathbf{Ab}}}$	
	75Ni25Co-B	**75Ni25Co-B**
773	$6.3726*10^{-11}$	$7.5257*10^{-10}$
823	$6.3783*10^{-11}$	$7.5325*10^{-10}$
873	$6.3809*10^{-11}$	$7.5382*10^{-10}$
923	$6.3852*10^{-11}$	$7.5482*10^{-10}$

973	$6.3983*10^{-11}$	$7.5498*10^{-10}$

Appendix E:

Permission of Reproduction from the Copyright Owner:

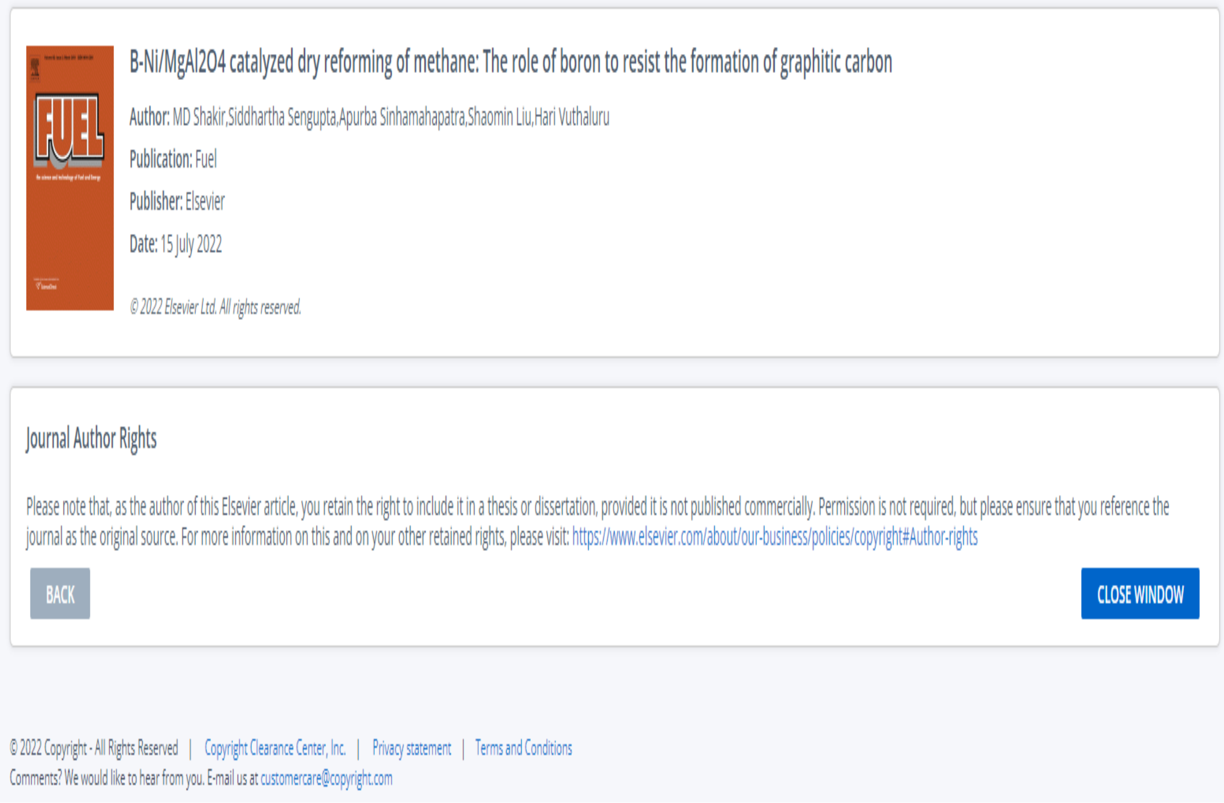

B-Ni/MgAl2O4 catalyzed dry reforming of methane: The role of boron to resist the formation of graphitic carbon

Author: MD Shakir,Siddhartha Sengupta,Apurba Sinhamahapatra,Shaomin Liu,Hari Vuthaluru

Publication: Fuel

Publisher: Elsevier

Date: 15 July 2022

© 2022 Elsevier Ltd. All rights reserved.

Journal Author Rights

Please note that, as the author of this Elsevier article, you retain the right to include it in a thesis or dissertation, provided it is not published commercially. Permission is not required, but please ensure that you reference the journal as the original source. For more information on this and on your other retained rights, please visit: https://www.elsevier.com/about/our-business/policies/copyright#Author-rights

© 2022 Copyright - All Rights Reserved | Copyright Clearance Center, Inc. | Privacy statement | Terms and Conditions
Comments? We would like to hear from you. E-mail us at customercare@copyright.com

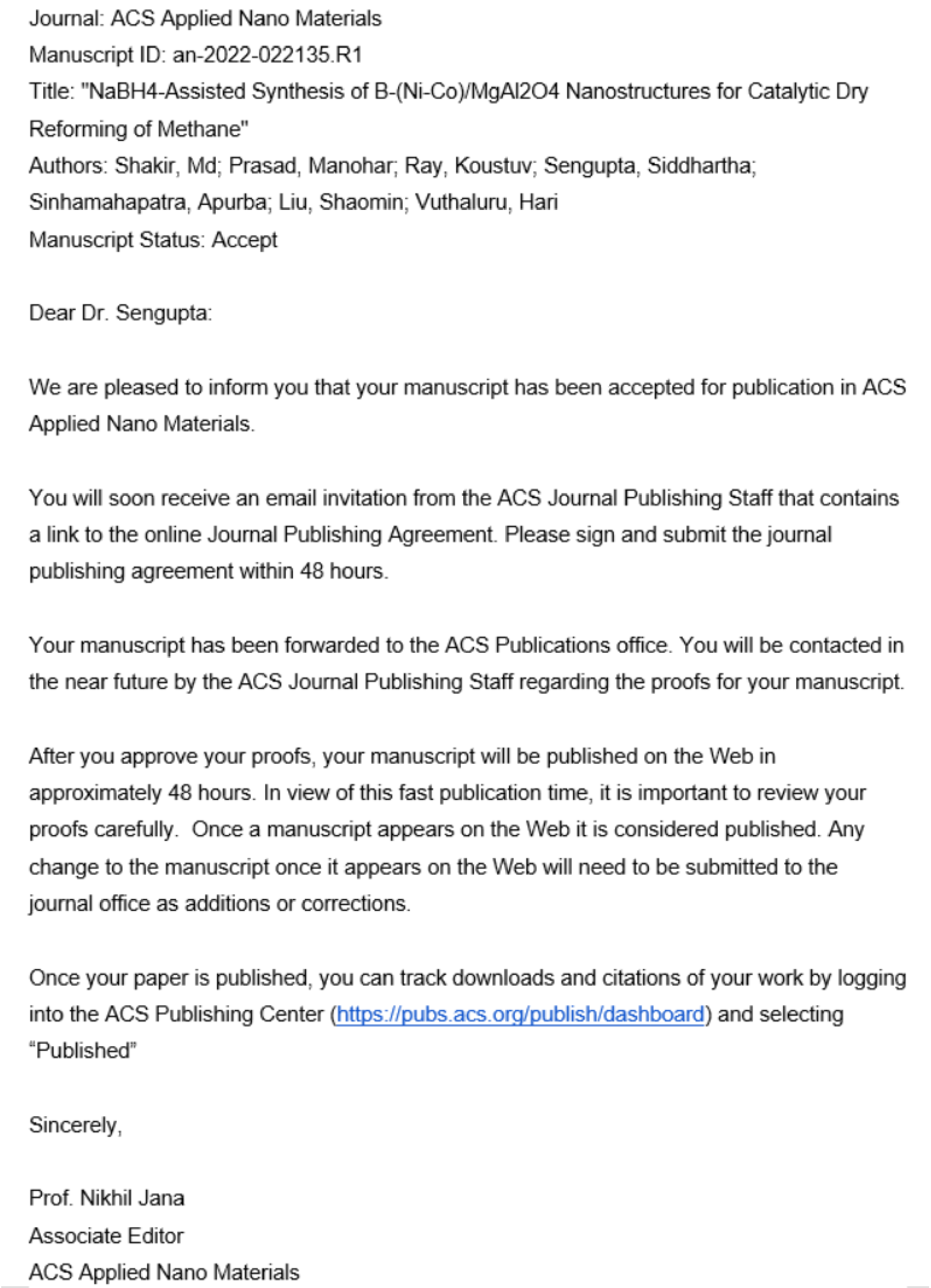

Journal: ACS Applied Nano Materials
Manuscript ID: an-2022-022135.R1
Title: "NaBH4-Assisted Synthesis of B-(Ni-Co)/MgAl2O4 Nanostructures for Catalytic Dry Reforming of Methane"
Authors: Shakir, Md; Prasad, Manohar; Ray, Koustuv; Sengupta, Siddhartha; Sinhamahapatra, Apurba; Liu, Shaomin; Vuthaluru, Hari
Manuscript Status: Accept

Dear Dr. Sengupta:

We are pleased to inform you that your manuscript has been accepted for publication in ACS Applied Nano Materials.

You will soon receive an email invitation from the ACS Journal Publishing Staff that contains a link to the online Journal Publishing Agreement. Please sign and submit the journal publishing agreement within 48 hours.

Your manuscript has been forwarded to the ACS Publications office. You will be contacted in the near future by the ACS Journal Publishing Staff regarding the proofs for your manuscript.

After you approve your proofs, your manuscript will be published on the Web in approximately 48 hours. In view of this fast publication time, it is important to review your proofs carefully. Once a manuscript appears on the Web it is considered published. Any change to the manuscript once it appears on the Web will need to be submitted to the journal office as additions or corrections.

Once your paper is published, you can track downloads and citations of your work by logging into the ACS Publishing Center (https://pubs.acs.org/publish/dashboard) and selecting "Published"

Sincerely,

Prof. Nikhil Jana
Associate Editor
ACS Applied Nano Materials

Attribution statement

Chapter 3. Paper "B-Ni/MgAl$_2$O$_4$ catalyzed dry reforming of methane: the role of boron to resist the formation of graphitic carbon", Fuel, Elsevier, 2022;
MD Shakir, Siddhartha Sengupta, Apurba Sinhamahapatra, Shaomin Liu, Hari Vuthaluru

<table>
<tr><th></th><th>Conception and Design</th><th>Acquisition of Data and Method</th><th>Data Conditioning and Manipulation</th><th>Analysis and Statistical Method</th><th>Interpretation and Discussion</th></tr>
<tr><td>Co-author 1
MD Shakir</td><td>✓</td><td>✓</td><td>✓</td><td>✓</td><td>✓</td></tr>
<tr><td colspan="6">Co-author 1 acknowledgment: I acknowledge that these represent my contribution to the above research output, and I have approved the final version.
Signature:</td></tr>
<tr><td>Co-author 2
Siddhartha Sengupta</td><td>✓</td><td></td><td>✓</td><td>✓</td><td>✓</td></tr>
<tr><td colspan="6">Co-author 2 acknowledgment: I acknowledge that these represent my contribution to the above research output, and I have approved the final version.
Signature:</td></tr>
<tr><td>Co-author 3
Apurba Sinhamahapatra</td><td>✓</td><td></td><td>✓</td><td>✓</td><td>✓</td></tr>
<tr><td colspan="6">Co-author 3 acknowledgment: I acknowledge that these represent my contribution to the above research output, and I have approved the final version.
Signature:</td></tr>
<tr><td>Co-author 4
Shaomin Liu</td><td></td><td></td><td></td><td></td><td>✓</td></tr>
<tr><td colspan="6">Co-author 4 acknowledgment: I acknowledge that these represent my contribution to the above research output, and I have approved the final version.
Signature:</td></tr>
<tr><td>Co-Author 5
Hari Vuthaluru</td><td>✓</td><td></td><td></td><td></td><td>✓</td></tr>
<tr><td colspan="6">Co-author 5 acknowledgment: I acknowledge that these represent my contribution to the above research output, and I have approved the final version.
Signature:</td></tr>
</table>

Chapter 4. Paper “NaBH$_4$-Assisted Synthesis of B–(Ni–Co)/ MgAl$_2$O$_4$ Nanostructures for the Catalytic Dry Reforming of Methane”, ACS Applied Nano Materials, 2022”.

MD Shakir, Manohar Prasad, Koustuv Ray, Siddhartha Sengupta, Apurba Sinhamahapatra, Shaomin Liu, Hari Vuthaluru

	Conception and Design	Acquisition of Data and Method	Data Conditioning and Manipulation	Analysis and Statistical Method	Interpretation and Discussion
Co-author 1 MD Shakir	✓	✓	✓	✓	✓
Co-author 1 acknowledgment: I acknowledge that these represent my contribution to the above research output, and I have approved the final version. Signature:					
Co-author 2 Manohar Prasad		✓	✓	✓	✓
Co-author 2 acknowledgment: I acknowledge that these represent my contribution to the above research output, and I have approved the final version. Signature:					
Co-author 3 Koustuv Ray		✓		✓	✓
Co-author 3 acknowledgment: I acknowledge that these represent my contribution to the above research output, and I have approved the final version. Signature:					
Co-author 4 Siddhartha Sengupta		✓		✓	✓
Co-author 4 acknowledgment: I acknowledge that these represent my contribution to the above research output, and I have approved the final version. Signature:					
Co-author 5 Apurba Sinhamahapatra		✓		✓	✓
Co-author 5 acknowledgment: I acknowledge that these represent my contribution to the above research output, and I have approved the final version. Signature:					
Co-author 6 Shaomin Liu		✓		✓	✓
Co-author 6 acknowledgment: I acknowledge that these represent my contribution to the above research output, and I have approved the final version. Signature:					
Co-Author 7 Hari Vuthaluru		✓		✓	✓
Co-author 7 acknowledgment: I acknowledge that these represent my contribution to the above research output, and I have approved the final version. Signature:					